NTNU – Trondheim
Norwegian University of
Science and Technology

Simulation of Low Salinity Waterflooding in a Synthetic Reservoir Model and Frøy Field Reservoir Model

Knut Even Holter

Earth Sciences and Petroleum Engineering
Submission date: June 2012
Supervisor: Jan-Åge Stensen, IPT

Norwegian University of Science and Technology
Department of Petroleum Engineering and Applied Geophysics

Preface

This thesis was written at the department of Petroleum Engineering and Applied Geophysics spring 2012, at the Norwegian University of Science and Technology. The academic supervisor for this thesis was Jan Åge Stensen from NTNU.

I would like to thank Jan Åge Stensen for kind advices and discussions. I would also like to thank Geir Frode Kvilaas and Det Norske Oljeselskap for allowing use of the simulation model of the Frøy field, and making this thesis possible.

I hereby declare that the work on this thesis is made independently and in accordance with the rules set down by the Examination regulations made by the Norwegian University of Science and Technology, Trondheim. The references are according to the Society of Petroleum Engineers' Style Guide updated 31st of August 2011.

Knut Even Holter

Trondheim, June 2012

Abstract

Most of the large petroleum discoveries have already been made, but the demand for energy is still increasing. To meet the demands, new methods for getting the existing resources from the subsurface up to the surface have to be applied. These methods include the Enhanced Oil Recovery (EOR) methods, methods to increase the hydrocarbons production from already existing fields. Low Salinity Waterflooding is an EOR method which has been given a lot of attention the last decades, and it has shown a great potential both during laboratory experiments and field scale tests. Low Salinity Waterflooding is applied by injecting water with a lower salinity than the existing connate water. Doing this provokes some chemically and physically processes that together tend to enhance the recovery in some petroleum reservoirs. The amount of incremental oil produced is, however, very dependent on the initial reservoir properties.

The purpose of this project was to investigate the possible options regarding low salinity waterflooding in ECLIPSE 100 through simulations of a synthetic reservoir model. Large wettability sensitivity was observed, indicating that the oil/water relative permeability, saturation and capillary pressure profiles play a major role during simulations when the BRINE option is activated. Results obtained after injection of brines with different salinities showed an increase in oil recovery with a decrease in salinity of the injected brines. An initial oil-wet reservoir with high residual oil saturation was observed to show the largest incremental recovery. A water-wet reservoir, however, resulted in the highest ultimate recovery. The reason for the increase in oil recovery could be seen in conjunction with a decrease in water production after breakthrough of the low saline brines.

After investigating the options included for low salinity waterflooding in ECLIPSE 100, a field evaluation of the potential of this as an EOR mechanism was simulated. A sector model of the Frøy field was obtained from Det Norske Oljeselskap. Initial reservoir properties and earlier laboratory experiments from cores in the same zone as the sector model had indicated a potential for LSW as a way to increase the oil production in the field. When the salinity in the reservoir reached below 5 kg/m^3 total dissolved salts (TDS), a reduction in residual oil saturation up to 7 % of PV was initiated. This reduction resulted in an up to 13 % increase in oil recovery of the initial oil in place during secondary recovery mode. Tertiary recovery mode showed almost the same incremental recovery as the secondary recovery

mode. A decrease in water cut was observed in conjunction with breakthrough of the low saline brines.

Even though the results obtained from low salinity waterflooding proved to be in the range of what was observed during earlier experiments from the Frøy field, the data added to the grid cells were no measured data. It should therefore be conducted new and accurate laboratory experiments, such that these data might be included in simulation models. This is especially important regarding parameters like relative permeability, saturation and capillary pressure. A full field investigation of the potential for low salinity waterflooding as a possible EOR mechanism should also be carried out, since the sector model only is valid for a small part of the reservoir. On the other side, as observed from simulation of a sector mode, the potential for low salinity waterflooding in the Frøy field seems to be large.

Sammendrag

De fleste store petroleumsfunnene har allerede blitt gjort, men etterspørselen for energi øker fortsatt. For å møte denne etterspørselen må nye metoder for å få opp de resterende ressursene fra undergrunnen opp til overflaten bli benyttet. Disse metodene omfatter metoder for å øke oljeutvinningen (EOR) i allerede eksisterende felt. Lavsalin flømming er en slik EOR metode som har fått mye oppmerksomhet de siste tiårene, og den har vist seg å ha et stort potensiale gjennom laboratorieforsøk og tester i feltskala. Lavsalin flømming gjennomføres ved å injisere vann med en lavere salinitet enn det opprinnelige formasjonsvannet. Dette har vist seg å provosere frem kjemiske og fysiske prosesser som sammen øker utvinningen i noen petroleumsreservoar. Mengden av økt utvinning avhenger av de initiale reservoar egenskapene.

Hensikten med denne oppgaven var å undersøke de forskjellige opsjonene som er tilgjengelig for simulering av lavsalin flømming i ECLIPSE 100. Dette ble bestemt og gjøres gjennom simulering av en syntetisk modell. Det ble observert en stor avhengighet av fuktegenskapene i modellen. Dette indikerte at olje/vann relativ permeabilitet, metning og kapillartrykksprofiler spiller en viktig rolle ved simulering når BRINE opsjonene er aktivert. Resultatene etter injeksjon av saltvann med forskjellig saltinnhold viste en økt oljeutvinning for injeksjon av saltvann med minkende salinitet. Det viste seg at det var det initiale oljefuktende reservoaret med en høy residual oljemetning som ga høyest økning i oljeproduksjon. Det var det vannfuktende reservoaret derimot som resulterte i høyest total oljeproduksjon. Grunnen for den økte oljeproduksjonen etter lavsalin flømming kan bli sett i sammenheng med en reduksjon i vannkutt etter gjennombrudd av saltvann med lav salinitet.

Etter å ha undersøkt opsjonene som finnes i ECLIPSE 100 med tanke på lavsalin flømming ble en feltevaluering av potensiale for dette som en EOR metode simulert. En sektormodell av Frøy feltet ble skaffet fra Det Norske Oljeselskap. De initiale reservoar egenskapene og tidligere laboratorieforsøk fra kjerneprøver i det samme området som sektormodellen hadde indikert et potensiale for lavsalin flømming som en metode for å øke oljeutvinningen i dette feltet på. Når saliniteten i reservoaret ble lavere en 5 kg/m^3 med totalt oppløste salter, ble en reduksjon av residual oljemetning opp til 7 % av porevolum initiert. Denne reduksjonen resulterte i en opp til 13 % økning i oljeproduksjon av initialt olje til stede

gjennom en sekundær produksjonsmekanisme. Tertiær produksjonsmekanisme resulterte i tilnærmet samme økning i oljeutvinning som den sekundære produksjonsmekanismen. En reduksjon i vannkutt ble observert i sammenheng med gjennombrudd av saltvannet med lav salinitet.

Selv om resultatene fra lavsalin flømming viste seg å være i samme spekter som tidligere eksperimenter fra Frøy feltet, var dataene inkludert i denne modellen ikke målte data. Det bør derfor bli gjennomført nye og nøyaktige laboratorieforsøk så slik data kan bli implementert i simuleringsmodeller. Dette gjelder spesielt for parametere som relativ permeabilitet, metning og kapillærtrykk. En fullfelts undersøkelse for potensialet for lavsalin flømming som en EOR metode bør også bli gjennomført. Dette siden sektormodellen kun er gjeldende for et avgrenset område i reservoaret. Potensialet for lavsalin flømming viste seg derimot å være stort i Frøy feltet etter å ha undersøkt dette i sektormodellen.

Table of Contents

List of Figures

List of Tables

1. Introduction

Due to its accessibility and low costs, waterflooding is one of the most common methods for improving oil recovery. In the last decades however, the potential of injecting low salinity fluids instead of seawater with high salinity has widely been discussed. Many coreflooding experiments as well as single well tracer tests (SWCTT) have been applied to test the phenomena, and many have proved to be successful by showing increasing oil recovery (Morrow et al. (1996) and Rivet et al. (2010)).

Understanding the chemistry of both the injection brine and reservoir brine is the key for optimizing the effect of low salinity waterflooding. Previous results from coreflooding experiments have indicated that there is a correlation between the shale present in the reservoir and the injection and reservoir brine (Austad et al., 2010). Analysis of the reservoir properties have therefore turned out to be important. By injection of brines with lower salinity than the reservoir brine, the ionic double layer between the clay and oil interface has turned out to expand and thus weaken (Morgan, 2009). If the reservoir brine is being properly analyzed, the injection brine can be mixed to maximize the effect of the ionic exchanges taking place between the two brines and the clay surface.

For low salinity waterflooding to be any effective, some conditions have turned out to be necessary (Morrow and Buckley, 2011). There has to be a significant clay fraction present in the reservoir, connate water has to be present and an exposure to crude oil to create mixed-wet conditions must be possible. The initial wettability and end point saturations also seem to play an important role for the low salinity flooding to be effective (Ashraf et al., 2011).

Some field scale experiments have been applied to investigate the possibility of enhanced oil recovery by low salinity waterflooding. Seccombe et al. (2008) reported that low salinity waterflooding was an attractive depletion process for the Endicott field in Alaska based on coreflood studies, SWCTT, numerical simulation and geochemical modeling. Results from the SWCTT showed an additional oil recovery up to 26 %. Skrettingland et al. (2011) reported on the other side disappointing results from coreflooding experiments and SWCTT from the Snorre field. The advantage of low salinity waterflooding was low in both the Upper Statfjord formation and in the Lunde formation.

Despite the encouraging results obtained from laboratory experiments and SWCTT during the last decades, only a few papers regarding modeling of low salinity waterflooding have been released. The purposes of these papers are mainly to present simple models for translating corefloods and SWCTT's into field-scale estimates of the low salinity potential. In ECLIPSE 100 the low salinity waterflooding option is introduced by the LOWSALT keyword in the RUNSPEC section, and opens up the opportunity of including two different sets of relative permeability and saturation profiles during the simulation period. This means that the option mainly is based on the theory of a wettability alteration as a result of the low salinity waterflooding, and is hence strongly dependent on the wettability of the reservoir.

Due to the lack of knowledge regarding simulation of low salinity waterflooding it was decided to do an investigation of the potential of low salinity waterflooding as an EOR mechanism with simulations in ECLIPSE 100. All simulations were done in a Black Oil model. The LOWSALT option was tested for two different cases. The first included a simple synthetic reservoir model, while the other included simulations of a sector and a 2D model of the Frøy field operated by Det Norske Oljeselskap. Different sensitivity analyses were implemented, including injection brine salinity, tertiary versus secondary waterflooding and testing of the different salinity dependent functions in ECLIPSE 100.

2. General Aspects of Waterflooding

To understand the basic behind reservoir engineering there are many parameters that have to be described. Knowledge of these parameters is important for both the theoretical study of low salinity waterflooding and the results obtained from numerical simulations. The most important reservoir parameters regarding waterflooding will be presented in the sections below.

2.1 Porosity

Porosity is one of the most important parameters for the reservoir rock. It describes the storage capacity of the rock, and is described as the part of a rock that does not consists of solid grains but consists of open pores. Porosity is defined as the ratio of the pore volume (PV) to bulk volume (BV) (Torsæter and Abtahi, 2003). The porosity may be divided into total porosity and effective porosity. The total is the ratio of all the pore spaces in a rock to the BV of the rock, while the effective porosity is the ratio of all interconnected pore spaces in a rock to the BV. It may be classified according to its origin as either primary or secondary porosity. The primary porosity is also called the original porosity and is developed during the deposition of the rock. Secondary porosity is described as porosity that has developed after the deposition of the sediments, mainly due to geological activities. Several parameters influence the porosity, such as grain shape, grain size, sorting, packing and compaction. Porosity is measured as a fraction or most commonly as percentage [%].

$$\phi = \frac{PV}{BV} \qquad \textbf{(Eq. 2-1)}$$

ϕ is porosity, PV is pore volume and BV is bulk volume.

2.2 Permeability

The permeability of a porous medium is defined as the ability of a medium to transmit fluids (Torsæter and Abtahi, 2003). High permeability means that fluids easily can flow through the medium, while low permeability means that fluids have difficulties flowing through the medium. Several parameters such as the shape and size of the pore throats and the absence of fractures influence the permeability. The unit for permeability is usually darcy [D], denoted [m^2] in the SI unit system.

The most known method for calculating the permeability of a rock is by use of the Darcy's equation. Darcy performed a series of experiments on the relationship affecting the downward flow of water through sand and invented the Darcy's law which in general is expressed as (Torsæter and Abathi, 2003):

$$\boldsymbol{k = \frac{q*\mu}{A}\frac{\Delta P}{\Delta x}} \qquad \textbf{(Eq. 2-2)}$$

Where q is the rate, μ is the viscosity, A the surface area, k is permeability and $\frac{\Delta P}{\Delta x}$ the pressure gradient.

2.3 Relative Permeability

The definition of permeability stated above is only valid if the rock is 100% saturated with a single-phase fluid and it is defined as the absolute permeability. Usually this is not the case because petroleum reservoir rocks often are saturated with two or more fluids such as oil, water and gas. In presence of more than one fluid, effective permeability has to be introduced. It is defined as the ability of a porous medium to transmit fluids when the saturation is less than 100% (Torsæter and Abtahi, 2003). The relative permeability of a phase is further defined as the ratio between the effective permeability of the phase and the absolute permeability.

$$\boldsymbol{k_{rf} = \frac{k_r}{k}} \qquad \textbf{(Eq. 2-3)}$$

Where k_{rf} is the relative permeability to the different phases, k_f is the effective permeability for the phase and k the absolute permeability.

2.4 Saturations

The PV described above can be considered as the volume of all the pores in a medium. This volume can again be divided into volumes of different fluids in the pores, and the PV is then the sum of all these volumes;

$$\boldsymbol{PV = V_{oil} + V_{water} + V_{gas}} \qquad \textbf{(Eq. 2-4)}$$

Where PV is pore volume and V_{oil}, V_{water} and V_{gas} are the volume of oil, water and gas respectively.

By use of **Equation 2-5**, the saturation can be defined. The saturation of a fluid is the fraction of the PV occupied by a particular fluid. For a given core sample, the saturation is defined as

the ratio of the volume of a fluid in a given core sample to the PV of the given sample (Torsæter and Abtahi, 2003).

$$S_i = \frac{V_i}{PV} \quad \text{(Eq. 2-5)}$$

Where i denotes the fluid phases, oil, water or gas. S_i is the phase saturation, V_i is the phase volume and PV is pore volume.

The sum of all the saturations in a rock will be equal to 1. Other terms for saturation that should be introduced:

- S_{or} is the residual oil saturation. This term describes the oil that is left in the pores after all the recoverable oil has been either produced or removed by for example waterflooding.
- S_{wi} is the initial water saturation of a core sample or a reservoir. In a hydrocarbon reservoir, there will almost always be some water in the pores initially additional to the hydrocarbons.
- S_{wir} is the irreducible water saturation. This describes the amount of water that is stuck in the rock and cannot be displaced during waterfloods.

2.5 Surface and Interfacial Tension

The surface tension is defined as the tendency of a liquid to expose a minimum free surface, and the interfacial tension is the similar tendency which exists when two immiscible liquids are in contact (Torsæter and Abtahi, 2003). That means the forces needed to maintain the interface or the surface. Surface and interfacial tensions are results from molecular properties occurring at the surface or interface.

2.6 Wettability and Contact Angle

The wettability plays an important role for the production of hydrocarbons. It is the main factor for the flow processes in the reservoir rock and also determines the initial fluid distributions (Torsæter and Abtahi, 2003). A reservoir rock can initially be water-wet, intermediate-wet or oil-wet. For EOR methods, understanding the chemistry behind rock wettability and how the oil “sticks” to the surface of the rock is very important. Previous observations have indicated that a water-wet reservoir is most efficient for waterflooding (Anderson, 1987).

When a liquid is brought in contact with a solid surface, the liquid can either spread out over the whole surface or form small drops on the surface. For the case where the liquid spreads out, the contact angle (Θ) is close to maximum. If droplets tend to form, the contact angle decreases. The same tendency can be seen if one fluid is immersed in another fluid and brought in contact with a surface. For an oil-water system where oil is immersed in water, the surface tends to be oil-wet if the oil spreads out on the surface. If the oil forms a droplet, the wettability shifts to more water-wet with decreasing contact angles. For close to completely water-wet system, the solid will have almost no contact with the oil droplet.

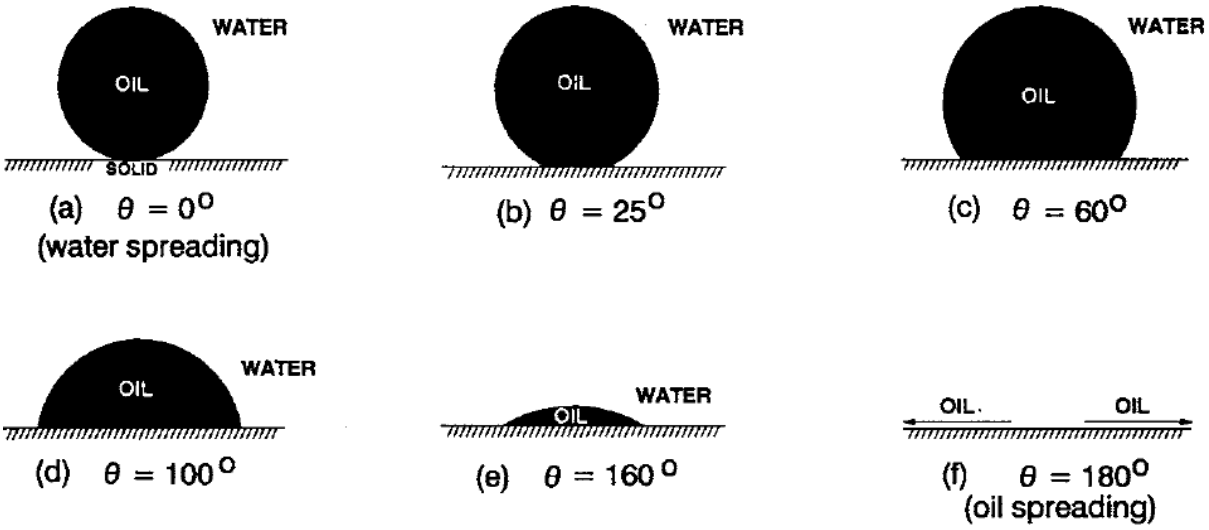

Figure 2-1: Different contact angles for oil-water systems (Morrow, 1990).

As indicated in **Figure 2-1** above, for a completely oil-wet system the contact angle is 180°. For a completely water-wet system, however, the contact angle is at its minimum, close to 0°.

2.7 Capillary Pressure

When two immiscible fluids are in contact, a discontinuity in pressure exists that separates them. The pressure difference between the two fluids is then defined as the capillary pressure (Torsæter and Abtahi, 2003). To determine the capillary pressure, P_c, the wetting and the non-wetting phases have to be known. An overview of different systems is found in **Table 2-1**. During waterflooding, the oil is displaced by water such that oil becomes the non-wetting phase and water the wetting-phase.

$$P_c = P_{non-wetting} - P_{wetting} \quad \text{(Eq. 2-6)}$$

P_c is the capillary pressure, $P_{non\text{-}wetting}$ and $P_{wetting}$ is the non-wetting and wetting phase pressure, respectively.

Table 2-1: Capillary pressure systems.

System	Wetting phase	Pc =
Oil/gas	Oil	Pg - Po
Oil/water	Water	Po - Pw
Gas/water	Water	Pg - Pw

P_g is the gas pressure, P_o is the oil pressure and P_w is the water pressure.

2.8 Production Mechanisms

During production of hydrocarbons there are two main different mechanisms that can occur. These mechanisms depend on which phase of the displaced and produced fluids are the wetting or the non-wetting.

2.8.1 Imbibition

The imbibition is the most common production mechanism during production of hydrocarbons. It appears when the non-wetting phase is displaced by the wetting-phase such that the amount of the wetting-phase in the reservoir or in the core sample increases. This process is often the mechanism of interest during waterflooding because it is the case when oil is displaced by water.

By displacement of oil by water, the relative permeability and capillary pressure curves may be obtained. As illustrated in **Figure 2-2** below, the imbibition process is affected by the S_{wir} and the S_{or}. Imbibition may be obtained either spontaneously or by adding force.

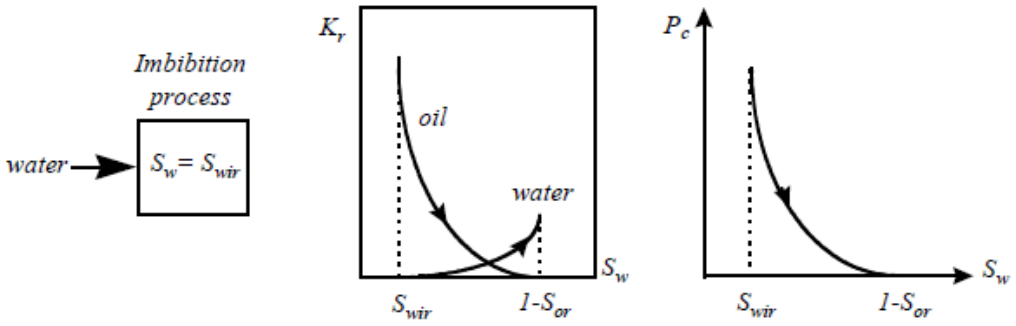

Figure 2-2: Imbibition process. Relative permeability and capillary pressure curves (Kleppe, 2011).

Where S_w is the water saturation, S_{wir} and S_{or} are irreducible water saturation and residual oil saturation, respectively. P_c is the capillary pressure and k_r is the relative permeability.

2.8.2 Drainage

The drainage process is obtained when the non-wetting phase is displacing the wetting-phase. This might be the case for gas-oil systems during gas injection, when gas as the non-wetting phase displaces oil.

For drainage to happen, the process has to be applied to a pressure higher than the threshold pressure, P_{cd}, as indicated on **Figure 2-3** below. An example can be used to describe this phenomenon. If a core 100 % saturated with water is displaced by oil, the oil needs to overcome the water pressure to be allowed to enter the core such that the capillary pressure will become positive.

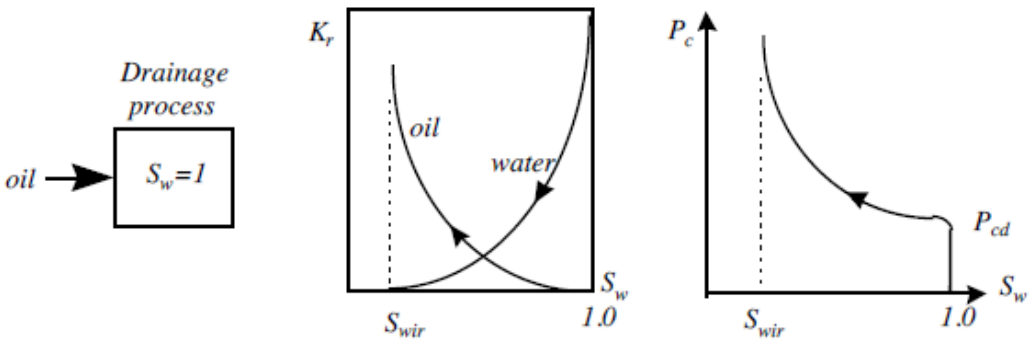

Figure 2-3: Drainage process. Relative permeability and capillary pressure curves (Kleppe, 2011).

Where S_w is the water saturation and S_{wir} is the irreducible water saturation. P_c is the capillary pressure, P_{cd} the drainage threshold pressure and k_r is the relative permeability.

Figure 2-2 and **Figure 2-3** used to describe the imbibition and drainage processes are for almost completely water-wet systems. The curves will depend on rock characteristics and wettability. For less water-wet conditions, the capillary pressure curves will have a negative part at high water saturations.

3. Low Salinity Waterflooding

3.1 Introduction

Low salinity waterflooding is an emerging EOR mechanism in the oil and gas industry. It has during many coreflood studies and single well chemical tracer tests (SWCTT) proven to have a high potential for enhancing oil recovery in certain reservoirs (Morrow et al. (1996), Seccombe et al. (2008) and Rivet et al. (2010)). The reason for this observed enhanced oil production has widely been discussed in the literature, but is not yet completely understood.

Low salinity waterflooding is injection of brines with a lower salinity, or at least a different salinity, than the initial formation brine salinity. If clay is present in the reservoir together with connate water this may cause reactions between the injected brine, the reservoir brine and the clay surface. These reactions are thought to trigger the pH in the reservoir for optimum conditions, start up an ionic exchange between the ions from the injected and reservoir brine or potentially mobilize some of the stuck oil by production of fines. This again might reduce the residual oil saturation and enhance oil recovery.

3.2 Literature Review

Conventional waterflooding has been applied for centuries for improving oil recovery in reservoirs, and is by far the most commonly used EOR technique up to date. Bernard (1967) however, presented experiments performed on sandstone cores where the salinity of the injection brines were changed during the waterflooding. It was well known that sandstones usually contained some clay, and that the clay was unaffected by saltwater but not by freshwater. The results from flooding on synthetic cores containing 2 % montmorillonite showed an up to 14 % increased oil recovery by changing the injected fluid from water containing 15 % NaCl to freshwater. Another interesting observation made during the experiments was a decrease in permeability and a small increase in pressure drop after the freshwater injection. Bernard suggested that this could be due to two cases. The first explanation was that the freshwater caused swelling of the clay, leading to a decrease in the available pore space which again gave a higher recovery. The second theory was that the freshwater dispersed the clay into fine particles that plugged flow channels, and that new flow channels were established again leading to an increased recovery. As a result of his

observations, Bernard concluded that waterflooding with distilled water or low salinity might result in an increased oil recovery.

Even though the results obtained from Bernard was encouraging, it was not until the 1990's that the potential for the low salinity waterflooding really was investigated. Morrow et al. (1996) performed a series of flooding experiments where they investigated the interaction between the injection brine and the formation brine. Standard flooding experiments were conducted with the same brines for the injected fluids as well as for the formation fluids. The new innovative experiments that were performed by Morrow et al. compared results from using standard experiments and the results from flooding with different injection brine and formation brine. Waterflood recoveries of a Prudhoe Bay crude oil on Berea Sandstone were determined. Two different brines were prepared, Brine 1 containing 4 % NaCl + 0.5 % $CaCl_2$ and Brine 2 containing 2 % $CaCl_2$. Brine 1 and 2 were then used as both the injected fluid and formation fluid in different combinations. The standard experiments for Brine 1 gave 16 % higher recovery than for Brine 2. The observations from the innovative experiments where Brine 1 and Brine 2 were used during mixed brine waterfloods resulted in recoveries intermediate to the results from the standard experiments. Results from the floods are presented in **Figure 3-1.**

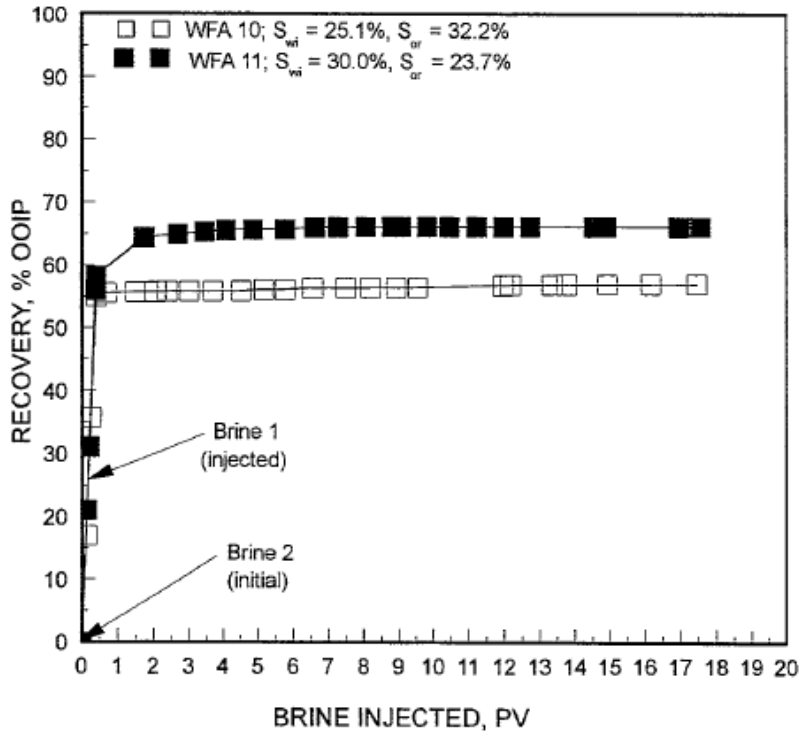

Figure 3-1: Increase in flooding efficiency during mixed-brine waterfloods (Morrow et al., 1996).

These unexpected results gave new interesting knowledge regarding the composition of the brines used during waterflooding. Old observation had concluded that it was the composition of the formation brine, connate water, which determined the displacement processes going on during waterflooding. The results obtained by Morrow et al., however, proved the opposite. If the old suggested theory should have been correct, the same results should have been obtained whether the formation brine and the injection brine were the same or not. As this was not the case, Morrow et al. concluded that the oil displacement was not only dominated by the composition of the initial formation brine. Another observation made during these experiments was that the results from the standard experiments performed gave different recoveries as well. The brines compositions were different, indicating that investigation of the crude oil/brine/rock (COBR) interactions might be crucial for optimal production during waterflooding.

These new observations lead to an increased research on this exciting subject the upcoming decades, and many laboratory experiments were conducted the following years. Both Tang and Morrow (1997) and Filoco and Sharma (1998) did similar experiments investigating the salinity effects of the injection and reservoir brines (RB). Their results, however, differed slightly. Tang and Morrow performed flooding experiments on Berea sandstone cores with the same injection and reservoir brine. They observed an increased recovery with a decreasing salinity of the injection brine. Their results also indicated that the salinity of the RB had an impact on oil recovery. The effect on recovery by lowering the salinity in the RB was pretty similar as the effect of lowering the salinity of the injected brine for the waterflooding case. For a spontaneous imbibition case, however, the low salinity effect was less for the RB salinity than for the injection brine salinity. Filoco and Sharma on the other side performed a series of centrifuge experiments on Berea sandstone to investigate the effect of both the injected and reservoir brine salinity. In contrast to Tang and Morrow, they observed a great dependence on the reservoir brine salinity and a low dependence for the injection brine. The reason for the increased recovery by the decrease in salinity for the RB, Foloco and Sharma indicated would be due to a wettability alteration towards oil-wet for high salinity RB.

Even due to an increasing research on low salinity waterflooding (LSW), the main mechanism behind the observed effects during low salinity waterflooding was still unclear. For a greater

understanding of these mechanisms, different sensitivity analyses were performed. Tang and Morrow (1999) conducted several flooding experiments to investigate low salinity waterflooding, and paid close attention to migration of fines during the oil production. It appeared to them that fines were produced in some of the cores that contained a certain amount of clay. To test if there was a clear relationship between this phenomena and oil recovery, they flooded a fired/acidized core with low salinity brines. A fired/acidized core would have a significantly reduced cation exchange capacity compared to a non-fired/acidized core and hence have a lower potential for fines migration. The results were as expected with no incremental recovery after LSW in these cores. As a result of this, Tang and Morrow concluded that adsorption of crude oil, the presence of potentially mobile fines and initial water saturations all have to be present for the low salinity effects (LSE) to be observed.

During low salinity waterflooding, a local increase in pH close to the clay surface has been observed during several laboratory experiments (Lager et al., 2006, RezaeiDoust et al., 2010 and Austad et al., 2010). It is also well known from the literature that the adsorption of ions depends on pH. Skauge et al. (1999) investigated the effect of organic acids and bases as well as oil composition on wettability and interfacial tension (IFT). The results indicated that the amount of acids and bases were proportional to the amount of polars (NSO and asphaltenes). A correlation between acid and base numbers was also observed. High acidic number (AN) yielded low base number (BN) and high BN resulted in low AN. It was also showed that an increase in asphaltene content might increase both AN and BN. Regarding the contact angle in the oil, the results showed a decrease in contact angle with an increase in the pH in the aqueous phase, and hence yielding more water-wet conditions. This is indicated in **Figure 3-2.** Sensitivity regarding the asphaltenes indicated an increased contact angle for an increase in asphaltene content, yielding more oil-wet conditions. Similar trends were also observed for the IFT alterations. A decrease in IFT was seen in conjunction with increased pH and a decrease in the amount of asphaltenes.

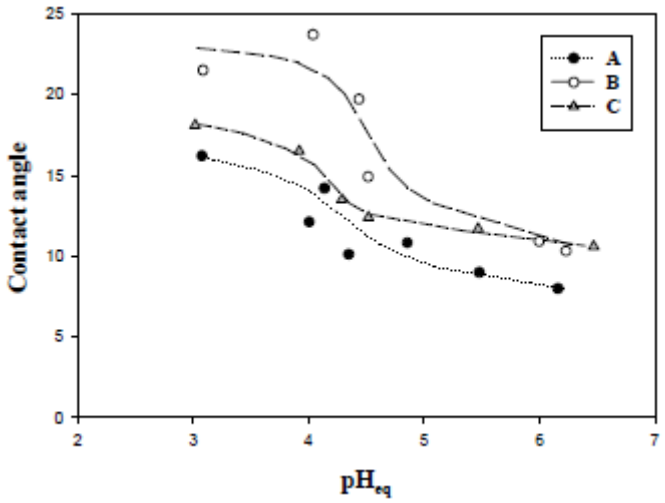

Figure 3-2: Contact angles as a function of pH in the aqueous phase (Skauge et al., 1999).

A recent laboratory experiment (Ashraf et al., 2010) has investigated the effect of wettability on secondary LSW. A low salinity waterflooding was carried out on Berea sandstone cores with varying wettabilities. The results showed that the neutral-wet core sample gave the highest ultimate recovery when standard synthetic brine (SB) was injected. The effect of low salinity waterflooding was, however, greatest for the water-wet core sample. An incremental oil recovery of 20 % of OOIP with injection of SB with 1 % of the initial SB salinity was observed.

The potential for LSW as an EOR mechanism for the North Sea has also been investigated. Several coreflooding experiments and a SWCTT have been conducted to evaluate the potential of LSW on the Snorre field. Skrettingland et al. (2011) reported, however, negative results both from the Upper and Lower Statfjord formation as well as the Lunde formation. A maximum of an incremental oil recovery of 2 % from the Statfjord formations were obtained by tertiary low salinity experiments. The result from the SWCTT was also disappointing, showing that no significant reduction in the Sor had taken place during the LSW. The reason for these results was concluded to be due to the initial wettability that was figured to be close to optimal for conventional waterflooding.

In the literature, low salinity waterflooding as a tertiary recovery mechanism has been given most attention (Morrow and Buckley, 2011). Gamage and Thyne (2011), however, performed experiments on outcrops and reservoir sandstones to compare secondary and tertiary oil recovery by low salinity waterflooding. Both single and two – phase experiments

were performed, and pressure drop and pH were continuously monitored. The single – phase coreflooding resulted in an increase in pH from 7.7 to 8.8 during low salinity waterflooding, and fines production was observed during some of the floodings. Incremental recovery was thought to be coincident with the decrease in salinity and increase in pH on the Berea outcrops. Similar pH increases were not observed during LSW in the reservoir sandstone. Among each rock type and oil combination, secondary mode experiments produced more oil than the tertiary experiments. The incremental recovery from the secondary waterflooding varied from 6 – 22 % compared to the tertiary recovery. Nasralla et al. (2011) observed similar trends during waterflooding on Berea core samples with different brines from a Middle East field. In all cases, the injection brine with the lowest salinity gave the highest recovery during secondary recovery mode. The reason for this they concluded that could be due to cation exchanges taking place, thus reducing the attracting forces between crude oil and the rock surface by changing the rock surface charge. They observed, however, no improvement in oil recovery during tertiary oil recovery. They indicated that the reason for this was because no fines migration or clay swelling occurred after the tertiary recovery mode. Two suggested reason for this were proposed. The first was that the residual oil after the formation water injection formed a film that prohibited interactions between fresh water and clay. The second was that adsorption of divalent cations inhibited any clay swelling or fines migration.

3.3 Mechanisms

As indicated in the short literature review in the **Section 3.2**, the mechanisms behind the low salinity waterflooding is still not completely understood. A number of different proposed explanations have, however, been presented. An overview of the most plausible explanations is found in the following sections.

3.3.1 Multicomponent Ionic Exchange

Understanding the chemistry of the rocks and brines is the key to investigate possible reasons for enhanced oil recovery (EOR) by low salinity waterflooding (LSW). The Multicomponent Ionic Exchange (MIE) is a theory based on chemical investigations of interactions between the reservoir brine and the injection brines. Reservoir, especially oil-

wet, sandstones contain some clay particles within the sand particles that have a negatively charged surface. The oil in these reservoirs is held on to the surface of the negatively charged clay particles mainly due to divalent cations, such as Ca^{+} and Mg^{2+} , positively charged ions that can form two bonds with other ions. As a result, the oil in these reservoirs might form complex organic polar compounds.

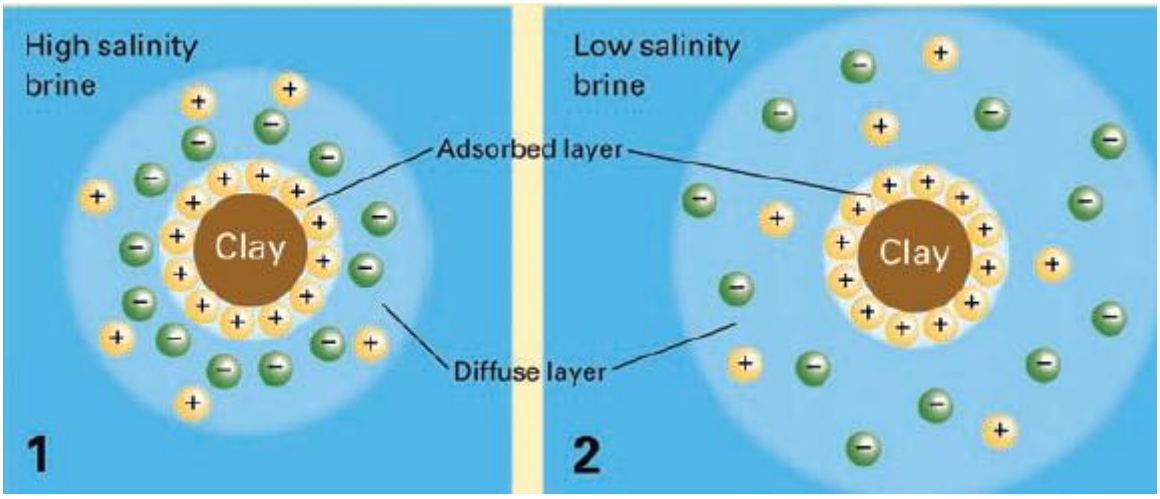

Figure 3-3: The concept of the double layer (Morgan, 2009).

If further on such oil bearing reservoirs are immersed in brine, a diffuse layer forms around the formation structure as illustrated above in **Figure 3-3**. These layers vary in thickness and stability depending on the salinity of the brine they are submerged in and the amount of active ions in place.

Flooding of these reservoirs by injection of water that has a lower salinity than the initial formation brine might cause some changes in the grain chemistry and result in an expansion of the diffuse layer. As earlier described, the diffuse layer is salinity dependent and expands with low salinity and reduces with high salinity. Free cations from the injected fluid might react with the divalent ions in the diffuse layers. For example might free Na^{+} ions exchange with the divalent ions, such as Mg^{2+} and Ca^{+}, holding the oil in place and thus release the oil stuck in the adsorbed layer.

Many experiments have supported and indicated the consequences of this theory, both in laboratory and in field scale. Lager et al. (2008) observed a significant increase in Mg-ions and a small increase in Ca-ions in the produced water immediately after breakthrough of the low salinity (LS) brine. The amount of Mg-ions later on became below the detection limit.

This can be described by the MIE theory. As the free ions from the injected brines such as Na^+ ions are reacting with the divalent Mg and Ca-ions already in place, the divalent ions are released from the diffuse layers in the same matter as the oil. The "new" free ions then can be transported away from the reservoir together with the produced water and hydrocarbons. This increases the amount of ions in the produced water as illustrated in **Figure 3-4** below. When all of the Mg-ions are "produced", the Mg-ions from the injected brine will be absorbed by the formation and the amount of Mg-ions in the produced water will approximately vanish. This is the case not only for magnesium, but also for other divalent ions initially in place in the reservoir. When the formation is fully saturated with ions, however, production of the initial ions might again appear.

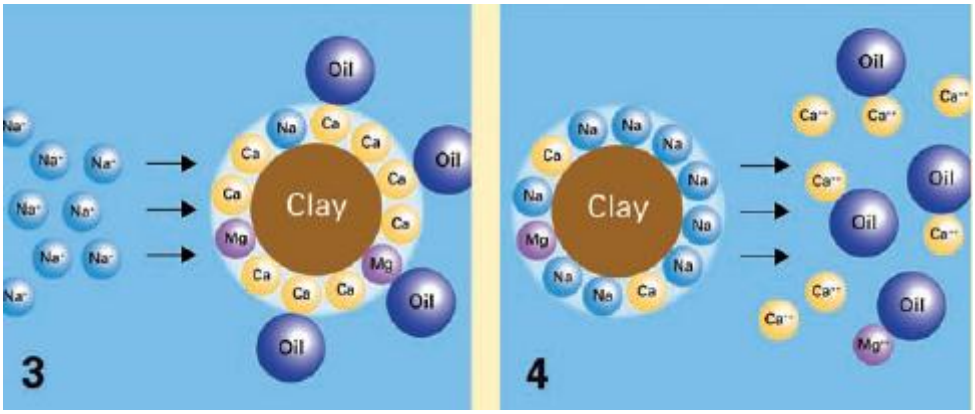

Figure 3-4: MIE in practice, to the left: before MIE, to the right: after MIE (Morgan, 2009).

The MIE theory is described in details by Lager et al. (2006). They suggested that 8 different possible mechanisms might describe how the adsorption to the clay minerals appears, whereas 4 of them will be strongly affected by cation exchange occurring during LSW.

The first mechanism, adsorption by cation exchange, appears when molecules containing quaternized nitrogen or heterocyclic rings replace the exchangeable ions initially bound to the clay surface. The second is described by ligand bonding which is a direct bonding between multivalent cations and a carboxylate group, resulting in detachments of organic-metallic complexes from the mineral surface. Cation bridging is the third suggested mechanism that is strongly affected by cation exchange occurring during LSW. It is described as a weak adsorption mechanism that appears between polar functional group and exchangeable ions on the clay surface. In the presence of highly solvent ions, such as Mg^{2+}, however, water bridging might appear. This is the fourth mechanism, and involves solvation

of the exchangeable cations by water molecules. The different mechanisms are illustrated in **Figure 3-5** below.

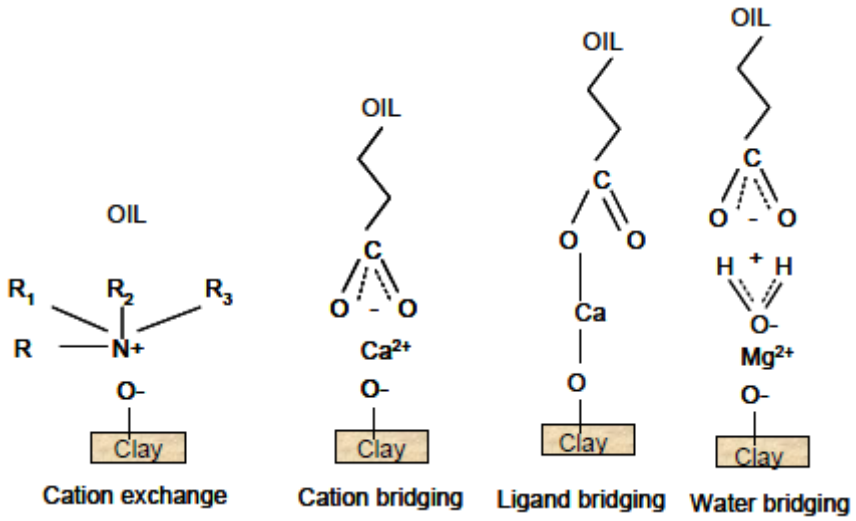

Figure 3-5: Mechanism describing the adsorption to the clay minerals during MIE (Seccombe et al., 2008).

As earlier described it is mainly the oil-wet reservoirs that contains this negatively charged clay surfaces which trap the oil to the surface, creating complex organic polar compounds. The MIE theory works such that a wettability alteration towards more water-wet conditions can appear. During LSW, MIE might take place, and remove the organic polar compounds from the clay surface and replace them with uncomplexed cations. This will lead to an enhanced oil recovery due to a wettability alteration towards more water-wet conditions, which has proven to be better than oil-wet conditions during conventional waterflooding (Anderson, 1987).

Lager et al. (2006) also performed an experiment to prove this theory. The experiment was performed on a North Slope core by replacing all the multivalent cations present in the reservoir with Na^+ - ions. By doing this, the effect of the MIE should be decreased significantly. As the core was fully saturated with Na^+-ions, the core was flooded with oil. The waterflooding experiment flooded at first high salinity water (HSW) with only NaCl. Then a LSW with only NaCl was conducted before a tertiary injection of LSB containing Ca^{2+} and Mg^+ was done. From the theory, this waterflooding should give no increased oil recovery by the LSW with or without the multivalent cations because no organic complexes were present to be desorbed, and all mobile oil had already been displaced. The results from the experiment

matched the predictions. These results indicated the importance of the MIE, and that this might be the primary driving force for the observed EOR by LSW.

3.3.2 pH alteration

The pH is a measure of acidity or basicity of an aqueous solution, and depends on the amount of hydrogen ions, H^+, in place (Zumdahl, 2009). High concentration of H^+-ions yields acidic conditions, low pH, while a basic condition is the opposite leading to high pH. Most connate water in reservoirs is considered to be acidic due to dissolved CO_2, H_2S and other sour atoms and a pH around 5-6 is expected. This low pH environment enhances the adsorption of both acidic and basic components onto the clay surface (RezaeiDoust et al., 2010). The presence of especially CO_2 is suggested to work as a pH buffer, such that the pH of a reservoir up to 10 is unlikely in most petroleum reservoirs.

During LSW, a local increase in pH close to the clay surface has been observed during several LSW laboratory experiment (Lager et al., 2006, RezaeiDoust et al., 2010 and Austad et al., 2010). Lager et al. (2006) proposed this to be due to two simultaneous reactions. A dissolution of carbonates which results in an excess of OH^-, and a cation exchange between clay minerals and the invading water.

$$CaCO_3 = Ca^{2+} + CO_3^- \quad \textbf{(Eq. 3-1)}$$

$$CO_3^{2-} + H_2O = HCO_3^- + OH^- \quad \textbf{(Eq. 3-2)}$$

As seen from the mathematical evidence in **Equation 3-1** (Lager et al., 2006) above, the dissolution of carbonates results in an excess of OH^- yielding an increase in pH. The cation exchange on the other side, **Equation 3-2** (Lager et al., 2006), works such that the mineral surface will exchange H^+ from the injected fluid with cations previously adsorbed. This will again lead to a decrease of H^+, and yields an increase in pH. If an increase in pH up to or above 9 would have appeared, this would be equivalent to alkaline waterflooding. LSW was earlier suggested to work like an alkaline waterflooding (Mcguire et al., 2005). Alkaline waterflooding has turned out to be an effective EOR method because of a reduction in interfacial tension. Due to the initial pH buffer, however, Lager et al. figured that this was not a possibility because pH alternation towards such high values could not be obtained. They also noted that low salinity effects were observed for lower pH values.

Austad et al. (2010) made another suggestion for the reason for this pH alteration, somewhat close to the theory by Lager et al. (2006). They figured the increase in pH to be due to ion exchanges in the reservoir or in the core. When injection of water with lower salinity than the initial formation water is conducted, desorption of especially Ca^{2+} might occur such that the equilibrium in the reservoir is disturbed. To compensate for the loss of cations, a substitution of Ca^{2+} and H^{+} might take place. This is indicated in **Figure 3-6** below. A decrease in in H^{+} will then happen, resulting in an increase in pH.

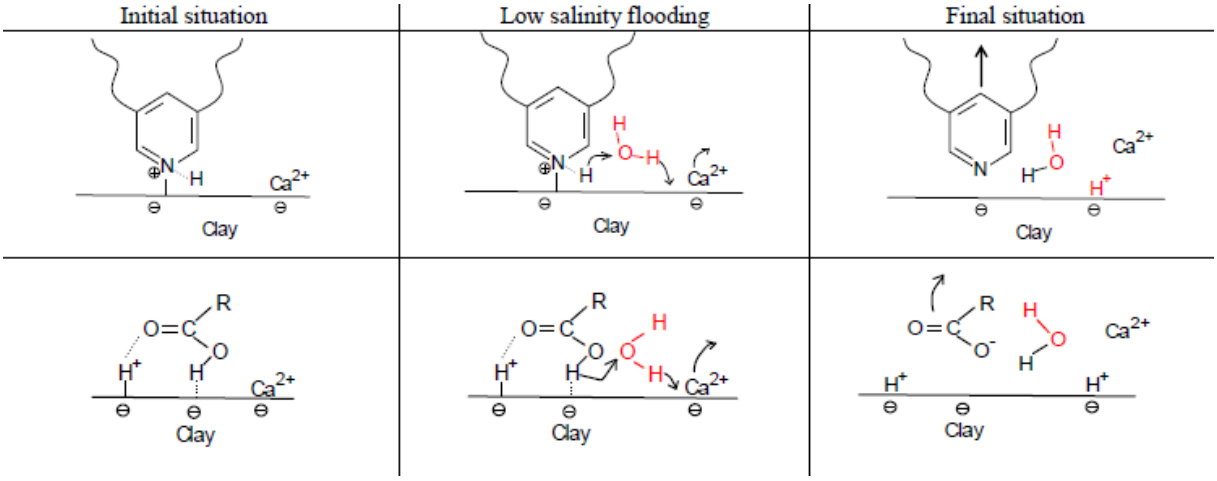

Figure 3-6: Proposed mechanism for LSE. Upper: Desorption of basic material. Lower: Desorption of acidic material (Austad et al., 2010).

The ionic exchange can be described mathematically by a numerous of equations and chemical reactions. Using Ca^{2+} as an example, **Equation 3-3** (Austad et al., 2010) below, as the reactive cation to describe the case above:

$$\boldsymbol{Clay - Ca^{2+} + H_2O = Clay - H^{+} + Ca^{2+} + OH^{-}} \quad \textbf{(Eq. 3-3)}$$

The local increase in this pH close to the clay surface causes reactions between adsorbed basic and acidic material as in an ordinary acid-base proton transfer reaction, **Equation 3-4** (Austad et al., 2010) and **Equation 3-5** (Austad et al., 2010). This might again lead to increased water-wet conditions and further on an increase in oil recovery.

$$\boldsymbol{Clay - NHR_3^{+} + OH^{-} = Clay + R_3N + H_2O} \quad \textbf{(Eq. 3-4)}$$

$$\boldsymbol{Clay - RCOOH + OH^{-} = Clay + RCOO^{-} + H_2O} \quad \textbf{(Eq. 3-5)}$$

As mentioned earlier, it has been stated that there is no clear relationship between effluent pH and oil recovery (Sheng, 2011). The increase in pH is seen more as a consequence of the LSE than the cause for the observed LSE.

3.3.3 Fines Migration

Production of fines has been observed several times in sandstone reservoirs in conjunction with low salinity waterflooding (LSW), and the reason for this phenomenon has widely been discussed in the literature and considered as one of the reasons for the low salinity effects (LSE).

Tang and Morrow (1999) observed production of fines during LSW of a CS-sandstone. During the LSW, a significant permeability reduction was observed. This was thought to be due to that migration of fines blocked some of the available pore space. They also concluded that the possibility of fines migration was a necessity because the LSE was eliminated during firing/acidizing of a Berea sandstone core, and waterflooding of this core showed almost no additional oil recovery by LSW. Further on Tang and Morrow discussed the theory regarding fines migration in details.

When low salinity brines (LSB) are injected, the double layer, as discussed under the MIE section above, is expanded due to a reduction of the ion concentration. This again might enhance the tendency for stripping of fines, because the double layer experiences a reduced stability.

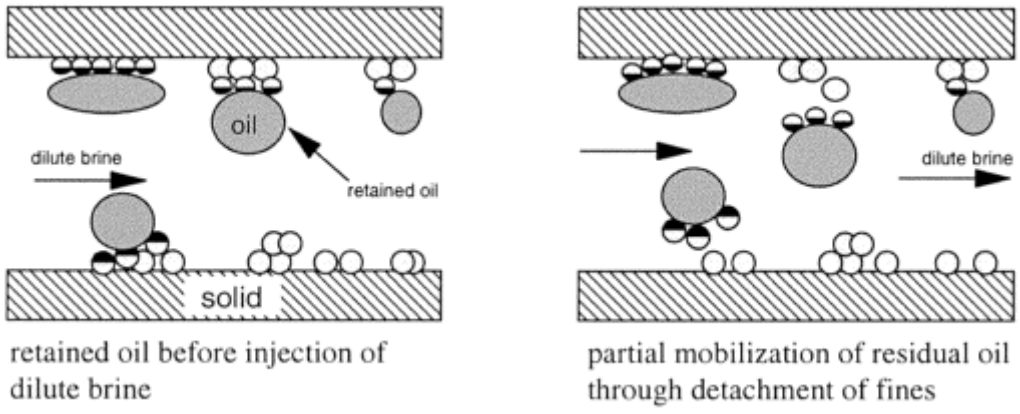

Figure 3-7: Mobilization of trapped oil due to migration of fines (Tang and Morrow, 1999).

Tang and Morrow suggested that diluted brine injection lead to mobilization of the trapped oil as a result of migration of fines. This is illustrated in **Figure 3-7** above and was thought to increase the oil recovery. The amount of extra oil produced was, however, considered to be greatly affected by the COBR interaction. If for instance a core was 100 % saturated with oil,

such that no connate water was in place, no additional oil recovery was observed during LSW.

The reason for this increased oil recovery by migration of fines was considered to be due to a wettability alteration towards more water- wet conditions. The presence of hydrocarbons in the adsorbed layer caused formation of, as mentioned earlier, complex organic-metallic ions. As these complexes were stripped away the system became more water-wet.

Migration of fines is, however, more suggested to be a cause of the MIE either than for the LSE alone. Many later experiments (Tang and Morrow, 1999 and Ashraf et al., 2010) have not shown any fines production during LSW, and they have questioned the theory of fines migration as the case of increased oil recovery with decreasing salinity. The conclusion so far is that fines migration is rather an effect than a cause.

3.3.4 Summary

All the proposed mechanisms tend to yield a wettability alteration towards more water-wet conditions. This is mainly a result of the chemical reactions happening between the clay surface and the injected and reservoir brines. These reactions might decrease the residual oil saturation and increase the oil recovery by mobilization of some of the trapped oil. The reduction in residual oil saturation is dependent on the initial rock properties and strongly dependent on the amount of clay in the reservoirs and the presence of and the salinity of the connate brine. Unfortunately, only few of these rock properties are included in simulators, and thus limit the accuracy during simulations of augmented waterfloodings such as low salinity waterflooding.

In simulators, such as ECLIPSE 100, the proposed wettability alteration towards more water-wet conditions is the base for the options regarding simulation of low salinity waterflooding. Limited data are available from after injection of low salinity brines. Since wettability is the major uncertainty, relative permeability, saturation and capillary pressure data should be measured before and after low salinity waterflooding. These measurements can be done in either laboratories or by SWCTT's and be included in simulators.

4. Modeling Low Salinity Waterflooding

Despite the growing interest in low salinity waterflooding as an EOR mechanism, only a few papers regarding modeling of low salinity waterflooding have been published. The purposes of these papers are mainly to present simple models for translating corefloods and SWCTT's into field-scale estimates of the low salinity potential. Previous proposed models of low salinity waterflooding have based their theory on the suggested low salinity mechanisms which is thought to yield a wettability alteration. This problem is mainly solved by adding sets of salinity dependent curves for saturations, relative permeability and capillary pressure. These sets will then be different for flooding with high salinity brines and for flooding with low salinity brines. In addition to this wettability alteration, there are many other effects of low salinity waterflooding that have been discussed for modeling LSW. This includes salinity dependency, mixing of connate water and injection water, connate-water banking and dispersion.

Coreflood studies have shown that the salinity of the injection brine plays a major role while injecting low salinity brines. The results have, however, not proven any proportional relationship between the salinity of the injection brine and oil recovery. Tests have shown that the salinity of the injection brine has to be significantly lowered for any effect to be observed. McGuire et al. (2005) showed no benefit from a SWCTT for lowering the salinity of the injection brine from 23 000 ppm to 7 000 ppm, but observed a significant increase in oil recovery by lowering it to 1 700 ppm. They concluded that LSE might be observed after lowering the injection brine salinity to less than approximately 5 000 ppm. This obviously varies from reservoir to reservoir, and proves that investigation of the COBR relationship plays a major role for optimization of the injection brine.

During waterflooding, the injected water might mix with the connate water, displace it or potentially bypass it. Previous models have mainly used the standard assumption that connate water is displaced by the injected water with some degree of mixing. This means that the displacement will not be piston-like. The displacement process does, however, vary with injection rate. Previous observations (Salter and Mohanty, 1982) found that the measured dispersion coefficient increases roughly linearly with velocity rather than being constant. Dispersion can be simulated in two ways. The first way is by use of numerical dispersion which occurs because the salt mixes uniformly within each grid block. The second

way is by connate-water banking. Connate-water banking is thought to occur because much of the connate water is displaced by the injected water. Earlier suggested theories indicated that it was the connate water that actually displaced the oil, such that the composition of the injected water was irrelevant. This has, however, been proven to be wrong indicating that for instance the salinity of the injected fluid actually plays a major role on recovery despite the connate-water banking.

During conventional secondary waterflooding, the Buckley-Leverett solution consists of a shock front and a spreading wave. For low salinity waterflooding, however, the Buckley-Leverett solution consists of two fronts. The first corresponds to the transition between low and high salinity, while the second front corresponds to the transition between high water saturation and connate water at high salinity. It addition to this, a connate-water bank is located between these two fronts. This is illustrated in **Figure 4-1** below.

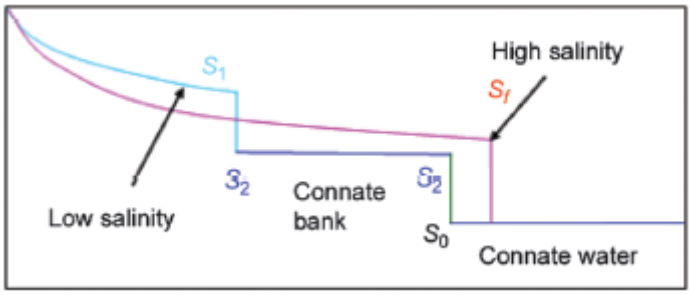

Figure 4-1: Bukley – Leverett solution for secondary low salinity waterflooding (Jerauld et al., 2008).

For tertiary waterflooding as well, there has been observed a difference in the Bukley-Leverett solution for low salinity waterflooding. This solution clearly indicates how a reduction in S_{or} might take place and is illustrated in **Figure 4-2**.

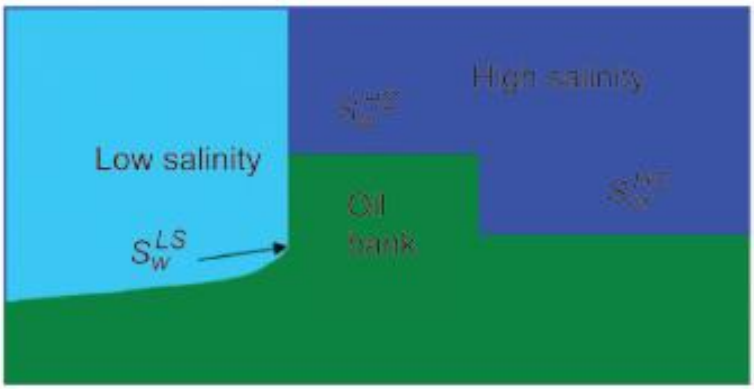

Figure 4-2: Bukley – Leverett solution for tertiary low salinity waterflooding (Jerauld et al., 2008).

It is to note that the ordinary Bukley-Leverett front has a higher velocity for conventional waterflooding than for low salinity waterflooding. This means that breakthrough of conventional waterflooding is observed to be quicker than for low salinity waterflooding (Jerauld et al., 2008).

The results from simulations are strongly dependent on the dispersion. Numerical dispersion appears mainly due to errors after discretization of the flow equations and might give misleading results. It can cause a smearing of otherwise sharp saturation fronts (Fanchi, 1983) and especially affects the time for breakthrough of the injected fluid. AlSofi and Blunt, (2010), however, proposed a new model to minimize the errors from numerical dispersion during augmented waterflooding. Rather than offering an improved discretization scheme, they proposed a simple model for addressing numerical dispersion. The new model assumed segregation-in-flow instead of the traditional instant mixing assumption, and this required replacement of some of the traditional equations. **Equation 4-1** for the fractional flow was replaced by **Equation 4-2.** Polymers are here just used as an example of concentration of the solute in water.

$$\boldsymbol{f_w = \frac{1}{1+\frac{\mu_w(C)\, k_{ro}}{k_{rw}(C)\, \mu_o}}} \qquad \textbf{(Eq. 4-1)}$$

$$\boldsymbol{f_{aq} = (1-C)f_w + Cf_p = (1-C)\frac{1}{1+\frac{\mu_w\, k_{ro}}{k_{rw}\, \mu_o}} + C\frac{1}{1+\frac{\mu_p\ \ k_{ro}}{k_{rwp}\, \mu_o}}} \qquad \textbf{(Eq. 4-2)}$$

Where μ_w, μ_o, μ_p is water, oil and polymer viscosity respectively, k_{ro}, k_{rw}, k_{rwp} is oil, water and injected aqueous phase (polymer) relative permeability, C is concentration of a relevant solute in water (polymer, salt, for instance) and f_{aq}, f_w, f_p is the fractional flow of the aqueous phase, water and polymer.

In the limits of no polymer (or other solvent) and fully saturated with polymers, **Equation 4-1** and **4-2** give the same fractional flows. Then the transport equations needed modifications, and **Equation 4-3** was replaced by **Equation 4-4.**

$$\boldsymbol{\phi \frac{\partial C S_w}{\partial t} + q_t \frac{\partial C f_w(S_w, C)}{\partial x} = 0} \qquad \textbf{(Eq. 4-3)}$$

$$\boldsymbol{\phi \frac{\partial}{\partial t}(S_w C) + q_t \frac{\partial}{\partial x}\left(f_p C\right) = 0} \qquad \textbf{(Eq. 4-4)}$$

Where ϕ is porosity, ϕ_f is fractional porosity, C is concentration of a relevant solute in water, S_w is water saturation, f_w is water fractional flow, f_p is polymer fractional flow, and q_t is total rate.

The new proposed model was found to resolve the saturation fronts during Bukley-Leverett solutions more efficient than the old model. This was especially obtained because the segregation-in-flow assumption did suggest a presence of a connate bank region, and the secondary shock become more self-sharpening.

To illustrate the effectiveness of the new numerical scheme a streamline based simulator was applied to compare numerical and analytical solutions in a 1D, 2D and 3D case for injection of polymers. By use of the proposed phase segregation scheme during the 1D case, a significant reduction in required number of grid blocks for an accurate solution was observed. In the conventional scheme, 1 000 grid blocks were necessary to resolve the front. For the segregation-in-flow numerical scheme, however, only 50 grid blocks were necessary to resolve the front with approximately the same accuracy. If the number of grid blocks were smaller than 1 000 for the conventional scheme, smearing occurred which lead to erroneous prediction in the oil production. The reduction in grid blocks for the new scheme was a consequence of significant less smearing of the polymer concentration front.

For the 2D polymer case, a much more distinct connate bank was observed for the segregation-in-flow scheme compared to the conventional scheme. This was due to less dispersion of the polymer front. During the 3D polymer case, the conventional scheme predicted higher oil production at early time than the new scheme, yielding less accurate results. It should be mentioned that a segregation option is available in commercial simulators. It is, however, only used for calculating effective fluid properties but not transport.

5. Low Salinity Waterflooding: Options in ECLIPSE 100

In ECLIPSE 100, there are many options included to investigate the impact of brine composition. The purposes of these options are to see the how the reservoirs depend on injection brine salinity and initial reservoir brine salinity. This is primarily done by introduction of the BRINE model. This model adds an extra separate salt phase to the already existing phases, and a mass conservation equation for the new phase is solved for each grid block in the reservoir model (**Equation 5-1,** Schlumberger, 2011). The brine is further on assumed to only exist in the water phase (Schlumberger, 2011).

$$\frac{d}{dt}\left(\frac{VS_wC_s}{B_w}\right) = \sum\left[\frac{Tk_{rw}}{B_w\mu_{s\,eff}}(\delta P_w - \rho_w g D_z)\right]C_s + Q_w C_s \qquad \text{(Eq. 5-1)}$$

Where ρ_w is the water density, Σ is the sum over neighboring cells, C_s is the salt concentration in the aqueous phase, $\mu_{s\,eff}$ is the effective viscosity of the salt, D_z is the cell center depth, B_w is the formation volume factor for water, T is transmissibility, k_{rw} is the water relative permeability, S_w is the water saturation, V is the block pore volume, Q_w is the water production rate, P_W is water pressure and g is gravity acceleration.

To activate the low salinity option in ECLIPSE, the keyword LOWSALT is introduced in the RUNSPEC section of the model. This automatically activates the BRINE option and allows the user to introduce two separate salinity dependent sets of saturation, relative permeability and capillary pressure curves for the already existing phases. This option works such that it is possible to change the set of curves when switching the injection brine from high salinity to low salinity. In addition to these salinity dependent curves, an interpolation between the curves might also be added. The LSALTFNC keyword in the PROPS section opens up this opportunity. This keyword is set to input two weighting factors controlling and calculating the saturation end points, the water and oil relative permeabilities and the water-oil capillary pressure when the LOWSALT option is active. The interpolation is conducted by a set of equations (**Equation 5-2, 5-3** and **5-4**):

$$k_{rw} = F_1 k_{rw}^L + (1 - F_1)k_{rw}^H \qquad \text{(Eq. 5-2)}$$

$$k_{ro} = F_1 k_{ro}^L + (1 - F_1)k_{ro}^H \qquad \text{(Eq. 5-3)}$$

$$P_{cow} = F_2 P_{cow}^L + (1 - F_2)P_{cow}^H \qquad \text{(Eq. 5-4)}$$

Where F_1 and F_2 are functions of the salt concentration, k_{rw} is the water relative permeability and k_{ro} is the oil relative permeability, P_{cow} is oil-water capillary pressure. The subscripts H and L stand for high salinity and low salinity curves respectively.

The end point saturations are calculated by the following set of equations (**Equation 5-5, 5-6, 5-7** and **5-8**):

$$\boldsymbol{S_{wco} = F_1 S^L_{wco} + (1 - F_1) S^H_{wco}} \quad \textbf{(Eq. 5-5)}$$

$$\boldsymbol{S_{wcr} = F_1 S^L_{wcr} + (1 - F_1) S^H_{wcr}} \quad \textbf{(Eq. 5-6)}$$

$$\boldsymbol{S_{wmax} = F_1 S^L_{wmax} + (1 - F_1) S^H_{wmax}} \quad \textbf{(Eq. 5-7)}$$

$$\boldsymbol{S_{owcr} = F_1 S^L_{owcr} + (1 - F_1) S^H_{owcr}} \quad \textbf{(Eq. 5-8)}$$

Where F_1 and F_2 are functions of the salt concentration, S_{wco} is the connate water saturation, S_{wcr} is the critical water saturation, S_{wmax} is the maximum water saturation and S_{owcr} is the critical oil saturation in water. The subscripts H and L stand for high salinity and low salinity curves, respectively.

In the REGIONS section it is possible to define which of the profiles that belongs to either the high salinity or low salinity injection brine. This if done by adding the two keywords SATNUM and LWSLTNUM. They determine the high salinity saturation functions and low salinity table number to each grid block, respectively. In addition to what has already been described it is necessary to have input data for the low salinity water PVT. This is done in the PROPS section by adding the keyword PVTWSALT followed by two recorded tables. The first table includes reference pressure and salt concentration. The second input table contains salt concentration, water formation volume factor, water compressibility, water viscosity and water viscosibility. These parameters should vary slightly from the water containing no salt due to a difference in water composition.

To set the initial salt concentration for the connate water, the keywords SALTVD or SALT should be added in the SOLUTION section. SALTVD comprise a table of salt concentration versus depth. The keyword SALT, however, should be followed by one real number for every grid block specifying the initial salt concentration. For setting the wanted injection brine salinity, input in the SCHEDULE section is necessary. The keyword WSALT after the name of the injection wells sets the salt concentration in the brines for the injection wells (Schlumberger, 2011).

6. Synthetic Model

A simple 10x10x3 model was decided to be applied to test the options regarding low salinity waterflooding in ECLIPSE 100. The purpose of this was to get to know the options in ECLIPSE 100 and evaluate the potential of low salinity waterflooding as a tertiary and a secondary EOR mechanism in a synthetic reservoir model.

The low salinity options in ECLIPSE are very dependent on relative permeability and saturation profiles, and hence strongly dependent on wettability. To illustrate this, different wettability profiles were generated by use of the Corey Model. The Corey Model is a simple model used to generate wanted saturation and relative permeability profiles by use of only a few equations and empirical parameters. **Equation 6-1, 6-2, 6-3, 6-4** and **6-5** are the base case for the Corey Model for a system with two phases, oil and water (Behrenbruch and Goda, 2006).

$$k_{rw} = S_*^{N_w} E_w \quad \text{(Eq. 6-1)}$$

$$k_{ro} = (1 - S_*)^{N_o} E_o \quad \text{(Eq. 6-2)}$$

$$E_w = k_{rw}(S_{or}) \quad \text{(Eq. 6-3)}$$

$$E_o = k_{ro}(S_{wi}) \quad \text{(Eq. 6-4)}$$

$$S_* = \frac{S_w - S_{wi}}{1 - S_{wi} - S_{or}} \quad \text{(Eq. 6-5)}$$

Where k_{rw} and k_{ro} are relative permeability of water and oil respectively, S_* is normalized water saturation, E_w, E_o, N_w and N_o are empirical parameters.

A number of sensitivity analyses were simulated and tested. This included not only the wettability profiles, but also the effect of injection brine salinity on tertiary and secondary imbibition, injection time and amount of injected fluids.

6. 1 Initialization of the Synthetic Model

The reservoir could initially and after low salinity waterflooding be considered as water-, neutral- or oil-wet. By use of the Corey Model, three different saturation and relative permeability profiles were generated to describe the three different wettabilities. As earlier mentioned it is possible to have two inputs for relative permeability and saturation profiles when the LOWSALT option is included in ECLIPSE 100. One of the profiles is to be used during conventional waterflooding and one to be used during low salinity waterflooding

(LSW). During most of the sensitivity analyses, the reservoir was initially considered slightly oil-wet and then reconsidered to be slightly water-wet after low salinity waterflooding. This was because this has been suggested to have the largest effect of low salinity waterflooding (Vledder et al., 2010). The three relative permeability and saturation profiles determined by the Corey Model are presented in **Table 6-1** and **Figure 6-1**. The main differences are seen in residual oil saturation (S_{or}).

Table 6-1: Corey parameters for the synthetic model.

	Water-wet	Mixed-wet	Oil-wet
Swi	0.2	0.2	0.2
Sor	0.1	0.2	0.3
Ew=Krw(Sor)	0.6	0.8	0.8
Eo=Kro(Swi)	0.8	0.8	0.5
Nw	3	2	3
No	2	2	3

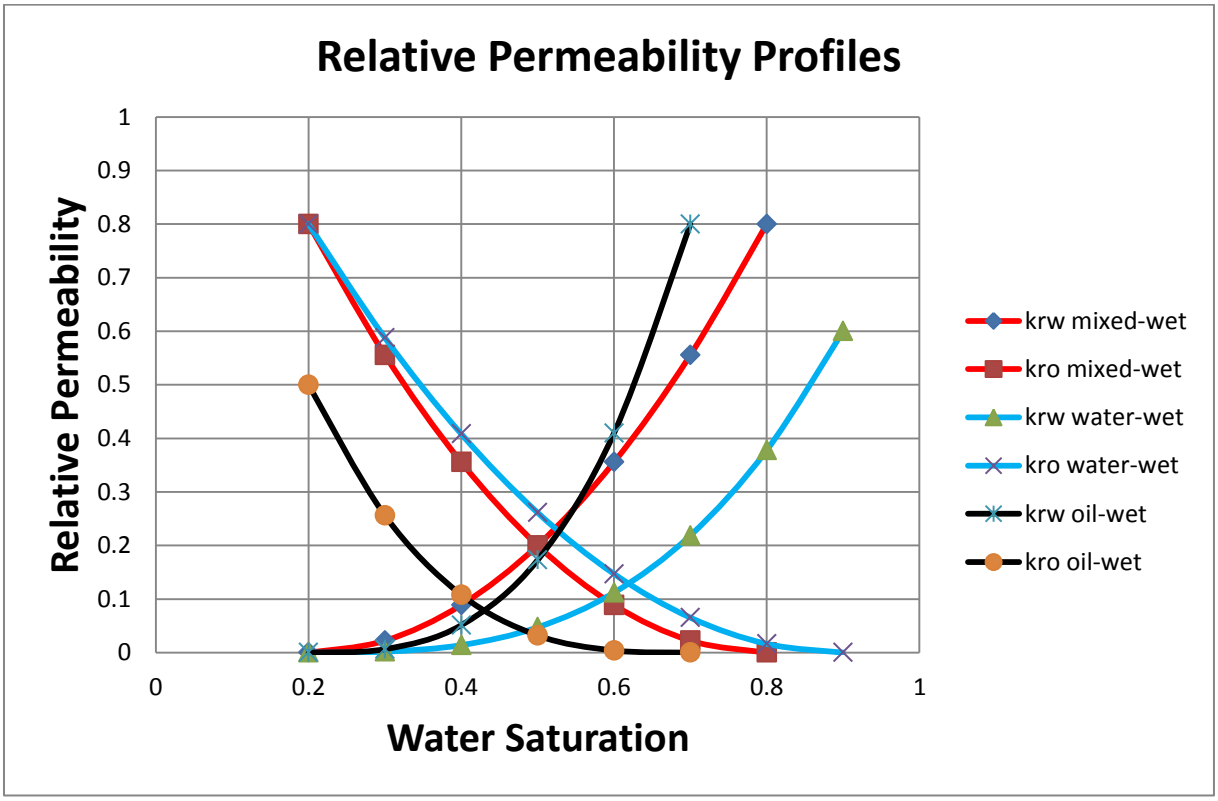

Figure 6-1: Oil-, mixed- and water-wet relative permeability profiles for the synthetic model.

The different wettability profiles were mainly generated to yield a difference in residual oil saturation during waterflooding, because the oil recovery is highly dependent on this variable. The slightly oil-wet case has a high S_{or} and is predicted to yield the lowest ultimate recovery. An oil-wet reservoir is characterized by low oil relative permeability, high water relative permeability and high S_{or} and has proven to have a low potential for conventional waterflooding. Crossover point for an oil-wet reservoir, where the water and oil relative permeabilities are equal, should as a rule of thumb occur below water saturation of 50 % PV (Anderson, 1987). The mixed-wet case has an intermediate S_{or} and equal values of water and oil relative permeability. A water-wet reservoir is characterized by low S_{or}, low water relative permeability and high oil relative permeability. The water-wet case applied in this model has, however, a relatively high water relative permeability at maximum water saturation. This is on the other side not thought to influence the recovery as much as the low residual oil saturation. Crossover point for a water-wet reservoir, where the water and oil relative permeabilities are equal, should as a rule of thumb occur above water saturation of 50 % PV (Anderson, 1987). This case is proposed to give the highest ultimate recovery. There is no clear relationship between the different wettability profiles, and they are created to test the low salinity options in ECLIPSE 100 and to see if there is a potential for LSW as an EOR mechanism. The high reduction in S_{or} is applied to illustrate the high dependency of this variable during waterflooding. The oil-wet case is, however, of most interest when applied initially because the field-case from the Frøy field has indicated an initial oil-wet reservoir behavior (Det Norske Oljeselskap, 2008). This will be discussed in **Chapter 7**. When referring to oil-, mixed- and water-wet profiles in the next sections, it is referred to the profiles generated and described above.

The reservoir model was a two phase model, containing only oil and water for simplifications. Capillary pressures were neglected due to lack of data. The initial connate water salinity was set to 35 kg/m^3 TDS, approximately the same salinity as regular seawater. From the literature, the effect of low salinity waterflooding was only observed after a significant decrease in salinity, below 5000 ppm (McGuire, 2005). Therefore the effect of low salinity waterflooding was decided to start after injection of brines with salinities below 5 kg/m^3 TDS, which is equal to 5000 ppm. This was set in the LSALTFNC. In the LSALTFNC it could also be decided how much of either the high salinity or low salinity saturation and

relative permeability profiles that were used during injection of brines with different salinities. The initial LSALTFNC is found in **Table 6-2** below.

Table 6-2: Initial LSALTFNC for the synthetic model.

Salt Concentration	F1	F2
[kg/m3]		
0	1	1
1	0.8	1
4	0.2	1
5	0	0
35	0	0
45	0	0

Two wells, one injector and one producer, were added to the model and placed diagonally with respect to each other. They were set to be controlled by reservoir fluid volumes, RESV, with rates of 200 m^3/day. The simulation time was set to 80 time steps of 30 days each or 2400 days, approximately 6.6 years after the start in 1990. Starting date is just illustrative. Initial reservoir properties are shown in **Table 6-3** below.

Table 6-3: Reservoir properties for the synthetic model.

Layer	1	2	3	Units
Number of blocks	100	100	100	
Depth	0.58	0.84	0.47	[m]
Width (X & Y)	500	500	500	[m]
PermX	4500	3300	2400	[mD]
PermY	4500	3300	2400	[mD]
PermZ	1050	1800	500	[mD]
Porosity	0.25	0.25	0.25	
Swi	0.2	0.2	0.2	

Initial salt concentration in the reservoir is illustrated in **Figure 6-2.** It was set to be 35 kg/m^3 TDS or approximately equal to normal seawater. The well placements are also illustrated. INJ is the water injector, and OP is the oil producer.

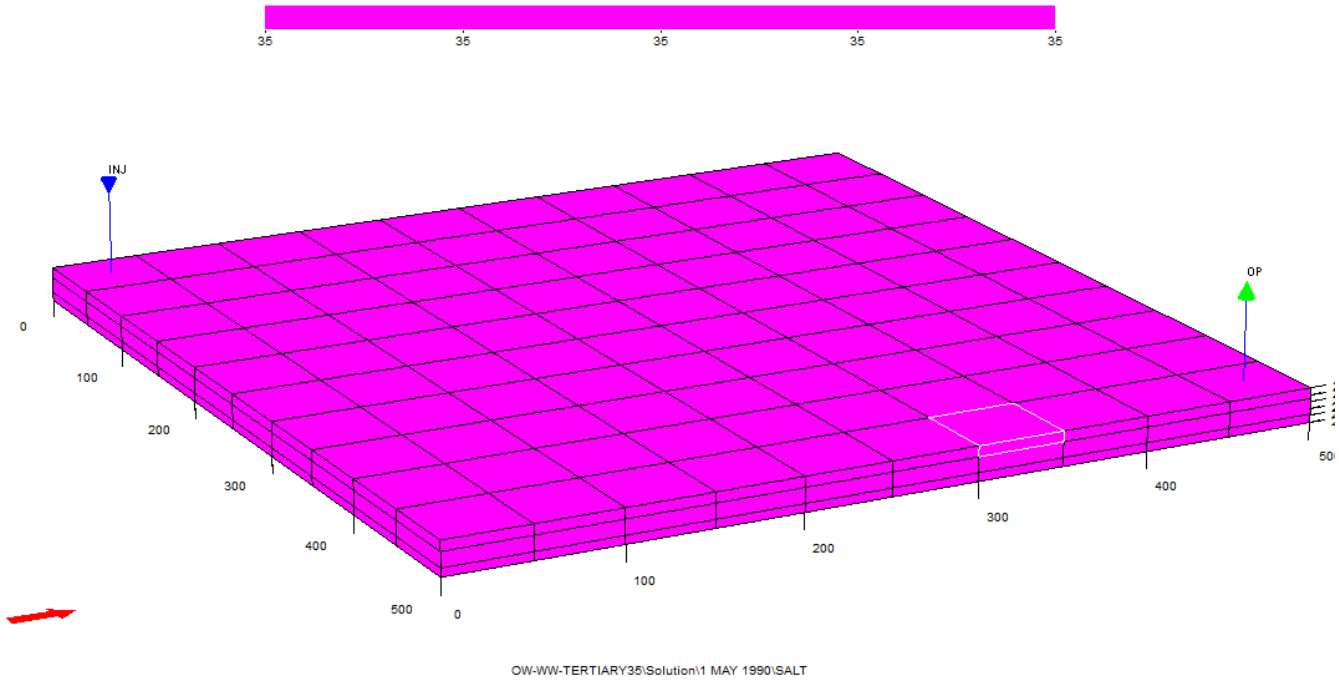

Figure 6-2: Initial salt concentration and well placements in the synthetic model.

6.2 Effect of Brine Salinity; Secondary Imbibition

To see the effect of low salinity waterflooding on secondary imbibition, brines with different salinities were injected. Injection of brine with 35 kg/m^3 TDS was initially carried out to set a base case recovery, and then flooding of brines with 10, 5, 4, 3, 2, 1 and 0 kg/m^3 TDS were conducted. The wettability was set to initially be oil-wet, and the more water-wet set of saturation and relative permeability profiles were applied during low salinity waterflooding (LSW). The results are presented graphically in **Figure 6-3** below, where the field oil efficiency (FOE) or oil recoveries are found. Ultimate recoveries can be seen in **Figure 6-4**.

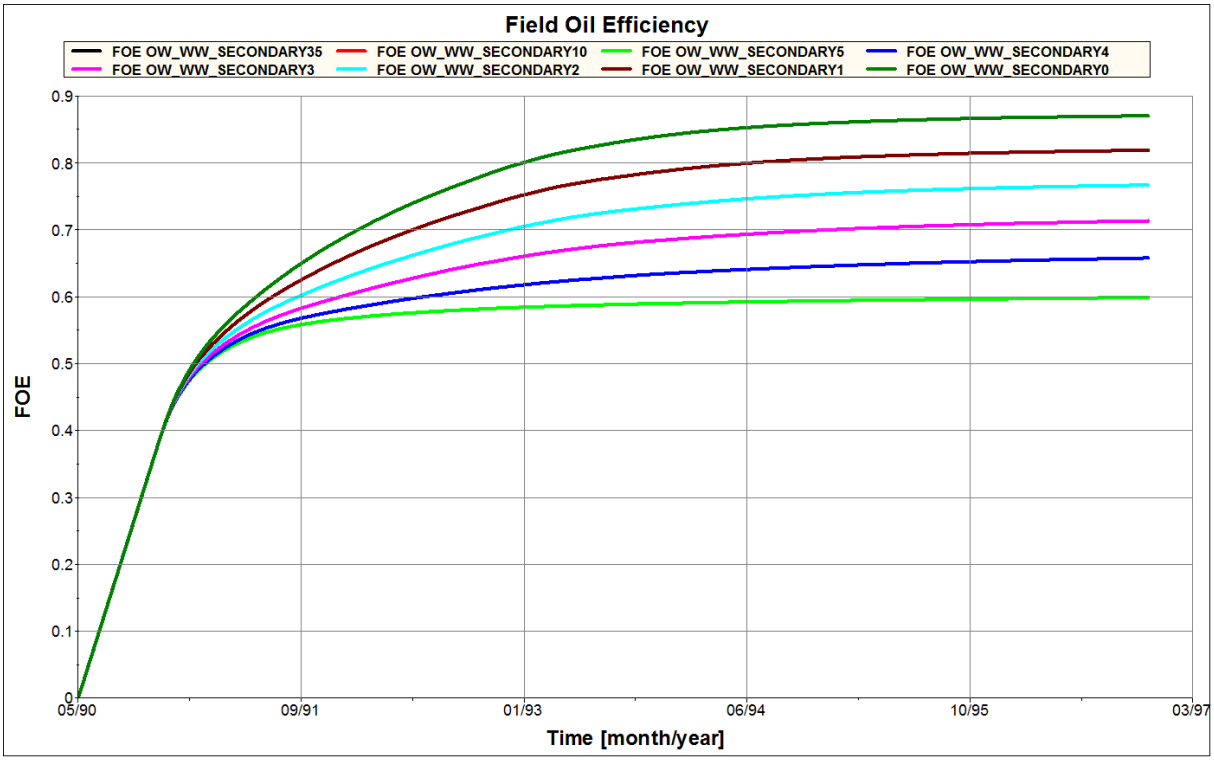

Figure 6-3: Oil recovery for secondary LSW with injection brine salinities of 35, 10, 5, 4, 3, 2, 1 and 0 kg/m^3 TDS.

Brine Salinity	Oil Recovery
[kg/m3]	[%] OIIP
35	59.89
10	59.89
5	59.89
4	65.78
3	71.33
2	76.67
1	81.88
0	87.02

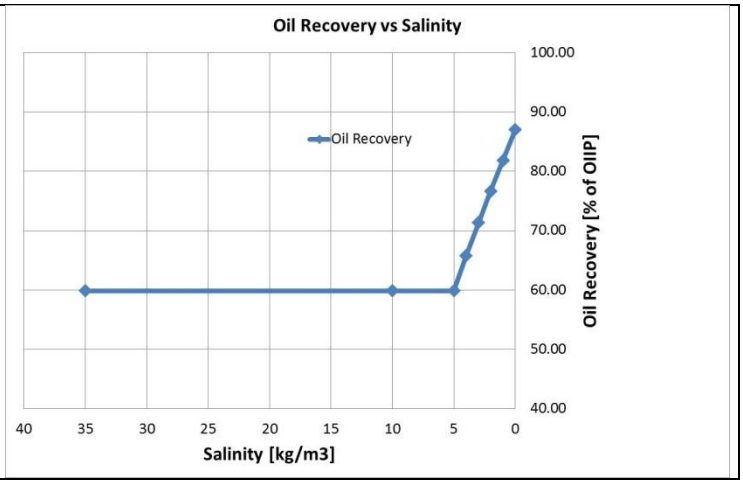

Figure 6-4: Ultimate oil recovery as a function of injection brine salinity during secondary LSW.

The results matched the prediction and the earlier observations described in the literature. It clearly showed an increase in oil recovery with a decrease in salinity of the injected brines. That no incremental recovery was seen for injection of brines with 10 and 5 kg/m^3 TDS was expected from the model, because the low salinity effects were set to start at salinities below 5 kg/m^3 TDS.

To investigate the low saline water behaviour, the salt concentration in the production well (WSPC) and the oil prodcution rate (FOPR) for the 35 kg/m^3 and 1 kg/m^3 TDS cases are found in **Figure 6-5**. The produced salt concentration is equal the first 7 month before breakthrough of the low saline water appears. Almost immediately after the beakthrough, the oil is recovered more efficient for the case where 1 kg/m^3 TDS is injected compared to case where seawater is injected. One of the reasons for the higher oil recovery when low salinity water is injected instead of seawater in this model is indicated in **Figure 6-6.** The water cut (FWCT) is significantly lower for the low salinity waterflooding than the conventional waterflooding. This indicates a more effiencient waterflooding, and that the ratio of water to total liquid produced is lower for the low salinity waterflooding cases.

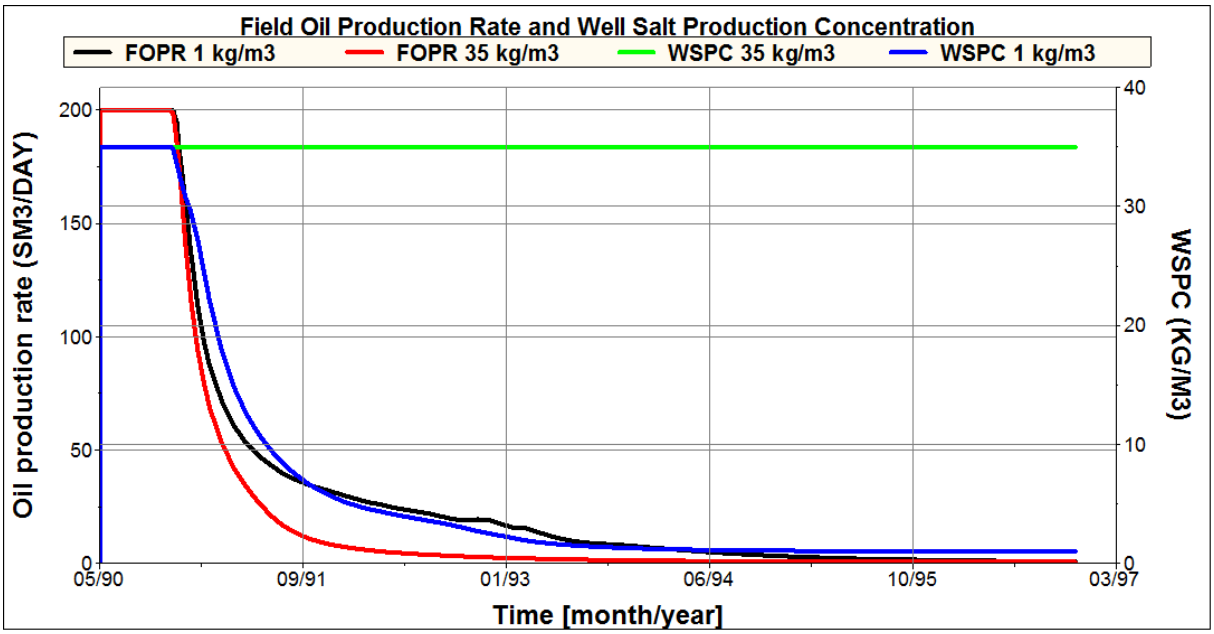

Figure 6-5: Oil production and well salt production concentration for secondary LSW with injection brine salinities of 35 and 1 kg/m^3 TDS.

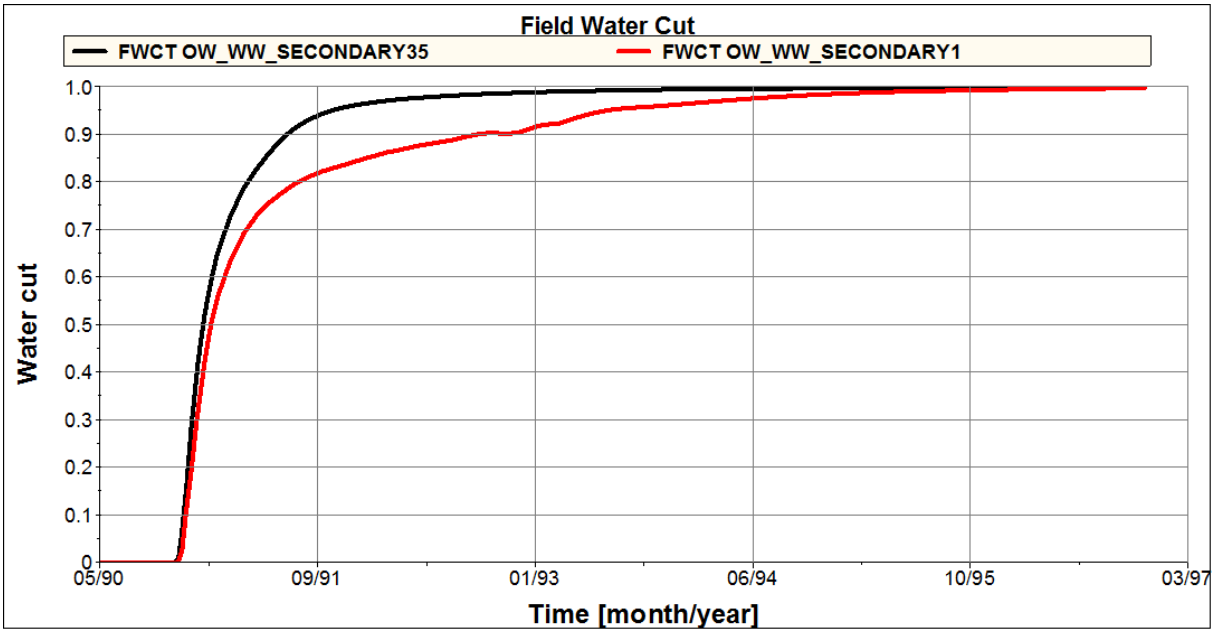

Figure 6-6: Water cut for secondary LSW with injection brine salinities of 35 and 1 kg/m^3 TDS.

6.3 Effect of Brine Salinity; Tertiary Imbibition

The injection of low salinity brines were started slightly after the oil production started to flatten out, after 15 time steps of 30 days each, or approximately after 1.2 years. The tertiary injection continued throughout the simulation period. Prior to the tertiary flooding, flooding of brine with 35 kg/m^3 TDS or equal to the initial connate water salinity was conducted. The tertiary recovery was done by flooding of brines with salinities of 10, 5, 4, 3, 2, 1 and 0 kg/m^3 TDS. Wettabilities ranged from oil- to water-wet. Tertiary imbibition was also applied to compare the incremental recovery obtained from secondary imbibition. The results from the injection of different brine salinities are presented in **Figure 6-7**, and the ultimate recoveries can be found in **Figure 6-8.** Comparison of secondary and tertiary flooding is shown in **Figure 6-9**.

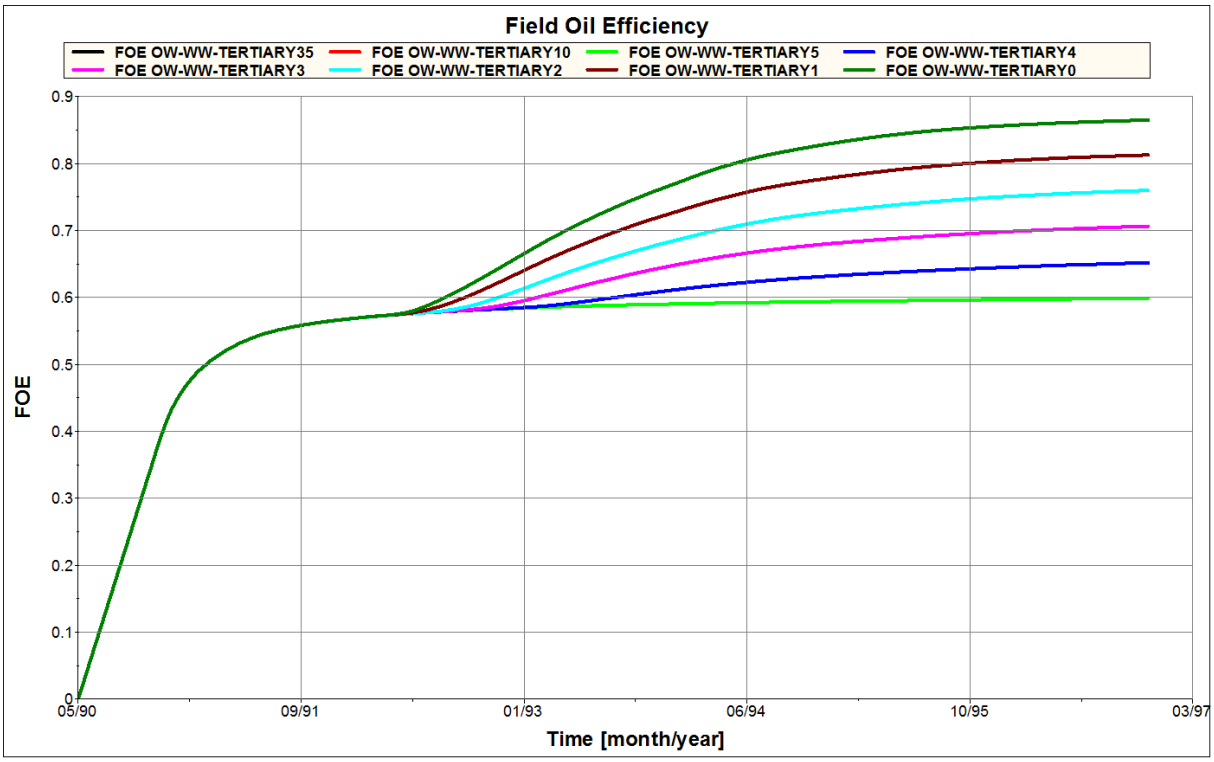

Figure 6-7: Oil recovery for tertiary LSW with injection brine salinities of 35, 10, 5, 4, 3, 2, 1 and 0 kg/m^3 TDS.

Brine Salinity	Oil Recovery
[kg/m3]	[%] OIIP
35	59.89
10	59.89
5	59.89
4	65.16
3	70.63
2	75.97
1	81.26
0	86.48

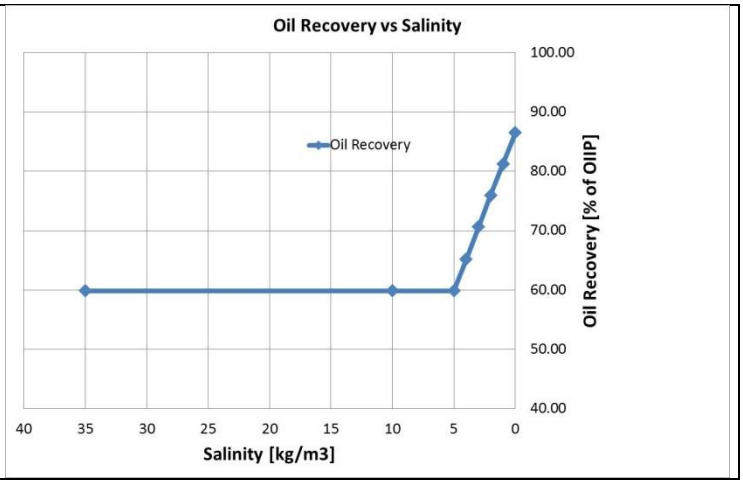

Figure 6-8: Ultimate oil recovery as a function of injection brine salinity during tertiary LSW.

As predicted from the model, no incremental recovery was seen for injection of brines with salinities above 5 kg/m^3 TDS. This was again because the low salinity effect was set to start at salinities below this critical value. Regarding the oil recovery, an increase in recovery was seen in conjunction with a decrease in salinity. From the literature, this was as expected. It is to note that both the rate of recovery and ultimate recovery increased with a decrease in salinity of the injected brines.

Comparison of secondary and tertiary recovery showed only a minor difference in ultimate recovery. The secondary recovery mechanism produced only approximately 0.6 % more oil than the tertiary recovery mechanism for injection if brines with salinities of 1 kg/m^3 TDS. This is probably because the same sets of relative permeability and saturation profiles were applied to all grid cells, and that the same reductions in residual oil saturation appeared after the LSW. The rate of recovery was naturally higher for the secondary case than for the tertiary case, mainly due to an earlier injection of low salinity brines. Oil recoveries are found in **Figure 6-9** below for tertiary and secondary flooding of 1 kg/m^3 TDS.

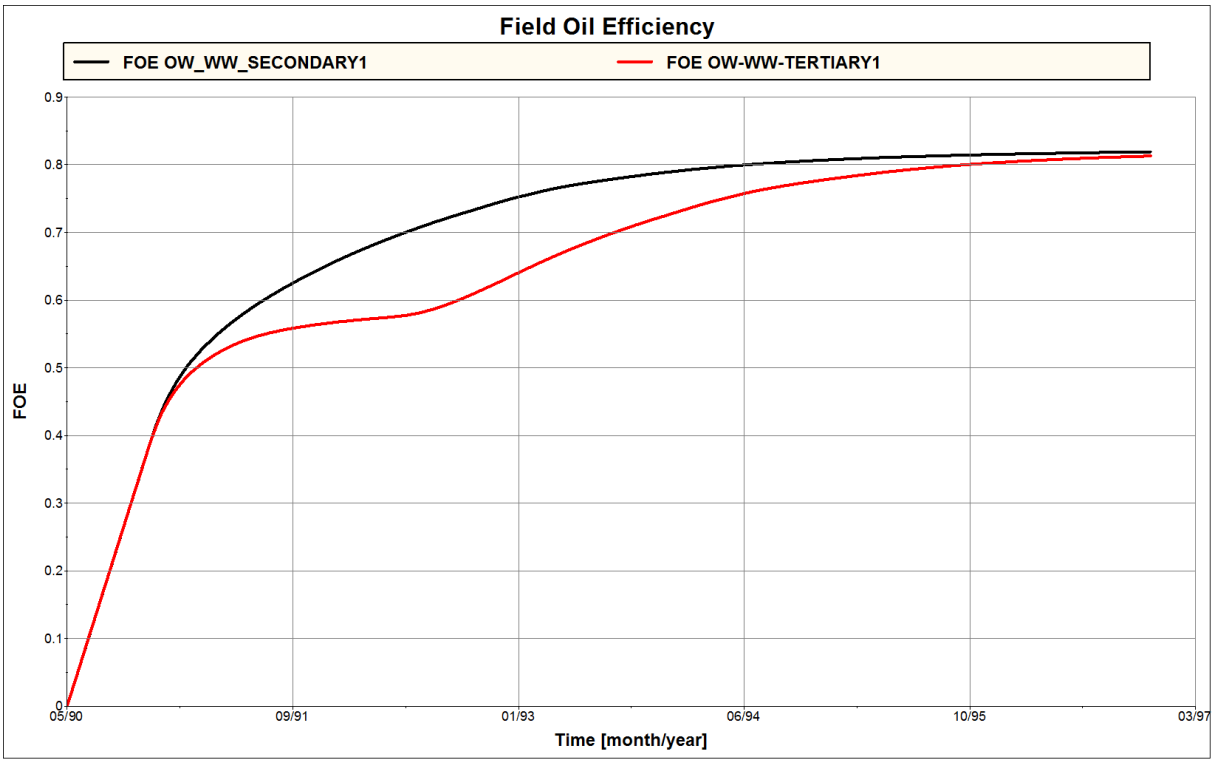

Figure 6-9: Oil recovery comparisons between secondary and tertiary LSW for injection brine salinity of 1 kg/m^3 TDS.

If the simulation period had been shorter, the difference in tertiary and secondary recovery modes might have been bigger. One suggested reason for the small difference observed is because both modes have been simulated long enough for the effect of low salinity waterflooding to be maximized. Different behavior in the field water cut and oil production did, however, occur. This is illustrated in **Figure 6-10**, where both water cut and oil production rate for the different recovery modes are found. It turned out that even due to the different production rate and water cut behavior, the difference on oil recovery was almost negligible.

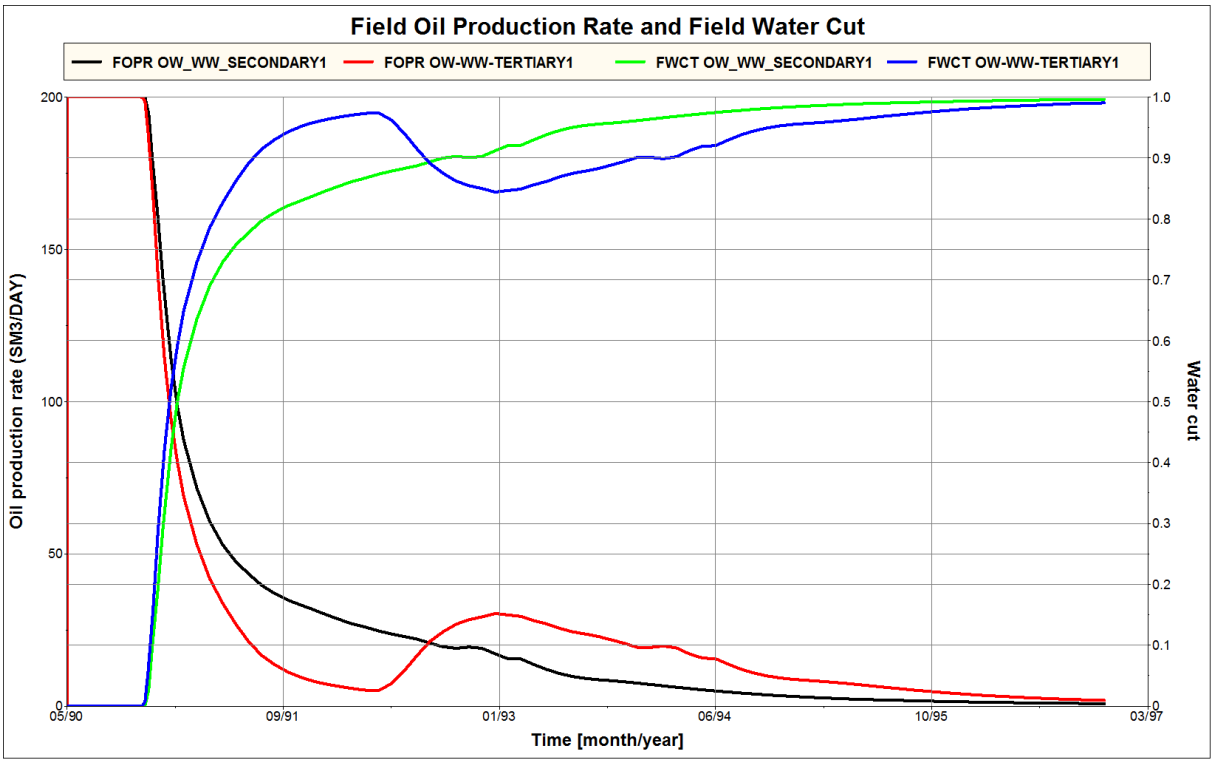

Figure 6-10: Oil production rate and water cut comparisons between secondary and tertiary LSW for injection brine salinity of 1 kg/m^3 TDS.

6.4 Effect of Injection Time during Tertiary Recovery

To optimize tertiary imbibition, wateflooding should be initiated when the reservoir pressure and the oil production start to decline. The purpose of this is to give the reservoir pressure support and to stop or at least reduce the reduction in oil production and extend the plateau rate. In this sensitivity analyses, injection of brines with 1 kg/m^3 TDS were implemented at different times. The base case is from the tertiary recovery described in the section above. One injection time was set prior to the base case and the other to be conducted later in the simulation period. It is to note that all the injection times are after the oil production has started to decline and stabilize. The injection times were after 10, 15 (base case), 25, 35 and 45 time steps of 30 days each. Wettabilities ranged from oil- to water-wet as the other sensitivity analyses. The results are presented in **Figure 6-11**.

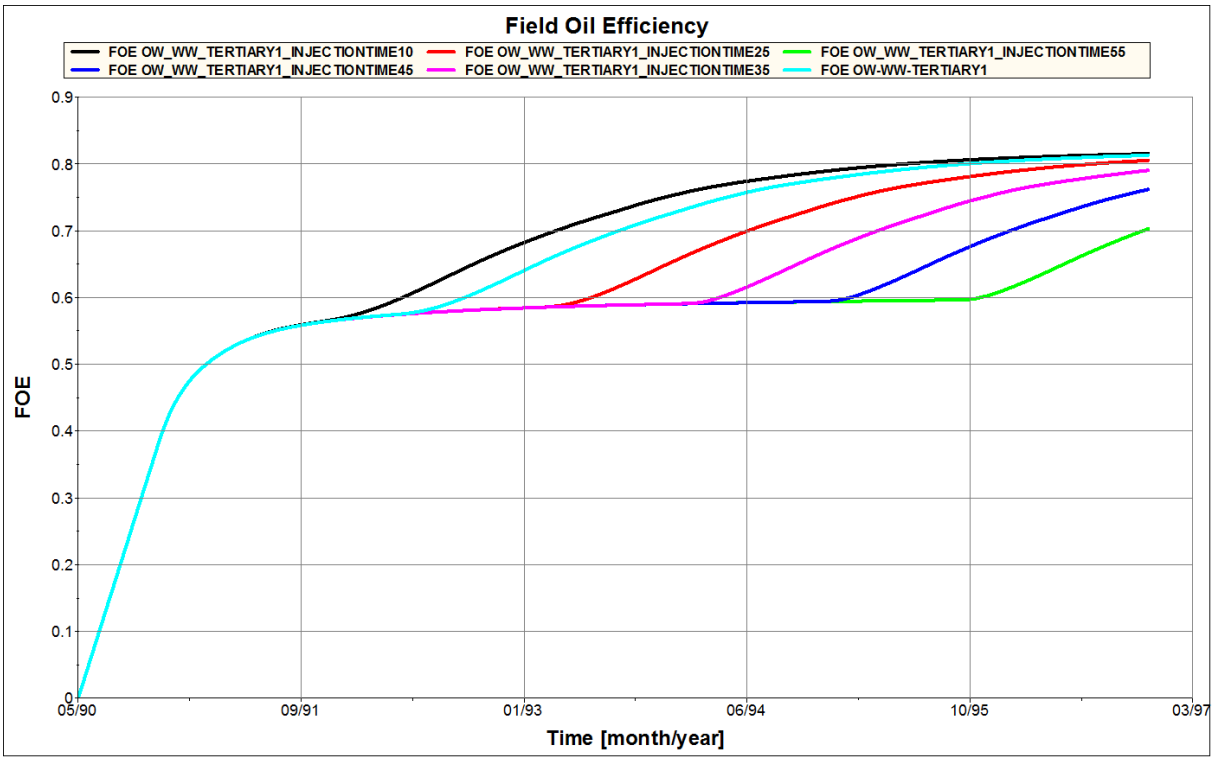

Figure 6-11: Oil recovery for different injection times during tertiary LSW with injection brine salinity of 1 kg/m^3 TDS.

An increase in oil recovery was seen in conjunction with an earlier injection time. This was as expected because an early injection time means injection of more low salinity brines and this should increase the effectiveness of the low salinity waterflooding. The difference in ultimate recovery was however not very large compared to the rate of recovery. It is also to note that the ultimate recoveries for the latest injection times have not been reached. From the interpretations, they should probably be a little less than for the earlier injection times.

6.5 Effect of Wettability on Tertiary Imbibition

As described earlier, the low salinity option in ECLIPSE 100 allows the user to have two sets of input of relative permeability and saturation profiles. Initially the reservoir could be considered as oil-, neutral or water-wet and after injection of low salinity brines reconsidered as one of them. From the Corey Model, relative permeability and saturation profiles were generated to give the three different wettabilities as discussed in **Section 6.1**. In this sensitivity analysis, combinations of the different wettabilites have been simulated and tested for tertiary injection of brines with 1 kg/m^3 TDS. The results are presented in **Figure 6-12** and **Table 6-4** below.

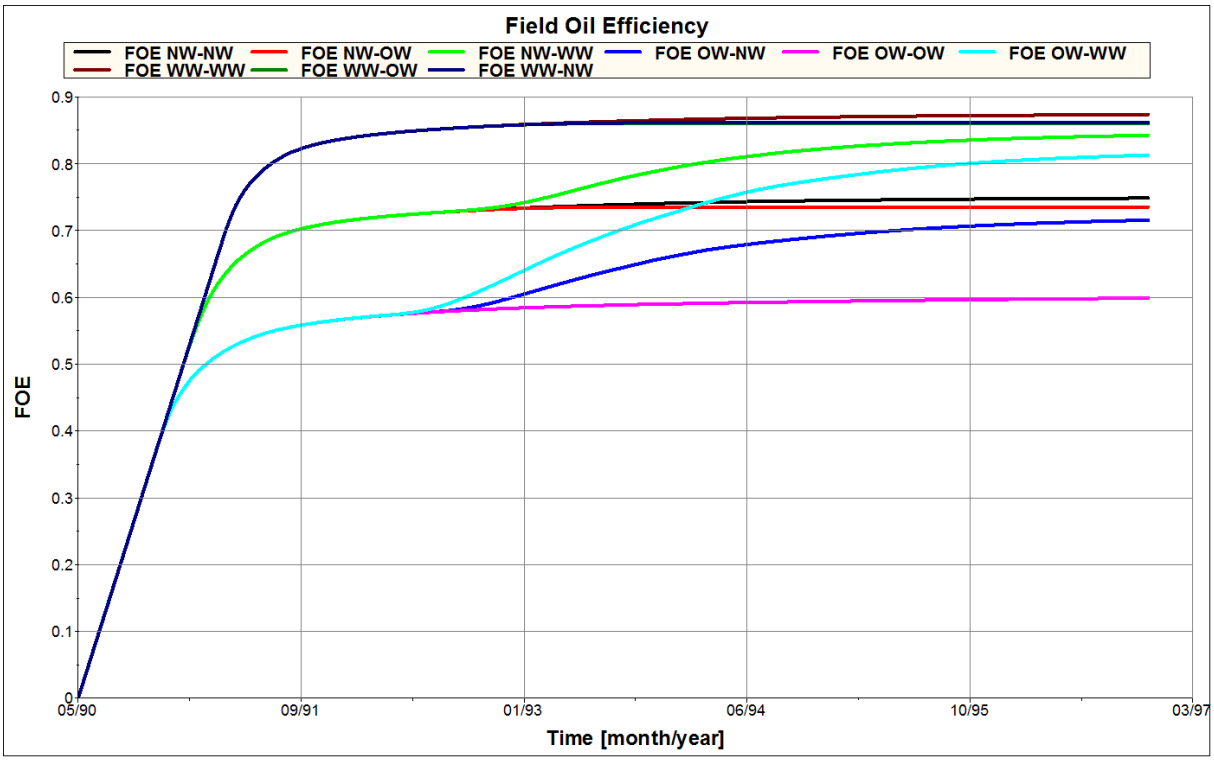

Figure 6-12: Oil recovery for different wettability alterations during tertiary LSW with injection brine salinity of 1 kg/m^3. TDS.

Table 6-4: Oil recovery for different wettability alteration during tertiary LSW with injection brine salinity of 1 kg/m^3 TDS.

Wettability Alteration	Recovery % of OIIP	Incremental Recovery
OW-OW	59.9%	0.0%
OW-NW	71.5%	11.6%
OW-WW	81.3%	21.4%
NW-OW	73.5%	-1.3%
NW-NW	74.8%	0.0%
NW-WW	84.2%	9.4%
WW-OW	86.0%	-1.3%
WW-NW	86.1%	-1.2%
WW-WW	87.3%	0.0%

Where OW, NW and WW are oil-wet, neutral-wet and water-wet relative permeability profiles, respectively.

The highest recoveries were seen from the cases were the reservoir initially was considered water-wet, and the lowest recoveries were seen from the cases were the reservoir initially was considered oil-wet. Mixed-wet recoveries were between the two extremes. For the cases where the reservoir initially was oil-wet, the effect of low salinity waterflooding was, however, the biggest. It resulted in an incremental recovery of up to 21.4 % of OIIP. This is most likely because of the large reduction in S_{or} when changing the relative permeability and saturation profiles from oil-wet to water- or mixed-wet. When the reservoir initially was considered water-wet, no effects were seen. When changing the wettability from water-wet to one of the other profiles, the recovery actually decreased. This is mainly because no reduction in S_{or} happened after changing from conventional to low salinity waterflooding, meaning that the initial properties were close to optimum for conventional waterflooding. The S_{or} actually increased when the wettability was altered from water-wet to mixed- or oil-wet.

6.6 Effect of Slug Sizes

While evaluating EOR, the amount of fluids injected should be carefully considered. This is the case especially when the economically aspects are to be evaluated. If this is not properly done, the extra amount of cash earned from the incremental oil recovered might be less than the costs of the external fluids. For a worst case scenario, this might therefore turn out not to be feasible. In this sensitivity analyses, a short evaluation of the recovery as an effect of different volumes of injected low salinity brines have been conducted. The different cases includes injection of low salinity brines with a salinity of 1 kg/m^3 TDS for 1, 5, 10, 15, 20 and 30 time steps of 30 days each. Both before and after injection of low salinity brines, brines with a salinity of 35 kg/m^3 TDS were injected. Base case recovery was set for injection of 65 time steps of 30 days each (tertiary injection as described earlier), and the wettabilities ranged from oil-wet to water-wet. The results are presented in **Figure 6-13** below.

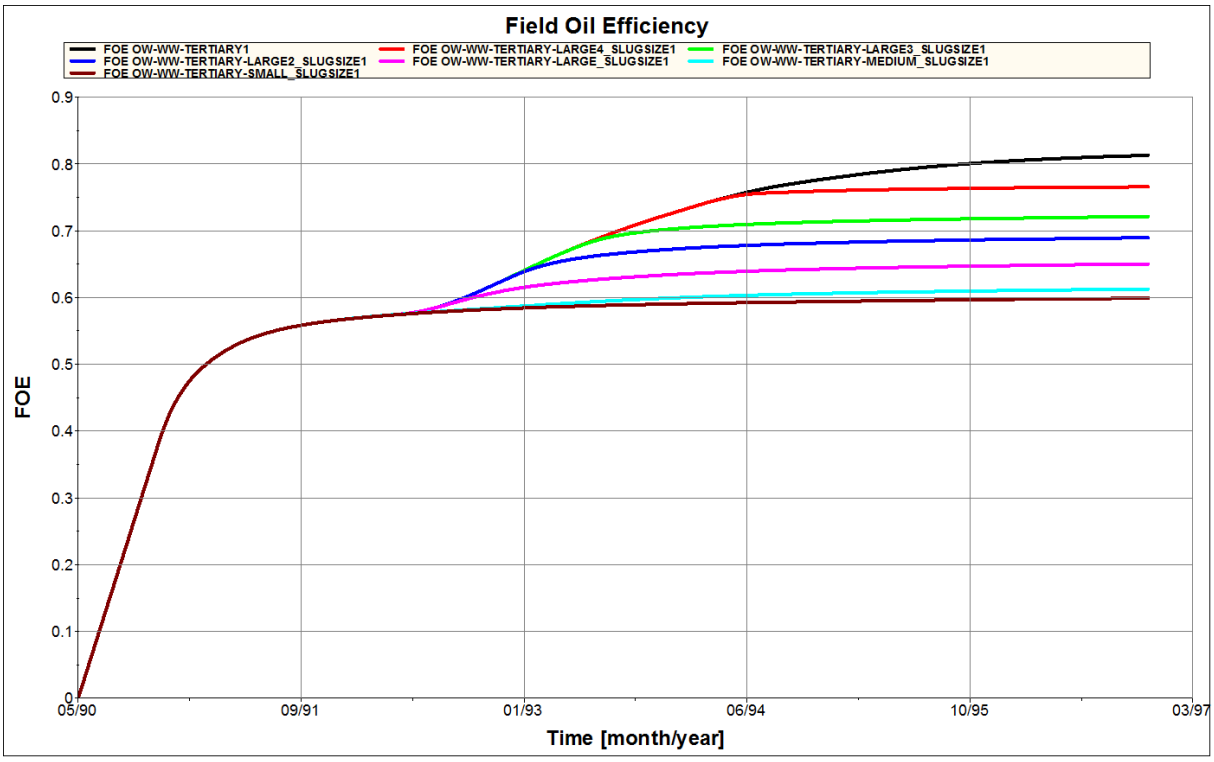

Figure 6-13: Oil recovery for different slug sizes during LSW with injection brine salinity of 1 kg/m^3 TDS.

The effect of different slug sizes was as predicted, showing an increase in recovery with an increase in slug size. It seems, however, that there is no linear relationship between the amount of fluids injected and recovery. It's easier to illustrate this by use of volume calculations. The amount of fluids injected and total recovery is seen in **Table 6-5**.

Table 6-5: Oil recovery versus PV injected for different slug sizes during tertiary LSW with injection brine salinity of 1 kg/m^3 TDS.

Total PV	**118125**	**[Rm3]**				
Injection time	Time	Total time	Rate	Inj V	Inj PV	Total recovery
[time steps]	[day]	[day]	[Rm3/day]	[Rm3]		[%]
1	30	30	200	6000	0.05	59.9
5	30	150	200	30000	0.25	61.2
10	30	300	200	60000	0.51	65.0
15	30	450	200	90000	0.76	68.9
20	30	600	200	120000	1.02	72.1
30	30	900	200	180000	1.52	76.5
65	30	1950	200	390000	3.30	81.3

The recovery increased significantly when the injected brine volume was low, but as the volume increased the amount of extra oil produced decreased. When the injected brine volume increased from 6 000 to 180 000 Rm^3 the incremental recovery was approximately 16.6 %. For the increase in injected volumes from 180 000 to 390 000 Rm^3, the incremental recovery was just around 4.8 %. This clearly shows how important it is to evaluate the amount of fluids that should be injected during EOR processes. For economically evaluations, this should naturally be taken into consideration.

To illustrate the effectiveness of the different slug sizes, live 2D screen shots of the salt distribution at different time steps can be used. In **Figure 6-14** and **Figure 6-15,** the salt distributions after injection of low salinity brines for the largest and the smallest slug sizes can be seen. The screen shots are taken from 24 August 1991, 21 September 1991, 23 October 1991 and 22 November 1991. For the smallest slug size, the salt concentration does not decrease significantly. For any incremental oil recovery to be observed, the salt concentration needs to be below 5 kg/m^3 in the grid cells. As this rarely happens, the effect of low salinity waterflooding will not be very large. For the largest slug size, however, a

severe drop in salt concentration appears, such that more of the optimum relative permeability and saturation profiles are being applied.

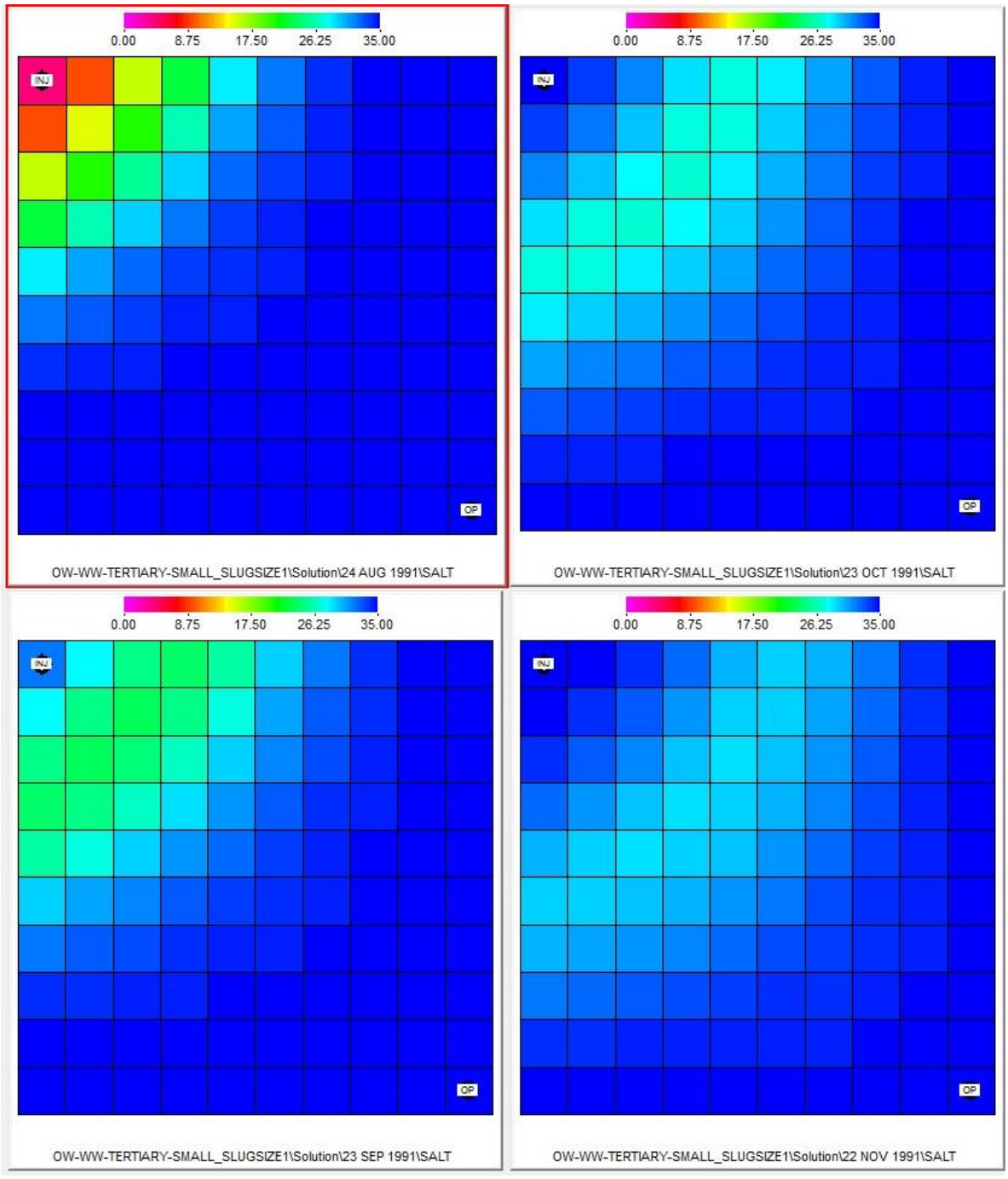

Figure 6-14: Salt distribution for small slug size with injection brine salinity of 1 kg/m^3 TDS.

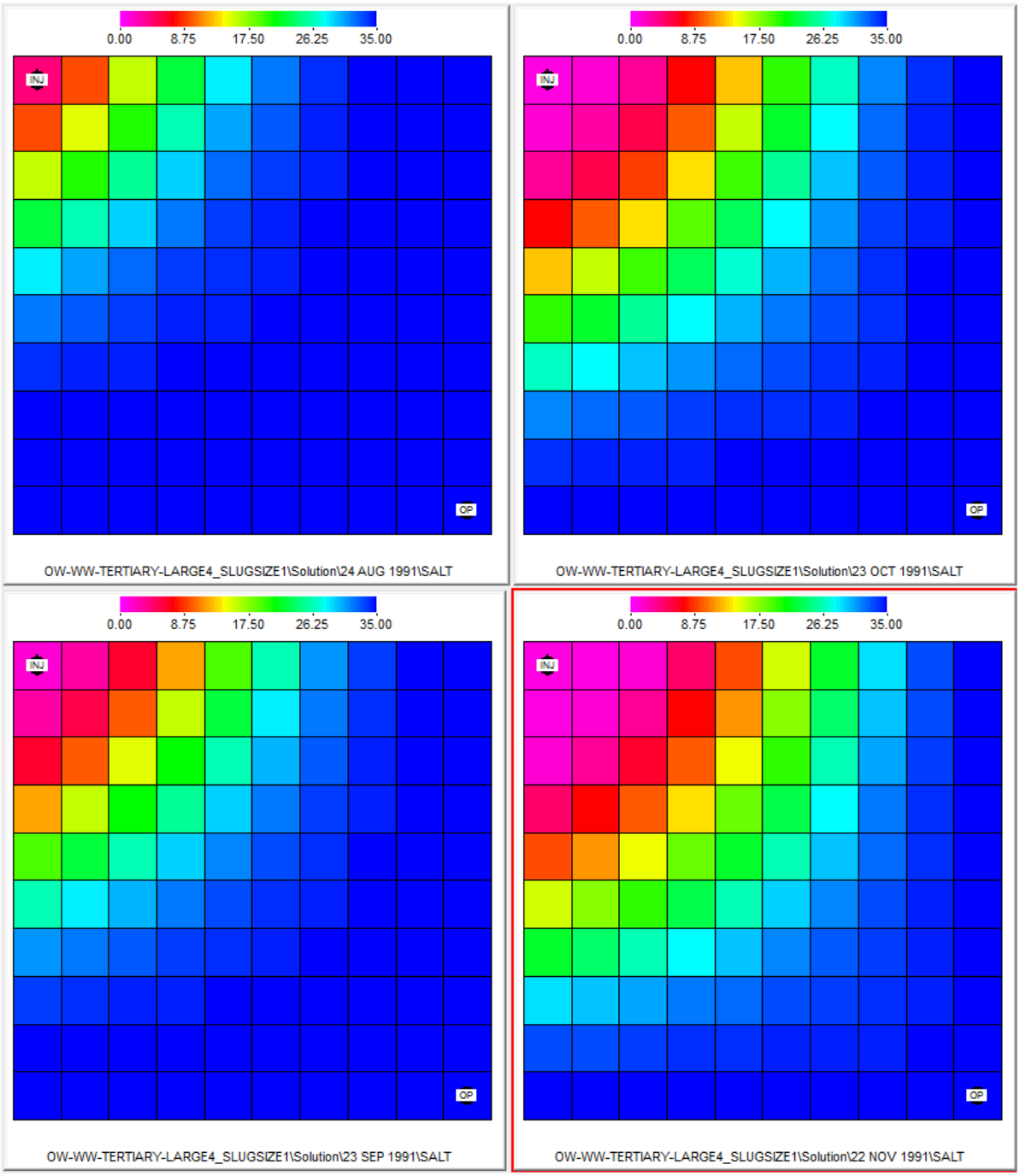

Figure 6-15: Salt distribution for large slug size with injection brine salinity of 1 kg/m^3 TDS.

6.7 Effect of Endpoint Saturations and Relative Permeability Interpolation

The LSALTFNC determines how much of the low salinity and high salinity relative permeability and saturation profiles that should be used for different injected brine salinities. The base case was discussed in **Section 6.1**. Two other LSALTFNC were made. One function were generated such that only data from the low salinity profiles were used for brine salinities below 5 kg/m^3 TDS, and only data from the high salinity profiles was used for salinities above the same value. The second case used less data from the low salinity profiles for the different injection brine salinities than the base case. The cases can be seen in **Table 6-6** below, and the results are plotted in **Figure 6-16**. Wettabilities again ranged from oil- to water-wet, and the injection brine salinity was 1 kg/m^3 for a secondary recovery.

Table 6-6: Different LSALTFNC for the synthetic model.

Salt Concentration [kg/m3]	F1	F2
0	1	1
1	1	1
4	1	1
5	0	0
35	0	0
45	0	0

Salt Concentration [kg/m3]	F1	F2
0	1	1
1	0.6	1
4	0.4	1
5	0	0
35	0	0
45	0	0

.

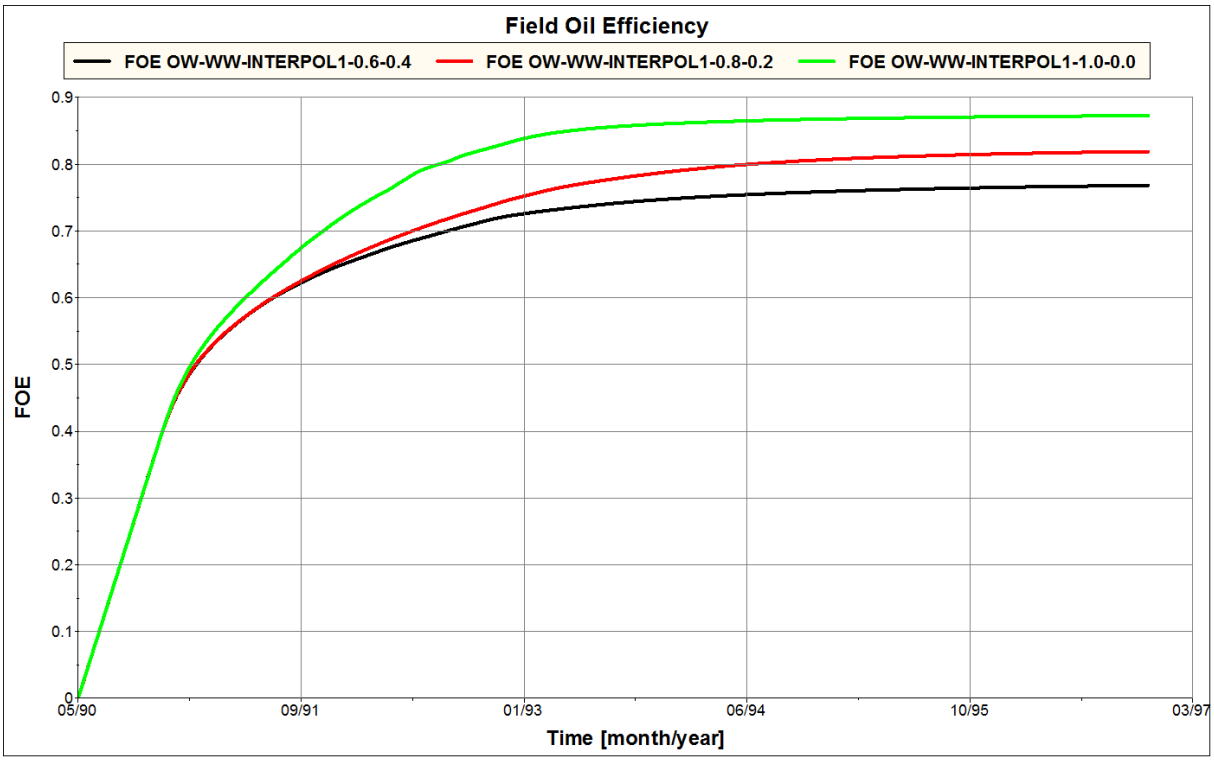

Figure 6-16: Oil recovery for different interpolations during secondary LSW with injection brine salinity of 1 kg/m^3 TDS.

The highest recovery was achieved for the case where only data from the low salinity profiles were used for brine salinities below 5 kg/m^3 TDS, and only data from the high salinity profiles for salinities above the same value. The recovery was observed to decrease with a reduction in the amount of the low salinity profiles that were used. This was expected, because the case that gave the highest recovery maximizes the effect of low salinity waterflooding in this model for all grid cells with salinities below 5 kg/m^3 TDS. The effect is highest when only the most optimum profile for waterflooding is used. Both the two other cases also have a large effect, but not to the same degree.

6.8 Summary of the Results Obtained from the Synthetic Model

The model worked well, and most of the results were as expected. Due to the initialization of the model, most of the results were also easy to predict. The effect of the low salinity waterflooding was very high for some of the cases simulated. This observation was mainly due to a large difference in residual oil saturation for the different saturation and relative permeability profiles. When shifting from oil-wet to water-wet, the residual oil saturation was set to decrease with 20 % of PV, from 30 to 10 %. During the tertiary injection of brine with a salinity of 0 kg/m^3 TDS, an increase in recovery of around 27 % was observed when the wettability was altered from oil- to water-wet.

Approximately no difference was observed between tertiary and secondary recovery modes. As already discussed, the proposed reason for this is that the same properties are given to all grid cells after initiation of low salinity waterflooding (LSW). The long simulation period also influenced the minor difference observed, because both cases were simulated long enough to reach maximum effects of the low salinity waterflooding.

This model was very homogenous, and this made the predictions even easier. The only heterogeneity in this model was seen in the layer depth. No transmissibility or permeability barriers were included such as faults or impermeable zones. This clearly optimizes the effect of waterflooding, because the injected fluids can flow easily through the reservoir and displace the oil. It should also be mentioned that the only low salinity waterflooding mechanism that ECLIPSE 100 takes into account is the proposed wettability alteration. The amount of clay in the reservoir does for instance not matter, and the proposed fines migration can only be implemented by decreasing the permeability. pH is not taken into consideration at all.

The BRINE option in ECLIPSE 100 turned out to be very sensitive to relative permeability, and especially residual oil saturation. It is important to be aware of this during simulation of such augmented waterflooding, and input from experimental data is needed for accurate simulations. It might therefore also be essential to conduct several precise experiments from different zones to figure out which zones in a reservoir that responds positively to low salinity waterflooding. Other inputs such as the LSALTFNC and different injected slug sizes

also seem to affect the oil recovery, and needs to be measured properly before applied in simulation models.

6.10 Uncertainties

During simulations, it is the numerical dispersion that often causes erroneous prediction. This has, however, not been investigated in this model. The largest discussable uncertainties will then probably depend on the BRINE option in ECLIPSE 100, and how the reservoir depends on the change in reservoir properties as a result of the brine dependency.

The synthetic model was taken from one of the example files found in the ECLIPSE 100 input files. It was initially prepared for injection of surfactants and contained none of the required keywords for initiation of the BRINE model. The variables needed to commence the BRINE option were only illustrative and might not give very reliable results because of little available data on this subject. The decrease in residual oil saturation of 20 % of pore volume would for instance improve the oil displacement questionably high, and this was also what was observed after the low salinity waterflooding. An increase up to 25 % of OOIP in oil recovery after tertiary LSW has been observed from the literature (Morrow and Buckley, 2011). Despite this the 27 % increase in oil recovery after the secondary low salinity waterflooding might indicate an overestimated potential for this as an EOR mechanism.

The drastic increase in oil recovery might also be seen in conjunction with the homogeneities found in the synthetic model. A homogeneous reservoir will be very efficient for waterflooding, because the oil easily is displaced and will hence be strongly dependent on the residual oil saturation. This again might lead to erroneous evaluations of potentially EOR mechanisms, because few real field reservoirs will have such homogeneous reservoir behavior. Most reservoirs will contain some permeability barriers such as faults and other no-flow boundaries.

6.9 Conclusion

Results obtained from simulations of the synthetic model clearly showed that waterfloods depend on the BRINE and low salinity models. Even though the data inputted in this model only are illustrative and no data are taken from laboratory measurements, it is possible to say that there is a large potential for low salinity waterflooding. A significant increase in

recovery was seen in conjunction with a decrease in salinity of the injected brines under the conditions included in this model.

Both the secondary and tertiary recovery mode responded to the initiated wettability alteration and showed almost similar ultimate recovery. This indicates that the amount of low salinity brines injected should be carefully investigated. As the tertiary recovery is implemented at a later stage, the amount of fluids injected is smaller compared to secondary recovery mode. If the rate of recovery is not the determining factor, tertiary recovery mode should be initiated if the economically aspects are to be considered. The slug sizes, however, have to be large enough so the salinity in the reservoir will reach below 5 kg/m^3 TDS so the initiated effect of low salinity waterflooding can occur.

7. Frøy Field

To evaluate the possibility of LSW as an EOR mechanism, it is important to know the basic behind the Frøy field itself. Some historical production and basic reservoir engineering are presented in the next sections.

7.1 Introduction

The Frøy field is located in the North Sea in production license 364, Blocks 25/2 and 25/5, approximately 32 km southeast of the Frigg field and 25 km northeast of the Heimdal field. This is shown in **Figure 7-1**. The current Production License was awarded in 2006. The licensees are Det Norske Oljeselskap ASA (50 %) and Premier Oil Norge AS (50 %). The field is operated by Det Norske Oljeselskap ASA, but is currently shut down. A new Plan for Development and Operation (PDO) was prepared in 2008, but due to the financial crisis the operations were delayed. The new operations are, however, planned to start within a few years depending on feasibility and other operations.

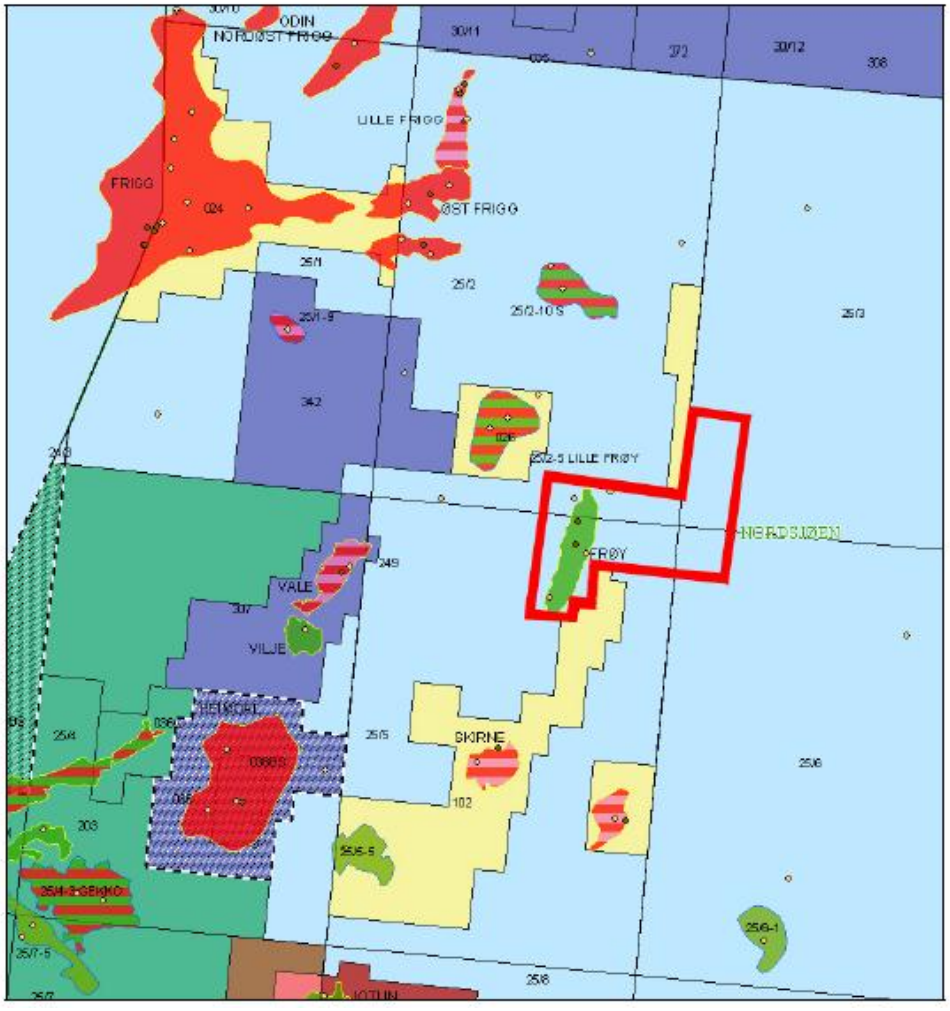

Figure 7-1: Frøy field location (Det Norske Oljeselskap, 2008).

7.2 Production History

The Frøy field was discovered in 1987 when a discovery well found a 76-m thick oil-bearing Brent sequence. The development solution consisted of a normally unmanned wellhead platform with 15 well slots and one-stage processing. Liquid and gas were transported to the Frigg platform for further processing.

During the first production period, 5.6 MSm^3 of oil was recovered from the Frøy field. This was obtained from six production wells with pressure support from four water injection wells. The total gross oil and gas production were 5.9 MSm^3 and 1.7 GSm^3, respectively. Because of unfortunate wettability behavior in the formation, the water volume that needed to be injected to prove any efficient was huge. A total of 8.6 MSm^3 water was injected and 2.4 MSm^3 water was produced. The monthly average production and injection rates are found in **Figure 7-2** below (Det Norske Oljeselskap, 2008).

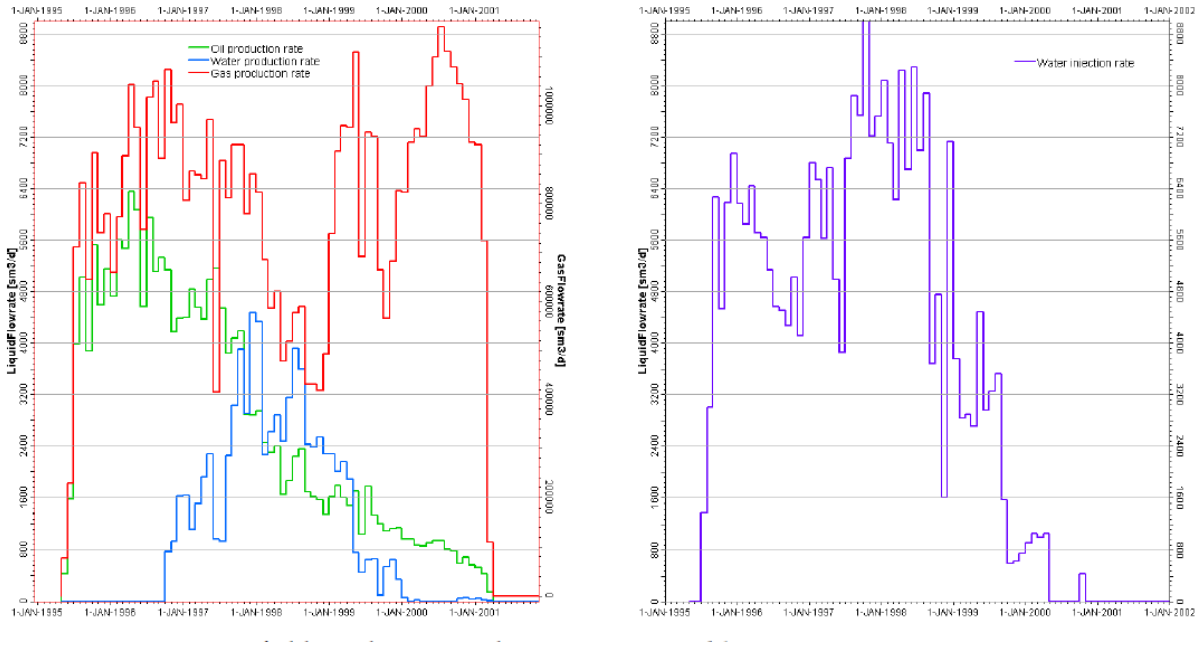

Figure 7-2: Oil production (green), water production (blue), gas production (red) and water injection (purple) for the Frøy field (Det Norske Oljeselskap, 2008).

7.3 Geology

The Frøy field has a very heterogeneous geology and is surrounded by a number of faults and dippings. The main formation is a westward-dipping monoclinal fault block, and the Frøy field is defined as an elongated three-way dip closure (west, south and north) with an up-thrown fault closure to the east.

Four main faults comprise the structural framework of the Frøy field; the crestal horst, the down flank area, the Northeastern segment and the undrilled Southeastern segment. Production from the crest and the western down flank segments were conducted from 1995 to 2001. The oil is situated in the Middle Jurassic Hugin and Sleipner sandstone Formations. See **Figure 7-3** for a geological overview with the wells drilled up to date. Segment 5, 6 and 7 are all in the water zone. (Det Norske Oljeselskap, 2008).

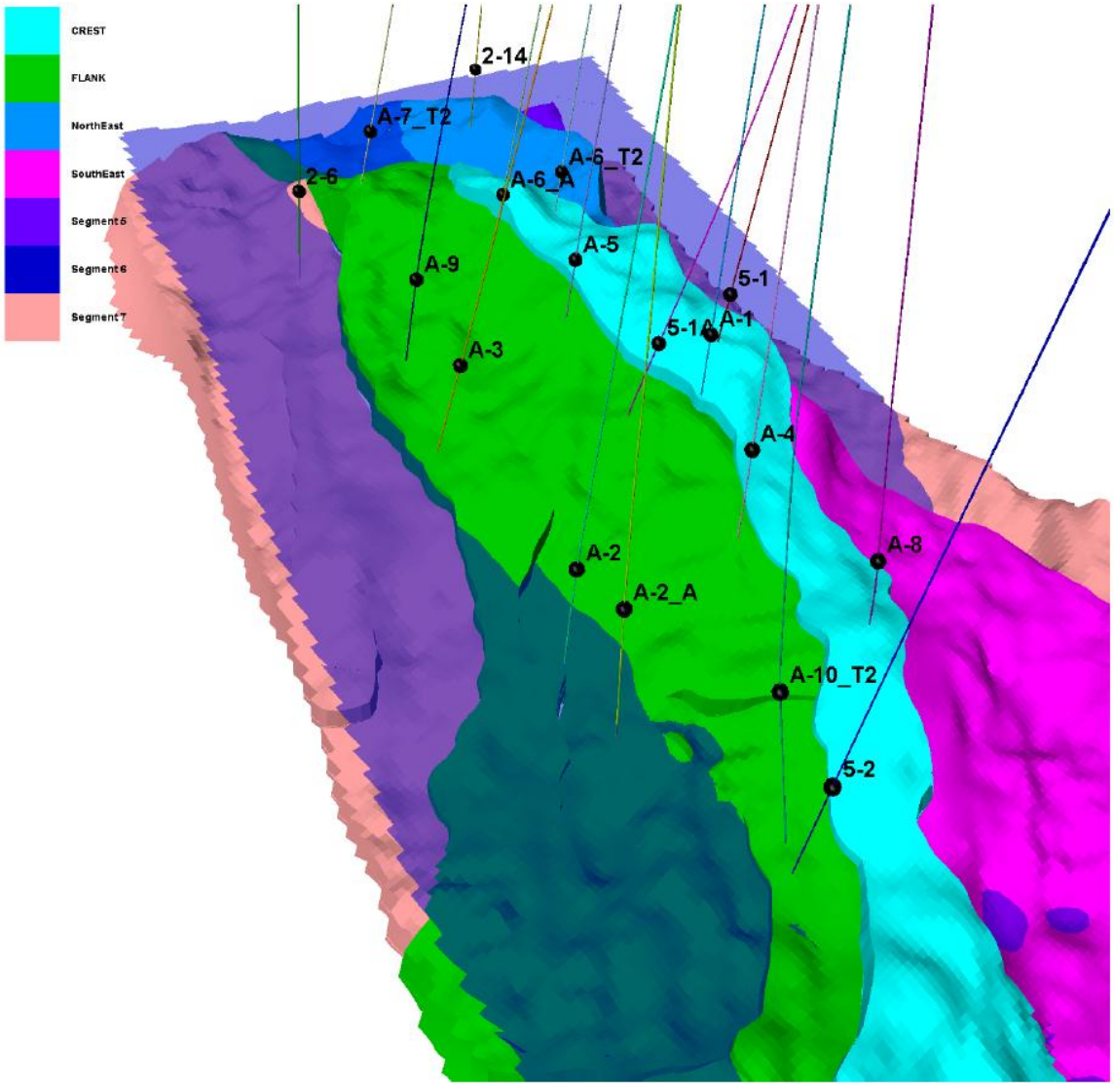

Figure 7-3: Segments and well placement in the Frøy field (Det Norske Oljeselskap, 2008).

7.4 Reservoir Engineering

The Frøy field was under production from 1995 to 2001. It proved to be more complex than originally estimated and it was observed an earlier water breakthrough than proposed. Together with the formation water, the injection water also provoked severe $BaSO_4$ scaling. The early water breakthrough, severe scaling and low oil prices made the operator abandon the field with a record low recovery factor of 18 % of OOIP in 2001.

The reservoir properties are heterogeneous as well. Vertical permeability varies from 1 up to 1000 mD. Initial reservoir temperature and pressure were estimated to be 103 °C and 308 bar at 2970 mTVD, respectively. Oil water contact (OWC) is at 3175 mTVD and gas oil contact (GOC) is at approximately 2900 mTVD. Water depth is 120 m, and the saturation pressure is at 270 bar. From a special core analysis (SCAL) the Corey parameters regarding relative permeability were obtained, indicating an oil-wet reservoir formation. Large uncertainties were proposed for the residual oil saturation, and this is incorporated by letting the critical oil saturation both with respect to water and gas displacement be allowed to vary between 10 and 45 %. This gives a mean value at approximately 25 %. The crude oil in the Frøy field has a viscosity and density at 20 °C of 5.97 cP and 0.829 g/cc, respectively (Lehne, 2010).

A large history-matching of the previous production history has been applied to optimize the full-field 3D reservoir simulation model. The model showed that the field had a severe heterogeneity than what was interpreted from the geological data. By introduction of barriers or semi-barriers into the model, a better match of the production data was obtained. Such barriers or semi-barriers may be results of sedimentary features such as coal and shale, leading to a decrease in permeability in certain zones. Relative permeability was also used as a matching parameter in the history-matching. The data was as mentioned taken from the SCAL analysis and proved to be unfavorable for waterflooding, meaning that a large amount of fluids was needed to be injected to obtain a sufficient reduction in the residual oil saturation. The history-matching results from the field oil and water production can be found in **Figure 7-4**. (Det Norske Oljeselskap, 2008).

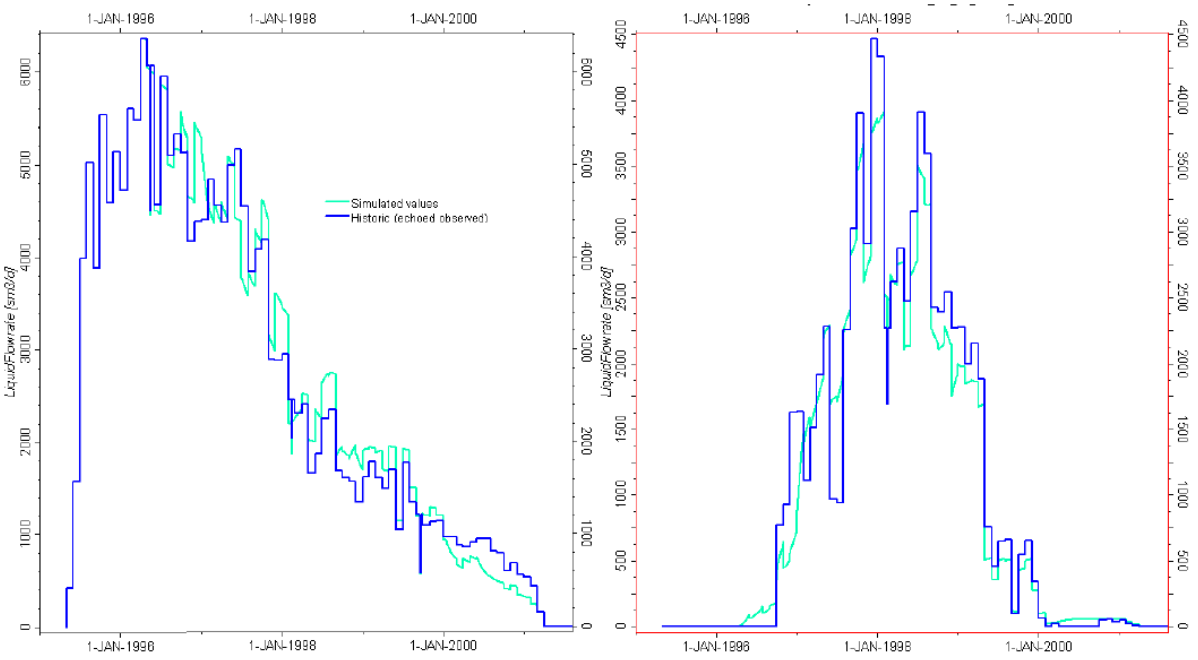

Figure 7-4: History match; simulated field oil production (turquoise), historic field oil production (blue), simulated water production (turquoise) and historic water production (blue) (Det Norske Oljeselskap, 2008).

7.5 Low Salinity Waterflooding Potential at the Frøy Field

As previously discussed, the Frøy field is currently shut down due to economically reasons. The new production strategy includes simultaneous water and gas injection (SWAG), but the reservoir properties also indicate a potential for low salinity waterflooding (LSW) as an EOR mechanism.

From the literature it is well known that reservoirs need to contain a certain amount of clay for LSW to be any effective. A XRD and CT scan has been carried out on core samples from the Frøy field, and these analyses indicated that the cores contain some clay (Lehne, 2010). Average clay mineral content was varying from 1.5 – 5 %. The initial wettability is also exciting, having proved to be slightly oil-wet. Since the main mechanism behind LSW is an alteration of the wettability towards more water-wet conditions, an oil-wet reservoir should have a large EOR potential. This is also proven in the synthetic model in **Section 6.2**, where it was the initial oil-wet reservoir that gave the largest effect of LSW. Based on the Corey parameters obtained from the PDO, the relative permeabilites for the high, low and base cases are presented in **Table 7-1** and **Figure 7-5** below (Det Norske Oljeselskap, 2008).

Table 7-1: Corey parameters for the Frøy sector model (Det Norske Oljeselskap, 2008).

	Case High	Base Case	Case Low
Swi	0.12	0.12	0.12
Sor	0.05	0.08	0.12
Krw(Swi)	1	1	1
Ew=Krw(Sor)	0.6	0.8	1
Eo=Kro(Swi)	1	1	1
Nw	1.8	1.3	1
No	5	5.5	6

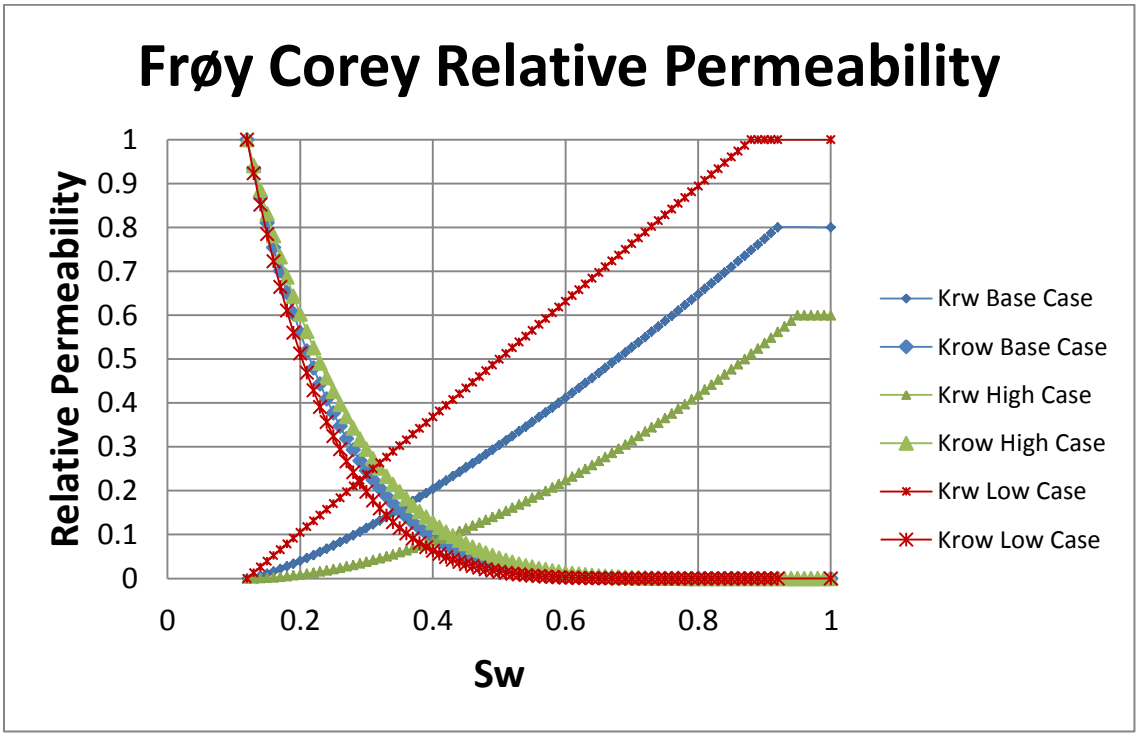

Figure 7-5: Relative permeability profiles based on Corey parameters in the Frøy sector model.

Some laboratory investigations of the potential for low salinity waterflooding (LSW) in the Frøy field have also been carried out. Hadia et al. (2011) conducted several flooding experiments at high temperature and low pressure on cores from different locations in the Frøy field. Synthetic formation brine and crude oil from the Frøy field were used in the experiments. Low salinity injection brines were prepared by adding required volume of

deionized water into high salinity injection brine. A total of three injection brines were prepared, and the brine with highest salinity (IB) had salinity approximately equal to the reservoir brine. The two other brines were made such that they had salinities of 10 % (10 % IB) and 1% (1 % IB) of the brine with the highest salinity.

Amott-Harvey method was used to find the initial wettability of a plug, and the results indicated a neutral-wet behavior. The wettabilities the rest of the plugs were assumed to be close to the same as for the plug that was measured. After performing the flooding experiments with different injection brines, the results varied from core to core. LSW, however, resulted in improved oil recovery varying from 6 to 14 %. The residual oil saturations were reduced from 4 to 9 % of pore volume at core scale. Some cores did on the other side not react to the LSW, and Hadia et al. concluded that the wettability alteration towards more optimum for low salinity effects (LSE) in these cores did not occur. A significant reduction in permeability was also observed during the experiment, probably due to an increase in differential pressure. This reduction in permeability was seen in conjunction with the increase in clay content as a consequence of low salinity waterflooding. The final conclusion was that there is a significant potential for LSW as an EOR process at the Frøy field. A summary of the coreflooding experiment is found in **Figure 7-6**.

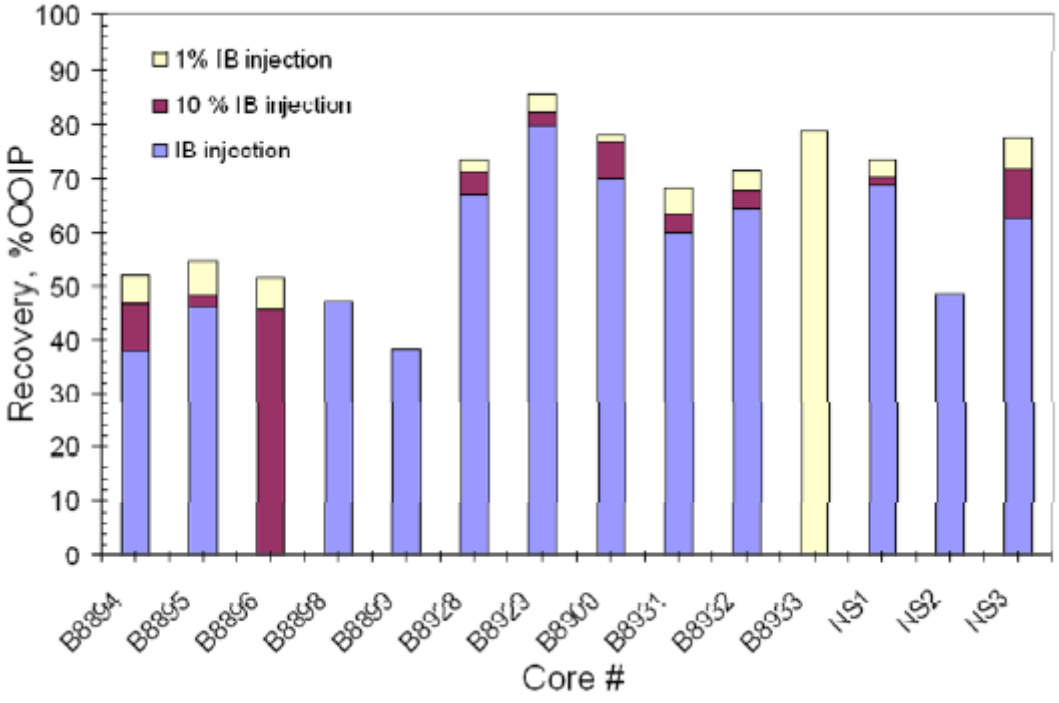

Figure 7-6: Oil recovery from LSW on different core samples from the Frøy field (Hadia et al., 2011).

Some of the cores from the laboratory experiment performed by Hadia et al. (2011) were taken from well 25/5-A-7 which is just north of the sector model, but in the same segment. This is illustrated in **Figure 7-3** in **Section 7-3**. Cores from this well showed an incremental recovery up to 14 % after low salinity waterflooding and an ultimate recovery varying from around 50 % to 75 %. Different reservoir properties, such as permeability and porosity, are probably the main reasons for the large difference in ultimate recovery. The reservoir properties vary with depth, and the cores are taken from different depths in the same well. Because the sector model is from the same segment and the properties should be close to what is obtained from core analyses, recoveries in the range of what was obtained from the laboratory experiment is expected. Lehne (2010) also observed that most of the cores experienced a reduction in relative permeability and residual oil saturation during injection of brines with low salinity in these cores. This is presented in **Figure 7-7** and **Figure 7-8**.

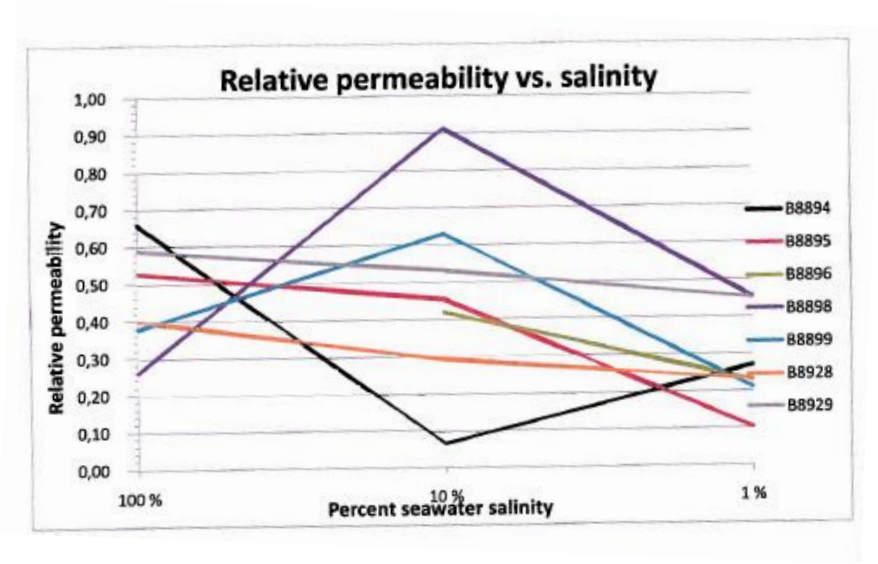

Figure 7-7: Relative permeability versus salinity (Lehne, 2010).

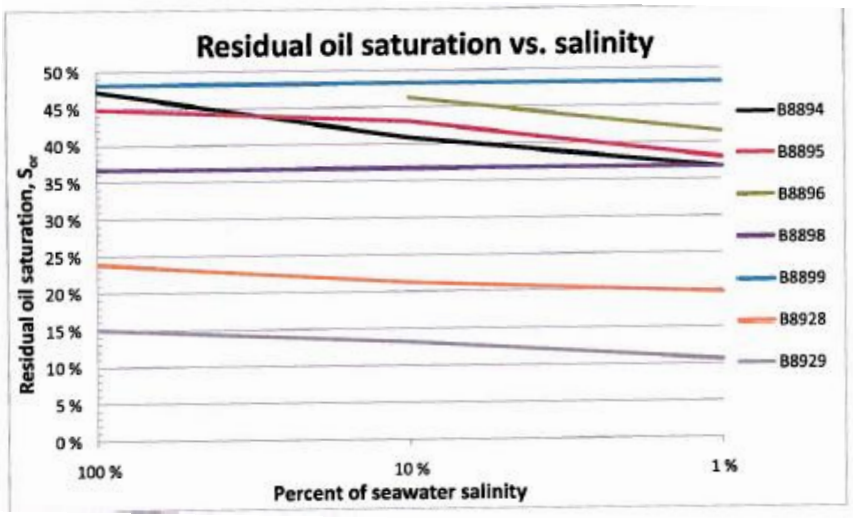

Figure 7-8: Residual oil saturation versus salinity (Lehne, 2010).

7.6 The Frøy Sector Simulation Model

A sector model of the full Frøy field simulation model was made to investigate the potential for low salinity waterflooding as an EOR mechanism. The full field model itself includes 36 layers with 74 and 107 layers in X- and Y-direction, and the simulation model is really divided into cells of 100x100 meters size. The sector model is taken from the western part of the reservoir, between the two largest faults in the reservoir model for simplifications. An overview of the placement of the sector model with respect to the full field simulation model can be seen in **Figure 7-9**. All the wells included in the model are also illustrated. The well placement for the sector model, however, is incorrect.

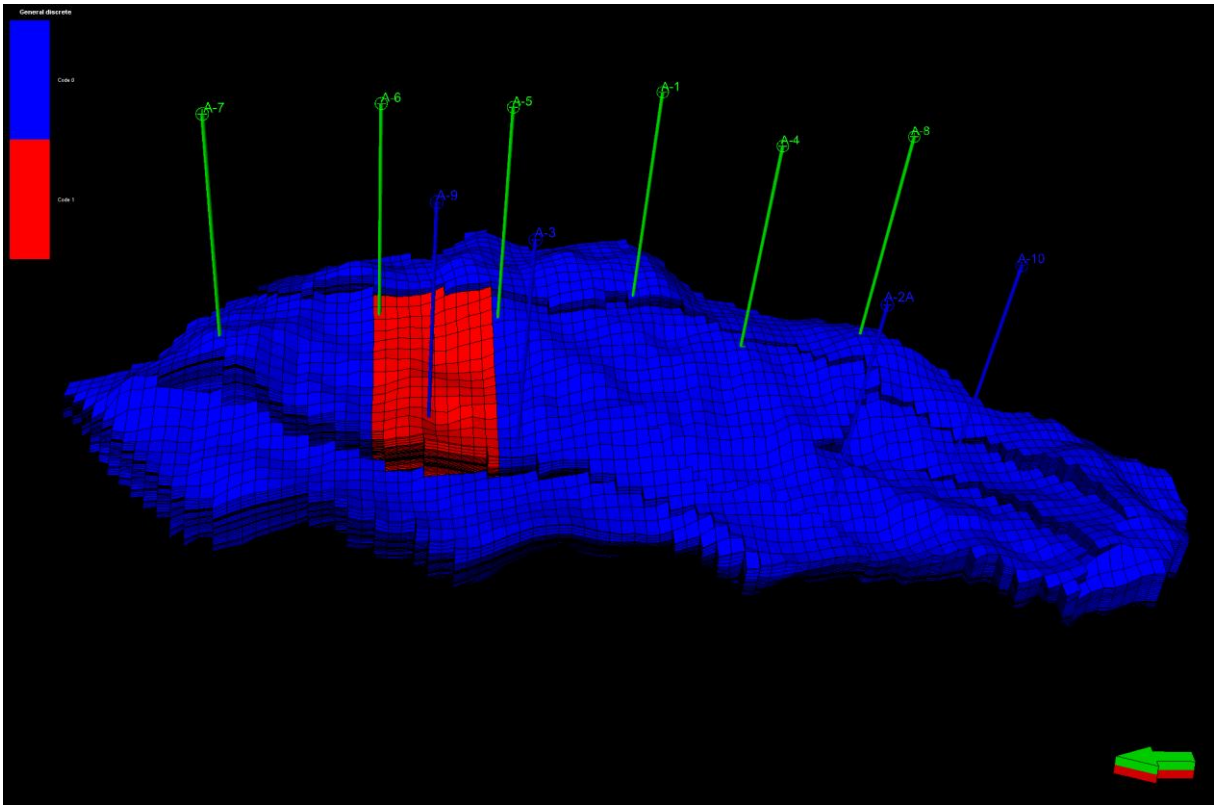

Figure 7-9: Frøy sector model location. The red zone indicates the sector model (Det Norske Oljeselskap, 2012).

7.7 Initialization of the Frøy Sector Model

The base case model was obtained from Det Norske Oljeselskap ASA, and the sector model was made by assigning ACTNUM values of 0 to the rest of the grid blocks from the full field model. This means that the grid blocks located outside the sector section is set to be none-active. It was decided to use ECLIPSE 100 2011 as the simulator, and a black oil model was applied.

All reservoir properties except relative permeability were kept unchanged during the simulation period. The properties vary throughout the reservoir and are not easy to present, but the most important parameters are found in **Appendix A** in **Figure 10-1, 10-2, 10-3** and **10-4**. The simulation period was initially from 1995 – 2030, but was extended to 2035 to get a better overview of the results. Two wells were added to the model, one oil producer and one injector for injection of water with different salinities. They were initiated in 2012. Initial completion data were generated from PETREL and not changed. The wells were placed in each end of the sector model, directly ahead of each other. It was decided to control the wells by rates and voidage replacement, such that injected water was equal to the amount of fluids produced. This was set in the WCONPROD and WCONINJP in the SCHEDULE section, and the oil production rate was set to be 800 Sm^3/day. As assigned in the WCONINJP, the injection water rate was set to be equal to the fluid production rate to minimize the pressure drop in the reservoir. A bottom hole pressure (BHP) limitation in the injector was also set to be at 450 bar. This was done to avoid extrapolation for pressures above 500 bar, because this was the maximum oil pressure in the model and PVT data for values above this was not included in the model. A BHP limitation was also set in the producer at 100 bar to make the simulation more realistic. Uncontrolled drawdown pressure as a result of too low BHP might lead to well damages such as sand production (Tiffin et al., 2003).

Gas, oil, water and dissolved gas were the phases included in the model. It is important to note that the saturation table End-point Scaling option was included in this model. This option scales the end-points of the relative permeability curves for each cell. It provides a mechanism for redefining values for connate, critical and maximum saturations in the saturation tables describing the flow of the reservoir fluids (Schlumberger, 2011). A short discussion of this option is found in **Appendix C**.

To implement the BRINE option in the model, the same procedure as in the synthetic model was conducted. This is described in **Chapter 5**. The initial connate water salinity was set to be 38 kg/m^3 TDS or approximately the same salinity as regular seawater in the Frøy field in the Utsira formation. Low salinity effects were set to start after injection of 5 kg/m^3 TDS in the same way as in the synthetic model, and the initial LSALTFNC is found in **Table 7-2**.

Table 7-2: LSALTFNC for the Frøy field.

Salt Concentration	F1	F2
[kg/m3]		
0	1	1
1	0.8	1
4	0.2	1
5	0	0
35	0	0
45	0	0

The initial unscaled oil-water relative permeability, saturation and capillary pressure profiles consisted of 4 different SATNUM. They were assigned to different regions in the model, but were equal before the End-point Scaling was implemented. The unscaled saturation profiles are found in **Figure 7-10** and the unscaled capillary pressure profile is found in **Figure 7-11**. After flooding with low salinity brines a new SATNUM, LWSLTNUM, was assigned to all the grid cells in the reservoir. Gas relative permeability, saturation and capillary pressure profiles were considered to be salinity independent. Due to lack of data, it was decided to only use capillary pressure from the high salinity function which is equal to the unscaled capillary pressure.

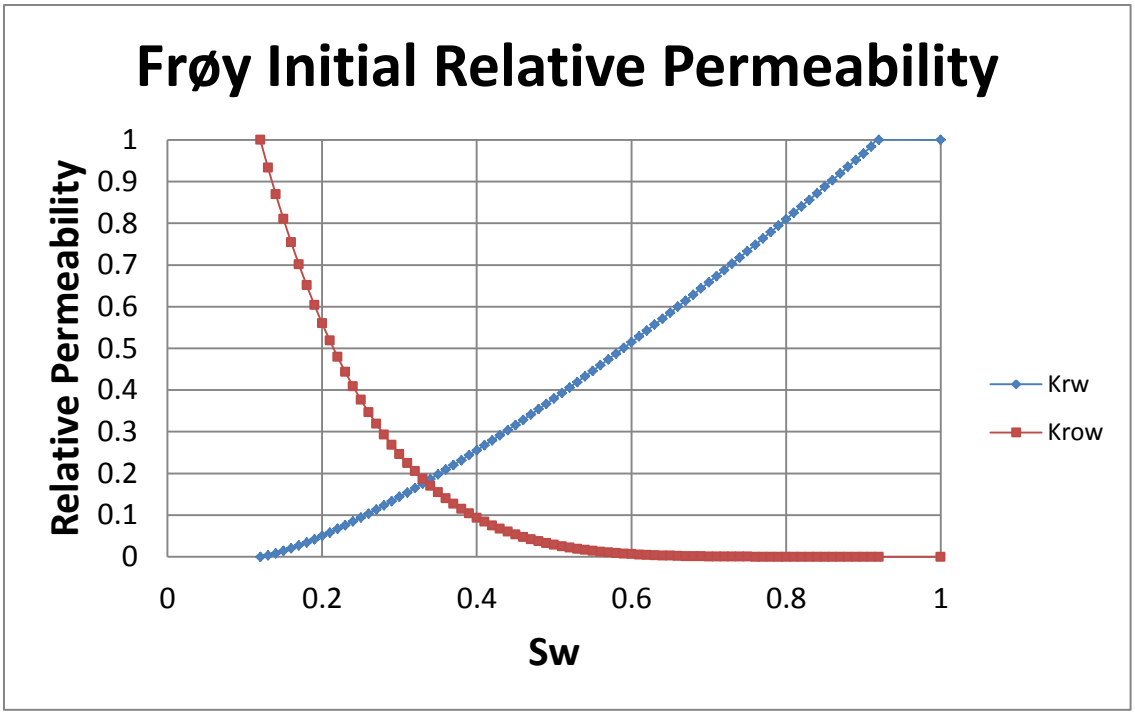

Figure 7-10: Initial unscaled relative permeability profile in the Frøy sector model.

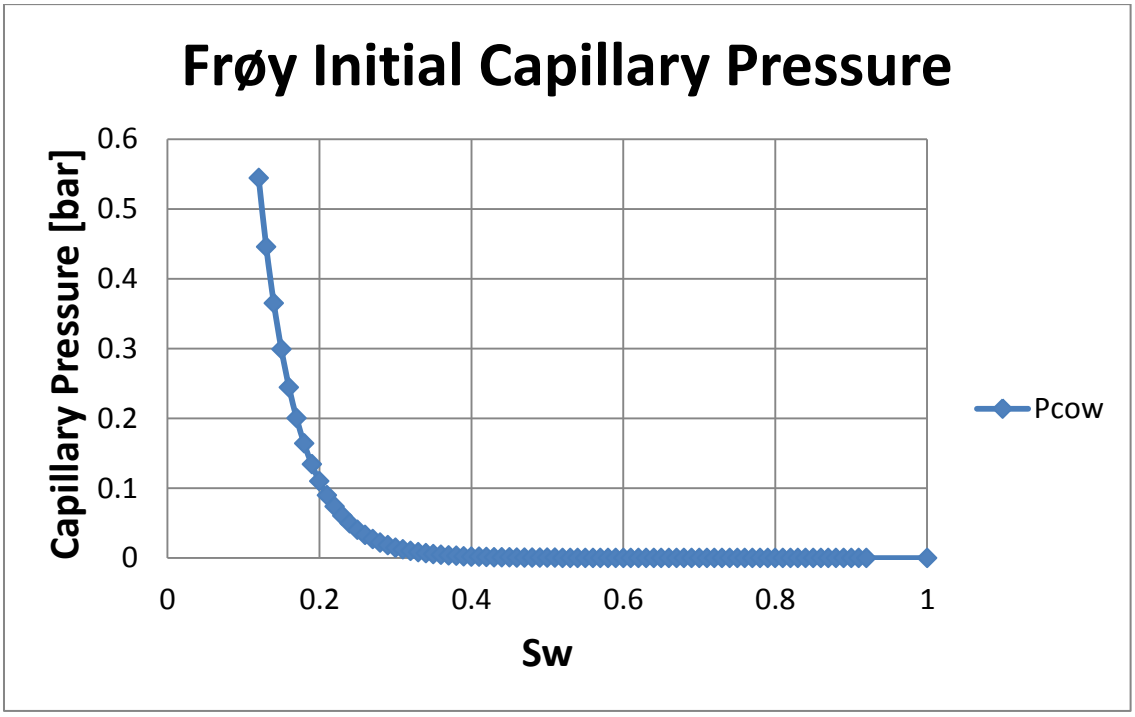

Figure 7-11: Initial unscaled capillary pressure profile in the Frøy sector model.

In **Figure 7-12** below, the oil saturation distribution immediately after initialization of the wells can be found. The well placements are also illustrated. Well INJ_2D and PROD_2D are

closed and are inactive. They are only implemented in the 2D model which is used to see the oil saturation profiles throughout the simulation period. This will be discussed later.

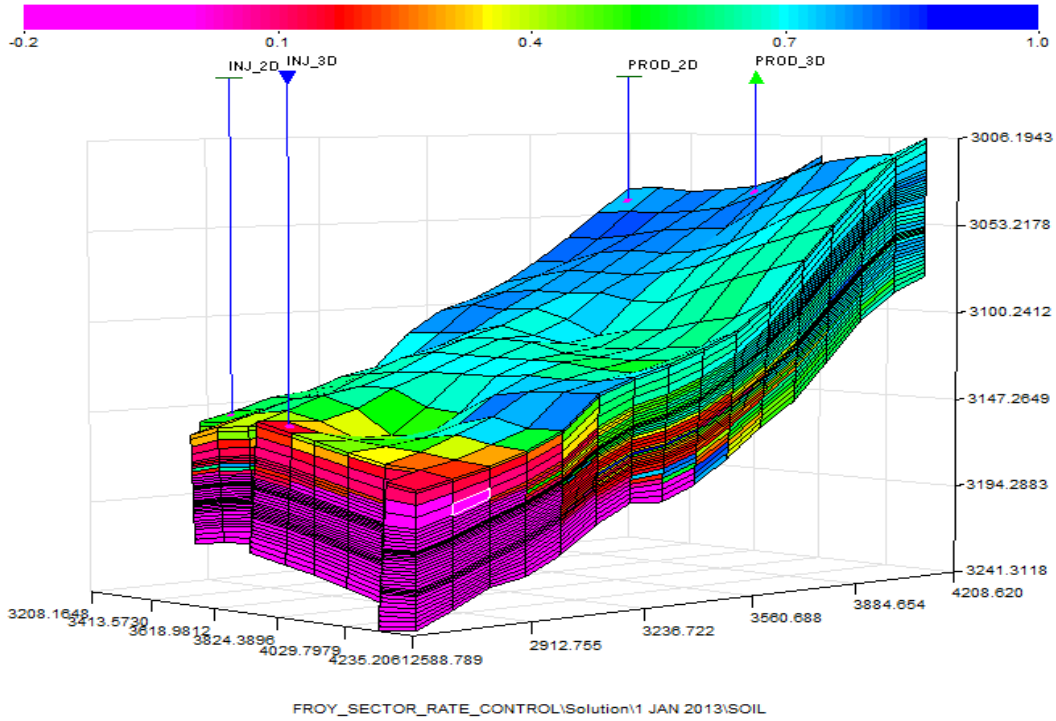

Figure 7-12: Initial oil saturation distribution in the Frøy sector model.

To investigate the potential of low salinity waterflooding as an EOR mechanism in the Frøy field different sensitivity analyses were conducted. Investigations of injection brine salinities in both secondary and tertiary recovery modes were carried out. The results from the waterfloodings will be presented in the next sections.

7.8 Effect of Brine Salinity; Secondary Imbibition

The effect of injection brine salinities on secondary oil recovery in the Frøy sector model was implemented by injection of brines with different salinities from the beginning of the simulation period. A base recovery was set by injection of water with the same salinity as the initial connate water, 38 kg/m^3 TDS. Further on, brines with salinities of 10, 4, 3, 2, 1 and 0 kg/m^3 TDS were injected. The initial relative permeability, saturation and capillary pressure curves were set equal to the one already included in the model. After initiation of the low salinity waterflooding, the relative permeability and saturation profiles were set to the high case included in the PDO as described in **Section 7.5**. The main differences in these two profiles are seen in residual oil saturation (S_{or}) and water relative permeability. Residual oil saturation was set to decrease with 7 % of PV compared to the unscaled relative permeability profile when only the low salinity relative permeability and saturation profiles were applied. Due to the End-point Scaling option, however, this reduction might vary significantly throughout the reservoir. Lehne (2010) observed a reduction in S_{or} ranging from 0 to 11 % of PV during laboratory experiments, meaning that the initiated reduction in S_{or} in this model should be in the same range.

Capillary pressure was as already discussed not changed, and the initial capillary pressure profiles were kept constant throughout the simulation period. Since it was decided to start the low salinity waterflooding effects after injection of brines below salinities of 5 kg/m^3 TDS, no incremental recovery was expected for the injection of brines with 10 kg/m^3 TDS. The oil recovery, field oil efficiency (FOE), from the different brine salinities are found in **Figure 7-13**, and the ultimate recoveries can be seen in **Figure 7-14.** The model is history matched from 1995 to 2008, and the wells were not initiated before 2012. It was therefore decided to start the analyses from the beginning of 2012.

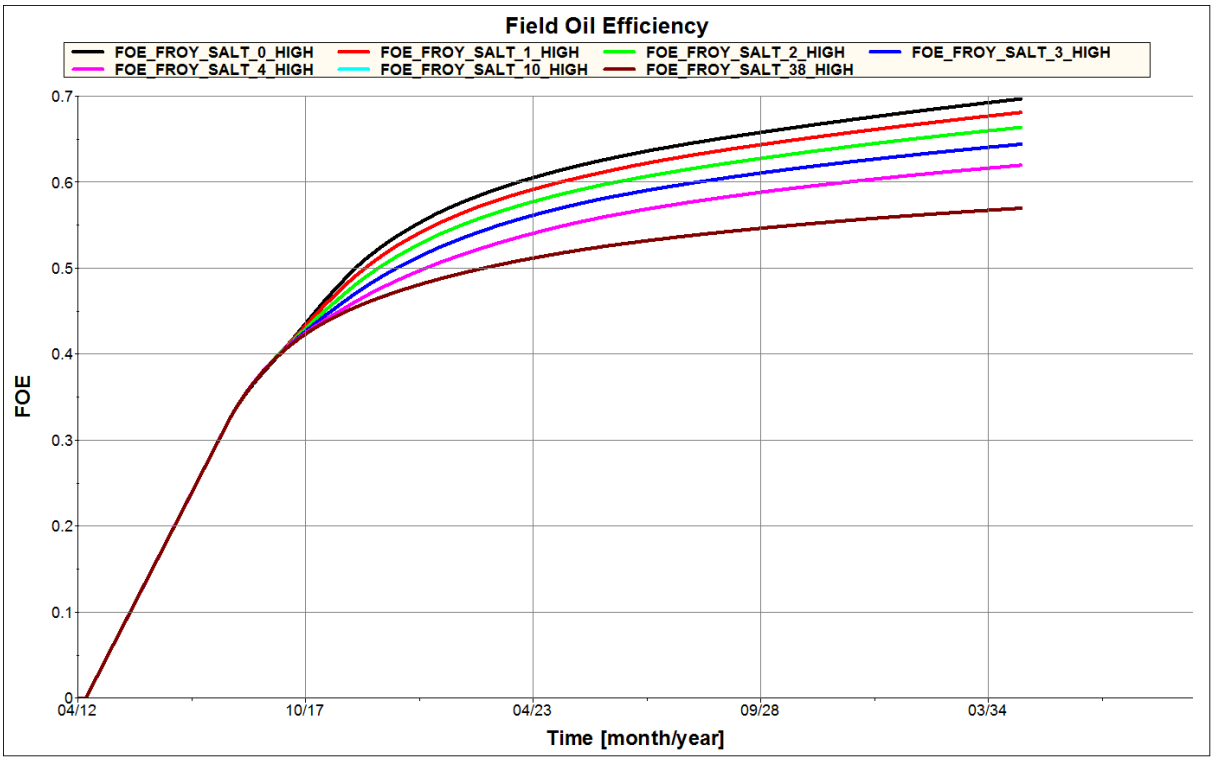

Figure 7-13: Oil recovery for secondary LSW with injection brine salinities of 38, 10, 4, 3, 2, 1 and 0 kg/m^3 TDS.

Brine Salinity	Oil Recovery
[kg/m3]	[%] OIIP
38	56.95
10	56.95
5	56.95
4	61.94
3	64.39
2	66.34
1	68.08
0	69.66

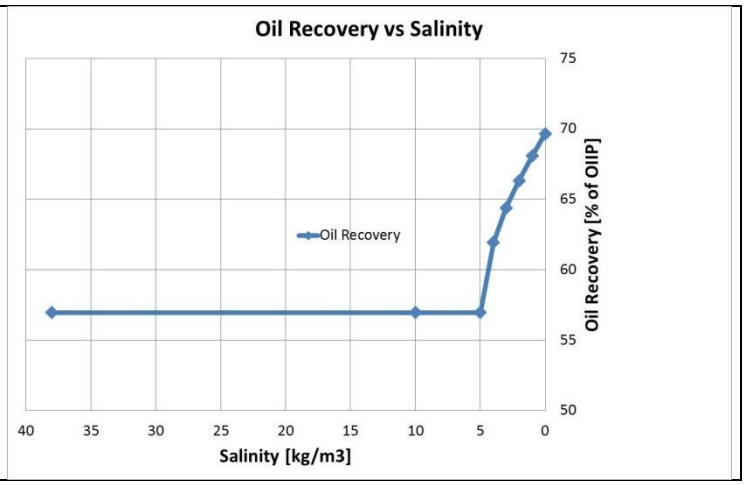

Figure 7-14: Ultimate oil recovery as a function of injection brine salinity during secondary LSW.

The results clearly showed an increase in oil recovery with a decrease in salinity for the injection brine. Injection of brine with 10 kg/m^3 TDS showed no incremental recovery as expected, and it produced the same amount of oil as regular seawater injection. The effect of the low salinity waterflooding was, however, not as big as in the synthetic model. In the synthetic model, a maximum incremental recovery from lowering the injection brine salinity was approximately 28 % of oil initially in place (OIIP). In the Frøy sector model, the oil recovery increased from around 57 to around 70 % of OIIP, yielding a maximum of 13 % incremental recovery of OIIP after lowering the injection brine salinity. As indicated in **Figure**

7-13 the ultimate recoveries have not yet completely been reached. It seems, however, to follow the same trend such that further effects of low salinity waterflooding only would result in a small additional increase in oil recovery.

The oil recoveries from the different injection brine salinities were equal until around October 2017. This is most likely because it takes some time before the injected low salinity brines reach the oil production well, due to for instance connate water banking. This is illustrated in **Figure 7-15** where the well production salinities (WSPC) for the different brine injection salinities are presented. Except from the seawater injection, the production brine salinity did not vary much before the middle of 2015. This contributes to the small difference seen in the oil recovery at the beginning of the production period. The low salinity effects were not set to start before the salinities were below 5 kg/m^3 and this was not reached in either of the cases until almost October 2017 when the oil recoveries started to differ.

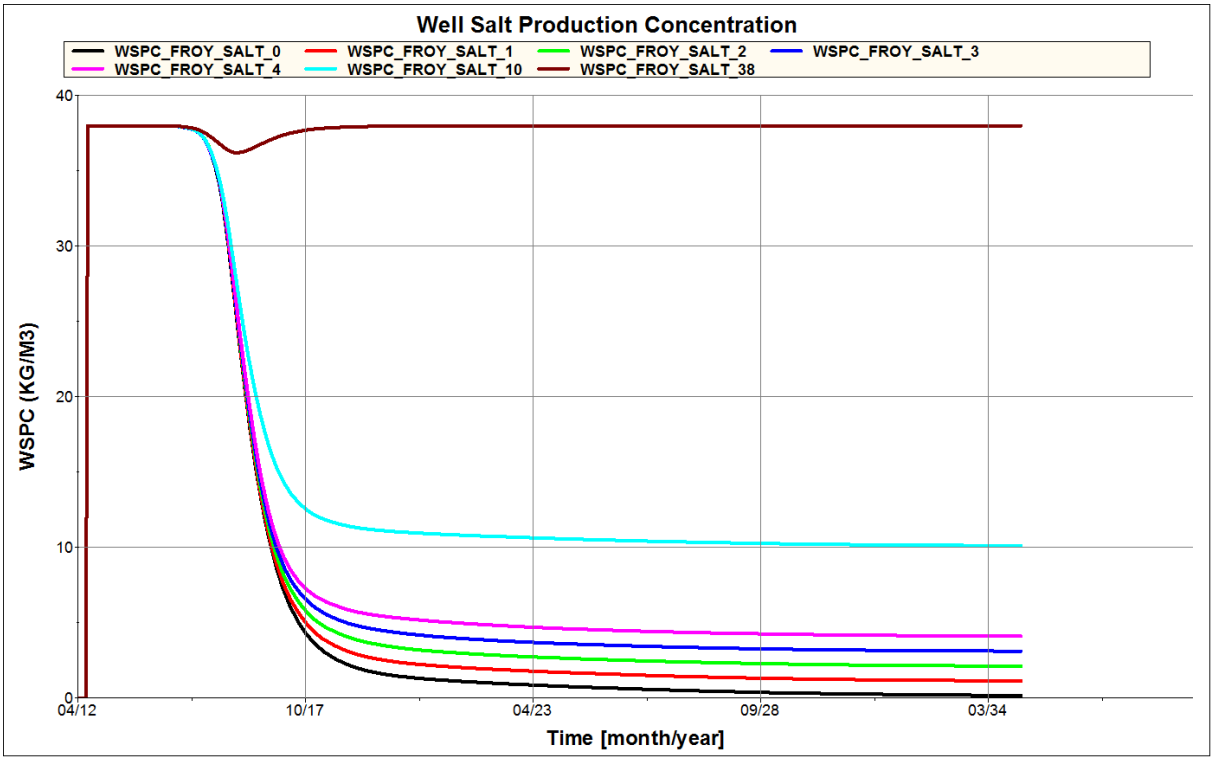

Figure 7-15: Well salt production concentration for secondary LSW with injection brine salinities of 38, 10, 4, 3, 2, 1 and 0 kg/m^3 TDS.

The reason for the observed increase in recovery with a decrease in injection brine salinity in this model might be described by the wettability alteration to less oil-wet condition. This alteration triggers the sweep efficiency during waterflooding, and the result of this is among

other a change in water cut. The water cut (FWCT) for the different cases are illustrated in **Figure 7-16**.

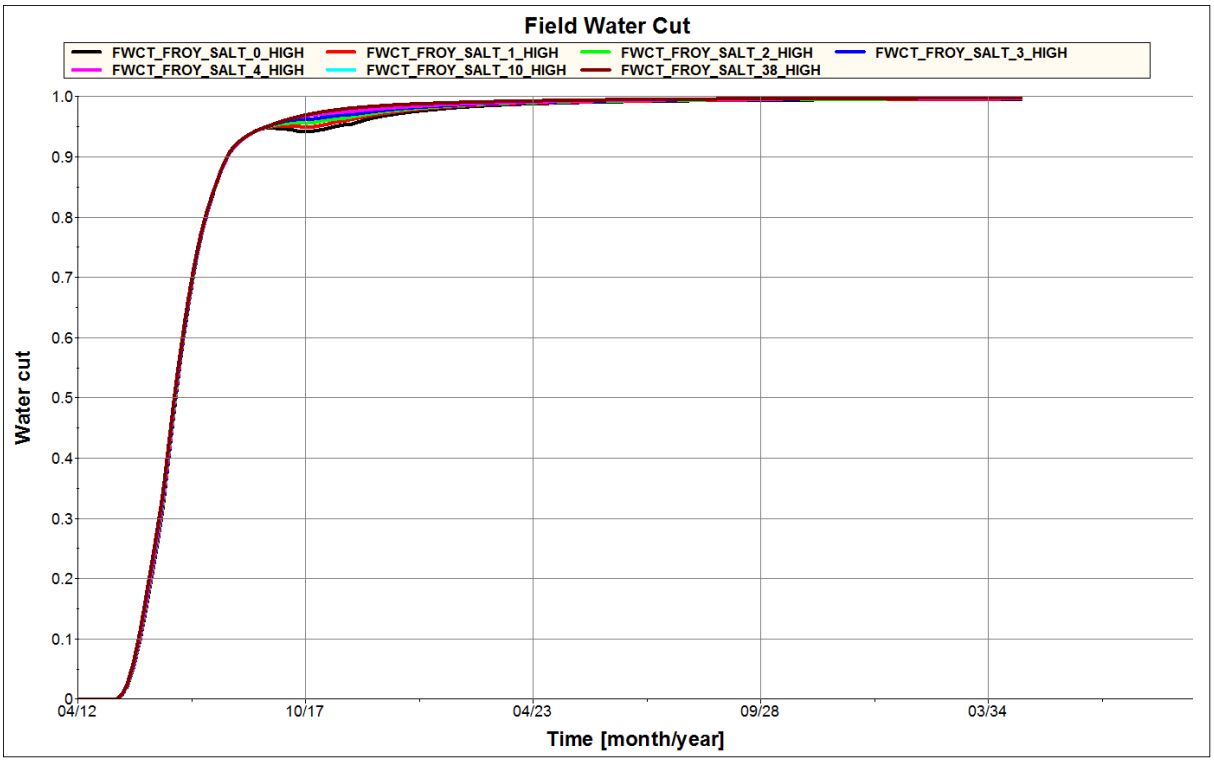

Figure 7-16: Water cut for secondary LSW with injection brine salinities of 38, 10, 4, 3, 2, 1 and 0 kg/m^3 TDS.

Again, no differences were seen until breakthrough of the low salinity brines occurred. After breakthrough, however, the water cut decreased slightly for the cases where the injected brines had lower salinities than the initial formation brine. This trend continued for almost 5 years, and would improve the oil recovery in the reservoir. As a result of the reduction in water cut, an increase in field oil production rate (FOPR) was observed. This is indicated in **Figure 7-17**. Approximately at the same time as the water cut decreased, the field oil production rate increased and got a new peak. The increase in oil production after the new peaks appeared and the oil production at the end of the simulation period are presented in **Table 7-3**. Incremental oil production is defined as the difference of the top oil production in the new peak and oil production before the start of the peak. An overview of the oil production rate and water cut for injection of 1 kg/m^3 TDS brine is found in **Figure 7-18** and **Figure 7-19**, where it is evident that the reduction in water cut leads to a rise in oil production.

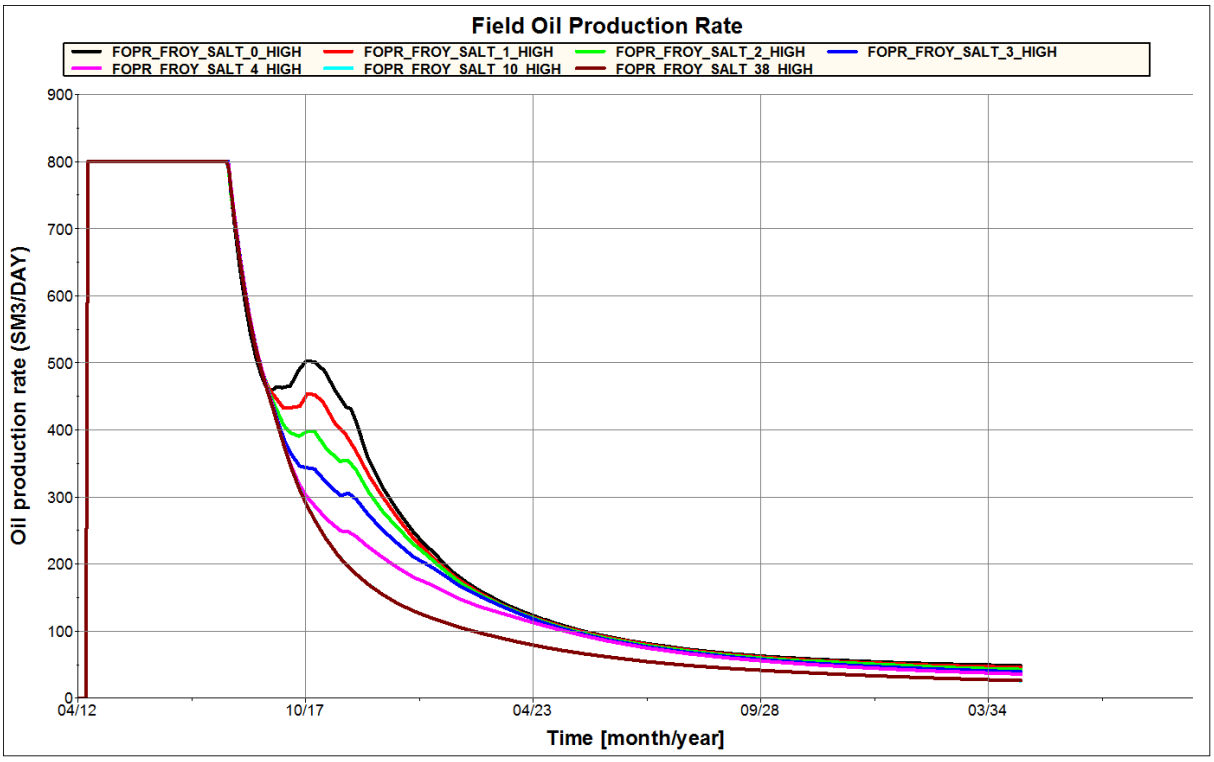

Figure 7-17: Oil production rate for secondary LSW with injection brine salinities of 38, 10, 4, 3, 2, 1 and 0 kg/m^3 TDS.

Table 7-3: Increase in oil production rate and oil production rate at the end of simulation period during secondary LSW after injection of brines with salinities of 0, 1, 2, 3, 4, 10 and 38 kg/m^3 TDS.

Injection Brine Salinity	Oil Production Before New Peak	Oil Production at New Peak	Incremental Oil Production	Oil Production at End of Simulation
[kg/m3]	[Sm3/Day]	[Sm3/Day]	[Sm3/Day]	[Sm3/Day]
0	458.7	502.2	43.5	48.5
1	432.6	453.5	20.9	45.9
2	390.5	397.5	7.0	43.0
3	301.8	305.7	3.9	39.3
4	-	-	0.0	36.1
10	-	-	0.0	26.2
38	-	-	0.0	26.2

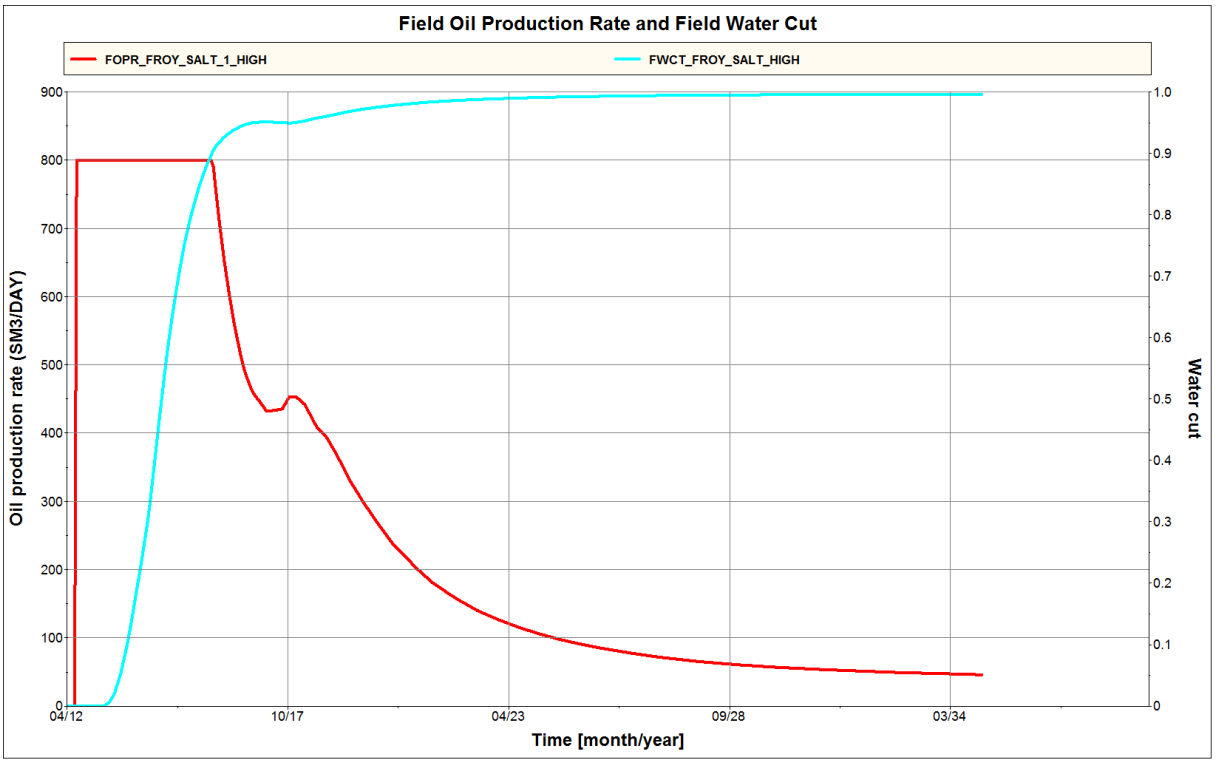

Figure 7-18: Oil production and water cut for 1 kg/m^3 TDS injection brine during secondary LSW.

Date	Oil Production	Water Cut
	[Sm3/Day]	[%]
4/2/2017	432.61	95.144
6/6/2017	433.00	95.053
8/26/2017	435.30	95.031
10/29/2017	453.54	94.902

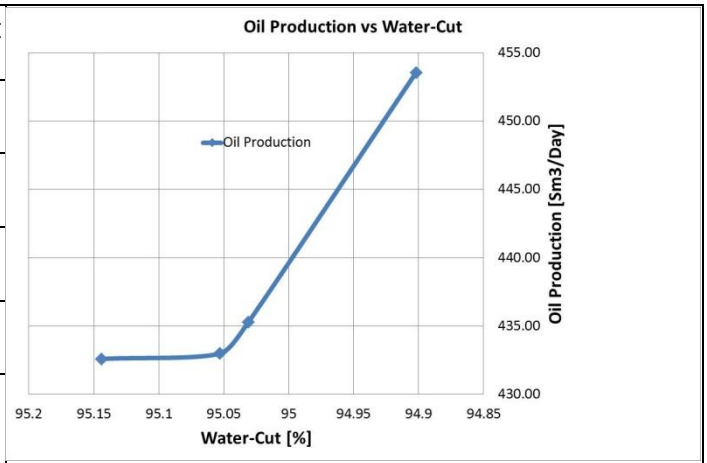

Figure 7-19: Oil production rate as a function of water cut after breakthrough of low saline brines during secondary LSW.

7.8.1 Oil Saturation Distribution

To illustrate the effectiveness of the low salinity waterflooding on the Frøy field, live screenshots were taken of the oil saturation during the production period. This was done to observe how the oil flows through the reservoir, and see if and how the oil was displaced more efficient during low salinity waterflooding compared to conventional waterflooding.

A 2D model of the Frøy field was obtained from the Det Norske Oljeselskap, and prepared for saturation analyses during injection of brines with salinities of 38 and 1 kg/m^3 TDS. Initial saturation distributions with the respective wells are found in **Figure 7-20**. The same well controls were applied as for the sector model, even though a production rate of 800 Sm^3/day probably is high for such a small model. All other reservoir properties were the same as in the sector model, except that the 2D model was limited by grid cells (X, 33, X). The 2D model was made by assigning ACTNUM values of 0 to the rest of the grid blocks from the full field model. This means that the grid blocks located outside the 2D section is set to be none-active. The LOWSALT option was implemented in the same way as described in **Chapter 5**.

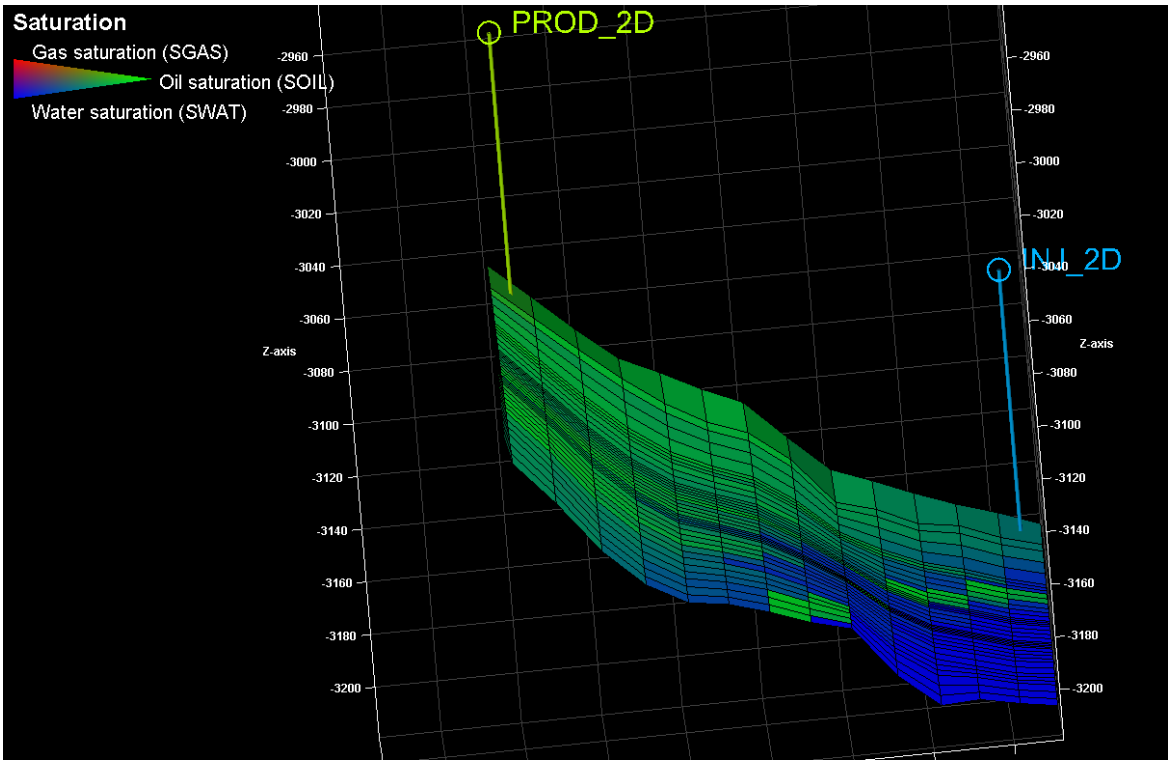

Figure 7-20: Initial saturation distribution in the Frøy 2D model.

The initial oil saturation was naturally equal for both the 1 and 38 kg/m^3 TDS cases. This is illustrated in **Figure 7-21** and **figure 7-22.**

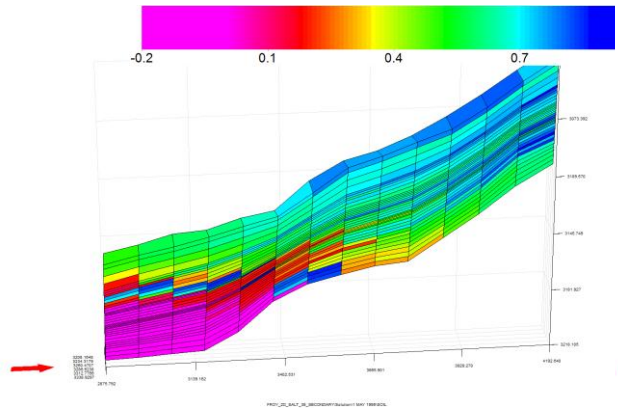

Figure 7-21: Initial oil saturation distribution in the Frøy 2D model.

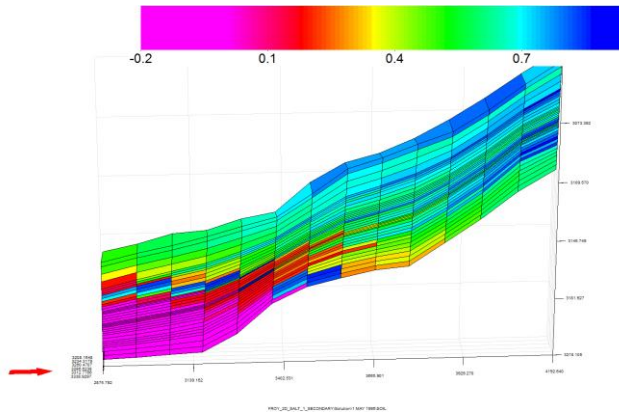

Figure 7-22: Initial oil saturation distribution in the Frøy 2D model.

It took, however, only a short period of time until large differences were seen in the oil saturation distribution. As discussed in the previous section, breakthrough of the low salinity brines in the sector model happened around April 2017. An overview of the oil saturation distribution for both cases from 1 January 2018 is therefore attached and is found in **Figure 7-23** and **Figure 7-24.** A significant difference was observed at this date. For the case where brine with 1 kg/m^3 TDS was injected, noticeable lower oil saturation was observed for large parts of the reservoir than for the case where brine with 38 kg/m^3 TDS was injected. This was probably due to a better sweep efficiency during the low salinity waterflooding compared to the conventional waterflooding as a result of the induced reduction in residual oil saturation and changes in relative permeability.

The initial residual oil saturation varies throughout the reservoir due to the End-point Scaling option, and predictions of the saturation distribution at the end of the simulation period were therefore hard to predict. After injection of brines with salinities below 5 kg/m^3 TDS, the residual oil saturation was set to decrease with 7 % of OIIP, from 0.12 to 0.05, compared to the unscaled residual oil saturations. Since more oil was produced during low salinity waterflooding than for conventional waterflooding, the reduction in residual oil saturation seems to favor the sweep efficiency in the 2D model. This is indicated in the oil saturation distribution for the end of the simulation period found in **Figure 7-25** and **Figure 7-26**. Significantly lower oil saturation was observed after the low salinity waterflooding was

conducted than the conventional waterflooding. This indicates that the initiated reduction in residual oil saturation has taken place. Due to the complexity of the reservoir, there are zones where the reduction in oil saturation is not that significant. In these zones, the oil production remains approximately equal for both types of waterfloodings. The remaining plots for the oil saturation distribution throughout the simulation period are found in **Appendix B**.

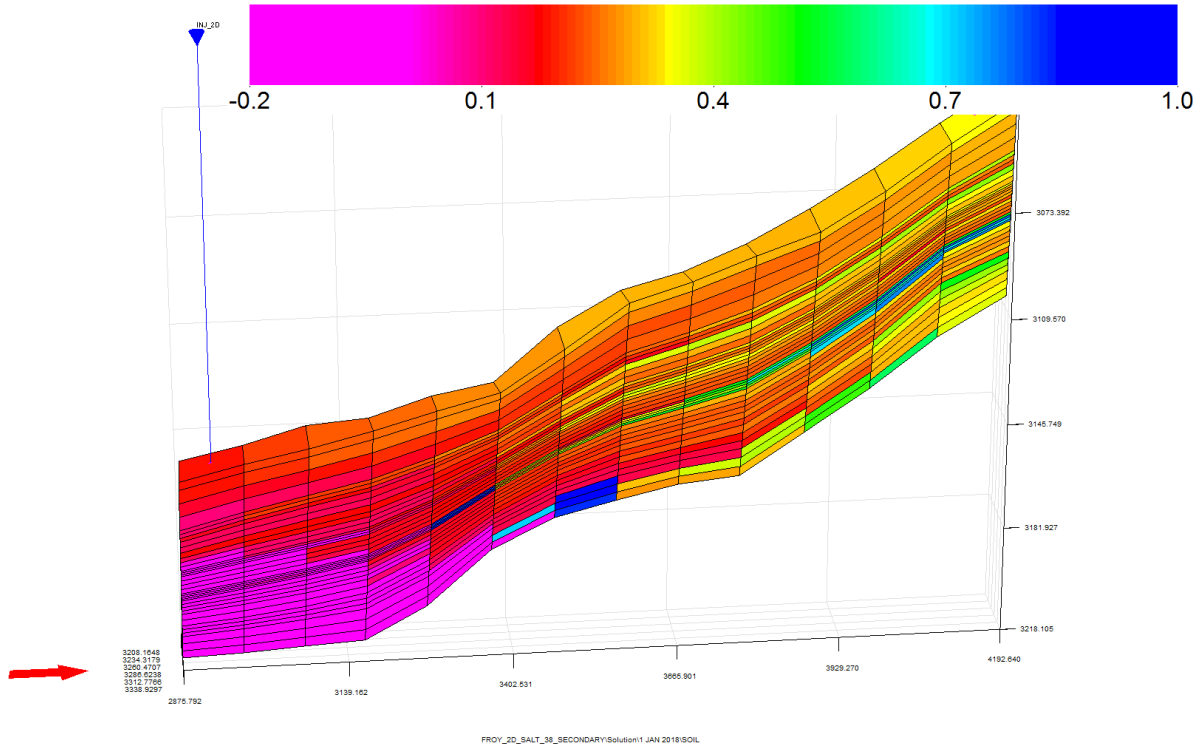

Figure 7-23: Oil saturation distribution 1 January 2018 for injection of brine with salinity of 38 kg/m^3 TDS.

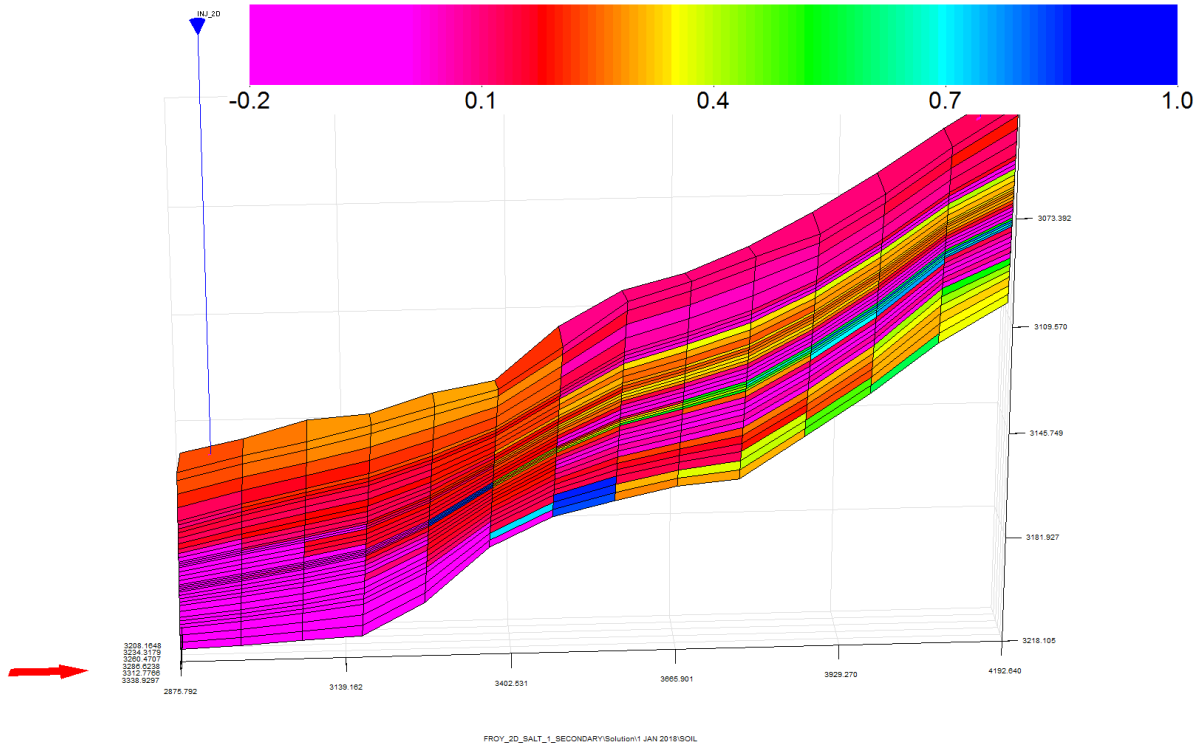

Figure 7-24: Oil saturation distribution 1 January 2018 for injection of brine with salinity of 1 kg/m^3 TDS.

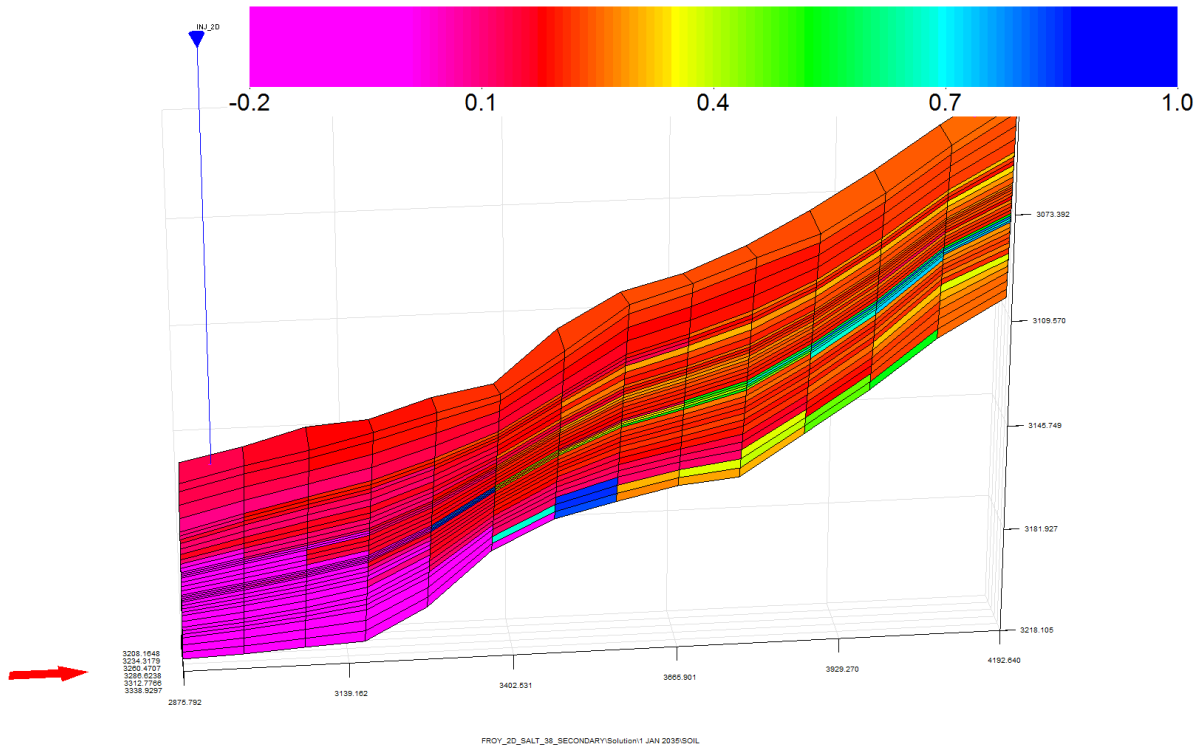

Figure 7-25: Oil saturation distribution 1 January 2035 for injection of brine with salinity of 38 kg/m^3 TDS.

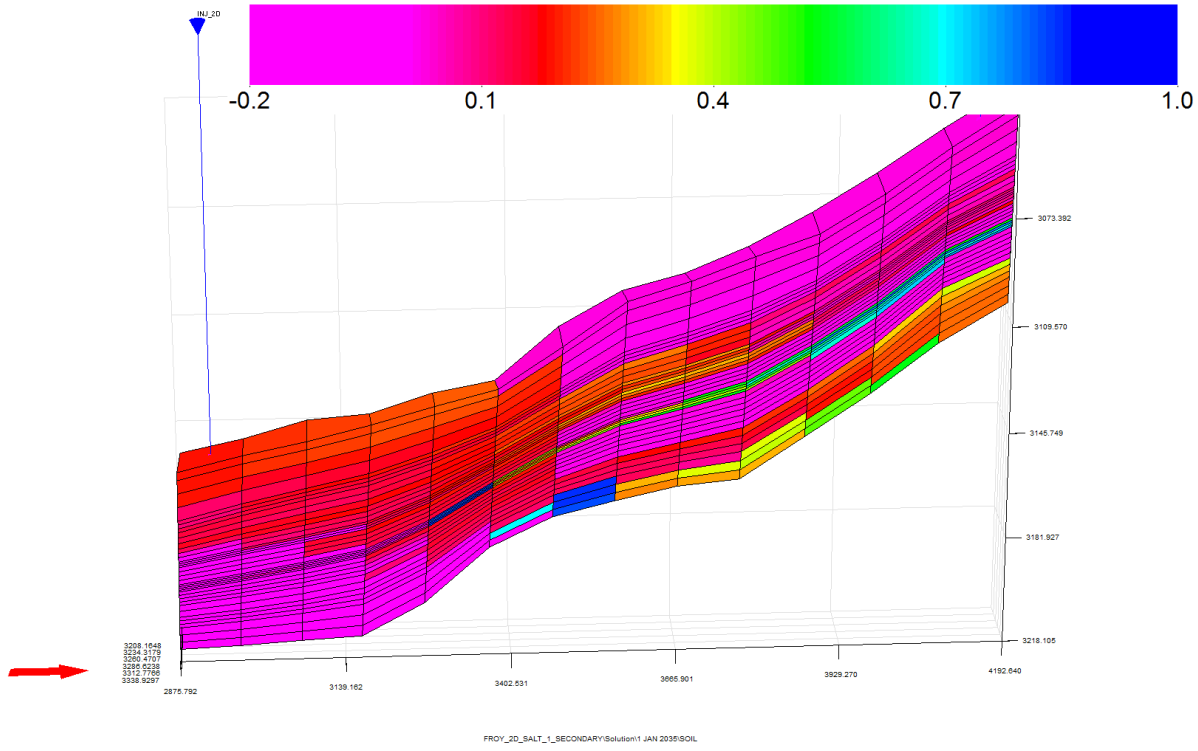

Figure 7-26: Oil saturation distribution 1 January 2035 for injection of brine with salinity of 1 kg/m^3 TDS.

7.9 Effect of Brine Salinity; Tertiary Imbibition

A base recovery was set by injection of brines with the same salinity as the initial connate water, 38 kg/m^3 TDS. On 1 January 2020 injection of brines with lower salinities were injected to investigate the potential for low salinity waterflooding as a tertiary EOR method in the Frøy field. The low salinity brines that were injected had salinities of 4, 3, 2, 1 and 0 kg/m^3 TDS. Wettabilites and capillary pressure were altered in the same way as described in **Section 7.8**. The oil recoveries, field oil efficiencies (FOE), after low salinity waterflooding are presented in **Figure 7-27.** Ultimate recoveries are found in **Figure 7-28.**

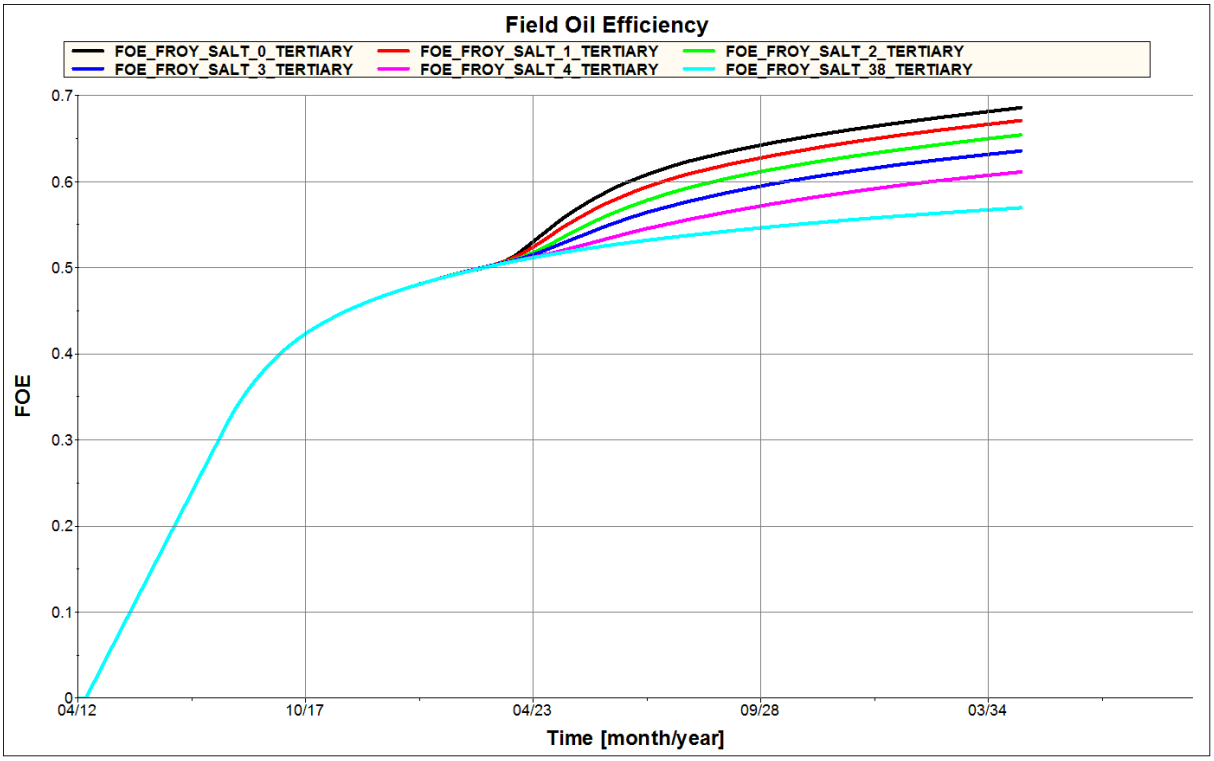

Figure 7-27: Oil recovery for tertiary LSW with injection brine salinities of 38, 4, 3, 2, 1 and 0 kg/m^3 TDS.

Brine Salinity	Oil Recovery
[kg/m3]	[%] OIIP
38	56.95
5	56.95
4	61.11
3	63.55
2	65.40
1	67.08
0	68.57

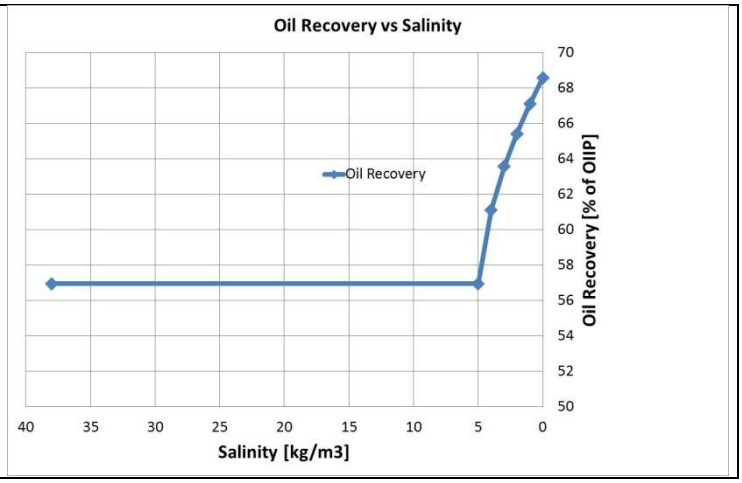

Figure 7-28: Ultimate oil recovery as a function of injection brine salinity during tertiary LSW.

A clear relationship between oil recovery and injection brine salinity was observed. With a decrease in injection brine salinity an increase in oil recovery occurred. This contributes to what is observed in some of the literature during earlier tertiary recovery by low salinity waterflooding (Lehne, 2010). The maximum incremental recovery from low salinity waterflooding was obtained after lowering the injection brine salinity to 0 kg/m^3 TDS. Oil recovery increased from around 57 to 68 %, yielding an incremental recovery of approximately 11 % after changing the injection brine salinity from 38 to 0 kg/m^3 TDS. As observed in the secondary recovery, the effect of low salinity waterflooding was not as high as in the synthetic model. The maximum increase in oil recovery was around 27 % in the synthetic model after tertiary recovery.

Even though the tertiary recovery was implemented on 1 January 2020, no difference in recovery was seen before around April 2023. This might be because it takes some time before water-breakthrough of the low salinity brines occur. This is illustrated in **Figure 7-29** where well salt production concentrations (WSPC) are found.

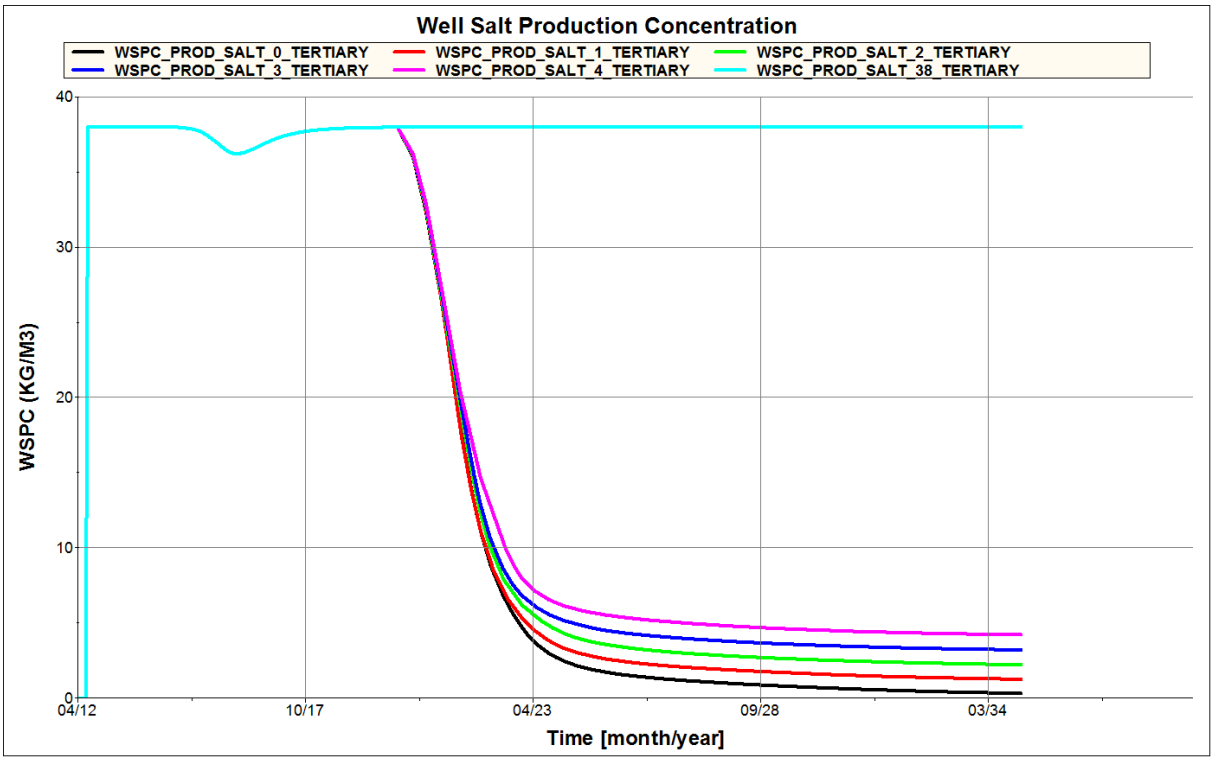

Figure 7-29: Well salt production concentration for tertiary LSW with injection brine salinities of 38, 4, 3, 2, 1 and 0 kg/m^3 TDS.

Since the effect of low salinity waterflooding was set to not start before the brine salinities were below 5 kg/m^3 TDS, no differences in recoveries were expected until the brine was lowered sufficiently. When the oil recovery starts to vary around April 2023, the brine salinities have reached low enough values for the low salinity effects to start. Another way to illustrate this is found in **Figure 7-30** and **Figure 7-31**. The field oil production rate (FOPR) for the 38 and 1 kg/m^3 TDS injection cases are plotted together with the WSPC to indicate the correlation between oil recovery and salinity. In **Figure 7-32**, oil production rate is found as a function of well salt production concentration for injection of brine with 1 kg/m^3 TDS.

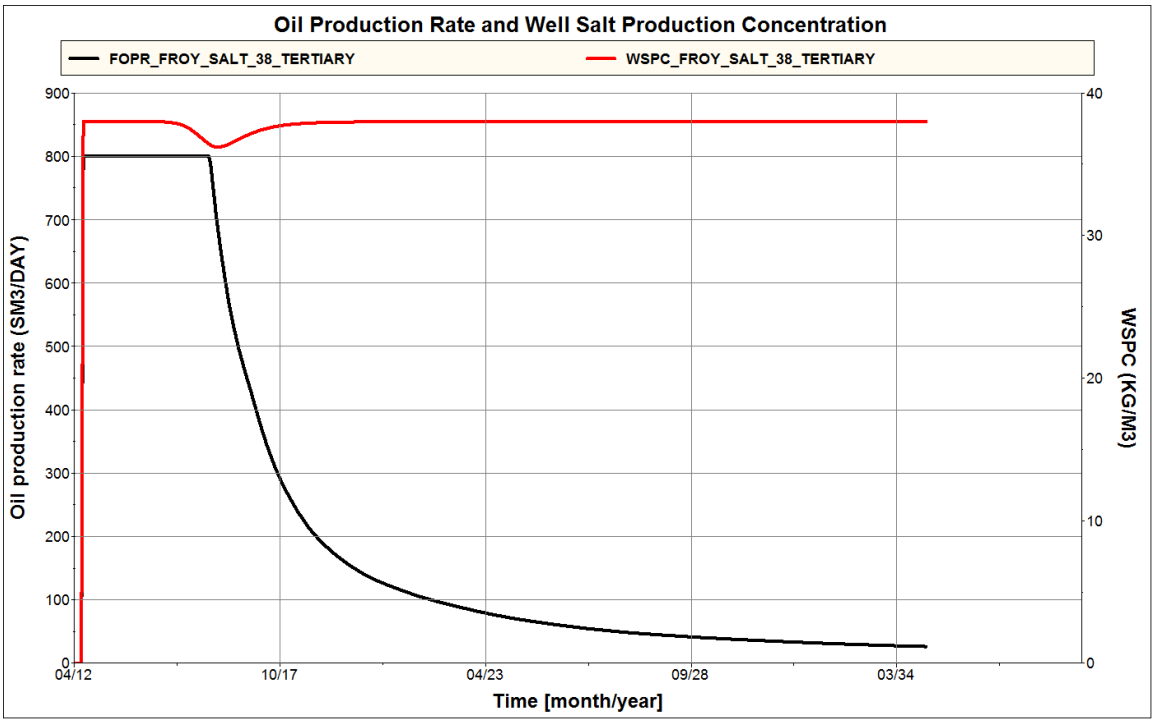

Figure 7-30: Oil production rate and well salt production salt concentration for injected brine with salinity of 38 kg/m^3 TDS during tertiary LSW.

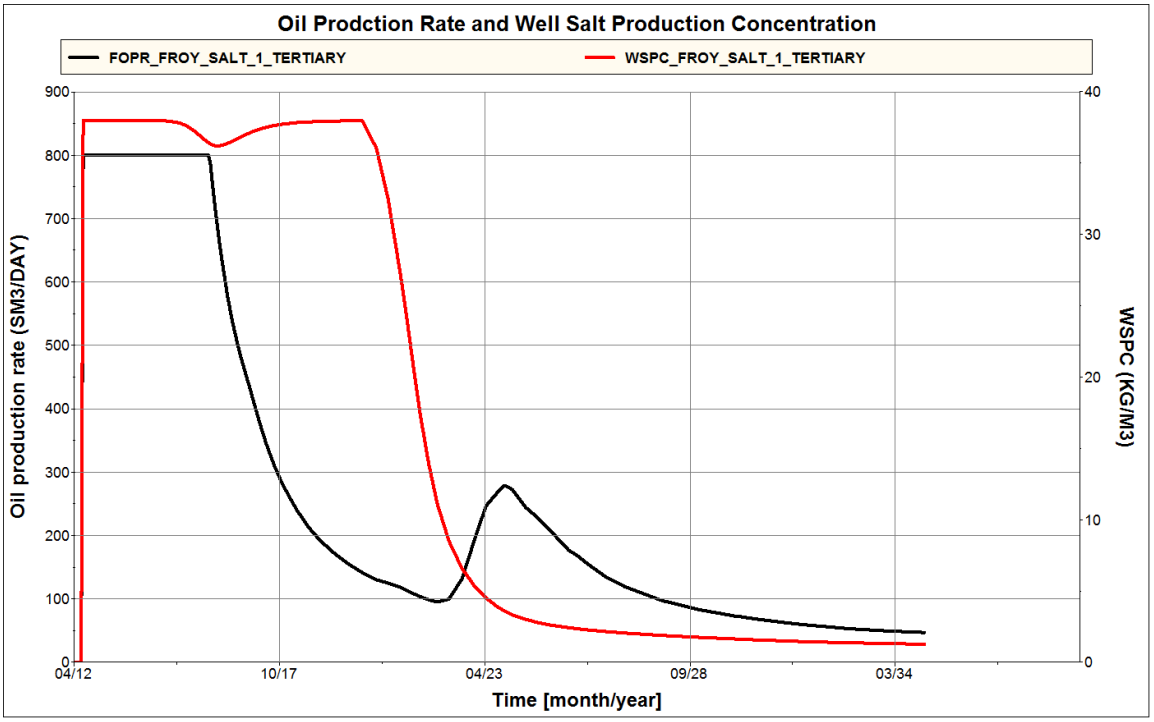

Figure 7-31: Oil production rate and well salt production salt concentration for injected brine with salinity of 1 kg/m^3 TDS during tertiary LSW.

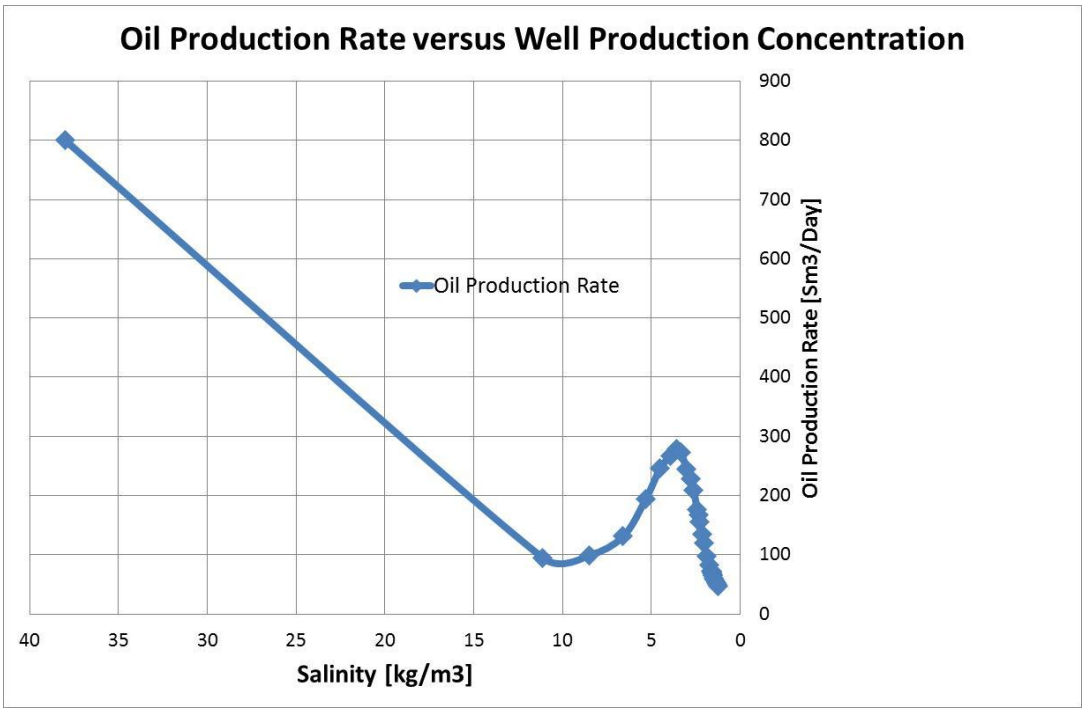

Figure 7-32: Oil production rate as a function of well salt production concentration for injection of brine with salinity of 1 kg/m^3 TDS during tertiary LSW.

When the salt concentration in the production well was kept constant at the same salinity as the initial connate water salinity, no increase in production rate during the simulation period was observed. In contrary, for the case where 1 kg/m^3 TDS was injected, the oil production rate got another peak after breakthrough of the low saline brine. The new peak, however, started somewhat before the well salt concentration was below 5 kg/m^3 TDS. This is probably because other parts of the reservoir than those close to the production well have reached salinities below the critical value.

A decrease in water cut (FWCT) was also observed during the tertiary oil recovery, and might be one of the reasons for the incremental oil recovery observed. The reduction started almost immediately after the breakthrough of the low salinity brines occurred and is illustrated in **Figure 7-33**. A rise in field gas production rate (FGPR) was also observed, and is indicated in **Figure 7-34**. One reason for this increase in gas production rate might be a result of different pressure variations in the reservoir during injection of brines with varying salinities. The initial saturation pressure was around 260 to 270 bar. During injection of the brines with low salt concentrations, the pressure in the reservoir dropped such that more gas might come out of solution and be produced. Average reservoir pressure (FPR) is seen in **Figure 7-35.**

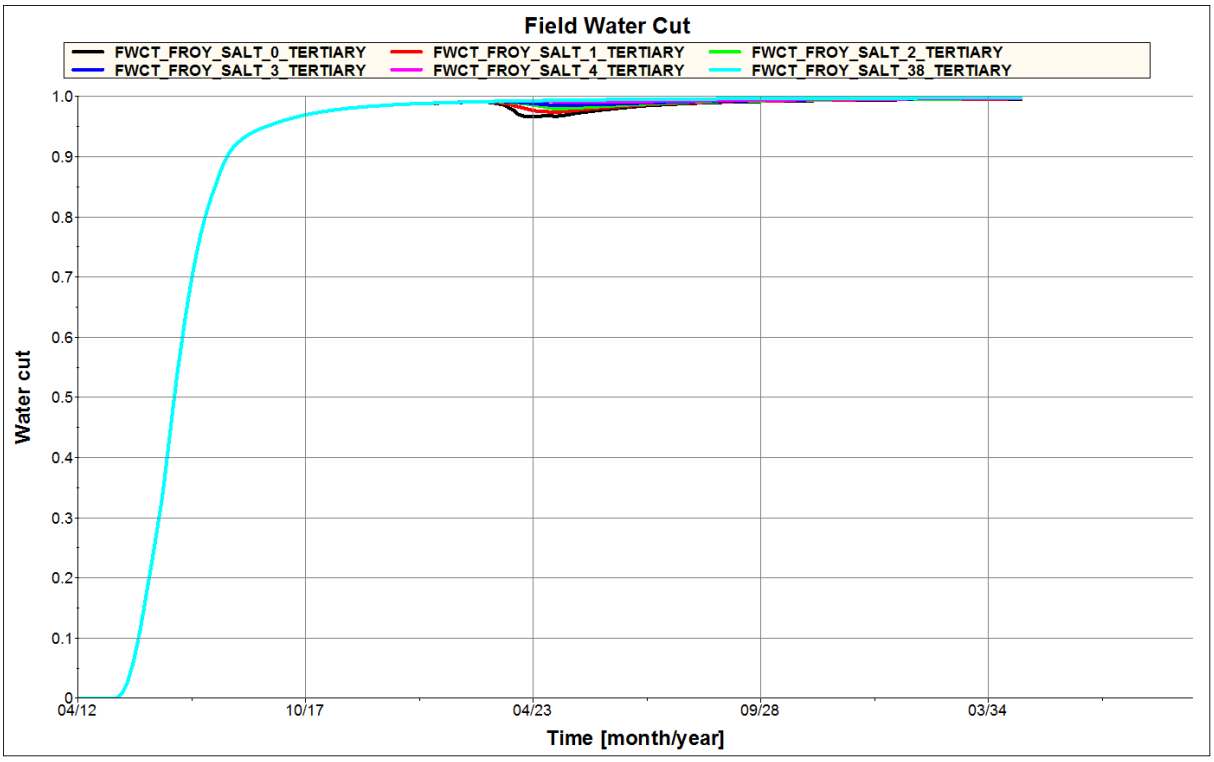

Figure 7-33: Water cut for tertiary LSW with injection brine salinities of 38, 4, 3, 2, 1 and 0 kg/m^3 TDS.

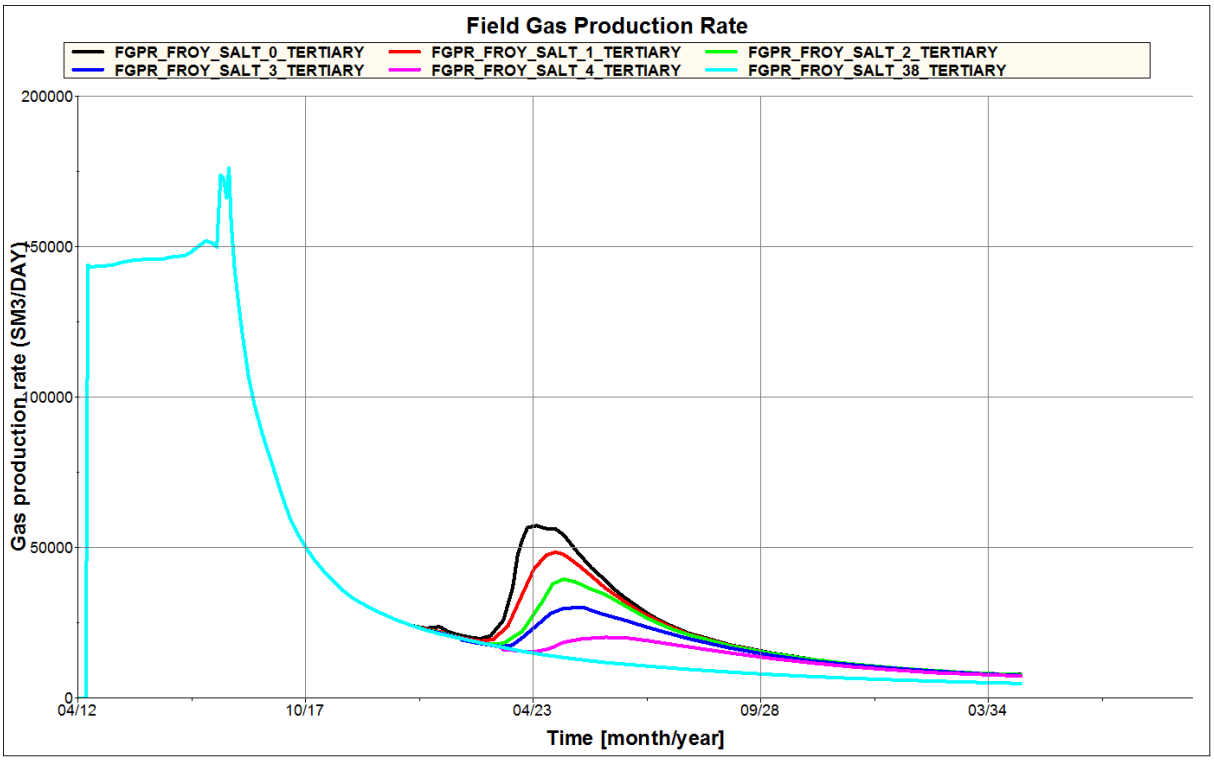

Figure 7-34: Gas production rate for tertiary LSW with injection brine salinities of 38, 4, 3, 2, 1 and 0 kg/m^3 TDS.

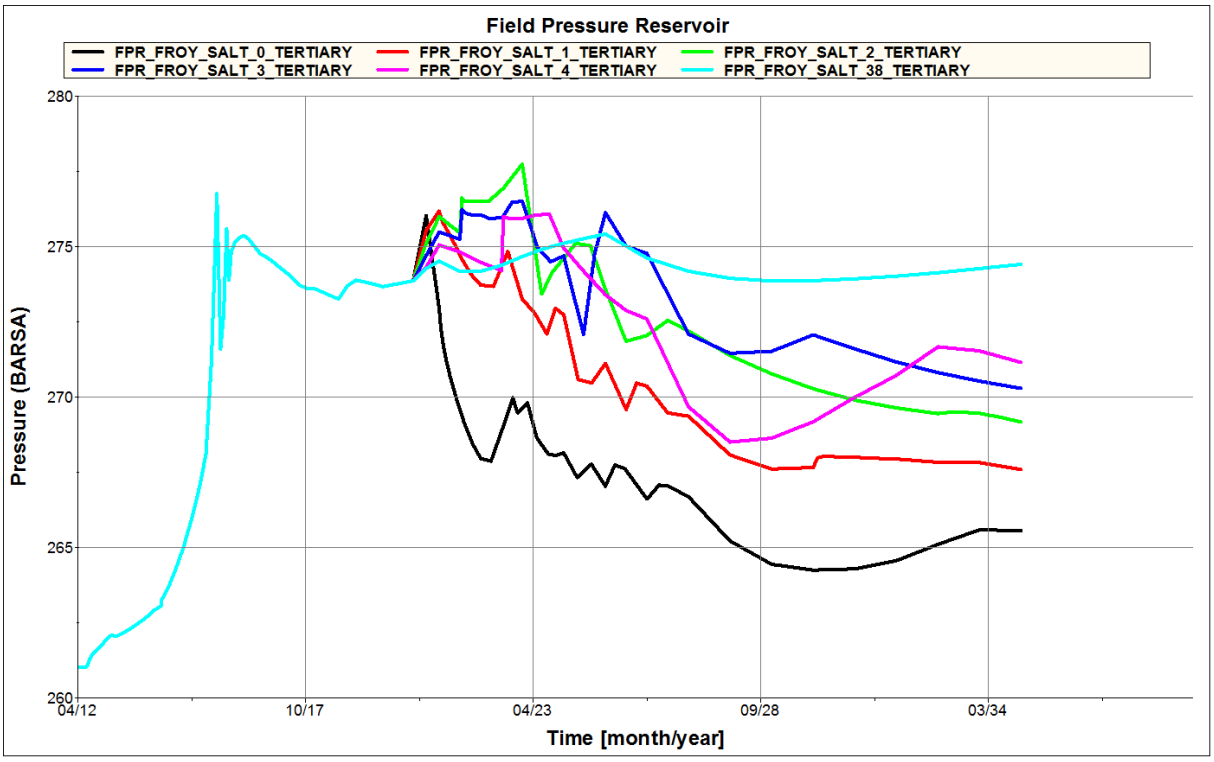

Figure 7-35: Reservoir pressure for tertiary LSW with injection brine salinities of 38, 4, 3, 2, 1 and 0 kg/m^3 TDS.

7.10 Tertiary versus Secondary Recovery by Low Salinity Waterflooding

Secondary recovery methods are implemented when the mobile oil still is in place and is conducted with external fluids, such as seawater or other augmented waterfloodings. In this model, this is launched by injection of low salinity brines immediately after initiation of the wells. Tertiary recovery methods are, on the other side, recovery after secondary recovery. It is characterized by injection of special fluids such as chemicals, miscible gases or injection of thermal energy. Tertiary recovery is initiated by injection of low salinity brines after injection of seawater in this model.

Based on the literature (Gamage and Thyne, 2011), the secondary oil recovery should be expected to be higher than the tertiary oil recovery by low salinity waterflooding. This was also the case in the synthetic model, but not very significant showing under 1 % difference in oil recovery. The results from secondary and tertiary recovery in the Frøy sector model obtained from the 1 kg/m^3 TDS waterflooding is presented in **Figure 7-36.**

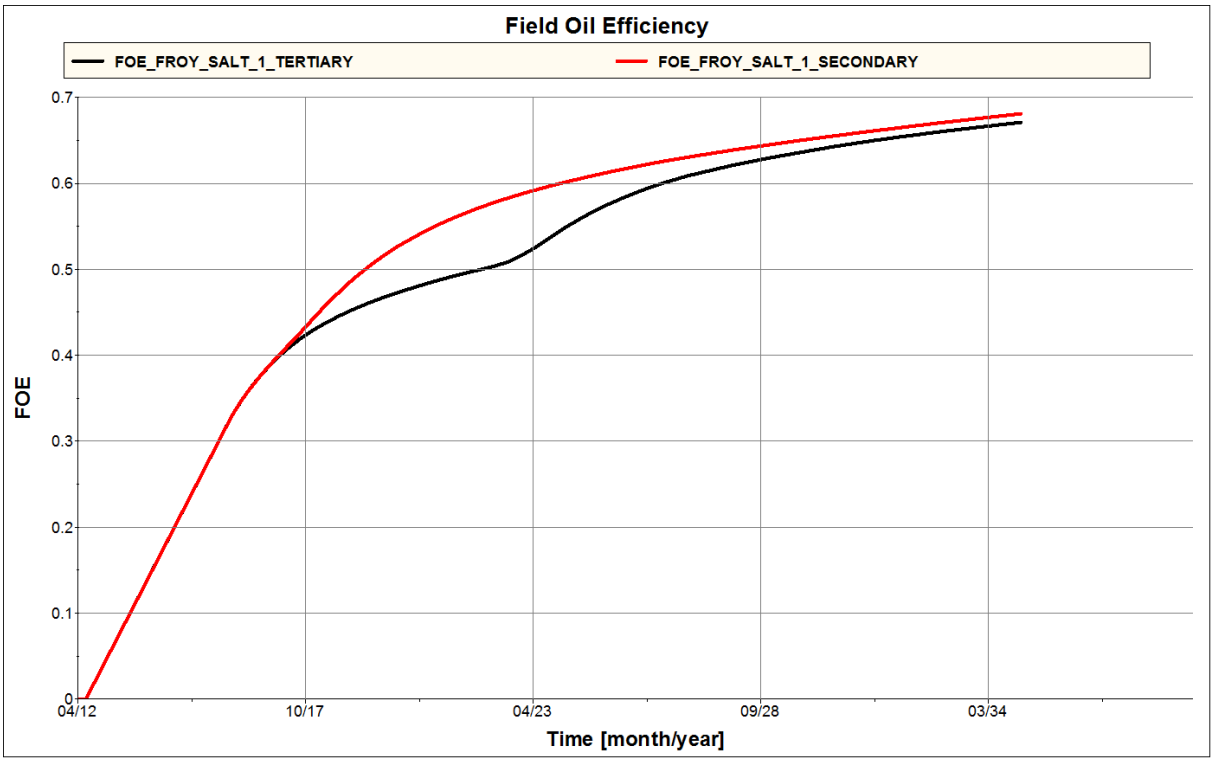

Figure 7-36: Oil recovery comparisons between secondary and tertiary LSW for injection brine salinity of 1 kg/m^3 TDS.

As indicated in **Figure 7-36**, the ultimate oil recovery varied only slightly between the secondary and tertiary oil recovery. The secondary had an ultimate oil recovery at approximately 68 % of OIIP, while the tertiary oil recovery showed an ultimate oil recovery

of approximately 67 % of OIIP. This is a smaller difference than what was observed by Gamage and Thyne (2011) during experimental investigation of the low salinity waterflooding potential during both secondary and tertiary recovery modes. The reason for this small difference in secondary and tertiary oil recovery mode in the Frøy sector model might be because both cases are given the same sets of relative permeability and saturation profiles after the low salinity waterflooding has taken place. This means that the same residual oil saturation is left in the reservoir after the waterflooding, and both recovery modes should in theory be equally efficient.

Previous tertiary laboratory experiments on the Frøy field have also proven to be effective (Lehne, 2010). Lehne experienced an up to almost 14 % incremental recovery of OIIP after reducing the salinity in the injection brine from 100 % (seawater) to 1 % (of seawater) salinity. He also observed the same incremental recovery whether seawater was injected prior to the injection of low saline brines or not. This indicated that the formation was unaffected by the seawater injection, causing no formation damage.

The main difference between secondary and tertiary recovery modes are the rate of recovery. Since the secondary recovery is conducted at an earlier phase, a quicker oil recovery than for the tertiary mode is expected. This is also the case in this model, and is illustrated by the oil production rate (FOPR) in **Figure 7-37**. Immediately after breakthrough of the low saline brines, an increase in oil recovery was seen for both recovery modes. The new production peaks were observed to occur at different times, but seemed to have similar effects on oil recovery as indicated in **Figure 7-36** for field oil efficiency.

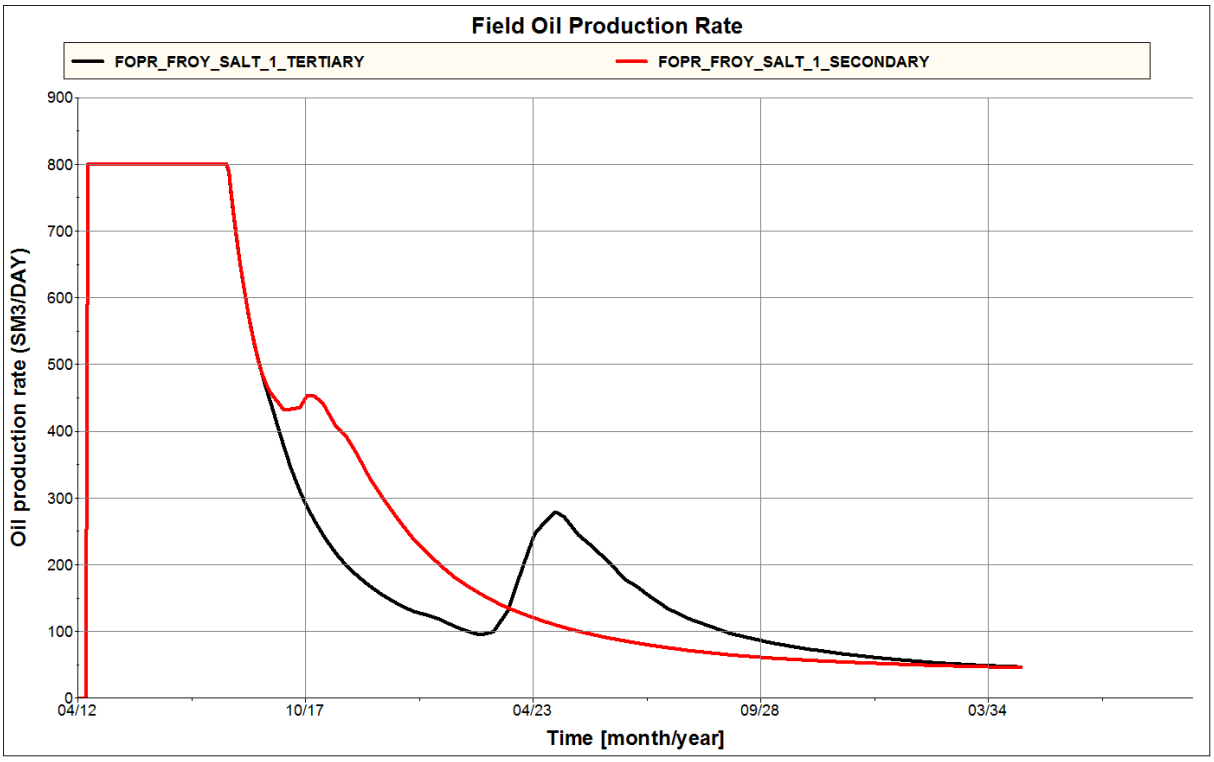

Figure 7-37: Oil production rate comparisons between secondary and tertiary LSW for injection brine salinity of 1 kg/m^3 TDS.

Even though the low saline water is cost efficient, the amount of fluids injected should be taken into consideration when the economically aspects are evaluated. A secondary recovery seems to yield only slight increase in recovery compared to the tertiary recovery mode. This even though the amount of low saline fluids injected is significantly higher.

The reason for the higher rate of recovery is as mentioned because of an earlier injection of the low salinity brine. Well salt production concentration for the two recovery modes can be found in **Figure 7-38** below. The concentration of salt in the production well undergoes the same behavior for both recovery modes, but the trend is shifted to the right for the tertiary recovery compared to the secondary recovery mode. This again can be seen in conjunction with the later injection of the low salinity brine.

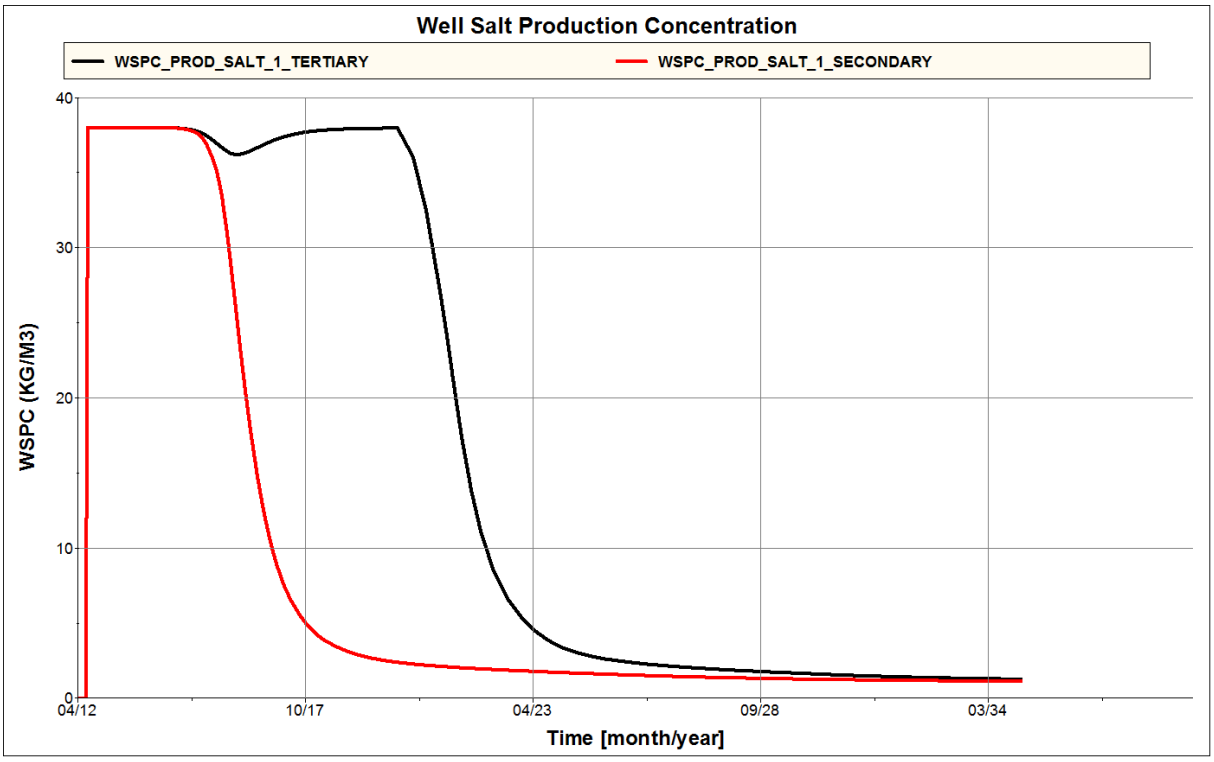

Figure 7-38: Well salt production concentration comparisons between secondary and tertiary LSW for injection brine salinity of 1 kg/m^3 TDS.

The reason for the small difference in oil recovery might be described by the water production. As seen in the earlier results presented for previous cases, the field water cut has experienced a reduction after the breakthrough of the low saline brines. In **Figure 7-39** the field water cut is found for both the tertiary and secondary recovery modes. Since the recoveries were almost similar, only small differences were observed in the water cut as well. It seems, however, that the secondary recovery experienced a somewhat less water cut than the tertiary recovery. Another way to illustrate water production is found in **Figure 7-40**, where the field water production total (FWPT) is seen. The total water production was observed to be slightly higher for the secondary than the tertiary recovery mode, indicating that this might be one the reasons for the small difference in oil recovery observed. Despite this slightly higher water production during the secondary recovery mode compared to the tertiary recovery mode, secondary produced some more oil. One reason for this might be the well control. As described in **Section 7.7**, the injection well is controlled by voidage replacement. When the production well produces more fluids, more water needs to be injected. Therefore it might be possible for the secondary recovery mode to produce both more oil and water. Total water injected (FWIT) is illustrated in **Figure 7-41**.

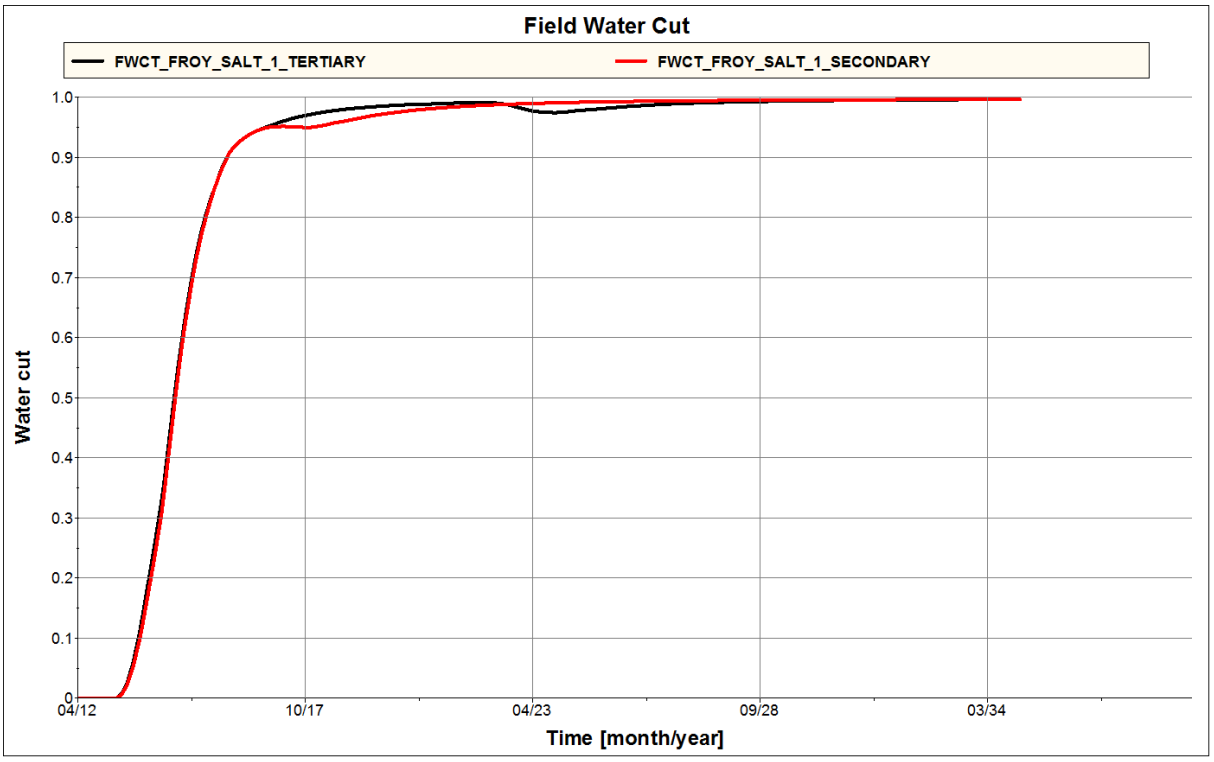

Figure 7-39: Water cut comparisons between secondary and tertiary LSW for injection brine salinity of 1 kg/m^3 TDS.

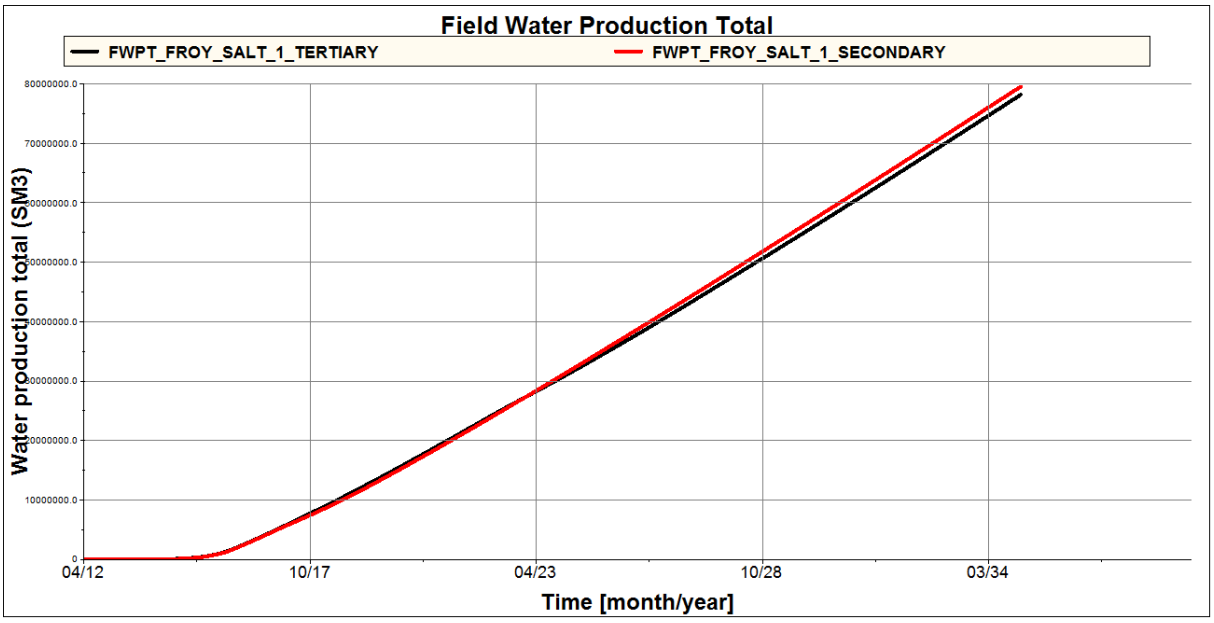

Figure 7-40: Total water production comparisons between secondary and tertiary LSW for injection brine salinity of 1 kg/m^3 TDS. Y-axis ranges from 10 000 000 to 80 000 000 SM3.

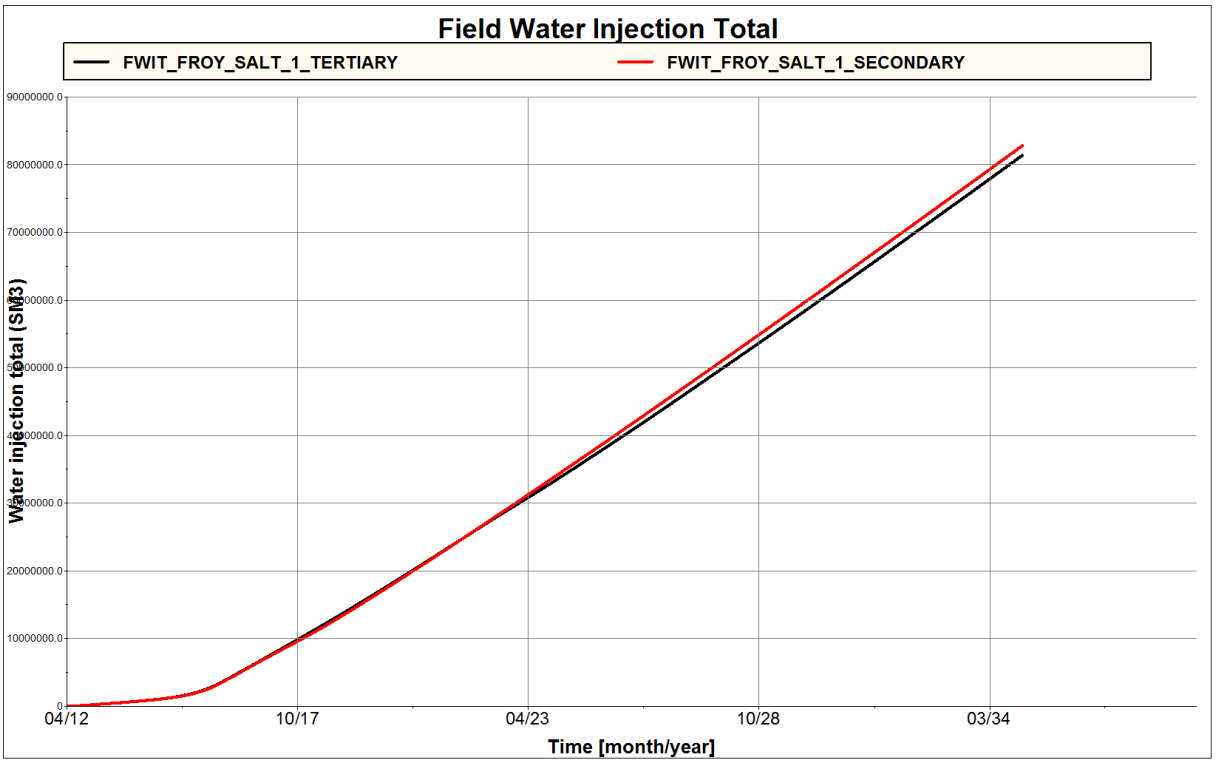

Figure 7-41: Total water injection comparisons between secondary and tertiary LSW for injection brine salinity of 1 kg/m^3 TDS. Y-axis ranges from 10 000 000 to 90 000 000 SM3.

7.11 Summary of the Results Obtained from the Frøy Field

The Frøy sector model contains large heterogeneities, and conventional waterflooding in the Frøy field has turned out not to be very efficient (Det Norske Oljeselskap, 2008). Simulated conventional waterflooding in the sector model gave a quick water breakthrough and an immediate high water cut. Injection of brines with low salinity, however, turned out to be very effective. The low salinity waterflooding yielded an incremental oil recovery up to 13 % of oil initially in place (OIIP), indicating a large potential as an EOR method in the Frøy field.

Injection of low saline brines showed similar trends as observed in the previous literature from many laboratory experiments. An increase in oil recovery was observed in conjunction with a decrease in salinity of the injected brines. The main proposed reason for the observed incremental recovery is the initiated wettability alteration towards less oil-wet conditions, with a lower water relative permeability and reduction in S_{or} during the simulation period. This alteration would enhance the sweep efficiency in the reservoir, so more oil could be produced. This is indicated in the section describing the oil saturation distribution in the reservoir. A water-wet reservoir has proven to be more efficient during waterflooding because it will let the injected water more easily imbibe into the matrix (Anderson, 1987). The injected water might then push the oil out more effectively, yielding a higher oil production by reducing the residual oil saturation. After injection of the low salinity brines, the residual oil saturation was set to decrease with 7 % of PV compared to the unscaled residual oil saturation. This gave an increase in oil recovery from approximately 57 to 70 % of OIIP during secondary recovery after lowering the injection brine salinity from 38 to 0 kg/m^3 TDS.

The tertiary oil recovery also showed similar trends to what has been observed during many laboratory experiments in the literature. A decrease in injection brine salinity caused an increase in oil recovery. The main reason for this is probably the same as for the secondary recovery mode, and the wettability alteration yielded a lower water cut and higher oil production rate. Maximum increase in oil recovery was seen after lowering the injection brine salinity from 38 to 0 kg/m^3 TDS, and resulted in an incremental oil recovery of approximately 11 % of OIIP.

Secondary oil recovery has during many laboratory experiments proved to have a significantly larger effect than tertiary recovery by low salinity waterflooding (Gamage and Thyne, 2011). This is, however, not the case in this simulated scenario. The secondary and tertiary recovery modes showed almost similar ultimate oil recovery, with approximately only 2 % difference for injection of brine with 0 kg/m^3 TDS. After the low salinity waterflooding, the same reservoir properties were given to all the grid blocks. This might be the reason why there was not observed any considerably difference in oil recovery. In addition, it should be mentioned that the simulation period has been extended to last for 23 years. During such a long simulation period, the rate of recovery does not influence the ultimate oil recovery that much. This is because both tertiary and secondary recovery modes both have reached the maximum effect of the low salinity waterflooding.

Based on previous experiments performed on cores from the Frøy field, the results seemed to be in the range of what was expected. Lehne (2010) observed an increase in recovery from tertiary low salinity waterflooding ranging from 6-14 % of OIIP. The observed reduction in S_{or} was ranging from approximately 0–11 % of PV. The increase in recovery obtained from simulation ranged from 4-13 % of OIIP depending on the salinity of the injected brines and with initiated reduction in S_{or} of 7 % of PV. It might therefore be possible to say that the results obtained from the simulations seem to be plausible.

7.12 Uncertainties

There are many uncertainties regarding simulation of low salinity waterflooding in the Frøy sector model. No effect of numerical dispersion has been investigated, but due to limitations in the simulator other things might as well give erroneous predictions.

As mentioned in **Section 3.3** a number of mechanisms have been proposed for trying to describe the reasons for the observed increase in recovery after low salinity waterflooding. The main factors controlling the effect from low salinity waterflooding seems to be the amount of clay present in the reservoir and the presence and the salinity of connate water. Even though it has been proved that there are some clay present in the reservoir (Lehne, 2010), there is no way to simulate the behavior of the clay. There might be large variations of the clay content and clay types throughout the reservoir. Since the effect of low salinity waterflooding during the simulations is set to be approximately equal for each grid block,

however, these variations might be overseen. The initial connate water saturation is on the other side more accurately measured, and large variations are implemented in the model. Similarities were also added for the connate water salinity, and all possible heterogeneities were neglected.

The End-point Scaling option included in the model makes the reservoir fluid behavior more heterogeneous and the predictions more difficult. When End-point Scaling is used, the high salinity tables are first scaled to these points before being used in the low salinity model. Even though the scaling does not apply to the low salinity tables (Schlumberger, 2011), large variations of the low salinity effects might occur within grid cells during the simulation of low salinity waterflooding. The wetting phases will somewhat vary throughout the reservoir, and the proposed decrease in residual oil saturation might not be equal in all the grid cells. This is also described in **Section 7.4**, where critical oil saturation both with respect to water and gas displacement was allowed to vary between 10 and 45 %.

Little data from laboratory experiments after low salinity waterflooding are available from the Frøy field. Lehne (2010) presented a reduction in residual oil saturation and relative permeability with a decrease in salinity of the injected brine, but no exact wettability measurements have been conducted after injection of low saline brines. This makes the predictions difficult since the data added for the low salinity waterflooding options are just illustrative. Even though the results obtained from laboratory experiments seems to be in the range of what was observed during the simulations, it should be mentioned that the data after low salinity waterflooding is not experimental data.

The capillary pressure after the low salinity waterflooding is set to be equal to the capillary pressure used during conventional waterflooding. No capillary pressure measurements have been conducted, and instead of making up new data it was decided to keep the capillary pressure constant throughout the simulation period. This is probably not a realistic scenario, since the capillary pressure would most likely change in conjunction with the changes in relative permeability and saturation profiles.

The oil saturation distribution obtained from the Frøy 2D model might not show very accurate results. The same well controls, as applied in the Frøy sector model, have been initiated and these values might not be representable for such a small model. Despite this,

some indications of a more efficient waterflooding during low salinity than conventional might nevertheless be seen.

7.13 Conclusion

By use of the options available in ECLIPSE 100 and data available from previous laboratory observations, a wettability alteration towards less oil-wet conditions were initiated in a Frøy field sector simulation model. This was done to investigate the potential for low salinity waterflooding as an EOR mechanism at the Frøy field. Even though the reasons for the observed effects after injection of brines with different salinities still are being discussed, it seems like the wettability alteration is the most likely explanation.

Based on the observed results from low salinity waterflooding in both the sector and a 2D model from the Frøy field, the potential for low salinity waterflooding as an EOR method seems to be exciting. The results obtained under the conditions used in the simulation model showed a large salinity dependency. A significant increase in oil recovery was seen in conjunction with a decrease in injection brine salinity. A maximum incremental recovery of 13 % of OIIP was obtained after lowering the injection brine salinity from 38 to 0 kg/m^3 TDS during secondary recovery mode. The reason for the observed increase in oil recovery was most likely the induced wettability alteration towards less oil-wet conditions. This alteration resulted in a reduction in residual oil saturation and water relative permeability which again resulted in a more efficient oil displacement by waterflooding. This more efficient oil displacement was thought to be due to a reduced water cut and hence lower water production.

Both secondary and tertiary recovery modes resulted in almost similar incremental oil recovery after low salinity waterflooding. If the economically aspects are considered, however, tertiary recovery mode is recommended because smaller volumes of low saline brines need to be injected.

7.14 Recommendations for Further Work

No real measurements have been performed on relative permeability, capillary pressure and wettability after low salinity waterflooding on core samples from the Frøy field. Previous experiments have only shown a decrease in relative permeability and residual oil saturation, but no exact wettability tests have been conducted. A natural next step would be to perform

new experiments and conduct such measurements. Data from these proposed experiments could further on be used as input in reservoir simulators for accurate predictions of the low salinity waterflooding potential in the Frøy field. This requires, however, more laboratory experiments from different zones and depths in the reservoir to investigate which of the zones it would be preferable to use low salinity waterflooding as an EOR mechanism.

The simulation model used in this project is just a sector model, and does only conclude that low salinity waterflooding is an interesting EOR mechanism in a small part of the Frøy field. A full field model is required to investigate the whole field potential, but the sector model does on the other side give indications of the fluid behavior and possible changes in the reservoir properties. For zones in the full field model that contain similar reservoir properties, the results would probably be in the same range. I would recommend to do simulations in the full field model to verify these effects.

As indicated in **Section 6.6**, the amount of low saline fluids that should be injected is necessary to investigate if the economically aspects are considered. Seccombe et al. (2008) showed that at low saline pore slug of 40 % of PV was the most optimum slug size for low salinity brine injection for the case of interest. It was mentioned, however, that this might vary for other reservoirs with different brine composition, exchange capacity or dispersivity and that they may require different slug sizes. It might therefor be useful to investigate the most optimum slug size for the Frøy field to optimize the feasibility of the reservoir.

The accuracy of the ECLIPSE 100 simulator has not been investigated with respect to numerical dispersion and other sources of error. It is therefore recommended to investigate the accuracy by changing the number of grid cells or to compare results obtained from ECLIPSE 100 with results obtained from other simulators. This might reduce or potentially remove possible simulation errors.

8. Numenclature

BV = Bulk volume, L^3, cm^3 [cc]

Bg = Gas formation volume factor

Bo = Oil formation volume factor

Bw = Water formation volume factor

$CaCO_3$ = Calcium carbonate

Ca^{2+} = Calcium ion

CO_3^{2-} = Carbonate ion

C_s = Salt concentration in the aqueous phase

E_o = Empirical parameter in the Corey Model

E_w = Empirical parameter in the Corey Model

F1 = Function of salt concentration

F2 = Function of salt concentration

f_w = Fractional flow of water

f_{aq} = Fractional flow of an aqueous phase

f_p = Fractional flow of polymer

H^+ = Hydrogen atom

H_2O = Water molecule

HCO_3^- = Hydrogen carbonate

k = Absolute permeability, L^2, mD [m^2]

k_{rf} = Relative permeability of a fluid, fraction

k_{ro} = Relative permeability of oil, fraction

k_{rw} = Relative permeability of water, fraction

N_o = Empirical parameter in the Corey Model

N_w = Empirical parameter in the Corey Model

OH^- = Hydroxide

P_{cd} = Drainage threshold pressure, m/Lt^2, bar [Psi]

P_{cow} = Oil-water capillary pressure, m/Lt^2, bar [Psi]

P_g = Gas pressure, m/Lt^2, bar [Psi]

PV = Pore volume, L^3, cm^3 [cc]

$P_{none\text{-}wetting}$ = Pressure of none-wetting phase, m/Lt^2, bar [Psi]

P_o = Oil pressure, m/Lt^2, bar [Psi]

P_w = Water pressure, m/Lt^2, bar [Psi]

$P_{wetting}$ = Pressure of wetting phase, m/Lt^2, bar [Psi]

Q_w = Flow rate of water, L^3/t, cc/hr

Q_t = Total flow rate, L^3/t, cc/hr

S_{or} = Residual oil saturation, fraction

S_{owcr} = Critical oil saturation in water

S_{wco} = Connate water saturation

S_{wi} = Initial water saturation, fraction

S_{wmax} = Maximum water saturation

S_* = Normalized water saturation

T = Transmissibility

V_g = Volume of gas, L^3

V_i = Volume of a fluid phase, L^3

V_o = Volume of oil, L^3

V_w = Volume of water, L^3

Greek Letters:

ϕ = Porosity [fraction]

ϕ_f = Porosity [fraction]

μ = Viscosity [cP]

μ_o = Viscosity of oil [cP]

$\mu_{s\,eff}$ = Effective viscosity of the salt

μ_w = Viscosity of water [cP]

θ = Contact angle [°]

ΔP = Differential pressure, m/Lt^2, bar [Psi]

$\Delta P/\Delta x$ = Pressure gradient [bar/m]

ρ_w = Density of water [g/cc]

Abbreviations:

COBR = Crude Oil Brine Rock

BHP = Bottom hole pressure

EOR = Enhanced Oil Recovery

FGPR = Field gas production rate

FOE = Field oil efficiency

FOPR = Field oil production rate

FPR = Field pressure reservoir

FVF = Formation volume factor

FWCT = Field water cut

FWIT = Field water injection total

FWPT = Field water production total

GOC = Gas oil contact

LS = Low salinity

LSB = Low salinity brine

LSI = Low salinity injection

LSW = Low salinity waterflooding

MIE = Multicomponent ionic exchange

OIIP = Oil initially in place

OOIP = Original oil in place

OWC = Oil water contact

RB = Reservoir brine

SCAL = Special core analyses

SWAG = Simultaneous water and gas (injection)

SWCTT = Single well chemical tracer test

TDS = Total dissolved salts

TVD = True vertical depth

WC = Water cut

WSPC = Well salt production concentration

9. References

AlSofi, A., M and Blunt, M., J. 2010. Control of Numerical Dispersion in Simulations of Augmented Waterflooding. Paper SPE 129658 presented at the 2010 SPE Improved Oil Recovery Symposium, Tulsa, Oklahoma, USA, 24-28 April 2010.

Anderson, W, G. 1987. Wettability Literature Survey – Part 6: The Effects of Wettability on Waterflooding. *Journal of Petroleum Technology 39* (12) 1605-1622. SPE-16471-PA.

Ashraf, A., Hadia, N., Torsæter, O. and Tweheyo, M.T. 2010. Laboratory Investigation of Low Salinity Waterflooding as Secondary Recovery Process: Effect of Wettability. Paper SPE 129012 presented at the SPE Oil and Gas India Conference and Exhibition, Mumbai, India, 20-22 January 2010.

Austad, T., RezaeiDoust, A, and Puntervold, T. 2010. Chemical Mechanism of Low Salinity Water Flooding in Sandstone. Paper SPE 129767 presented at the 2010 SPE Improved Oil Recovery Symposium, Tulsa, Oklahoma, USA, 24-28 April 2010.

Behrenbruch, P, and Goda, H, M. 2006. Two-Phase Relative Permeability Prediction: A Comparison of the Modified Brooks-Corey Methodology with a New Carman-Kozeny Based Flow Formulation. Paper SPE 101150 presented at the 2006 SPE Asia Pacific Oil & Gas Conference Exhibition, Adelaide, Australia, 11-13 September 2006.

Bernard, G.G. 1967. Effect of Floodwater Salinity on Recovery of Oil from Cores Containing Clays. Paper SPE1725 presented at the 38th Annual Californian Regional Meeting of the Society of Petroleum Engineers of AIME, Los Angeles, California, U.S.A. 26-27 October, 1967.

Deans, H.A. and Carlisle, C. Single Well Chemical Tracer Test Handbook, second edition. Laramie, Wyoming.

Det Norske Oljeselskap. 2012. Introduction to Frøy Reservoir Engineering. Det Norske Oljeselskap (Unpublished).

Eclipse Simulation Software Manuals. 2011. Schlumberger.

Fanchi J.R. 1983. Multidimensional Numerical Dispersion. *SPE journal* 23 (1) 143-151. SPE-9018-PA.

Filoco, P, R. and Sharma, M, M. 1998. Effect of Brine Salinity and Crude Oil Properties on Relative Permeabilities and Residual Saturations. Paper SPE 49320 presented at the 1998 SPE Annual Meeting, New Orleans, Los Angeles, U.S.A September 1998.

Frøy Redevelopment Project Plan for Development and Operation. August 2008. Det Norske Oljeselskap ASA and Premier Oil Norge AS.

Gamage, P. and Thyne, G. 2011. Comparison of Oil Recoveries by Low Salinity Waterflooding in Secondary and Tertiary Recovery Modes. Paper SPE 147375 presented at the SPE Annual Technical Conference, Denver, Colorado, U.S.A, 30 October – 2 November 2011.

Hadia, N., Lehne, H.H., Kumar ,K.G., Selboe, K., Stensen, J.Å. and Torsæter, O. 2011. Laboratory Investigation of Low Salinity Waterflooding on Reservoir Rock Samples from the Frøy Field. Paper SPE 141114 presented at the SPE Middle East Oil and Gas Show and Conference, Manama, Bahrain, 20-23 March 2011.

Hansen, T. 2011. Laboratory Investigation of Low Salinity Waterflooding as a Tertiary Recovery Process: Effect of Crude Oil Composition. Master Thesis, Norwegian University of Science and Technology, Trondheim, Norway.

Jerauld, G.R., Lin, C.Y., Webb, K.J and Seccombe, J.C. 2008. Modeling Low-Salinity Waterflooding. Paper SPE 102239 presented at the 2006 SPE Annual Technical Conference an Exhibition, San Antonio, Texas, 24-27 September.

Joel, C. 2010. Numerical Simulation of Low Salinity Waterflooding Wettability Alteration for Enhances Oil Recovery. Master Thesis, Norwegian University of Science and Technology, Trondheim, Norway.

Lager, A., Webb, K.J., Black, C. J.J., Singleton, M. and Sorbie, K.S. 2006. Low Salinity Oil Recovery – An Experimental Investigation. Paper SCA2006-36 presented at the International Symposium of the Society of Core Analysts, Trondheim, Norway, 12-16 September 2006.

Lager, A., Webb, K.J., Collins, I.R. and Richmond, D.M. 2008. LoSal^{TM} Enhanced Oil Recovery: Evidence of Enhanced Oil Recovery at the Reservoir Scale. Paper SPE 113976 presented at the 2008 SPE/DOE Improved Oil Recovery Symposium, Tulsa, Oklahoma, U.S.A., 19-23 April 2008.

Lehne, H. H. 2010. Low salinity Waterflooding. An Experimental Investigation of the Potential in the Frøy Field in the North Sea. Master Thesis, Norwegian University of Science and Technology, Trondheim, Norway.

McGuire, P.L., Chatman, J.R., Paskvan, F.K., Sommer, D.M. and Carini, F.H. 2005. Low Salinity Oil Recovery: An Exciting New EOR Opportunity for Alaska's North Slope. Paper SPE 93903 presented at the 2005 SPE Western Regional Meeting, Irvine, California, U.S.A, 30 March – 1 April 2005.

Morrow, N. 1990. Wettability and Its Effect on Oil Recovery. *J. Pet Tech 42 (12): 1476-1484.* SPE-21621-PA.

Morrow, N. and Buckley, J. 2011. Improved Oil Recovery by Low-Salinity Waterflooding. *J. Pet Tech 63 (5): 106-112*. SPE -129421-PA.

Morrow, N.R, Valat, M. and Yildiz, H. 1996. Effect of Brine Composition on Recovery of an Alaskan Crude Oil by Waterflooding. Paper SPE 96-94 presented at the 47th Annual Technical Meeting of the Petroleum Society, Calgary, Alberta, Canada, 10- 12 June 1996.

Nasralla, R, A., Alotaibi, M, B. and Nasr-El-Din, A. 2011. Efficiency of Oil Recovery by Low Salinity Water Flooding in Sandstone Reservoirs. Paper SPE 144602 presented at the SPE Western North American Regional Meeting, Anchorage, Alaske, U.S.A, 7-11 May 2011.

Petrophysics and Surface Chemistry Group, Petroleum Recovery Research Centre, New Mexico Tech. 2005. An Introduction to Wettability of Oil Reservoirs: http://baervan.nmt.edu/research_groups/petrophysics/group/intro-to-wettability.pdf

RezaeiDoust, A., Pentervold, P. and Austad, T. 2010. A discussion of the Low Salinity EOR potential for a North Sea Sandstone Field. Paper SPE134459 presented at the SPE Annual Technical Conference and Exhibition, Florence, Italy, 19-22 September 2010.

Rivet, S.M, Lake, L.W. and Pope, G.A. 2010. A Coreflood Investigation of Low-Salinity Enhanced Oil Recovery. Paper SPE 134297 presented at the SPE annual Technical Conference and Exhibition, Florenze, Italy, 19-22 September 2010.

Sadikhzada, Abulfaz. 2010. Simulation of Low Salinity Waterflooding in Simple Models. Semester project, Norwegian University of Science and Technology, Trondheim, Norway.

Seccombe, J.C., Lager, A., Webb,K., Jerauld, G. and Fueg, E. 2008. Improving Waterflood Recovery: LoSal^{TM} EOR Field Evaluation. Paper SPE 113480 presented at the 2008 SPE/DOE Improved Oil Recovery Symposium, Tulsa, Oklahoma, U.S.A., 19-23 April 2008.

Serhat, A. 2001. Estimation of fracture relative permeabilities from unsteady state corefloods. Journal of Petroleum Science and Engineering 30 (2001) 1-14.

Sheng, J.J. 2011. Modern Chemical Enhanced Oil Recovery: Theory and Practice. Kidlington, Oxford: Gulf Professional Publishing.

Skrettingland, K., Holt, K., Tweheyo, M.T and Skjevrak, I. 2011. Snorre Low-Salinity-Water Injection – Coreflooding experiments and Single-Well Field Pilot. Paper SPE 129877 presented at the SPE Improved Oil Recovery Symposium, Tulsa, 24-28 April 2011.

Tang, G, Q. and Morrow, N, R. 1997. Salinity, Temperature, Oil Composition, and Oil Recovery by Waterflooding. Paper SPE 36680 presented at the 1996 SPE Annual Technical Conference and Exhibition, Denver, Colorado, U.S.A 6-9 October, 1996.

Tang, G-Q. and Morrow, N.R. 1999. Influence of brine composition and fines migration on crude oil/brine/rock interactions on oil recovery. Journal of Petroleum Science and Engineering 24 (1999) 99-111.

Tiffin, D, L., Stein, M, H. and Wang, X. 2003. Drawdown Guidelines for Sand Control Completions. Paper SPE 84495 presented at the SPE Annual Technical Conference and Exhibition, Denver, Colorado, U.S.A 5-8 October 2003.

Torsæter, O. and Abtahi, M. 2003. Experimental Reservoir Engineering Laboratory Work Book, Norwegian University of Science and Technology, Trondheim, Norway.

Torsæter, O. 2012. Reservoir Engineering of Naturally Fractured Reservoir, First Part: Fractured Reservoir Description and Geometry. Norwegian University of Science and Technology, Trondheim, Norway.

Vledder, P., Fonseca, J, C., Wells, T., Gonzalez, I. and Ligthelm, D. 2010. Low Salinity Water Flooding: Proof of Wettability Alteration On A Field Wide Scale. Paper SPE 129564 presented at the 2010 SPE Improved Oil Recovery Symposium, Tulsa, Oklahoma, U.S.A, 24-28 April 2010.

Wu, Y-S. and Bai, B. 2009. Efficient Simulation for Low-Salinity Waterflooding in Porous and Fractured Reservoirs. Paper SPE 118830 presented at the 2009 SPE Reservoir Simulation Symposium, The Woodlands, Texas, USA, 2-4 February 2009.

Zumdahl, S.S. 2009. Chemical Principles, Sixth Edition. University of Illinois, Brooks/Cole, Cengage Learning.

APPENDICES

10. Appendix A: Frøy Field Reservoir Properties

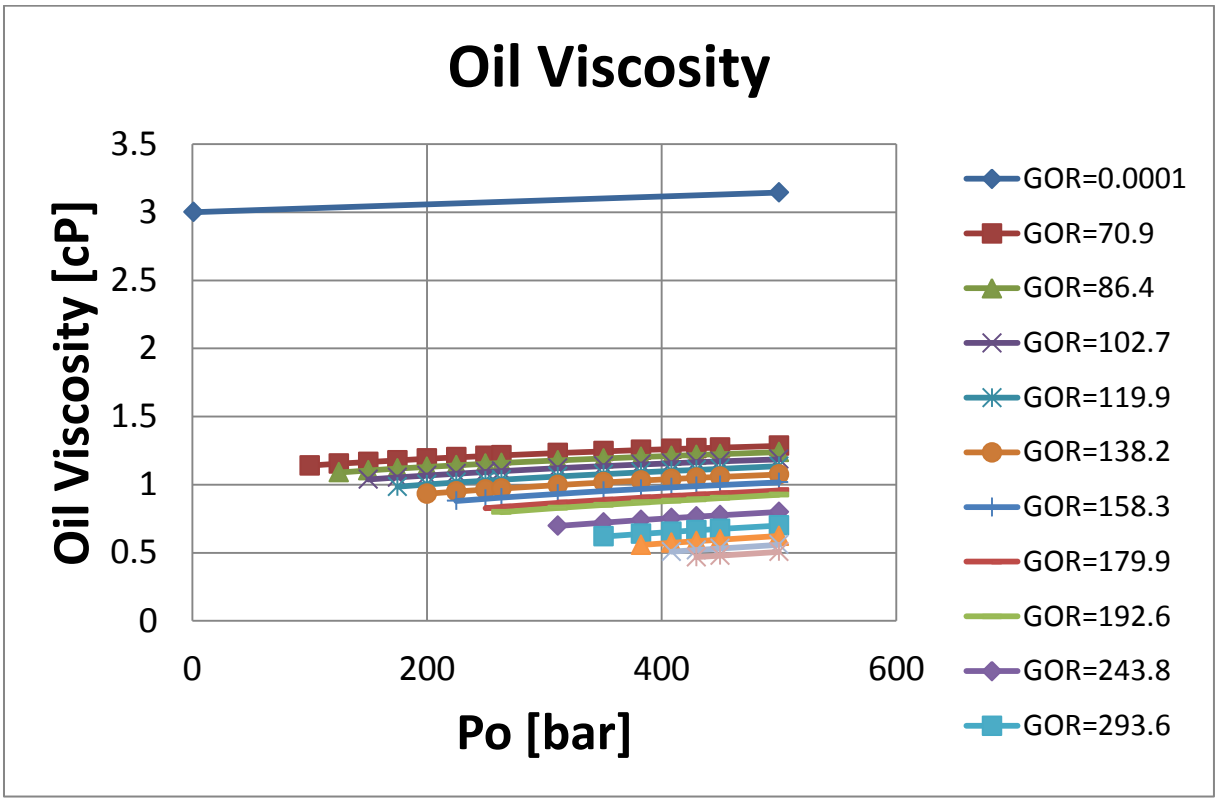

Figure 10-1: Oil viscosity versus oil pressure for different GOR.

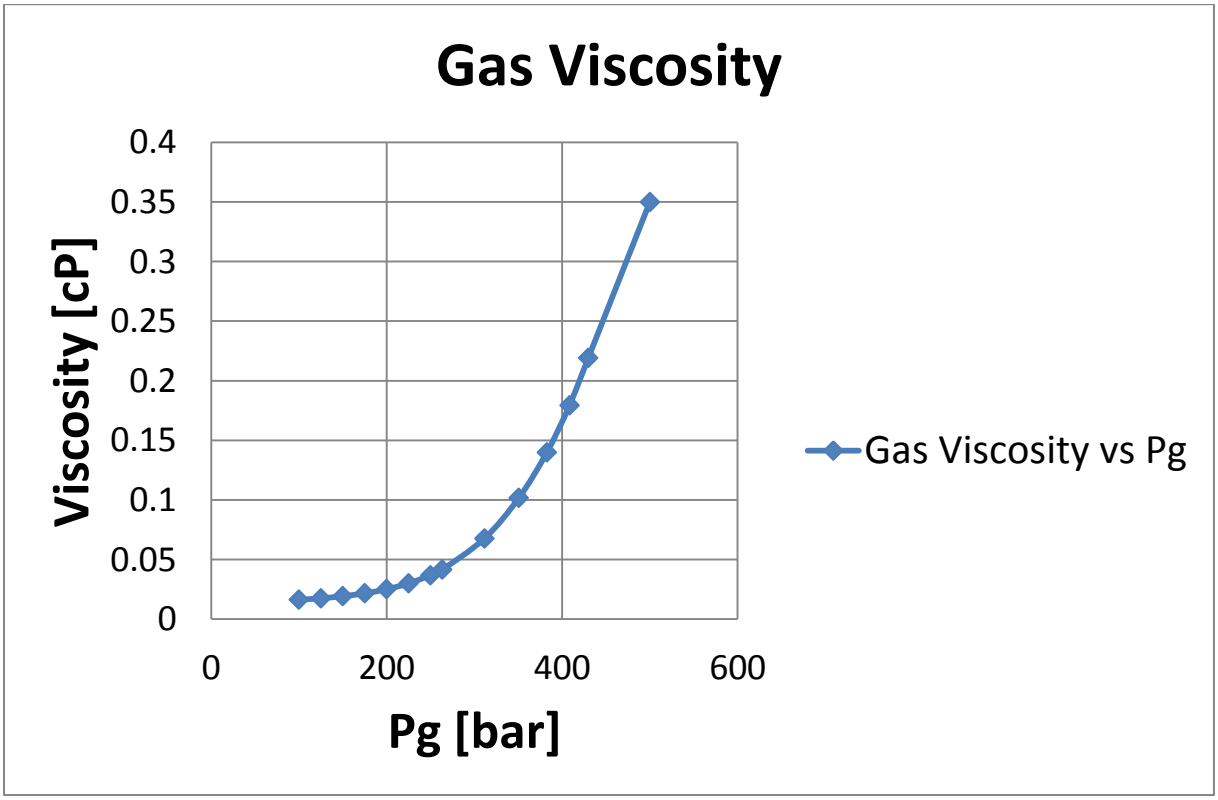

Figure 10-2: Gas viscosity versus gas pressure.

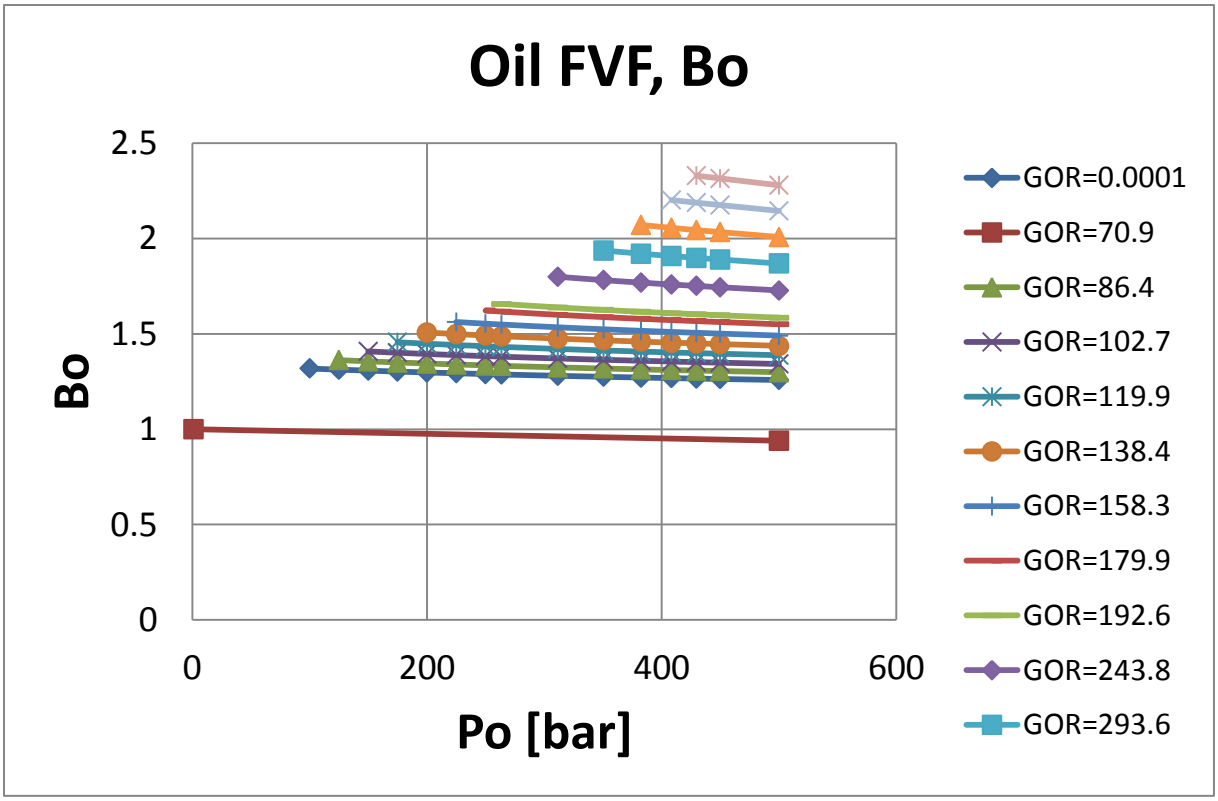

Figure 10-3: Bo versus oil pressure for different GOR.

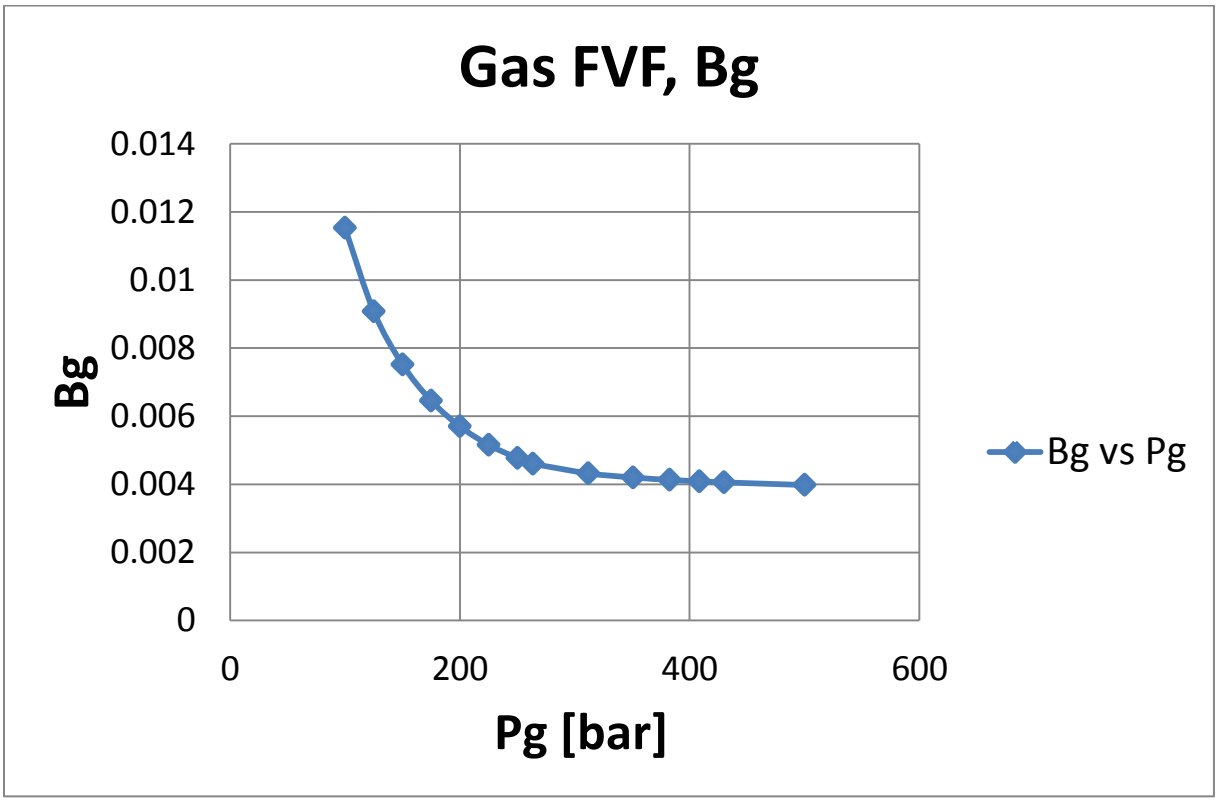

Figure 10-4: Bg versus gas pressure.

11. Appendix B: Frøy Field Oil Saturation Distribution

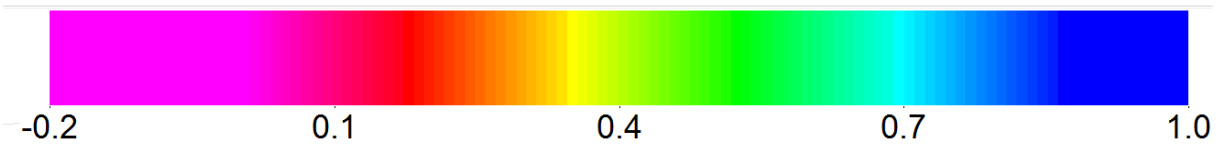

Year: 1995

Salinity of injection brine:

1 kg/m^3 TDS

38 kg/m^3 TDS

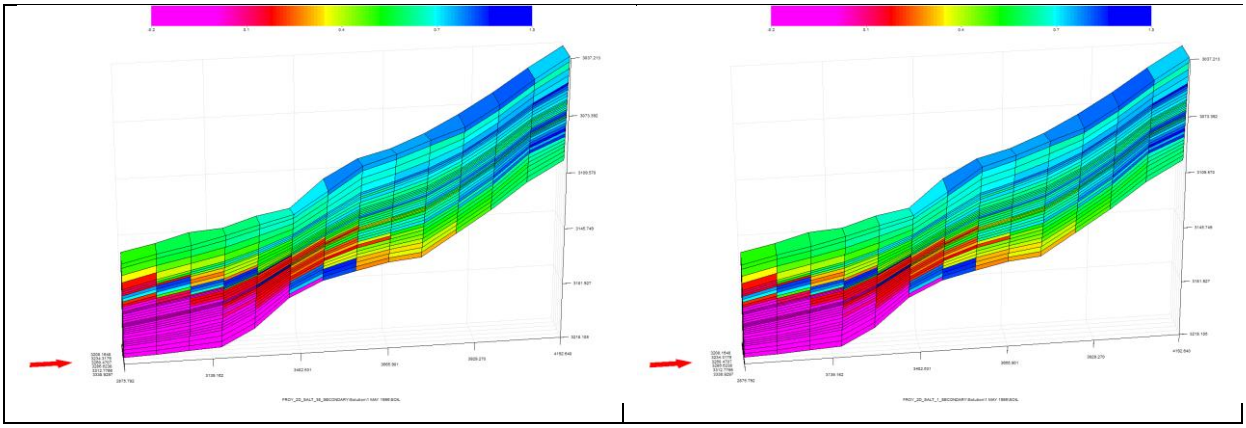

Figure 11-1: Oil saturation for different salinities 1995.

Year: 2012

Salinity of injection brine:

1 kg/m^3 TDS

38 kg/m^3 TDS

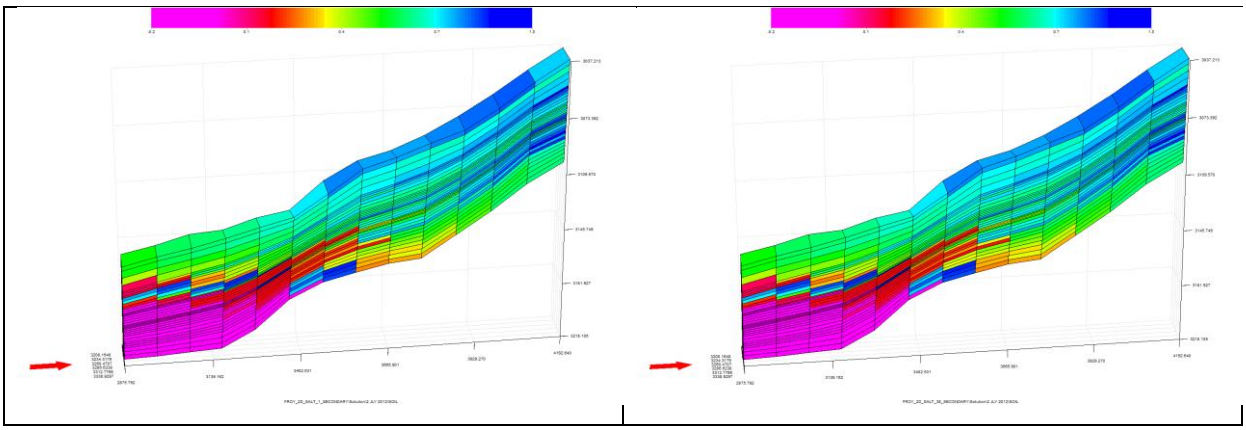

Figure 11-2: Oil saturation for different salinities 2012.

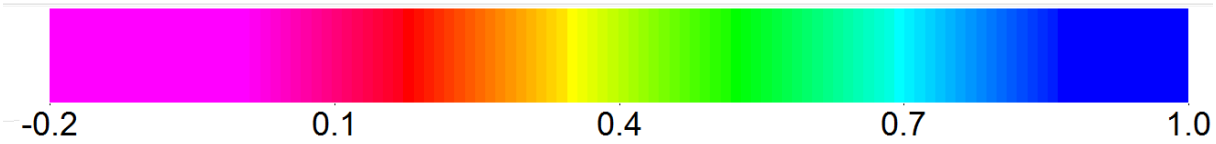

Year: 2013

Salinity of injection brine:

1 kg/m^3 TDS

38 kg/m^3 TDS

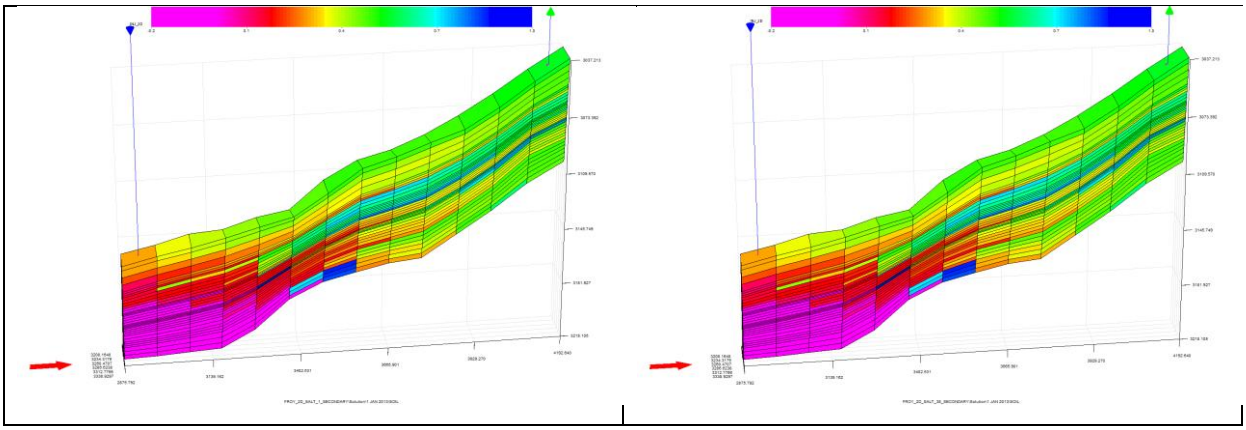

Figure 11-3: Oil saturation for different salinities 2013.

Year: 2014

Salinity of injection brine:

1 kg/m^3 TDS

38 kg/m^3 TDS

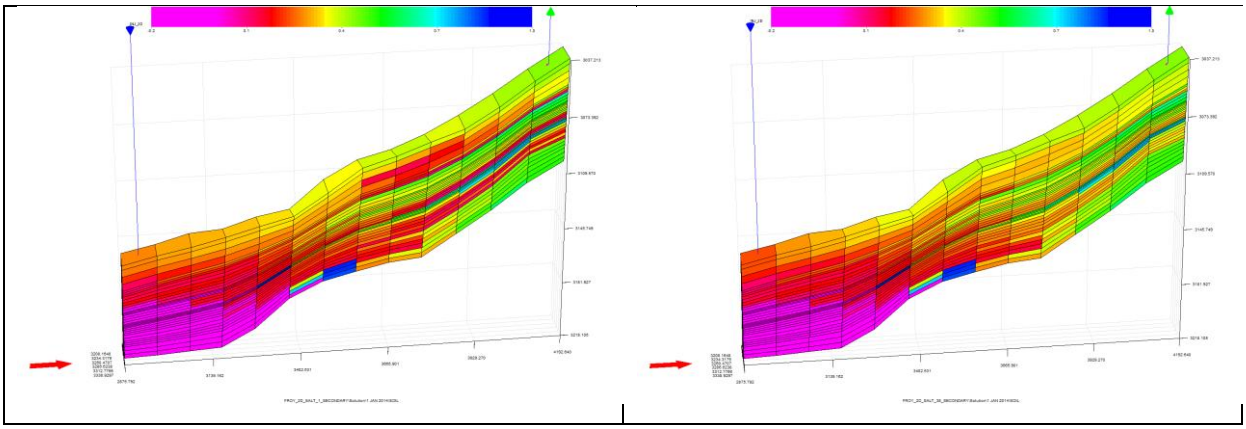

Figure 11-4: Oil saturation for different salinities 2014.

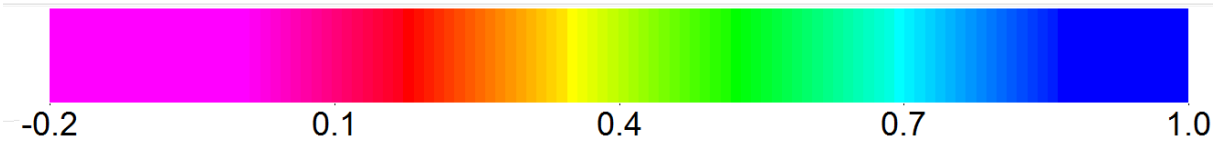

Year: 2015

Salinity of injection brine:

1 kg/m^3 TDS

38 kg/m^3 TDS

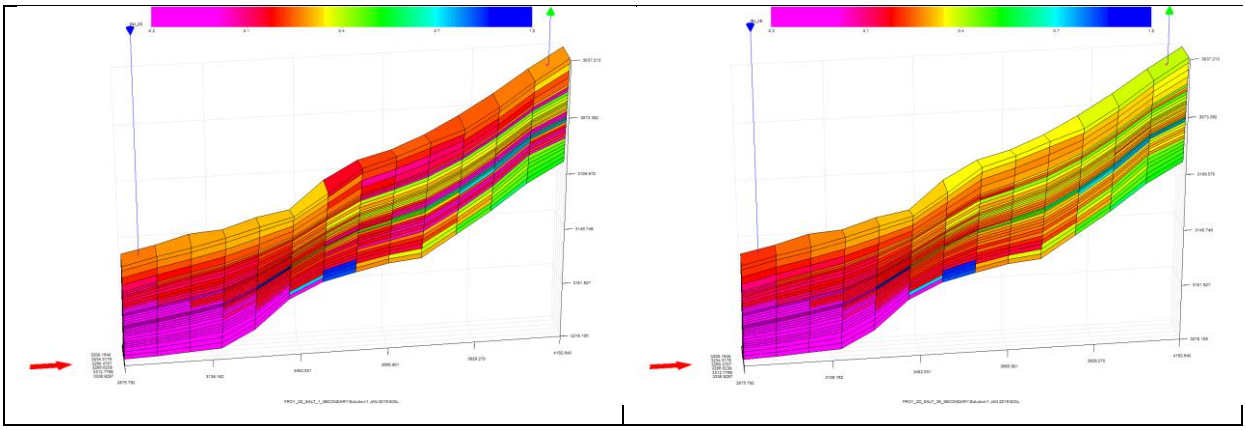

Figure 11-5: Oil saturation for different salinities 2015.

Year: 2016

Salinity of injection brine:

1 kg/m^3 TDS

38 kg/m^3 TDS

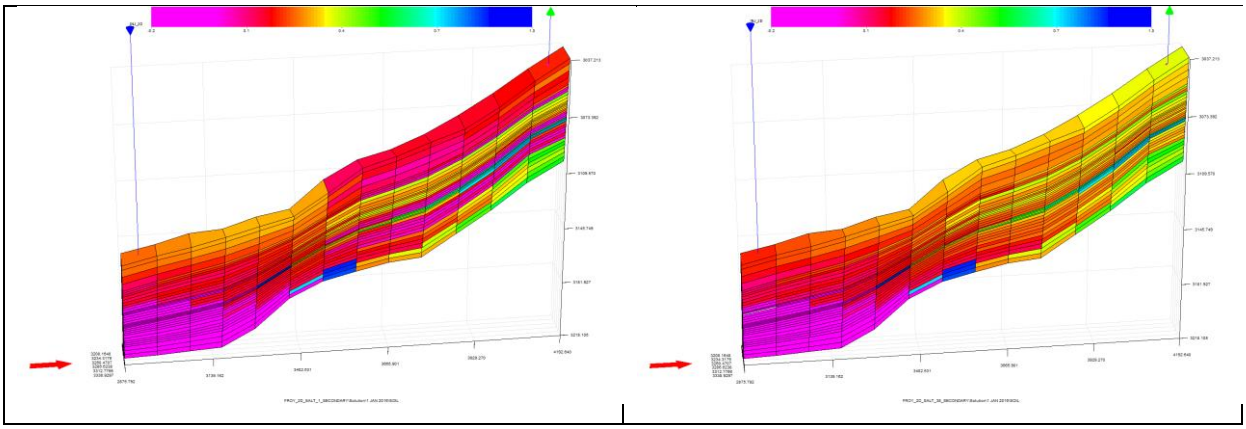

Figure 11-6: Oil saturation for different salinities 2016.

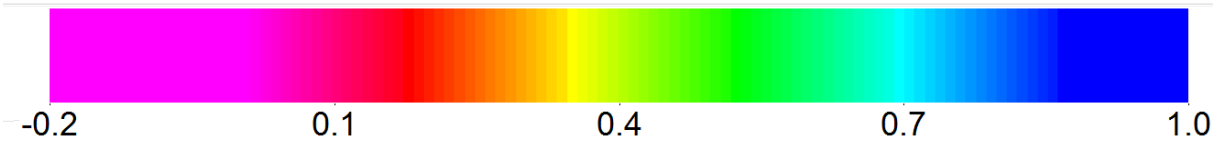

Year: 2017

Salinity of injection brine:

1 kg/m^3 TDS

38 kg/m^3 TDS

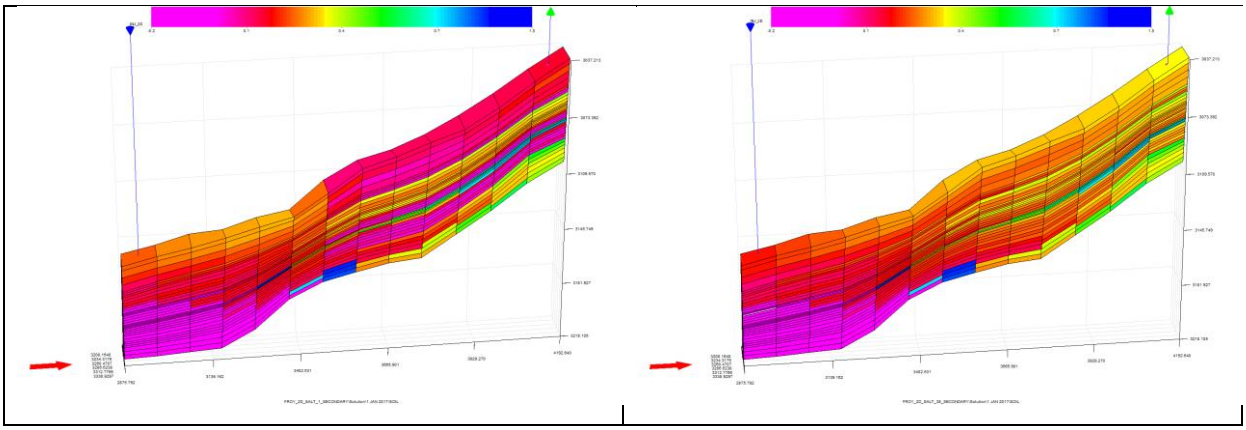

Figure 11-7: Oil saturation for different salinities 2017.

Year: 2018

Salinity of injection brine:

1 kg/m^3 TDS

38 kg/m^3 TDS

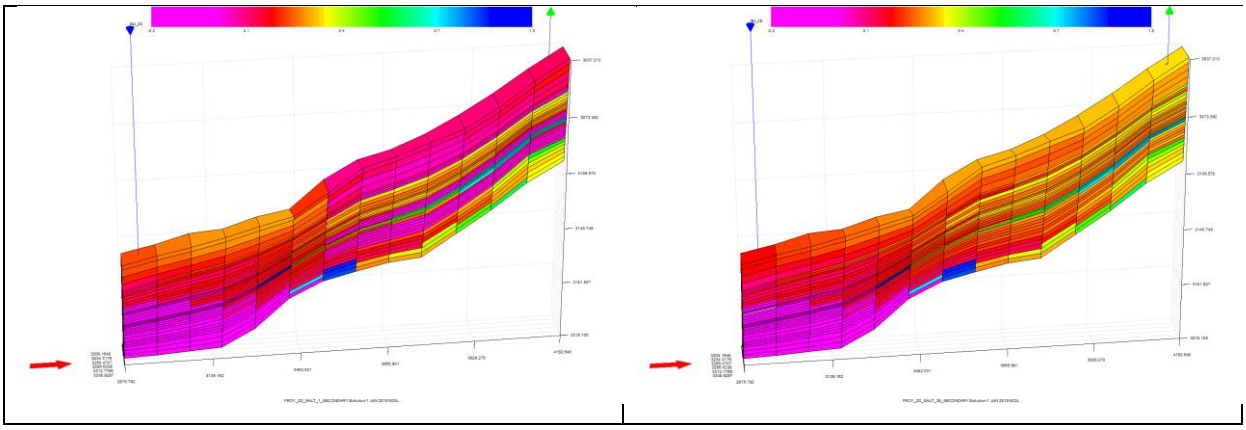

Figure 11-8: Oil saturation for different salinities 2018.

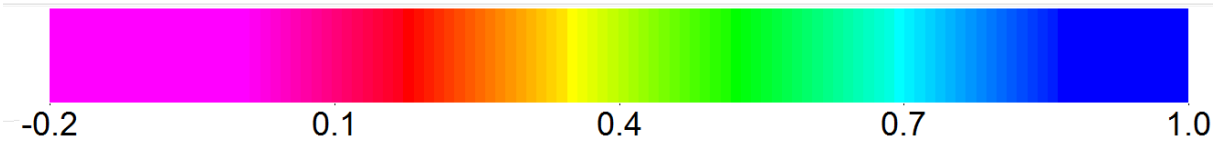

Year: 2019

Salinity of injection brine:

1 kg/m^3 TDS

38 kg/m^3 TDS

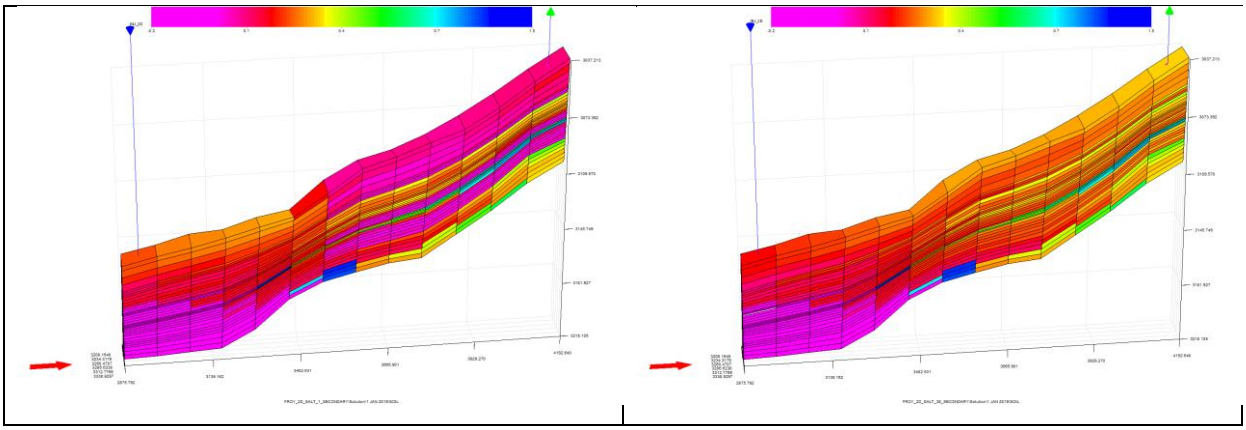

Figure 11-9: Oil saturation for different salinities 2019.

Year: 2020

Salinity of injection brine:

1 kg/m^3 TDS

38 kg/m^3 TDS

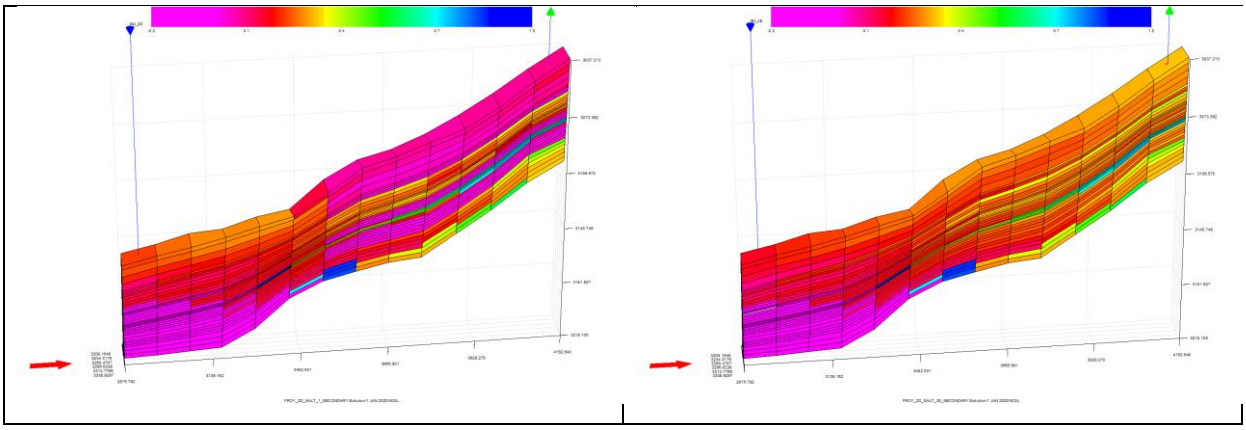

Figure 11-10: Oil saturation for different salinities 2020.

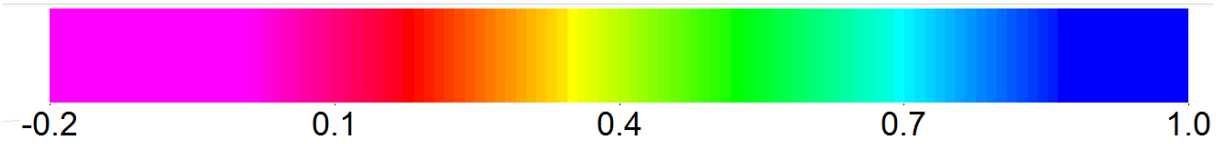

Year: 2021

Salinity of injection brine:

1 kg/m^3 TDS

38 kg/m^3 TDS

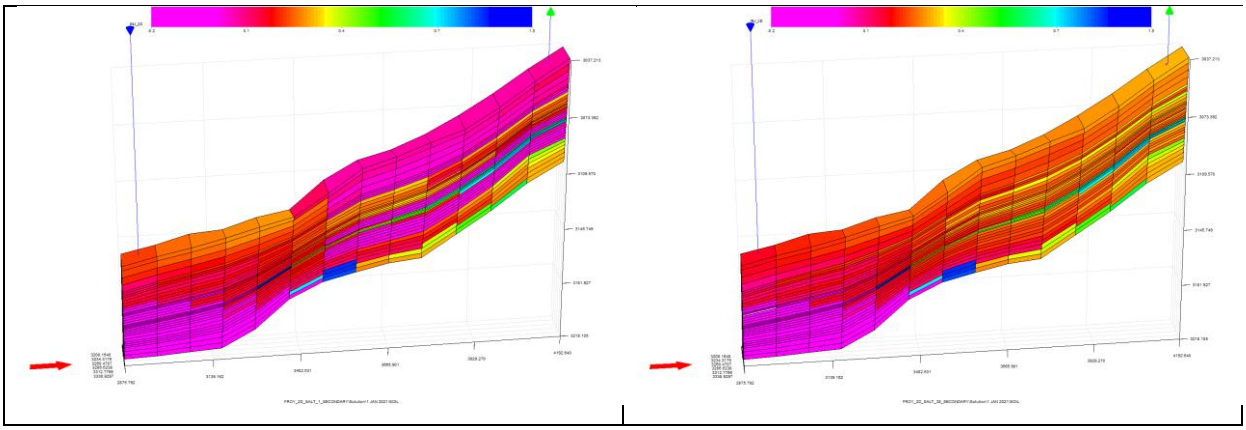

Figure 11-11: Oil saturation for different salinities 2021.

Year: 2022

Salinity of injection brine:

1 kg/m^3 TDS

38 kg/m^3 TDS

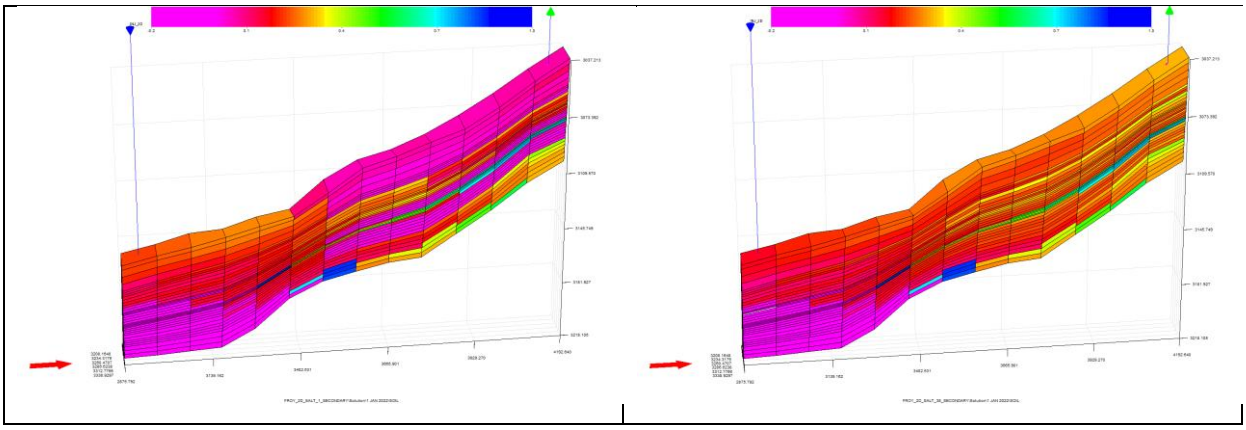

Figure 11-12: Oil saturation for different salinities 2022

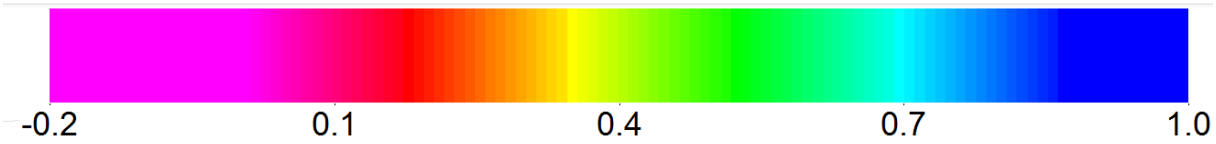

Year: 2023

Salinity of injection brine:

1 kg/m^3 TDS

38 kg/m^3 TDS

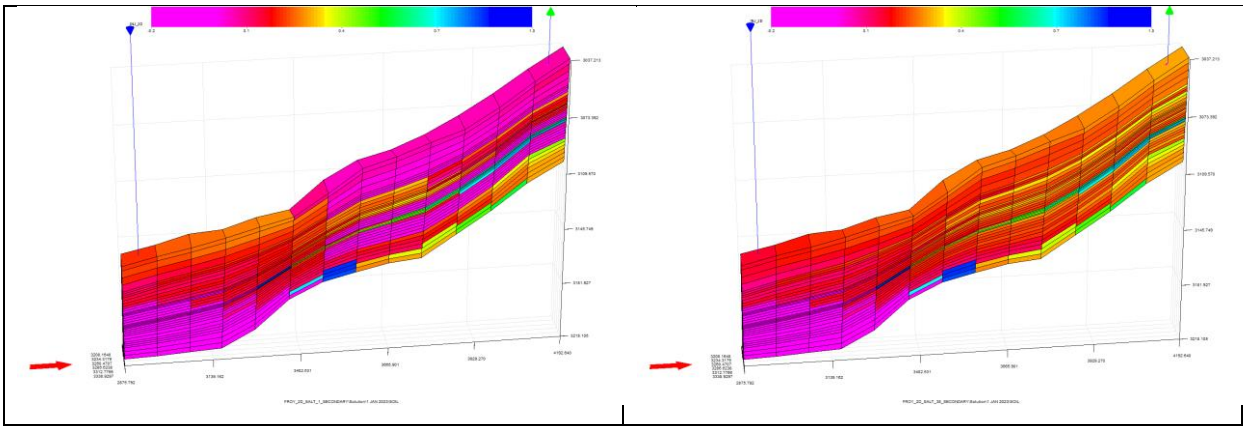

Figure 11-13: Oil saturation for different salinities 2023.

Year: 2024

Salinity of injection brine:

1 kg/m^3 TDS

38 kg/m^3 TDS

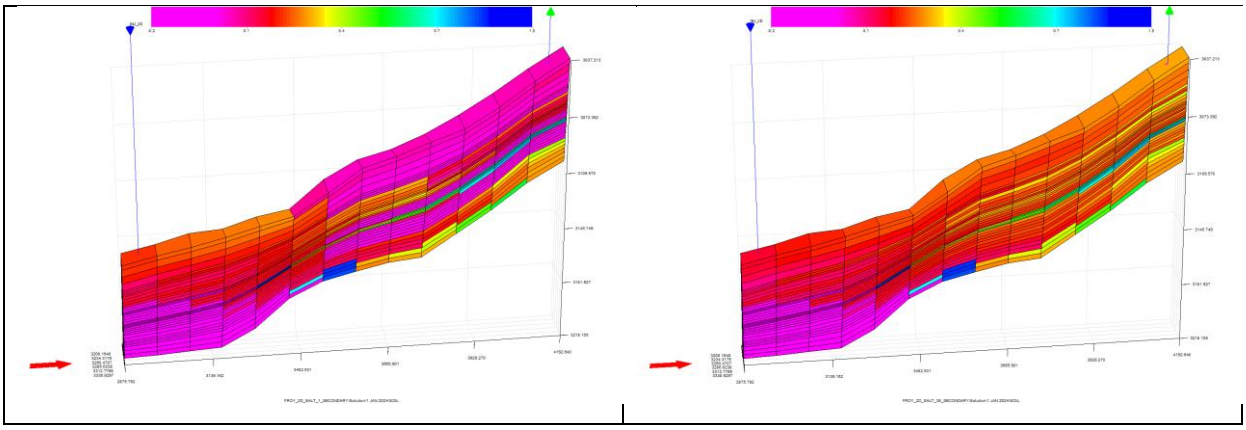

Figure 11-14: Oil saturation for different salinities 2024

.

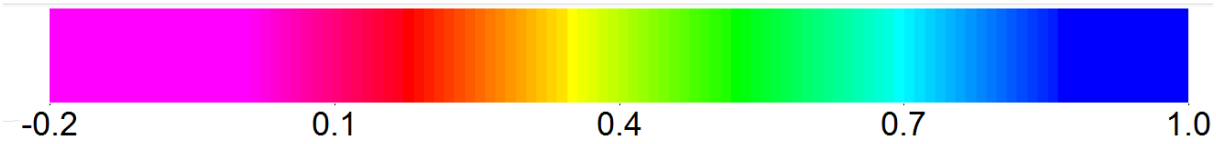

Year: 2025

Salinity of injection brine:

1 kg/m^3 TDS

38 kg/m^3 TDS

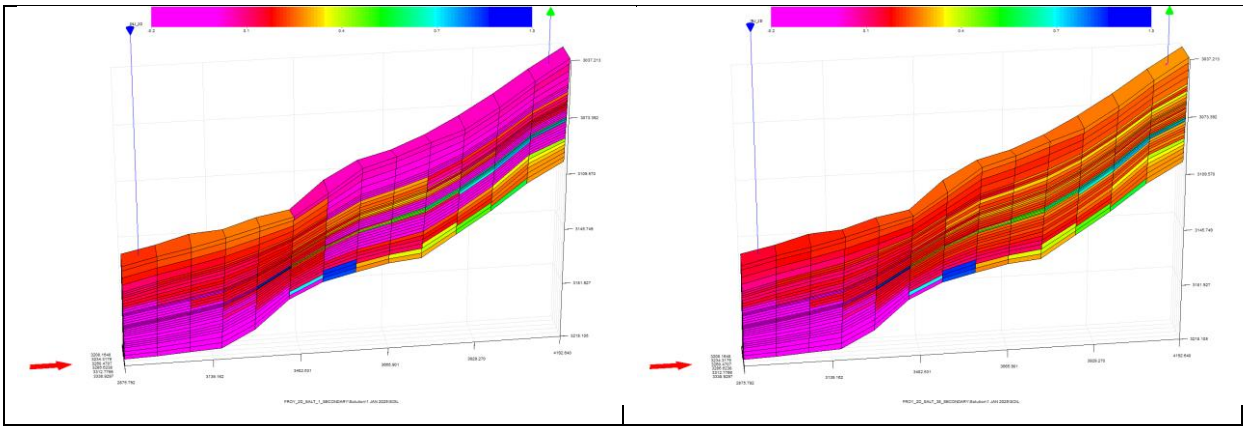

Figure 11-15: Oil saturation for different salinities 2025.

Year: 2026

Salinity of injection brine:

1 kg/m^3 TDS

38 kg/m^3 TDS

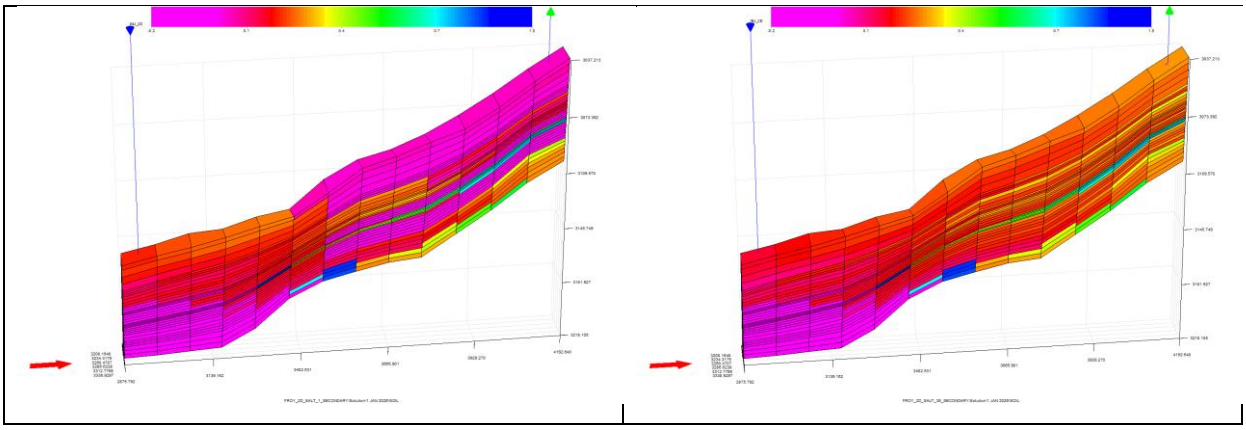

Figure 11-16: Oil saturation for different salinities 2026.

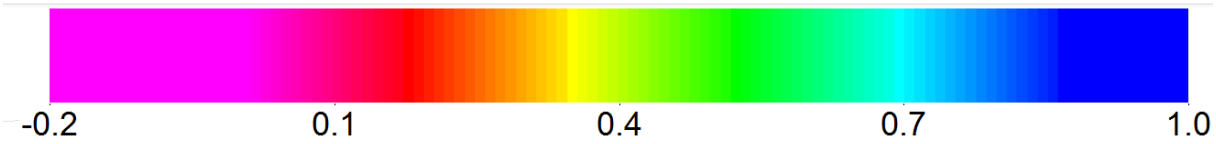

Year: 2027

Salinity of injection brine:

1 kg/m^3 TDS

38 kg/m^3 TDS

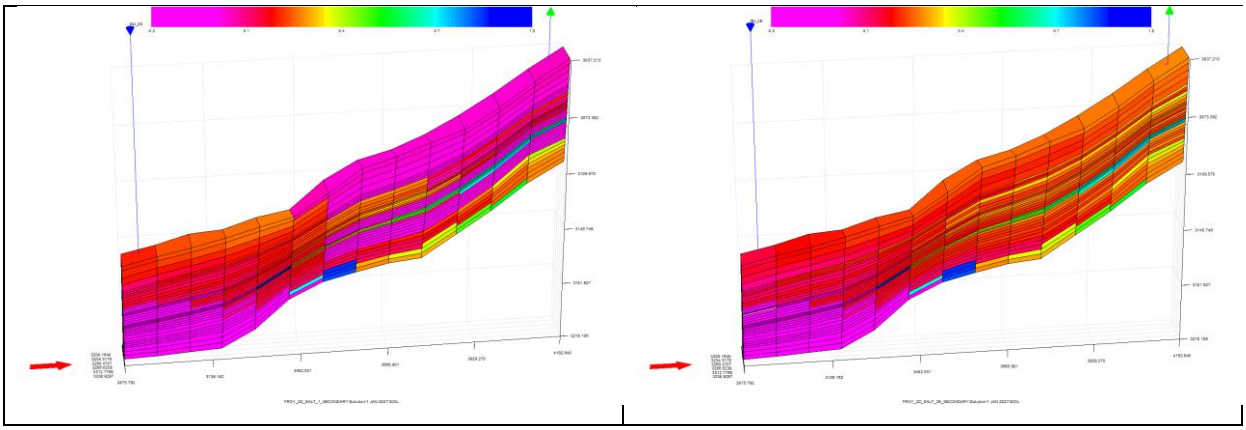

Figure 11-17: Oil saturation for different salinities 2027.

Year: 2028

Salinity of injection brine:

1 kg/m^3 TDS

38 kg/m^3 TDS

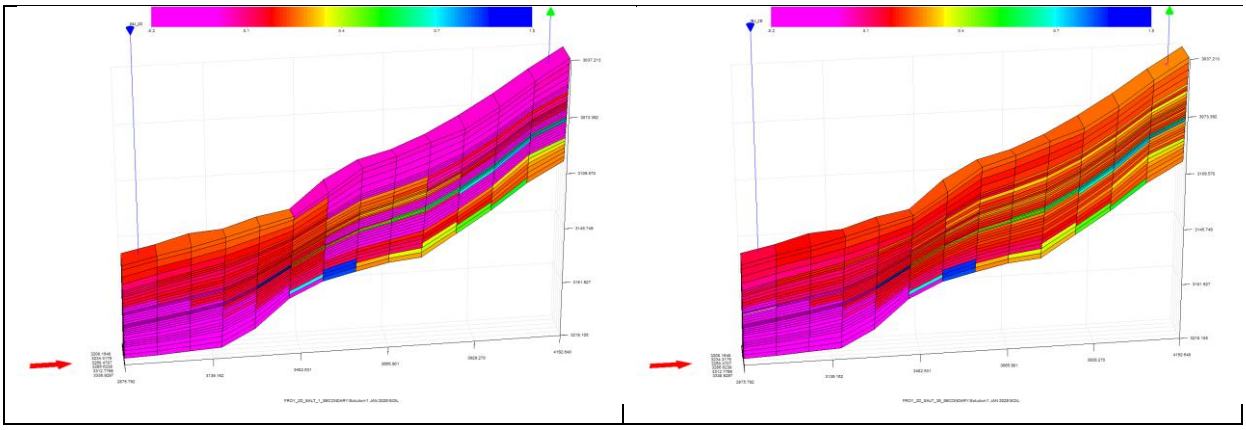

Figure 11-18: Oil saturation for different salinities 2028.

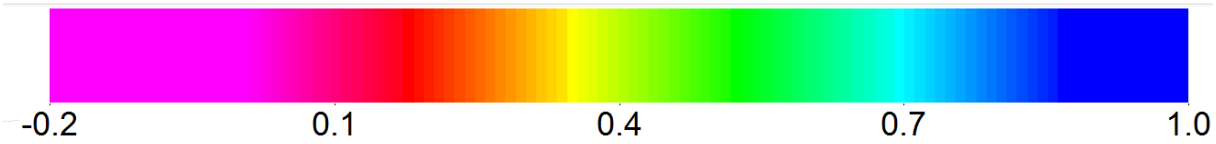

Year: 2029

Salinity of injection brine:

1 kg/m^3 TDS

38 kg/m^3 TDS

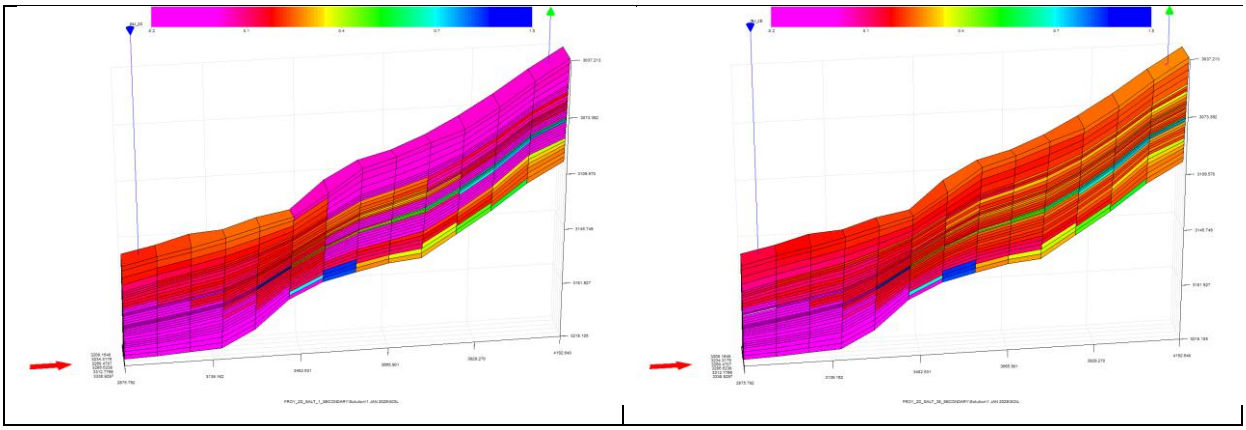

Figure 11-19: Oil saturation for different salinities 2029.

Year: 2030

Salinity of injection brine:

1 kg/m^3 TDS

38 kg/m^3 TDS

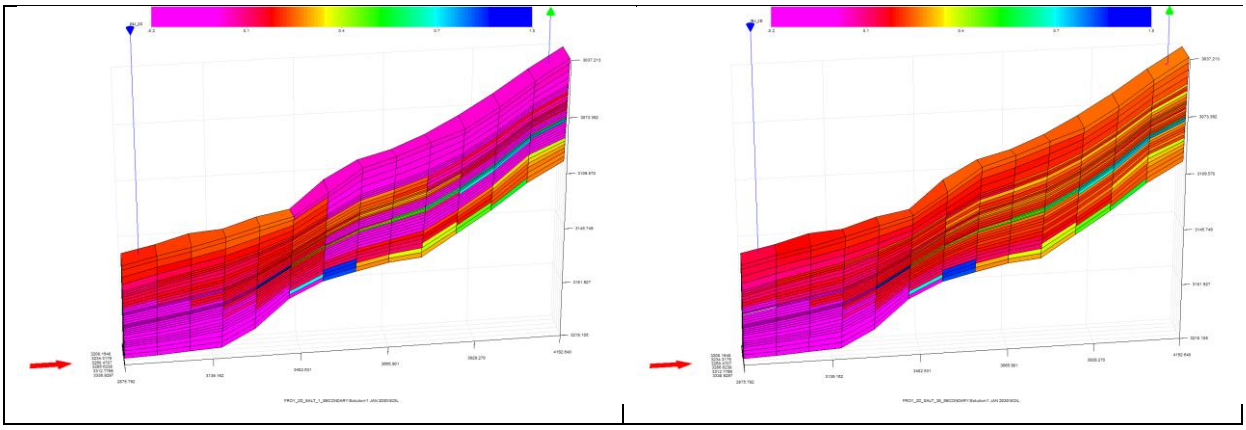

Figure 11-20: Oil saturation for different salinities 2030.

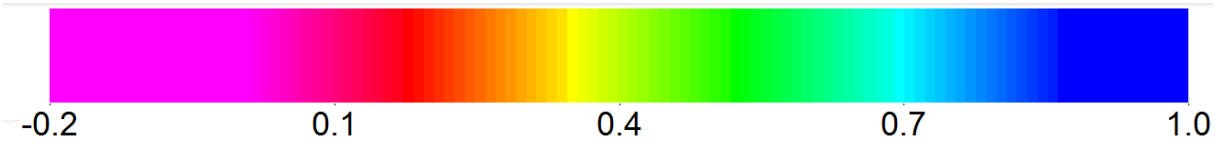

Year: 2031

Salinity of injection brine:

1 kg/m^3 TDS

38 kg/m^3 TDS

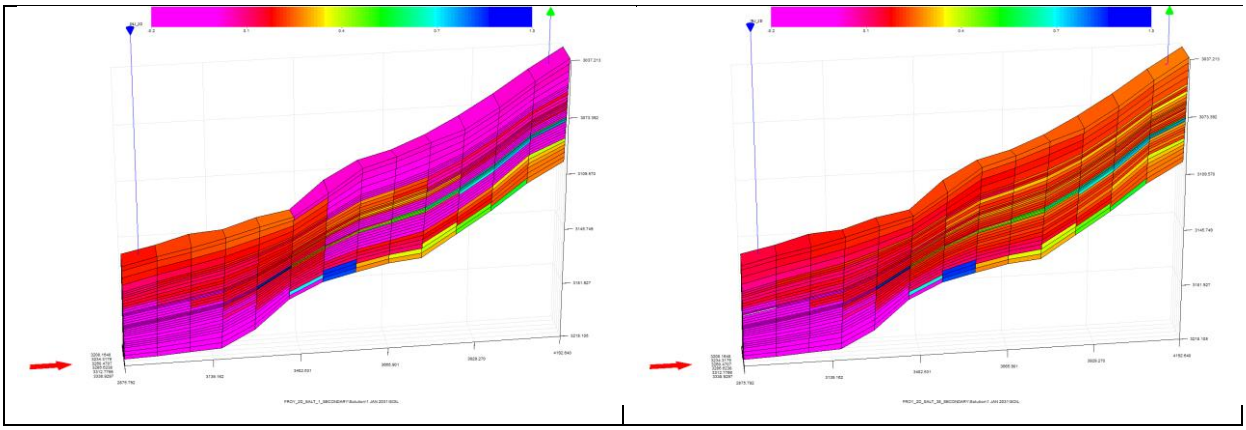

Figure 11-21: Oil saturation for different salinities 2031.

Year: 2032

Salinity of injection brine:

1 kg/m^3 TDS

38 kg/m^3 TDS

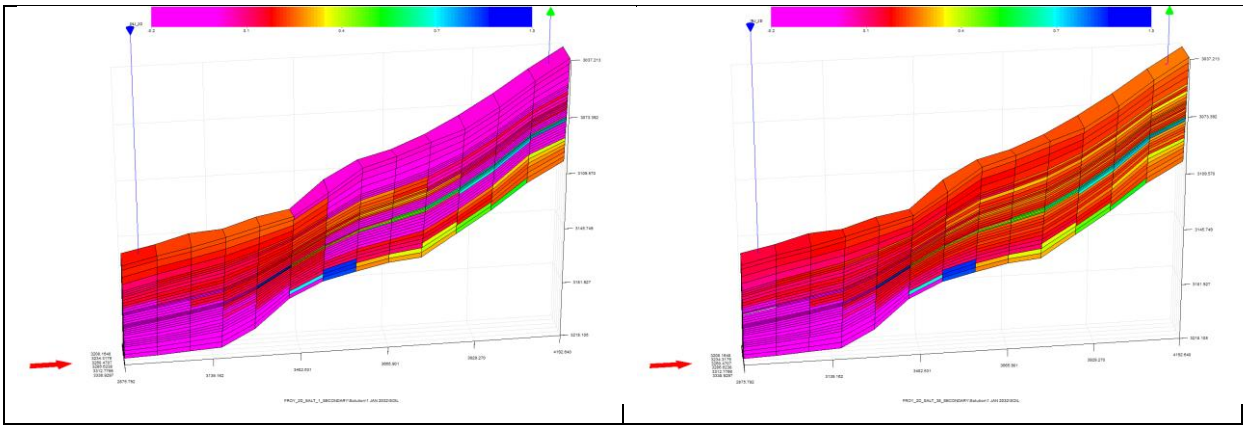

Figure 11-22: Oil saturation for different salinities 2032.

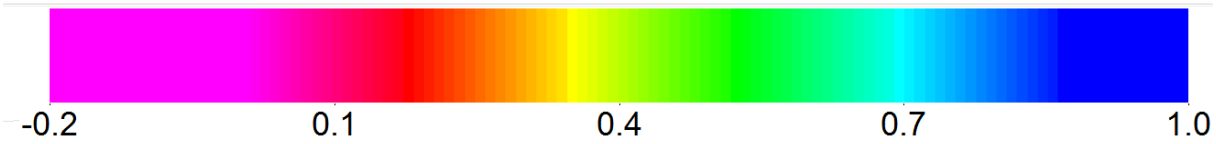

Year: 2033

Salinity of injection brine:

1 kg/m^3 TDS

38 kg/m^3 TDS

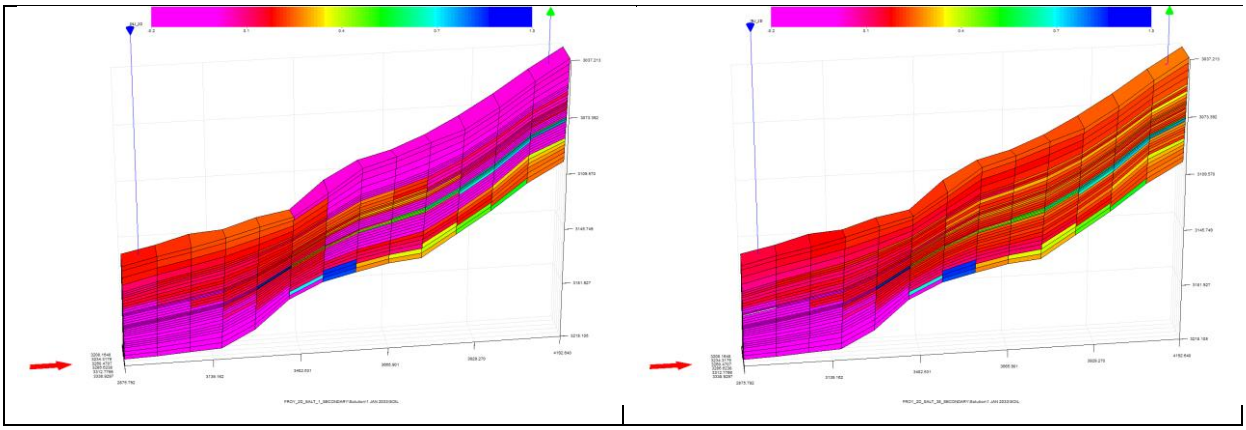

Figure 11-23: Oil saturation for different salinities 2033.

Year: 2034

Salinity of injection brine:

1 kg/m^3 TDS

38 kg/m^3 TDS

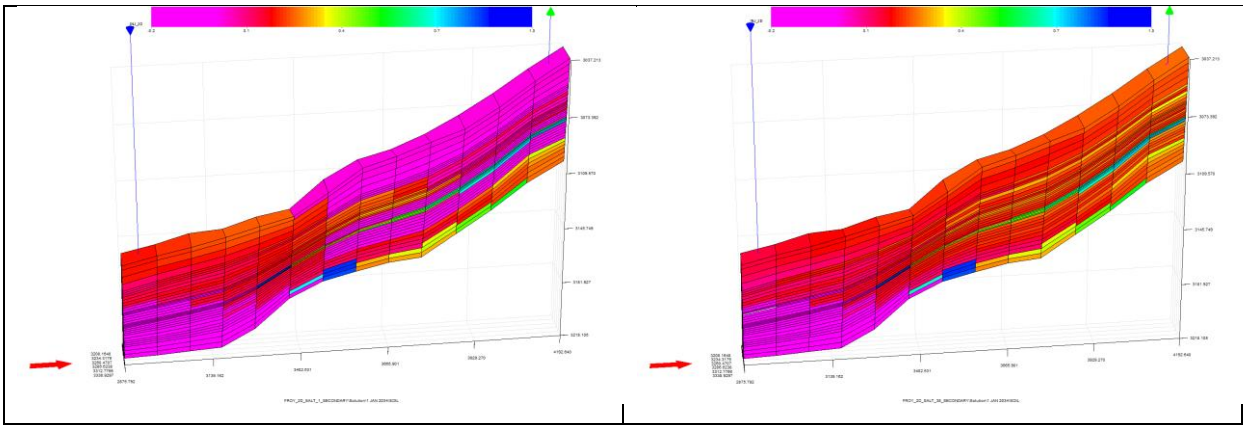

Figure 11-24: Oil saturation for different salinities 2034.

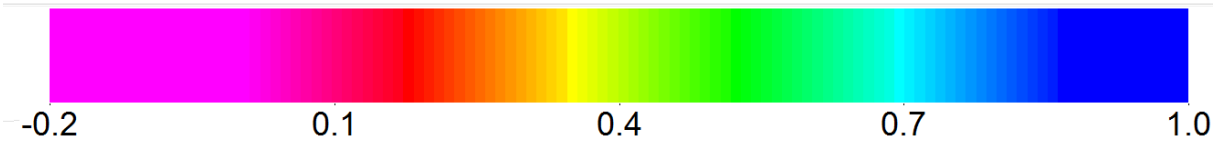

Year: 2035

Salinity of injection brine:

1 kg/m^3 TDS

38 kg/m^3 TDS

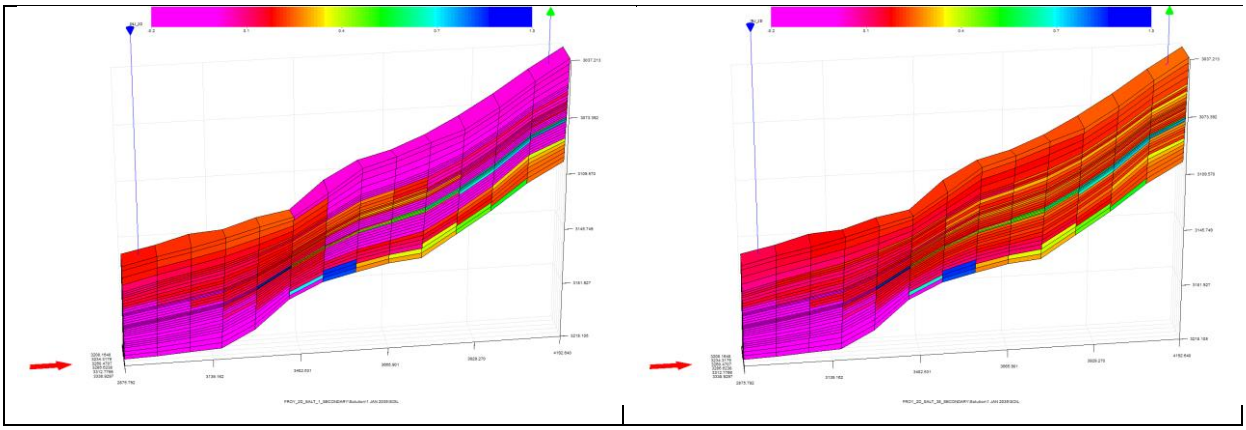

Figure 11-25: Oil saturation for different salinities 2035.

12. Appendix C: End-point Scaling in ECLIPSE 100

The End-point Scaling option in ECLIPSE 100 is enabled by adding the ENDSCALE keyword to the RUNSPEC section. It provides a mechanism for redefining values for the connate, critical and maximum saturations in the saturation tables described in the flow of the reservoir fluids (Schlumberger, 2011). The option is especially useful for modeling reservoirs containing large depth variations in the connate or the critical saturations for one or more of the phases. An overview of some of the relevant keywords for End-point Scaling with a short description is found below:

SOWCR –Specifies the critical oil-in-water saturation within each grid cell. It is the largest oil saturation for which the oil relative permeability is zero in an oil-water system. The SOWCR keywords also permit scaling of the oil-water relative permeability table used in computing the flow of oil between grid cells and well connections.

SWL -Specifies the connate water saturation within each grid cell. It is the smallest water saturation in a water saturation function table. The SWL keyword also permits scaling of the water capillary pressure table used in computing the initial water saturation distribution.

SWU – Specifies the maximum water saturation within each grid cell. It is the largest water saturation entry in a water saturation table.

SWCR – Specifies the critical water saturation within each grid cell. It is the largest water saturation for which the water relative permeability is zero. The SWCR keyword also permit scaling of the relative permeability table used in computing the flow of water between grid cells and well connections.

SGU- Specifies the maximum gas saturation within each grid cell. It is the largest gas saturation in a gas saturation function table.

SGCR – Specifies the critical gas saturation within each grid cell. It is the largest gas saturation for which the gas relative permeability is zero. The SGCR also permits scaling of the relative permeability table used in computing the flow of free gas between grid cells and well connections.

SOGCR – Specifies the critical oil-in-gas saturation within each grid cell. It is the largest oil saturation which the oil relative permeability is zero in an oil-gas-connate water system. The SOGCR keyword also permits scaling of the oil-gas relative permeability table used in computing the flow between grid blocks and well connections.

KRWR – This keyword scales the relative permeability of water within each grid block. It scales the relative permeability at residual oil saturation.

KRW - This keyword scales the relative permeability of water within each grid block. It scales the relative permeability at the maximum water saturation, typically at water saturation of 1.0.

The scaled saturations can be obtained by a linear transformation to determine equivalent saturation to be used for look-up in the unscaled table.

In the Frøy sector model, an alternative form for scaling is included. This form preserves the relative permeabilities at three saturation nodes, and is included by adding the keyword SCALECRS in the RUNSPEC section. If the keyword "YES" is added, the option is implemented. In three phase runs, the preserved end points are:

$$\boldsymbol{k_{rw};\ SWCR, (1 - SOWCR - SGL) and\ SWU} \quad \textbf{(Eq. 12-1)}$$

$$\boldsymbol{k_{rg};\ SGCR, (1 - SOGCR - SWL) and\ SGU} \quad \textbf{(Eq. 12-2)}$$

$$\boldsymbol{k_{row};\ SOWCR, (1 - SWCR - SGL) and\ (1 - SWL - SGL)} \quad \textbf{(Eq. 12-3)}$$

$$\boldsymbol{k_{rog};\ SOGCR, (1 - SGCR - SWL) and\ (1 - SWL - SGL)} \quad \textbf{(Eq. 12-4)}$$

Where $k_{rw,}$ $k_{rg,}$ k_{row} and k_{rog} is the water, gas, oil in water and oil in gas relative permeability respectively. SWCR is critical water saturation, SOWCR is critical oil-in-water saturation, SGL is connate gas saturation, SWL is connate water saturation, SWU is maximum water saturation, SGU is maximum gas saturation, SGCR is critical gas saturation and SOGCR is critical oil-in-gas saturation.

The scaling of the relative permeability might be conducted at the maximum phase saturation and at the critical/residual saturation of the associated phase. When the KRWR keyword is included, as it is in the Frøy sector model, the scaling will honor the relative

permeability at the critical saturation (SR) of the associated phase. In three phase runs, the SR will be:

$$\boldsymbol{SR = 1 - SOWCR - SGL} \quad \textbf{(Eq. 12-5)}$$

Where SR is critical saturation of the associated phase, SOWCR is critical oil-in-water saturation and SGL is connate gas saturation.

This means that two cases will be available, and they are presented below with water relative permeability as an example. The other phases are scaled in the same manner.

Case 1: SWCR ≤ SW ≤ SR

$$\boldsymbol{k_{rw}(S) = k_{rw}(S') \frac{KRWR(grid\ block)}{k_{rw}(S_r)(table)}} \quad \textbf{(Eq. 12-6)}$$

Case 2: SR ≤ SW ≤ SWU

$$\boldsymbol{k_{rw}(S) = KRWR + \frac{(k_{rw}(S')(table) - k_{rw}(S_r)(table)))}{(k_{rwmax}(table) - k_{rw}(S_r)(table))}(KRW - KRWR)} \quad \textbf{(Eq. 12-7)}$$

Where k_{rw} and KRW is unscaled and scaled relative permeability of water respectively, KRWR is scaled relative permeability of water at residual oil saturation, S' is the new saturation, S is saturation, S_r is the value of the displacing critical saturation in the table, k_{rwmax} is the maximum water relative permeability (taken from the saturation table).

Examples on two – and three point scaling are found in **Figure 12-1** and **Figure 12-2** below.

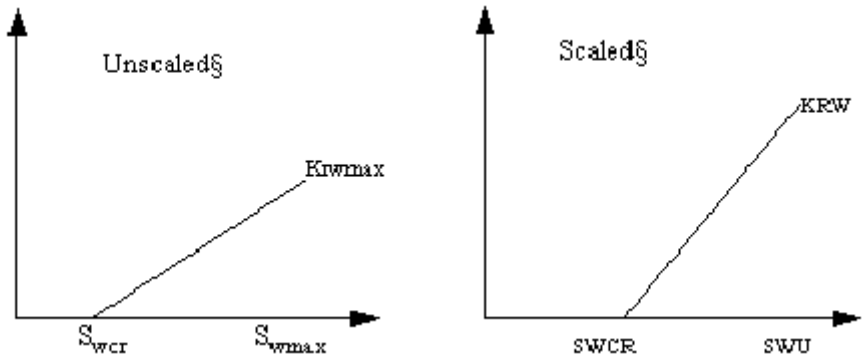

Figure 12-1: Two point End-point scaling example (Schlumberger, 2011).

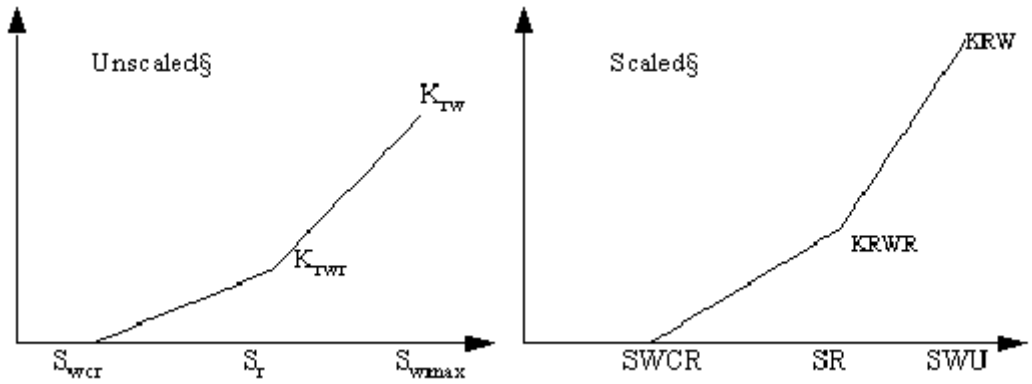

Figure 12-2: Three point End-point scaling example (Schlumberger, 2011).

In the Frøy sector model, the relevant files for End-point Scaling are found from the include files. These files are not found in the appendix because some of them contain many inputs. A short overview of the relevant files with description is found below:

G4_SWCR.INC – gives SWCR values for each grid block

G4_SWATINIT.INC – gives the initial water saturation in each grid block

SGCR_MULTNUM.MINC – uses MULTNUM to specify critical gas saturation for each SATNUM region

SOGCR_MULTNUM.MINC - uses MULTNUM to specify critical oil –in- gas saturation for each SATNUM region

MULTSWCR_4SATNUM.MINC - uses MULTNUM to specify critical water saturation for each SATNUM region

SOWCR_MULTUM.MINC - uses MULTNUM to specify critical oil-in-water saturation for each SATNUM region

KRWR_MULTUM.MINC - uses MULTNUM to specify different end point water relative permeabilities for each SATNUM region

To illustrate how the scaled relative permeability varies with different grid blocks, PETREL 2011 might be applied. In PETREL 2011 an option is included to make plots from the initial relative permeability, saturation and capillary pressure profiles. Some samples from depth variation in grid blocks (40, 33, XX) are found in the following figures. Notice that the unscaled relative permeabilities are equal;

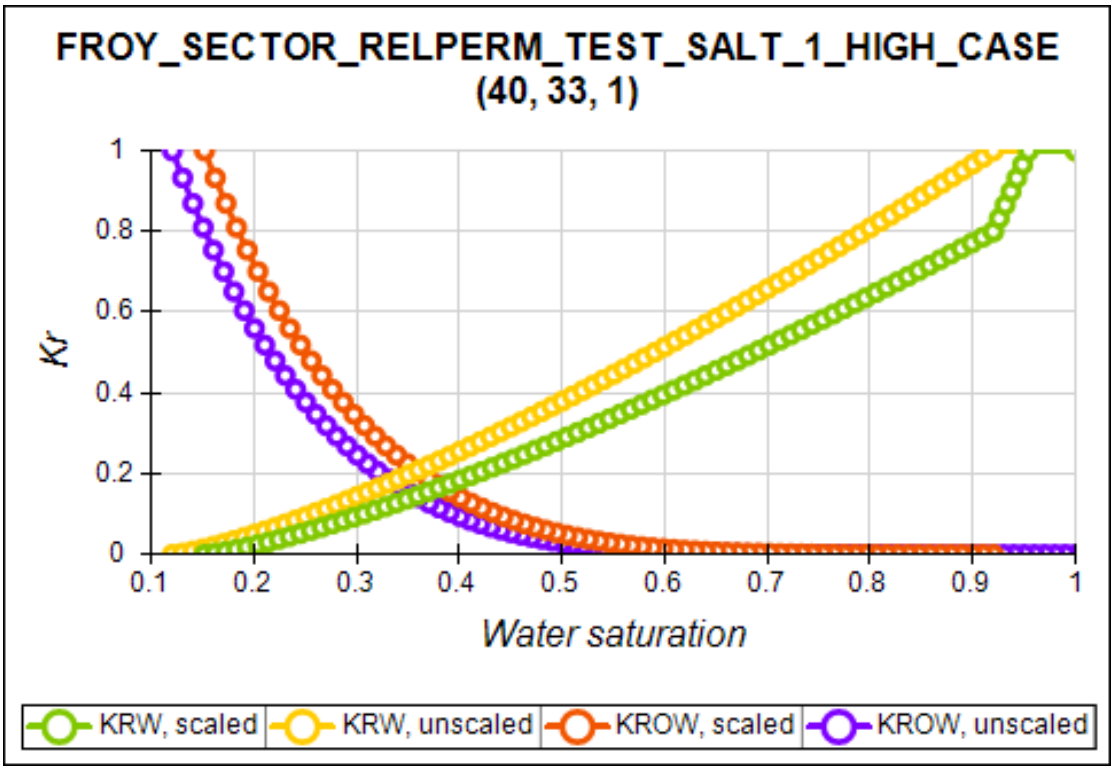

Figure 12-3: Scaled and unscaled relative permeabilites in grid cell (40,33,1).

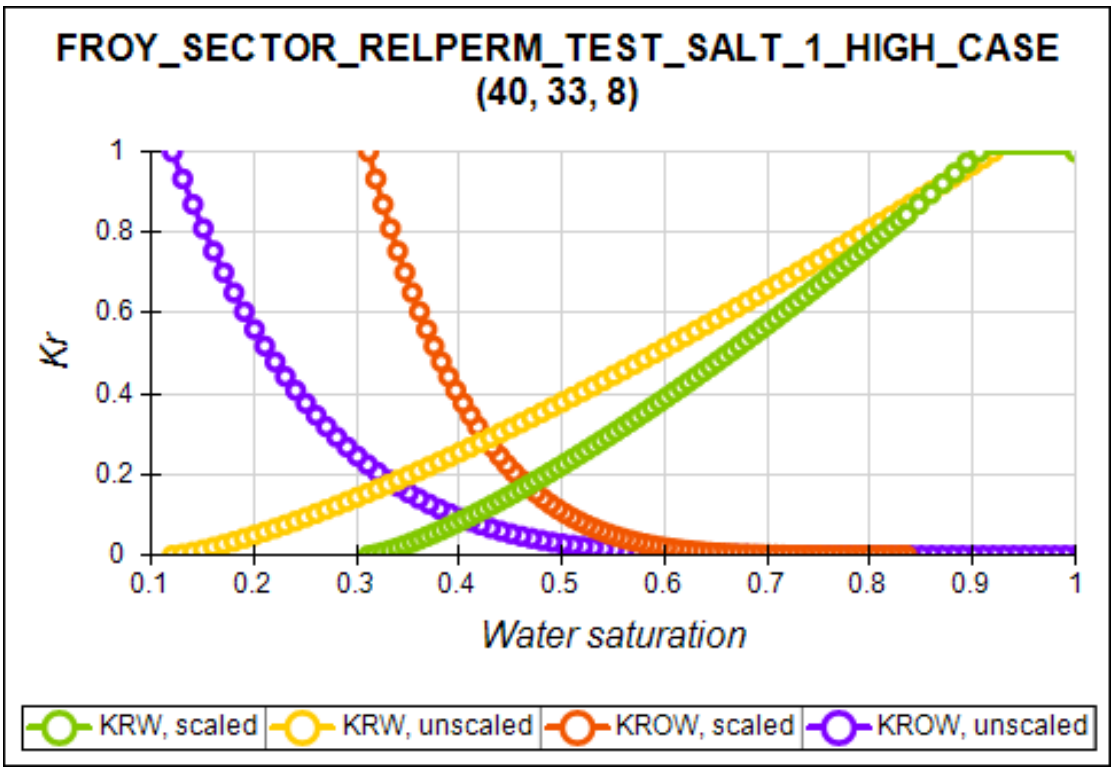

Figure 12-4: Scaled and unscaled relative permeabilites in grid cell (40,33,8).

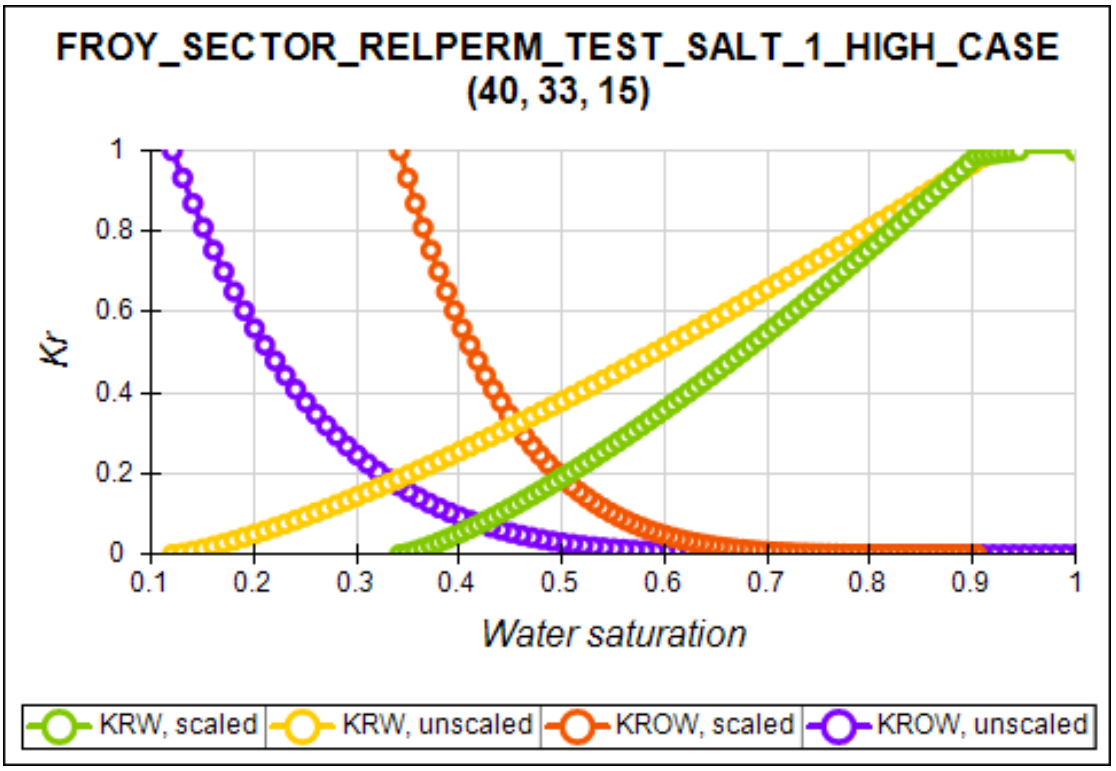

Figure 12-5: Scaled and unscaled relative permeabilites in grid cell (40,33,15).

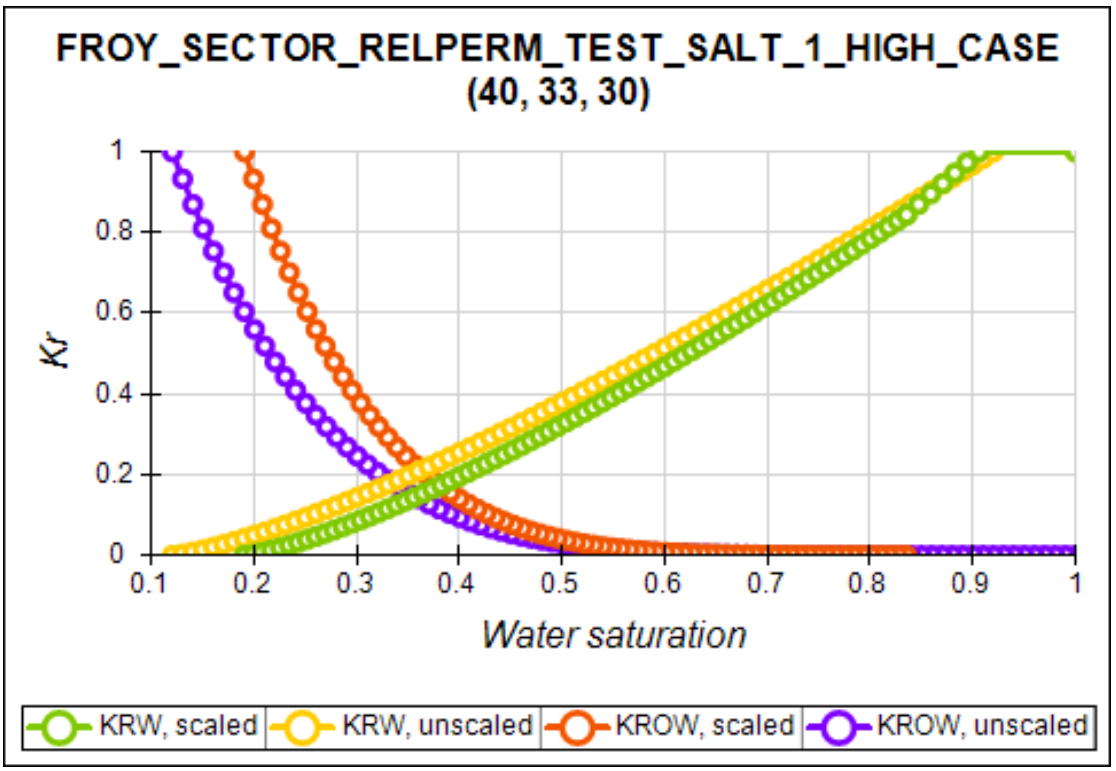

Figure 12-6: Scaled and unscaled relative permeabilites in grid cell (40,33,30).

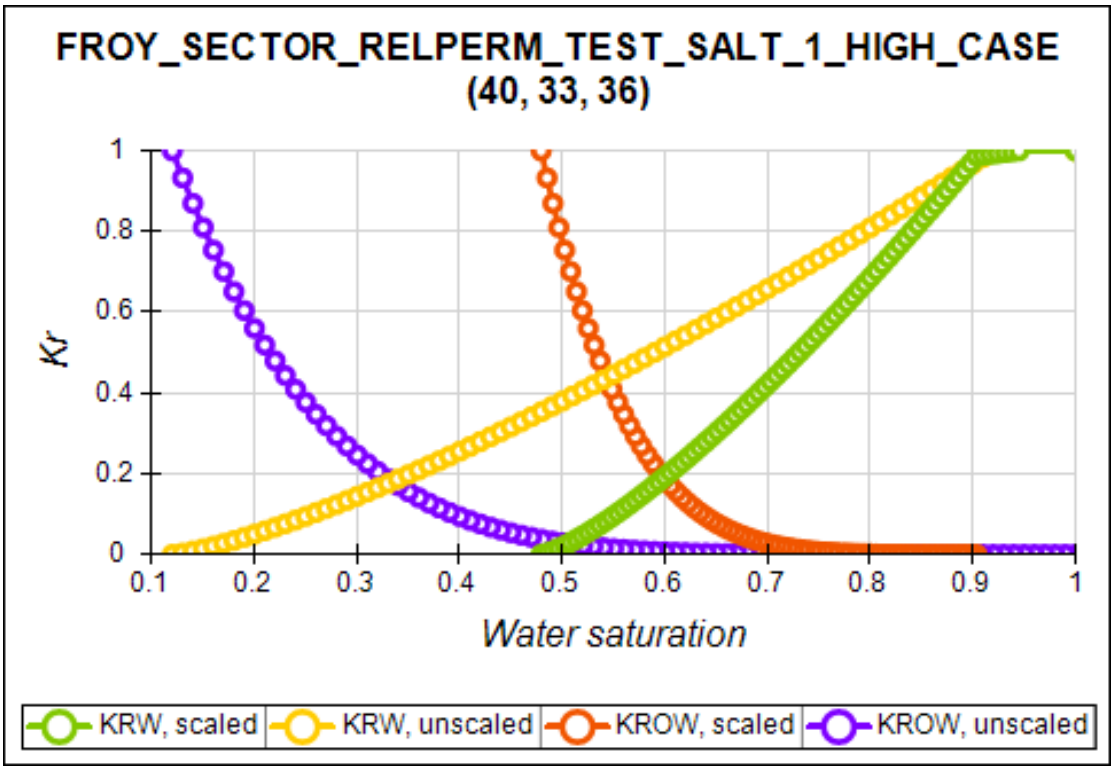

Figure 12-7: Scaled and unscaled relative permeabilites in grid cell (40,33,36).

It is also possible to scale the capillary pressure with respect to scaled water saturation, but since this is not implemented in the Frøy sector model it will not be discussed. Two plots are made from PETREL 2011 to illustrate that no depth variations regarding capillary pressure are included. They are found in **Figure 12-8** and **Figure 12-9**. The scaled capillary pressure will then also be equal to the unscaled capillary pressure.

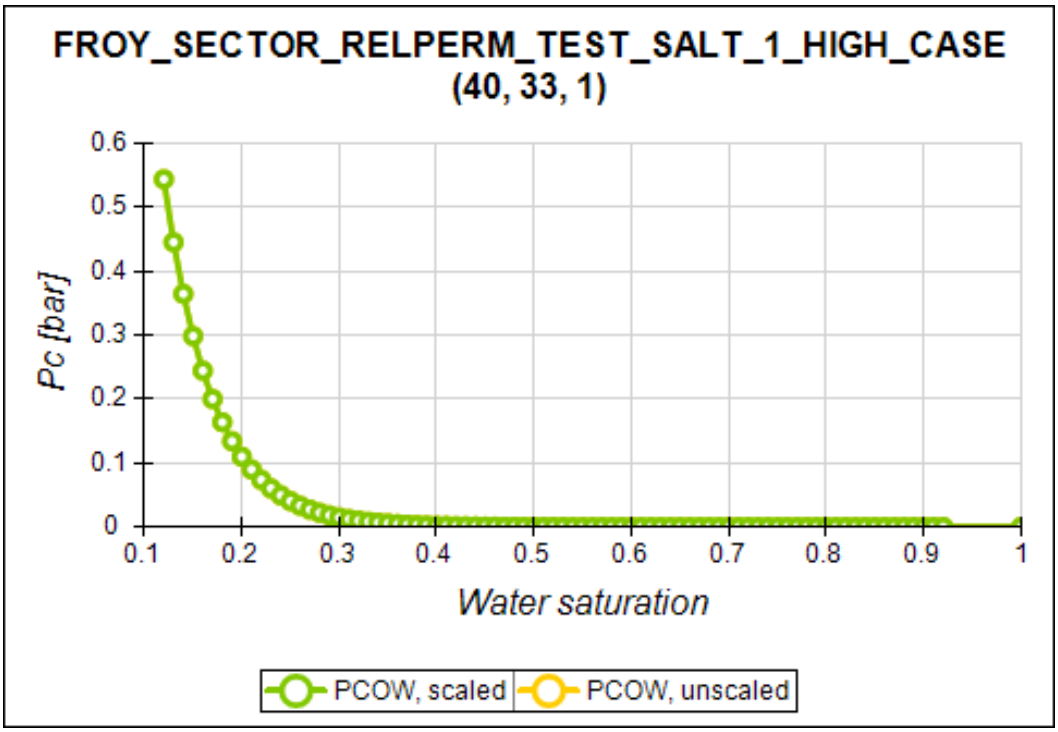

Figure 12-8: Scaled and unscaled capillary pressures in grid cell (40,33,1).

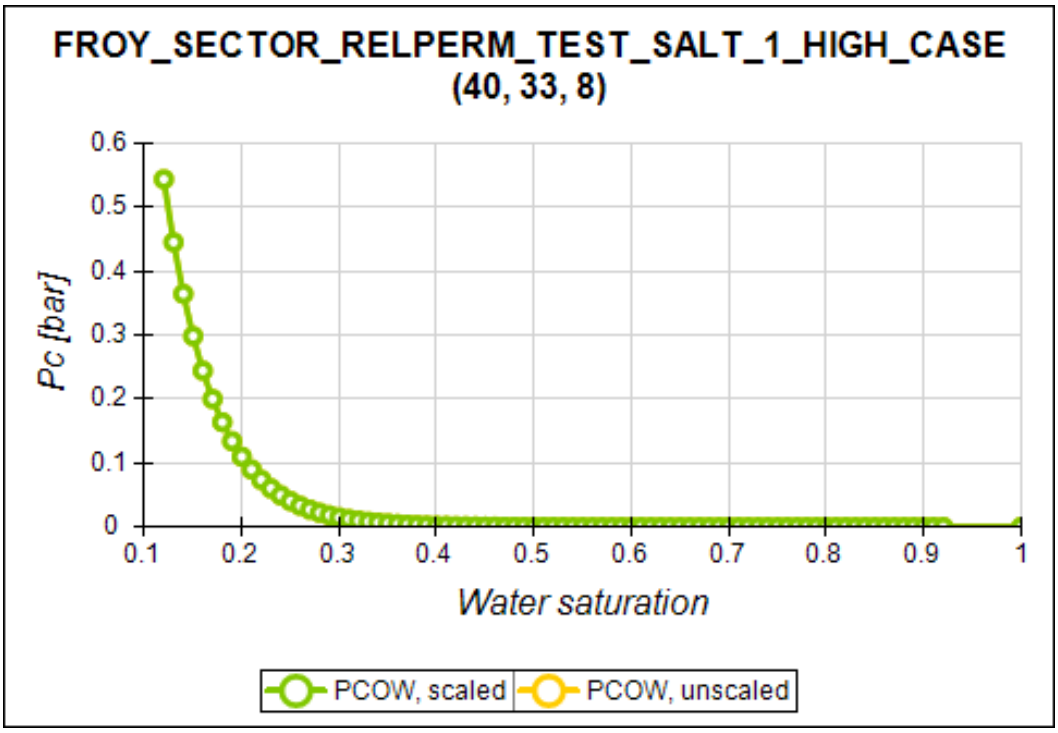

Figure 12-9: Scaled and unscaled capillary pressures in grid cell (40,33,8).

13. Appendix D: Single Well Chemical Tracer Test Description

The single well chemical tracer test is conducted as described below (Deans and Carlisle):

The SWCTT includes injection and back production of the initial formation water and reactive chemicals. An ester is injected and reacts partly with the oil and water. A material balance tracer is also injected to differentiate the injected volume and the formation volume being displaced. The chemicals are then pushed away from the wellbore. When the chemicals and the water is far enough away from the wellbore, the well is shut down. The shutdown period depends on how long time it takes before the wanted reactions have been done properly. The reactions include dissolution of the ester into an alcohol and an organic acid. It is the alcohol formed that makes the S_{or} measurement possible because it is not originally a part of the formation water.

The material balance tracer is most soluble in the water, and travels approximately with the same speed as the water. During production, the product alcohol separates from the unreacted ester tracer. The separation is because the product alcohol has approximately the same speed as the water and the ester production velocity is slower than the alcohol velocity because it must portioned between the oil and water phases.

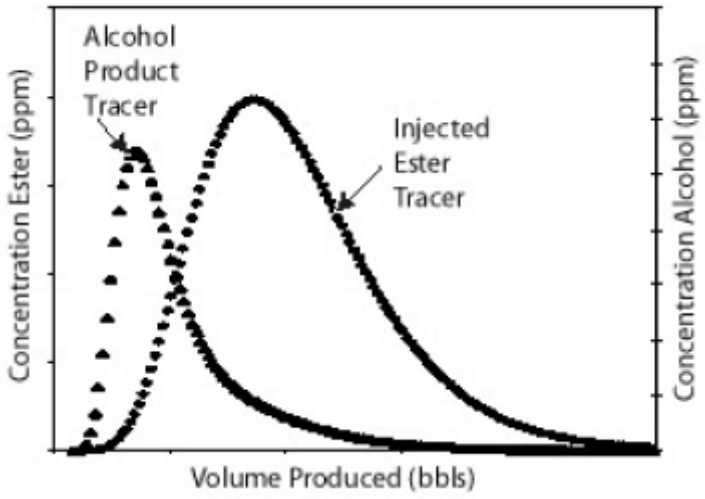

Figure 13-1: SWCTT description (Deans and Carlisle).

SWCTT for EOR evaluation is conducted by three steps:

1. A standard SWCTT is conducted to obtain the initial S_{or}
2. A volume of the EOR fluid is injected

3. A new SWCTT is repeated for the treated region, and the reduction in S_{or} for the two tests is a measure of the EOR flood performance.

14. Appendix E: ECLIPSE 100 Data File, Synthetic Base Case Model

```
RUNSPEC

TITLE

 Surfactant model test case.

DIMENS

  10   10    3  /

OIL

WATER

LOWSALT

METRIC

TABDIMS

-- NTSFUN NTPVT NSSFUN NPPVT NTFIP NRPVT

2 1 100 50 1 /

WELLDIMS

   2    3    1    2 /

GASFIELD

  'YES'  /


START

   1 'MAY' 1990  /
```

```
NSTACK
   40 /
 UNIFOUT
GRID    ============================================================
NEWTRAN
DXV
 10*50   /
DYV
 10*50  /
DZ
 100*0.58 100*0.84 100*0.47  /
PERMX
 100*4500 100*3300 100*2400 /
COPY
 'PERMX' 'PERMY' 1 10   1 10  1 3 /
/
PERMZ
 100*1050 100*1800 100*500 /
PORO
 300*0.25 /
TOPS
 100*2600 /
```

RPTGRID

/

PROPS ==========

LSALTFNC

-- Cs F1 F2 -- SATNUM 1

0.0 1.0 1.0

1.0 1.0 1.0

4.0 1.0 1.0

5.0 0.0 0.0

35.0 0.0 0.0

45.0 0.0 0.0

/

-- Cs F1 F2 -- SATNUM 2

0.0 1.0 1.0

1.0 1.0 1.0

4.0 1.0 1.0

5.0 0.0 0.0

35.0 0.0 0.0

45.0 0.0 0.0

/

/

--High salinity rel.perm, O-W

SWOF

-- Sw Krw Kro   Pc

0.2 0.0000 0.500 0.0

0.3 0.0064 0.256 0.0

0.4 0.0512 0.108 0.0

0.5 0.1728 0.032 0.0

0.6 0.4096 0.004 0.0

0.7 0.8000 0.000 0.0

/

--Low salinity rel.perm, W-W

0.2 0.000000 0.800000000 0.0

0.3 0.001740 0.587755102 0.0

0.4 0.013994 0.408163265 0.0

0.5 0.047230 0.261224490 0.0

0.6 0.111953 0.146938776 0.0

0.7 0.218659 0.065306122 0.0

0.8 0.377843 0.016326531 0.0

0.9 0.600000 0.000000000 0.0

/

PVDO

```
  200    1.0     0.47

  280    0.999   0.47

  300    0.998   0.47

/


ROCK

 270 .3E-5 /

DENSITY

 850. 1000. 10. /

PVTWSALT

 270.0 35.0/

 0.0  1.030  4.6E-5  0.5  0.0

10.0  1.030  4.6E-5  0.5  0.0 /

--RPTPROPS

   -- PROPS Reporting Options

--




REGIONS    ============================================================


SATNUM

-- High salinity = 1
```

```
 300*1 /

LWSLTNUM

-- Low salinity = 2

 300*2 /

--RPTREGS

-- 24*0 /

 RPTREGS

LWSLTNUM LSLTWNUM /

SOLUTION   ============================================================

SWAT

300*0.2 /

-- 50*0.2

-- 50*0.4 /

PRESSURE

300*200 /

SALT

300*35.0 /


RPTSOL

--

-- Initialisation Print Output

--
```

'PRES' 'SOIL' 'SWAT' 'RESTART=1' 'OILAPI' 'FIPTR=2' 'TBLK' 'FIPPLY=2' 'SURFBLK'

'FIPSURF=2' /

SUMMARY ===

WBHP

/

FWIR

FOPR

FOPT

FOE

FWCT

GSPT

'G' /

GSIR

'G' /

GSIT

'G' /

GSPR

'G' /

WSPR

'OP' /

WSPT

'OP' /

WSIR

'INJ' /

WSIT

'OP ' /

BSCN

1 1 1 /

1 1 2 /

4 4 1 /

5 5 1 /

7 7 1 /

10 10 1 /

/

BSIP

1 1 1 / salt in place

1 1 2 /

4 4 1 /

5 5 1 /

7 7 1 /

10 10 1 /

/

BOSAT

1 1 1 /

2 2 1 /

3 3 1 /

4 4 1 /

5 5 1 /

5 5 2 /

5 5 3 /

6 6 1 /

7 7 1 /

8 8 1 /

9 9 1 /

10 10 1 /

10 10 2 /

10 10 3 /

/

BOKR

1 1 1 /

1 1 2 /

4 4 1 /

5 5 1 /

7 7 1 /

10 10 1 /

/

BWKR

1 1 1 /

1 1 2 /

4 4 1 /

5 5 1 /

7 7 1 /

10 10 1 /

/

BWKR

1 1 1 /

1 1 2 /

4 4 1 /

5 5 1 /

7 7 1 /

10 10 1 /

```
/

--FUHCPVI

RUNSUM

SCHEDULE  ============================================================

RPTSCHED                              FIELD   16:55 18 APR 86

'PRES' 'SOIL' 'SWAT' 'RESTART=6' 'FIP=2' 'WELLS=2' 'SUMMARY=2' 'CPU=2'

'NEWTON=2' 'OILAPI' 'FIPTR=2' 'TBLK' 'FIPSALT=2' 'TUNING' 'SURFBLK' 'SURFADS'

'FIPSURF=2' /


WELSPECS

'OP'  'G'   10 10  2600  'OIL'  /

'INJ' 'G'   1  1   2600  'WAT'  /

/

COMPDAT

'OP     '   10  10  1   3 'OPEN'   0  .0   157E-3 /

'INJ    '   1   1   1   3 'OPEN'   0  .0   157E-3 /

/

WCONPROD

'OP' 'OPEN' 'RESV' 4* 200 0.0 4* /

/

WCONINJE

'INJ' 'WAT' 'OPEN' 'RESV' 1* 200  /
```

/

--UDQ

--DEFINE FUHCPV FOPV /

--UPDATE FUHCPV NEXT /

--/

--UDQ

--DEFINE FUHCPVI FWIT/FUHCPV /

--/

--TSTEP

-- 10*30 /

--/

--TSTEP

--10*30/

--WSALT

--INJ 10.0 /

--/

WSALT

'INJ' 35.0 /

/

TSTEP

80*30/

--WSALT

--'INJ' 35.0 /

--/

--TSTEP

--65*30/

--/

END

15. Appendix F: ECLIPSE 100 Data File, Frøy Field Low Salt Base Case Model

```
--
================================================================================
====================

-- Frøy Field G4 3D FFSM  2008

--

--   Updated Petrel model per. 05.09.2007

--

-- History Matcing September  2007

--         - intra-facies permeability                                          ; MULTPERM

--         - inter-region/facies transmisibility   ; MULTREGT

--         -          fault transmissibility              ; MUTFLT

--  - critical water saturation-          ; MULTSWCR - SWCRi = SWATINIT

--  - critical gas  saturation-           ; MULTSGCR - SGCRi = 0.0

--         - aquifer permeability               ; AQUCT - 4th param (mD)

--         - .

--         - RelPerm

--         - Fluid data

--

--

--
================================================================================
====================
```

-- 28.02.2008: This file is always copied from HM31_BASE to

-- experiment directories, even when choosing Simulate Selected cases

-- in MEPO. Consequently, any changes in experiments must be

-- represented in local include files e.g. SCALECRS.INC

--

==========

-- History matching April 2008

-- HM31_BASE represents a revised starting point for history

-- matching. A list of the modifications is given below.

-- - Some G3-faults are reintroduced to the G4-grid with

-- FAULTS keyword, G3TOG4_FAULTS.INC

-- - G3 fault multipliers are included, G3TOG4_MULTFLT.INC

-- - New PVT-data from DewPoint (April 2008) is included.

-- - Saturation function variations are now limited to the

-- end-point saturations and not the Corey-exponents.

-- - A-3 to A-1 high-perm. channel is (temporarily) removed

-- (EQUALPERM1.MINC)

-- - Range of permeability multipliers for channel and low-perm. facies

-- has been modified in MEPO uncertainty parameter.

-- History matching April 2008

```
--  HM31_BASE represents a revised starting point for history
--  matching. A list of the modifications is given below.
--    - Some G3-faults are reintroduced to the G4-grid with
--          FAULTS keyword, G3TOG4_FAULTS.INC
--    - G3 fault multipliers are included, G3TOG4_MULTFLT.INC
--    - New PVT-data from DewPoint (April 2008) is included.
--    - Saturation function variations are now limited to the
--      end-point saturations and not the Corey-exponents.
--    - A-3 to A-1 high-perm. channel is removed (EQUALPERM1.MINC)
--    - Range of permeability multipliers for channel and low-perm. facies
--      has been modified in MEPO uncertainty parameter.
-- May 2008:
--    - Additional faults (no throw) have been introduce to improve water
--      production match:
--       G3TOG4_NEWG4_FAULTS.INC
--       G3TOG4_NEWG4_MULTFLT.MINC
--    - Using same saturation functions for well connections as
--      connecting grid block *_BLOCKCONN*
-- June 2008:
--    - Barrier north of A-7 has been extended in EW-direction: MULTYX_A7N.MINC
--    - Well A-2 has been misrepresented probably for the whole G4
--      h.m. work, including round 1 in late fall 2007. An
```

```
--      approximation to the path of the correct sidetrack well A-2A
--      is now implemented in the schedule file:
--      G4_HIST_MB_A2A_BLOCKCONN.INC
--    - Permeabilities are lumped per facies and reservoir unit:
--      G4_FACIES_RU_PERM.GRDECL
-- July 2008:
--    - Well connection parameters are defaulted so that the
--      changes induced by e.g. permeability multipliers will
--      apply for the wells also.
--    - Lower perforations for A-1 well are moved west of 'purple'
--      fault: layers 29-31.



-- 18.7.2008
--  HM31_M2_29_8  - MEPO global value 15.2 ;Best Match so far ; 18.7.2008 )
--                  - lumped facies permeability
--                  - no VAPOIL ( consit. with 200807 compos.study)
--                  - Well -A1 perfs in reservoir unit 5-4 moved 1 cell west ;
--                    across major N-S fault i.e. from HORST to MAIN area
--                  - condition histmatch on LRAT ( .. rather than ORAT)
--                  - NB! A-7 BHP low; re-introduce well relperms for this well
--                   (ref. RM/Total wrt wettability vs. depth)
```

```
-- G4                          -       G4 3D subsurface model

--  _PDO                -       PDO consistent; DPSO_8P_6I_SWAG_NOWO_DC_REG

--                  _PVT    - update PVT; average properties @ 3088 mMSL TVD, no depth trends

--                  _F                  - more pessimitic base case fluid behaviour; DRSDT =
0.02 Sm3/Sm3/d

--                  _iGL    - continuous gas lift within gas handling capacity

RUNSPEC

TITLE

 Frøy Field History Match Production from May 1995 to June 2001

-- Model dimension 74 x 107 x 36 = 285 048 cells

DIMENS

-- nx  ny  nz

  74 107  36 /

-- use metric dimensions

METRIC

-- fluids

WATER

OIL

GAS

DISGAS

LOWSALT
```

```
-- VAPOIL

-- Use EndPoint Scaling for saturation regions

ENDSCALE

/

START

-- start date

 1 MAY 1995 /

GRIDOPTS

--  DirMult? MxMLTNM -- allow directional TransMult ( MULTREGT )

    YES      30 /

REGDIMS

-- MxFIPNM  FIPNUM

     10    30       /

FAULTDIM

-- MxFltSegm

    1750  /

EQLOPTS

-- options; MOBILE  QUIESC THPRES IRREVERS

/

EQLDIMS

--  NTEQUIL NDepNod in xxVD

     1     100      30   /
```

```
--THPRES

--  from / to equil reg  ThresHolPres

--    1     2              0.000

-- /

WELLDIMS

-- MXNW MxNCpW MxG  MxNWpG

   30    200    7    10 /

VFPPDIMS

-- mxflo  mxthp  mxwct mcgfr mxalq mxtab

   20    10     20     10   10     2     /

-- use unified I/O

UNIFIN

UNIFOUT

TABDIMS

-- NTSFUN NTPVT NSSFUN NPPVT NTFIP NRSPVT NRVPVT

-- 5=4 Fac.+1 Well (SATNUM5.INC)

    5     1     100   197    1*   197   197 /

-- -- Remove me: line below is with SATNUM.INC commented out in REGIONS

--    2     1     50   197    1*   197   197 /

AQUDIMS

-- Numaq lnaq inftab linftb  nanaq  aqconnbl

        4*              1      5000  /
```

```
-- run / check ?

 NOSIM

-- create save for fast restart

SAVE

/

NSTACK

-- prev sol.search dir stored

     50 /

MESSAGES

--  mess   comm   warn   prob   err    bug    -- ( .. /.. )

   1*    1*    1*    1*    1*    1*

   100000 50000  10000  3333333  100    1* /

--    100000 50000  10000  1     1     1* /

-- 02.06. Testing stop limit for severity 4 and 5 messages(PROBLEM,ERROR) to 1

--
================================================================================
====================

GRID

-- report/make *INIT and *GRID / *EGRID files

INIT

GRIDFILE

-- no/grid/Egrid EGRIDout

     2        1 /
```

```
-- 3D grid; 05.September

-- Using Facies RU lumped permeability

NOECHO

INCLUDE

  '../MEPO_Include/HM31_M2_29_8/G4_FACIES_RU_PERM.GRDECL'  /

ECHO

-- include Fault planes;

-- Split purple into 3 segments

-- PURPLE_N and PURPLE_S sealed off

-- PURPLE_C split into PURPLECT (layers 1 - 16) and PURPLECB (layers 17 - 36)

-- PURPLECT sealed off on up-flank side of fault

-- Northern part of WHITE separated from rest of the fault; new name WHITE_N

NOECHO

-- Modified all fault specifications to use X+ instead of X-

-- due to incorrect visualization in Petrel (also Y- to Y+)

INCLUDE

 '../MEPO_Include/HM31_M2_29_8/G4_FAULTS_NEW4.INC' /

INCLUDE

 '../MEPO_Include/HM31_M2_29_8/G3TOG4_NEWG4_FAULTS.INC' /

ECHO

-- Include the Multnum-regions

-- This is the facies+zone combinations
```

```
NOECHO

INCLUDE

 '../MEPO_Include/HM31_M2_29_8/G4_FACIES_GROUPS_2.INC' /

ECHO

-- MULTIREG; Internal for each facies

-- Channel/intertidal facies + Zones (3,4,5,6)

-- INCLUDE

-- 'MULTPERM.INC' /

--   'MULTPERM_2.MINC' /

-- 12.02.2008 regrouping

INCLUDE

  '../MEPO_Include/HM31_M2_29_8/MULTPERM_3.MINC' /

-- Across fault trans.multipl

-- Seal off yellow, red, beige 2, and all east of red

-- Rest is estimated (below)

--INCLUDE

--  '../MEPO_Include/HM31_M2_29_8/MULTFAULT.INC' /

--INCLUDE

--  '../MEPO_Include/HM31_M2_29_8/MULTFLT_NEW2.MINC' /

--INCLUDE

--  '../MEPO_Include/HM31_M2_29_8/G3TOG4_NEWG4_MULTFLT.MINC' /

-- 02.04.2008. Channel between A-3 and A-1 has been (temporarily)
```

```
-- removed in HM31_BASE case.

-- -- Artificial high permeability channel

-- -- between  A-3 and A-1. Tight bottom of channel

-- INCLUDE

--    'EQUALPERM1.MINC' /

--

-- -- Tighten the sides of high perm. channel between  A-3 and A-1

-- INCLUDE

--   'CH_SIDES.MINC' /

-- Vertical transmissibility multipliers.

-- Interface between layer 16 and 17 sealed off (bottom of layer 16)

INCLUDE

  '../MEPO_Include/HM31_M2_29_8/MULTZ.MINC' /

-- Reduce flow from north-west into A-7

-- Reduce even more.

--INCLUDE

--  '../MEPO_Include/HM31_M2_29_8/MULTYX_A7N.MINC' /

-- -- Reduce flow from south (A-9) into A-7

-- INCLUDE

--   'MULTY_A7S2.MINC' /

-- -- Reduce flow from north (high perm. channel) into A-4

-- INCLUDE
```

```
--   'MULTYX_A4N.MINC' /

-- -- Reduce pressure support from west towards A-5

-- INCLUDE

--   'MULTX_A5W.MINC' /

-- -- Limit producing volume for A-6 (North)

-- INCLUDE

--  'MULTY_A6N.MINC' /

-- -- Limit producing volume for A-6 (South)

-- INCLUDE

--  'MULTY_A6S.MINC' /

-- -- Limit producing volume / pressure support from north, A-8

-- Reincluding HM31_MANUAL2 exp 19,Latin Hypercube

--INCLUDE

-- '../MEPO_Include/HM31_M2_29_8/MULTY_A8N.MINC' /

-- Reduce size of model; cut segments to the south and south east

-- Remove segments southeast and northeast

NOECHO

--INCLUDE

--  '../MEPO_Include/HM31_M2_29_8/G4_ACTNUM.INC' /

--include sector model

INCLUDE

  '../Sector_ACTNUM/ACTNUM_3D.INC' /
```

```
NOECHO

-- Output the faults and active cells

-- RPTGRID

--  'FAULTS' 'IOCN' /

-- RPTGRID

--  'FAULTS' /

--
================================================================================
====================

EDIT

--
================================================================================
====================

PROPS


LSALTFNC

-- Cs F1 F2 -- SATNUM 1

0.0 1.0 1.0

1.0 0.8 0.8

4.0 0.2 0.2

5.0 0.0 0.0

35.0 0.0 0.0

45.0 0.0 0.0
```

/

-- Cs F1 F2 -- SATNUM 2

0.0 1.0 1.0

1.0 0.8 0.8

4.0 0.2 0.2

5.0 0.0 0.0

35.0 0.0 0.0

45.0 0.0 0.0

/

-- Cs F1 F2 -- SATNUM 3

0.0 1.0 1.0

1.0 0.8 0.8

4.0 0.2 0.2

5.0 0.0 0.0

35.0 0.0 0.0

45.0 0.0 0.0

/

-- Cs F1 F2 -- SATNUM 4

0.0 1.0 1.0

1.0 0.8 0.8

4.0 0.2 0.2

```
5.0 0.0 0.0

35.0 0.0 0.0

45.0 0.0 0.0

/


-- Cs F1 F2 -- SATNUM 5

0.0 1.0 1.0

1.0 0.8 0.8

4.0 0.2 0.2

5.0 0.0 0.0

35.0 0.0 0.0

45.0 0.0 0.0

/

-- Debug convergence issues (PVT)

DEBUG

 8*0 0 11*0 1 /

EXTRAPMS

 4 /

PMAX

-- Pmax(PVCO)  Pmax  Pmin  #nodes

  500        500   100    17 /

-- 28.02.2008: Test the effect of 2- vs. 3-point scaling in HM10_MANUAL
```

```
INCLUDE

  '../MEPO_Include/HM31_M2_29_8/SCALECRS.INC' /

-- initial water saturations using SWATINIT from Petrel

NOECHO

INCLUDE

 '../MEPO_Include/HM31_M2_29_8/G4_SWATINIT.INC' /

ECHO

-- write endpoint sats to *INIT

FILLEPS

-- Rock compressibility

INCLUDE

 '../MEPO_Include/HM31_M2_29_8/ROCK.INC' /

-- DewPoint data 2008 -Modified

-- Frøy 25/5-1 DST 3B BHS no 2

-- New Process,

INCLUDE

 '../Include/Props/MOD_3088m_NewProc_TEST.INC' /

-- ResLab Integration SCAL Review June 2007;

--  Base Case Ng = 2 ; Nog = 5.5, Sorg = 0.08 , Swi = 0.12 (NB! End-Point-Scaling)

-- INCLUDE

--  'SGOF_RESLAB200706.INC' /

--  'SGOF_RESLAB200706_NORM.INC' /
```

```
-- INCLUDE

--  'SGOF.MINC' /

-- INCLUDE

--  'SGOF4.MINC' /

INCLUDE

  '../MEPO_Include/HM31_M2_29_8/SGOF5.MINC' /

-- ResLab Integration SCAL Review June 2007;

--  Base Case Nw = 1.3 ; Now = 5.5, Sorg = 0.08 , Swi = 0.12 (NB! End-Point-Scaling)

--   NORMALIZED oil water relperm

--    straight line OW oil relperm for wells; "PI" not impacted by change in WCT

-- INCLUDE

--    'SWOF_RESLAB200706.INC' /

--    'SWOF_RESLAB200706_NORM.INC' /

-- INCLUDE

--    'SWOF.MINC' /

-- INCLUDE

--   'SWOF4.MINC' /

INCLUDE

  '../MEPO_Include/HM31_M2_29_8/SWOF5_SW1_TEST.MINC' /

-- ResLab Integration SCAL Review June 2007; critical oil saturation 8%

--  ( largest value where Kro = 0.0)

-- To be estimated (between 0.08 to 0.22)
```

```
-- SOWCR

--  285048*0.08 /

-- INCLUDE

--   'SOWCR.MINC' /

INCLUDE

  '../MEPO_Include/HM31_M2_29_8/SOWCR_MULTNUM.MINC' /

-- With SATNUM5.INC, adding critical value for SATNUM region 4, RU 1+2

EQUALS

  SOWCR 0.08 1 74 1 107 1 4 /

/

-- Connate water 12% ; i.e. smallest water saturation in an SATFUNC

SWL

   285048*0.12 /

-- critical water saturation; equal initial SWATINIT

NOECHO

INCLUDE

   '../MEPO_Include/HM31_M2_29_8/G4_SWCR.INC' /

ECHO


-- adjust SWCR to stall immediate water prod linked to new well relperm. ??

-- Match against watercut? (0.7 to 1.3)

-- INCLUDE
```

```
--  'MULTSWCR.INC' /
INCLUDE
   '../MEPO_Include/HM31_M2_29_8/MULTSWCR_4SATNUM.MINC' /
-- keep SWCR within "global" Swinit / 1- Sowcr (min / max) values
MINVALUE
 SWCR 0.12 /
/
MAXVALUE
  SWCR 0.7799 /
/
--Adjust the gas saturation table for connate water
SGU
 285048*0.88 /
-- Critical gas saturation; increase to slow gas front velocity
-- Vary between 0 and 0.1; Start value 0.07
-- INCLUDE
--  'SGCR.INC' /
--INCLUDE
--  'SGCR.MINC' /
INCLUDE
  '../MEPO_Include/HM31_M2_29_8/SGCR_MULTNUM.MINC' /
-- With SATNUM5.INC, adding critical value for SATNUM region 4, RU 1+2
```

```
EQUALS
  SGCR 0.07 1 74 1 107 1 4 /
/
-- Scaled critical oil-in-gas saturation
-- Interval to be decided
INCLUDE
  '../MEPO_Include/HM31_M2_29_8/SOGCR_MULTNUM.MINC' /
-- With SATNUM5.INC, adding critical value for SATNUM region 4, RU 1+2
EQUALS
  SOGCR 0.08 1 74 1 107 1 4 /
/


-- ResLab Integration SCAL Review June 2007;  Krw@Sorw = 0.8
-- To be estimated (0.2 to 0.8)
-- Eclipse 2007 has changed the end-scaling behaviour
-- -- Goes with 4satnum
-- COPY
--  KRW KRWR /
-- /
--


-- KRW
```

```
--  285048*0.8 /

-- -- Goes with 4satnum

-- INCLUDE

--   'KRW.MINC' /

-- INCLUDE

--   'KRW4.MINC' /

INCLUDE

  '../MEPO_Include/HM31_M2_29_8/KRWR_MULTNUM.MINC' /

-- With SATNUM5.INC, adding critical value for SATNUM region 4, RU 1+2

EQUALS

  KRWR 0.8 1 74 1 107 1 4 /

/

KRW

 285048*1.0000  /

--
================================================================================
======================

REGIONS

-- 4 Facies + 1 well in satnum

NOECHO

INCLUDE

  '../MEPO_Include/HM31_M2_29_8/SATNUM5.INC' /

ECHO
```

```
LWSLTNUM

285048*5 /


--FIPNUM from it 14 and on.

INCLUDE

 '../MEPO_Include/HM31_M2_29_8/FIPNUM.INC'  /

-- Not using FIPNUM, because it cannot be zero,

-- and MULTNUM is zero in some places

--COPY

--  MULTNUM  FIPNUM /

--/

--
================================================================================
====================

SOLUTION

--EQUIL

-- datum  pressure  owc   Pcowc  GOC  Pcgoc  RSVD  RVVD

--   2930    306    3176   0    2930   0     1   1  /

-- 10.06.2008: dataset 17, testing no fine grid equilibration

-- datum  pressure  owc   Pcowc  GOC  Pcgoc  RSVD  RVVD equil (default = -5)

--  2930    306    3176   0    2930   0     1   1   0 /

--  report SOLUTION data

-- RPTSOL
```

```
-- FIIP/region  Swi/Cell  Swcr/cell

--      'FIP=2'    'SWAT'     'SWCR'  /

--INCLUDE

-- '../MEPO_Include/HM31_M2_29_8/XXVD.INC' /

--include initial condition

INCLUDE

  '../Sector_ACTNUM/INIT.INC' /

-- Carter Tracy aquifer

-- Re-introduce, and couple to west

-- Maybe also south-west

-- Aquifer permeability: vary between 1 and 2000 mD; start value 333 mD

-- INCLUDE

--   'AQUCT.INC' /

--INCLUDE

--  '../MEPO_Include/HM31_M2_29_8/AQUCT.MINC' /

SALT

285048*38.00 /

--Restart

-- 78 : 1 Apr 2012

-- 79 : 1 Jul 2012

-- 80 : 1 Oct 2012

-- 81 : 1 Jan 2013
```

```
--RESTART

--   '../MEPO_Include/HM31_M2_29_8/HM31_M2_29_8sw1.UNRST'  80  /

--'Q:\Lisenser\PL364\Reservoir Engineering\1.0 Reservoir
model\G4_200709\MEPO_Include\HM31_M2_29_8\HM31_M2_29_8sw1.UNRST'   80  /

--/

-- Change Rs for undersaturated oil

OPERATE

  RS 6* 'ADDX' RS  24  1 /

/

-- Report SOLUTION data (initial state)

RPTSOL

 RESTART=2 /

--
================================================================================
====================

SUMMARY

INCLUDE

  '../Include/Summary/PRED_SWAG.SUM' /

--
================================================================================
====================

SCHEDULE

-- VFP tables (5.5" or 7", COMPDAT assumes 8.5")

NOECHO
```

```
--INCLUDE

--   '../INCLUDE/VFP/VLP_TUBING_7.Ecl' /

--  '../INCLUDE/VFP/VLP_TUBING_5.5.Ecl' /

ECHO

-- request warnings for PVT and VFP table extrapolation to *PRT

EXTRAPMS

 4 /

RPTSCHED

 CPU NEWTON FIP=3  WELLS /

RPTRST

 BASIC=2 /

-- Well specs ; here NEW G4 well locations"

--INCLUDE

-- '../Include/Well/G4_8P_6I_rB.INC' /

-- F&F gas consumption; 200 KSm3/d

GCONSUMP

  FIELD  200e+3  /

/

-- compositional study indicate DRSDT ~ 0.02 Sm3/Sm3/d .. or 0.03 Sm3/Sm3/d  ??

DRSDT

  0.3  /

-- production schedule 1.10.2012 -> 1.1.2030
```

--include sector model

RPTSCHED -- Generated : Petrel

FIP WELLS /

RPTRST -- Generated : Petrel

BASIC=3 FLOWS /

SKIP -- Generated : Petrel

--Hint: Select wells on the input tree, drop in with the blue arrow, then add rules with the rule pop-up

ENDSKIP -- Generated : Petrel

GRUPTREE -- Generated : Petrel

'GROUP 1' FIELD /

/

DATES -- Generated : Petrel

2 JLY 2012 /

/

WELSPECS -- Generated : Petrel

--'INJ_2D' is the simulation well name used to describe flow from 'Inj_2D'

--'INJ_3D' is the simulation well name used to describe flow from 'Inj_3D'

--'PROD_2D' is the simulation well name used to describe flow from 'Prod_2D'

--'PROD_3D' is the simulation well name used to describe flow from 'Prod_3D'

--

INJ_2D 'GROUP 1' 28 33 1* WATER /

INJ_3D 'GROUP 1' 26 37 1* WATER /

PROD_2D 'GROUP 1' 40 33 1* OIL /

PROD_3D 'GROUP 1' 40 37 1* OIL /

/

COMPDAT -- Generated : Petrel

INJ_2D 28 33 1 1 OPEN 1* 8.6762 0.19050 861.81 0.00 1* Z 19.50 /

INJ_2D 28 33 2 2 OPEN 1* 9.6419 0.19050 957.80 0.00 1* Z 19.51 /

INJ_2D 28 33 3 3 OPEN 1* 4.8302 0.19050 479.41 0.00 1* Z 19.42 /

INJ_2D 28 33 4 4 OPEN 1* 109.8869 0.19050 10904.44 0.00 1* Z 19.40 /

INJ_2D 28 33 5 5 OPEN 1* 2.0052 0.19050 198.93 0.00 1* Z 19.38 /

INJ_2D 28 33 6 6 OPEN 1* 2.0053 0.19050 198.93 0.00 1* Z 19.37 /

INJ_2D 28 33 7 7 OPEN 1* 14.5529 0.19050 1445.67 0.00 1* Z 19.51 /

INJ_2D 28 33 8 8 OPEN 1* 0.8149 0.19050 80.82 0.00 1* Z 19.35 /

INJ_2D 28 33 9 9 OPEN 1* 0.8155 0.19050 80.87 0.00 1* Z 19.33 /

INJ_2D 28 33 10 10 OPEN 1* 6.0874 0.19050 604.38 0.00 1* Z 19.45 /

INJ_2D 28 33 11 11 OPEN 1* 0.6689 0.19050 66.31 0.00 1* Z 19.30 /

INJ_2D 28 33 12 12 OPEN 1* 0.6699 0.19050 66.39 0.00 1* Z 19.28 /

INJ_2D 28 33 13 13 OPEN 1* 0.6710 0.19050 66.49 0.00 1* Z 19.26 /

INJ_2D 28 33 14 14 OPEN 1* 0.2822 0.19050 27.96 0.00 1* Z 19.25 /

INJ_2D 28 33 15 15 OPEN 1* 2.1617 0.19050 214.43 0.00 1* Z 19.36 /

INJ_2D 28 33 16 16 OPEN 1* 0.2825 0.19050 27.99 0.00 1* Z 19.24 /

INJ_2D 28 33 17 17 OPEN 1* 10.9598 0.19050 1087.40 0.00 1* Z 19.38 /

INJ_2D 28 33 18 18 OPEN 1* 10.9672 0.19050 1087.92 0.00 1* Z 19.37 /

INJ_2D 28 33 19 19 OPEN 1* 10.9755 0.19050 1088.55 0.00 1* Z 19.35 /

INJ_2D 28 33 23 23 OPEN 1* 0.7493 0.19050 74.19 0.00 1* Z 19.17 /

INJ_2D 28 33 25 25 OPEN 1* 9.1930 0.19050 911.21 0.00 1* Z 19.28 /

INJ_2D 28 33 27 27 OPEN 1* 9.2162 0.19050 913.19 0.00 1* Z 19.25 /

INJ_2D 28 33 28 28 OPEN 1* 9.2288 0.19050 914.27 0.00 1* Z 19.23 /

INJ_2D 28 33 29 29 OPEN 1* 15.3538 0.19050 1520.71 0.00 1* Z 19.21 /

INJ_2D 28 33 30 30 OPEN 1* 15.3752 0.19050 1522.42 0.00 1* Z 19.18 /

INJ_2D 28 33 31 31 OPEN 1* 0.1387 0.19050 13.72 0.00 1* Z 19.06 /

INJ_2D 28 33 32 32 OPEN 1* 0.1387 0.19050 13.72 0.00 1* Z 19.05 /

INJ_2D 28 33 33 33 OPEN 1* 0.1387 0.19050 13.72 0.00 1* Z 19.04 /

INJ_2D 28 33 36 36 OPEN 1* 0.1503 0.19050 14.86 0.00 1* Z 18.98 /

INJ_3D 26 37 1 1 OPEN 1* 23.4261 0.19050 2310.67 0.00 1* Z 18.79 /

INJ_3D 26 37 2 2 OPEN 1* 100.9621 0.19050 9967.78 0.00 1* Z 18.88 /

INJ_3D 26 37 3 3 OPEN 1* 30.9709 0.19050 3055.72 0.00 1* Z 18.82 /

INJ_3D 26 37 4 4 OPEN 1* 11.7827 0.19050 1163.75 0.00 1* Z 18.92 /

INJ_3D 26 37 5 5 OPEN 1* 2.3313 0.19050 230.38 0.00 1* Z 18.98 /

INJ_3D 26 37 6 6 OPEN 1* 2.3291 0.19050 230.22 0.00 1* Z 19.00 /

INJ_3D 26 37 7 7 OPEN 1* 2.3269 0.19050 230.07 0.00 1* Z 19.03 /

INJ_3D 26 37 8 8 OPEN 1* 0.8157 0.19050 80.68 0.00 1* Z 19.06 /

INJ_3D 26 37 9 9 OPEN 1* 0.8148 0.19050 80.61 0.00 1* Z 19.10 /

INJ_3D 26 37 10 10 OPEN 1* 0.8137 0.19050 80.53 0.00 1* Z 19.13 /

INJ_3D 26 37 11 11 OPEN 1* 0.4572 0.19050 45.26 0.00 1* Z 19.16 /

INJ_3D 26 37 12 12 OPEN 1* 0.4571 0.19050 45.26 0.00 1* Z 19.18 /

INJ_3D 26 37 13 13 OPEN 1* 0.4570 0.19050 45.27 0.00 1* Z 19.20 /

INJ_3D 26 37 14 14 OPEN 1* 0.2944 0.19050 29.16 0.00 1* Z 19.22 /

INJ_3D 26 37 16 16 OPEN 1* 0.2865 0.19050 28.38 0.00 1* Z 19.25 /

INJ_3D 26 37 17 17 OPEN 1* 10.5103 0.19050 1039.72 0.00 1* Z 19.08 /

INJ_3D 26 37 18 18 OPEN 1* 10.4973 0.19050 1038.77 0.00 1* Z 19.12 /

INJ_3D 26 37 19 19 OPEN 1* 10.4865 0.19050 1038.04 0.00 1* Z 19.15 /

INJ_3D 26 37 20 20 OPEN 1* 10.4734 0.19050 1037.08 0.00 1* Z 19.18 /

INJ_3D 26 37 22 22 OPEN 1* 1.1973 0.19050 118.81 0.00 1* Z 19.40 /

INJ_3D 26 37 25 25 OPEN 1* 6.4130 0.19050 635.80 0.00 1* Z 19.31 /

INJ_3D 26 37 27 27 OPEN 1* 6.4090 0.19050 635.64 0.00 1* Z 19.34 /

INJ_3D 26 37 28 28 OPEN 1* 6.4079 0.19050 635.64 0.00 1* Z 19.36 /

INJ_3D 26 37 29 29 OPEN 1* 12.8605 0.19050 1276.09 0.00 1* Z 19.39 /

INJ_3D 26 37 30 30 OPEN 1* 12.8449 0.19050 1275.05 0.00 1* Z 19.43 /

INJ_3D 26 37 31 31 OPEN 1* 0.1519 0.19050 15.11 0.00 1* Z 19.61 /

INJ_3D 26 37 32 32 OPEN 1* 0.1513 0.19050 15.05 0.00 1* Z 19.66 /

INJ_3D 26 37 33 33 OPEN 1* 0.1506 0.19050 14.99 0.00 1* Z 19.70 /

INJ_3D 26 37 34 34 OPEN 1* 0.2547 0.19050 25.36 0.00 1* Z 19.75 /

INJ_3D 26 37 36 36 OPEN 1* 0.2526 0.19050 25.18 0.00 1* Z 19.88 /

PROD_2D 40 33 1 1 OPEN 1* 86.8118 0.19050 8668.42 0.00 1* Z 20.06 /

PROD_2D 40 33 2 2 OPEN 1* 1.4111 0.19050 140.96 0.00 1* Z 20.10 /

PROD_2D 40 33 3 3 OPEN 1* 8.8027 0.19050 879.22 0.00 1* Z 20.09 /

PROD_2D 40 33 4 4 OPEN 1* 2.7357 0.19050 273.22 0.00 1* Z 20.07 /

PROD_2D 40 33 5 5 OPEN 1* 15.2273 0.19050 1521.97 0.00 1* Z 20.16 /

PROD_2D 40 33 6 6 OPEN 1* 15.2261 0.19050 1521.93 0.00 1* Z 20.17 /

PROD_2D 40 33 7 7 OPEN 1* 15.2248 0.19050 1521.89 0.00 1* Z 20.17 /

PROD_2D 40 33 8 8 OPEN 1* 6.1170 0.19050 611.67 0.00 1* Z 20.21 /

PROD_2D 40 33 9 9 OPEN 1* 6.1151 0.19050 611.54 0.00 1* Z 20.22 /

PROD_2D 40 33 10 10 OPEN 1* 0.7982 0.19050 79.76 0.00 1* Z 20.13 /

PROD_2D 40 33 11 11 OPEN 1* 0.2857 0.19050 28.55 0.00 1* Z 20.14 /

PROD_2D 40 33 12 12 OPEN 1* 0.2856 0.19050 28.54 0.00 1* Z 20.14 /

PROD_2D 40 33 13 13 OPEN 1* 0.2856 0.19050 28.55 0.00 1* Z 20.15 /

PROD_2D 40 33 15 15 OPEN 1* 0.3906 0.19050 39.04 0.00 1* Z 20.16 /

PROD_2D 40 33 17 17 OPEN 1* 7.7700 0.19050 777.28 0.00 1* Z 20.25 /

PROD_2D 40 33 18 18 OPEN 1* 7.7695 0.19050 777.27 0.00 1* Z 20.26 /

PROD_2D 40 33 19 19 OPEN 1* 7.7690 0.19050 777.25 0.00 1* Z 20.26 /

PROD_2D 40 33 20 20 OPEN 1* 7.7689 0.19050 777.28 0.00 1* Z 20.27 /

PROD_2D 40 33 25 25 OPEN 1* 11.5926 0.19050 1160.09 0.00 1* Z 20.29 /

PROD_2D 40 33 26 26 OPEN 1* 11.5889 0.19050 1159.81 0.00 1* Z 20.30 /

PROD_2D 40 33 27 27 OPEN 1* 11.5853 0.19050 1159.55 0.00 1* Z 20.31 /

PROD_2D 40 33 28 28 OPEN 1* 11.5819 0.19050 1159.30 0.00 1* Z 20.32 /

PROD_2D 40 33 29 29 OPEN 1* 12.5776 0.19050 1259.08 0.00 1* Z 20.33 /

PROD_2D 40 33 30 30 OPEN 1* 12.5722 0.19050 1258.66 0.00 1* Z 20.34 /

PROD_2D 40 33 31 31 OPEN 1* 0.1344 0.19050 13.44 0.00 1* Z 20.23 /

PROD_2D 40 33 32 32 OPEN 1* 0.1341 0.19050 13.42 0.00 1* Z 20.25 /

PROD_2D 40 33 33 33 OPEN 1* 0.1339 0.19050 13.39 0.00 1* Z 20.27 /

PROD_2D 40 33 34 34 OPEN 1* 0.1693 0.19050 16.94 0.00 1* Z 20.29 /

PROD_2D 40 33 35 35 OPEN 1* 0.1693 0.19050 16.94 0.00 1* Z 20.31 /

PROD_2D 40 33 36 36 OPEN 1* 0.1679 0.19050 16.81 0.00 1* Z 20.33 /

PROD_3D 40 37 1 1 OPEN 1* 4.4094 0.19050 440.11 0.00 1* Z 20.01 /

PROD_3D 40 37 2 2 OPEN 1* 13.7926 0.19050 1377.12 0.00 1* Z 20.05 /

PROD_3D 40 37 3 3 OPEN 1* 1.5537 0.19050 155.14 0.00 1* Z 20.05 /

PROD_3D 40 37 4 4 OPEN 1* 15.6983 0.19050 1568.73 0.00 1* Z 20.14 /

PROD_3D 40 37 5 5 OPEN 1* 16.1609 0.19050 1616.87 0.00 1* Z 20.27 /

PROD_3D 40 37 6 6 OPEN 1* 16.1715 0.19050 1618.35 0.00 1* Z 20.30 /

PROD_3D 40 37 7 7 OPEN 1* 2.2268 0.19050 222.72 0.00 1* Z 20.24 /

PROD_3D 40 37 8 8 OPEN 1* 5.0323 0.19050 503.95 0.00 1* Z 20.37 /

PROD_3D 40 37 9 9 OPEN 1* 5.0312 0.19050 504.00 0.00 1* Z 20.41 /

PROD_3D 40 37 10 10 OPEN 1* 0.6567 0.19050 65.75 0.00 1* Z 20.34 /

PROD_3D 40 37 11 11 OPEN 1* 2.5475 0.19050 255.36 0.00 1* Z 20.47 /

PROD_3D 40 37 12 12 OPEN 1* 0.3327 0.19050 33.32 0.00 1* Z 20.38 /

PROD_3D 40 37 13 13 OPEN 1* 0.3327 0.19050 33.33 0.00 1* Z 20.40 /

PROD_3D 40 37 14 14 OPEN 1* 0.6190 0.19050 62.01 0.00 1* Z 20.42 /

PROD_3D 40 37 15 15 OPEN 1* 4.7409 0.19050 475.63 0.00 1* Z 20.57 /

PROD_3D 40 37 16 16 OPEN 1* 0.6195 0.19050 62.09 0.00 1* Z 20.48 /

PROD_3D 40 37 17 17 OPEN 1* 10.6353 0.19050 1067.98 0.00 1* Z 20.67 /

PROD_3D 40 37 18 18 OPEN 1* 10.6363 0.19050 1068.44 0.00 1* Z 20.71 /

PROD_3D 40 37 19 19 OPEN 1* 10.6369 0.19050 1068.84 0.00 1* Z 20.75 /

PROD_3D 40 37 20 20 OPEN 1* 10.6378 0.19050 1069.29 0.00 1* Z 20.78 /

PROD_3D 40 37 25 25 OPEN 1* 11.3325 0.19050 1140.13 0.00 1* Z 20.88 /

PROD_3D 40 37 26 26 OPEN 1* 11.3300 0.19050 1140.27 0.00 1* Z 20.92 /

PROD_3D 40 37 27 27 OPEN 1* 11.3297 0.19050 1140.63 0.00 1* Z 20.96 /

PROD_3D 40 37 28 28 OPEN 1* 11.3293 0.19050 1141.00 0.00 1* Z 21.00 /

PROD_3D 40 37 29 29 OPEN 1* 10.8675 0.19050 1094.87 0.00 1* Z 21.04 /

PROD_3D 40 37 30 30 OPEN 1* 10.8635 0.19050 1094.83 0.00 1* Z 21.08 /

PROD_3D 40 37 31 31 OPEN 1* 0.1391 0.19050 14.00 0.00 1* Z 20.90 /

PROD_3D 40 37 32 32 OPEN 1* 0.1390 0.19050 13.99 0.00 1* Z 20.96 /

PROD_3D 40 37 33 33 OPEN 1* 0.1388 0.19050 13.98 0.00 1* Z 21.02 /

PROD_3D 40 37 35 35 OPEN 1* 0.1762 0.19050 17.77 0.00 1* Z 21.16 /

/

WCONINJE -- Generated : Petrel

INJ_2D WATER SHUT RATE 25.0000 1* 1* /

/

WCONINJP

```
 INJ_3D WATER  OPEN  450 1* 1* 1*  1.0 /

 PROD_3D /

 /

 WSALT

 INJ_3D 38.00 /

 /

--WECON                          -- Generated : Petrel

--  PROD_2D 10.00 7* RATE /

--  PROD_3D 10.00 7* RATE /

--  /

WCONPROD                         -- Generated : Petrel

 PROD_2D SHUT ORAT 20.00 /

 PROD_3D OPEN ORAT 800 1* 1* 1* 1* 100 /

 /

DATES                            -- Generated : Petrel

 1 JAN 2013 /

 /

WSALT

 INJ_3D 38.00 /

 /

DATES                            -- Generated : Petrel

 1 JAN 2014 /
```

/

WSALT

INJ_3D 38.00 /

/

DATES -- Generated : Petrel

1 JAN 2015 /

/

WSALT

INJ_3D 38.00 /

/

DATES -- Generated : Petrel

1 JAN 2016 /

/

WSALT

INJ_3D 38.00 /

/

DATES -- Generated : Petrel

1 JAN 2017 /

/

```
 WSALT
   INJ_3D 38.00 /
   /
DATES                    -- Generated : Petrel
 1 JAN 2018 /
/
 WSALT
   INJ_3D 38.00 /
   /
DATES                    -- Generated : Petrel
 1 JAN 2019 /
/
 WSALT
   INJ_3D 38.00 /
   /
DATES                    -- Generated : Petrel
 1 JAN 2020 /
 /
  WSALT
   INJ_3D 38.00 /
   /
DATES                    -- Generated : Petrel
```

```
 1 JAN 2021 /

/

 WSALT

   INJ_3D 38.00 /

   /

DATES                    -- Generated : Petrel

 1 JAN 2022 /

/

 WSALT

   INJ_3D 38.00 /

   /

DATES                    -- Generated : Petrel

 1 JAN 2023 /

 /

 WSALT

   INJ_3D 38.00 /

   /

DATES                    -- Generated : Petrel

 1 JAN 2024 /

/

 WSALT

   INJ_3D 38.00 /
```

```
  /
DATES                    -- Generated : Petrel
 1 JAN 2025 /
 /
 WSALT
   INJ_3D 38.00 /
  /
DATES                    -- Generated : Petrel
 1 JAN 2026 /
/
 WSALT
   INJ_3D 38.00 /
  /
DATES                    -- Generated : Petrel
 1 JAN 2027 /
/
 WSALT
   INJ_3D 38.00 /
  /
DATES
-- Generated : Petrel
 1 JAN 2028 /
```

```
/

 WSALT

  INJ_3D 38.00 /

  /

DATES                    -- Generated : Petrel

 1 JAN 2029 /

 /

 WSALT

  INJ_3D 38.00 /

  /

DATES                    -- Generated : Petrel

 1 JAN 2030 /

 /

 WSALT

  INJ_3D 38.00 /

  /

DATES                    -- Generated : Petrel

 1 JAN 2031 /

 /

 WSALT

  INJ_3D 38.00 /

  /
```

```
DATES                    -- Generated : Petrel
 1 JAN 2032 /
 /
 WSALT
  INJ_3D 38.00 /
  /
DATES                    -- Generated : Petrel
 1 JAN 2033 /
 /
 WSALT
  INJ_3D 38.00 /
  /
DATES                    -- Generated : Petrel
 1 JAN 2034 /
 /
 WSALT
  INJ_3D 38.00 /
  /
DATES                    -- Generated : Petrel
 1 JAN 2035 /
 /
 WSALT
```

```
    INJ_3D 38.00 /

    /

END
```